JOURNAL OF FLUID MECHANICS

VOLUME 10 PART 4

JUNE 1961

PUBLISHED BY

CAMBRIDGE UNIVERSITY PRESS

BENTLEY HOUSE, 200 EUSTON ROAD, LONDON, N.W.1

AMERICAN BRANCH: 32 EAST 57TH STREET, NEW YORK 22, N.Y.

Price 30*s.* (*U.S.A.* $5.00)

The JOURNAL OF FLUID MECHANICS exists for the publication of theoretical and experimental investigations of all aspects of the mechanics of fluids, and is issued in four parts per volume.

EDITORS

DR G. K. BATCHELOR, DR T. BROOKE BENJAMIN

Department of Applied Mathematics and Theoretical Physics, University of Cambridge, Free School Lane, Cambridge, England

ASSISTANT EDITORS

DR J. R. A. PEARSON, DR O. M. PHILLIPS

ASSOCIATE EDITORS

PROF. G. F. CARRIER

Pierce Hall, Harvard University, Cambridge 38, *Massachusetts, U.S.A.*

DR W. C. GRIFFITH

Lockheed Missiles and Space Division, Palo Alto, California, U.S.A.

M. J. LIGHTHILL

Royal Aircraft Establishment, Farnborough, Hampshire, England

PROF. R. R. LONG

School of Engineering, The Johns Hopkins University, Baltimore 18, *Maryland, U.S.A.*

DR P. G. SAFFMAN

Department of Mathematics, King's College, London, W.C. 2, *England*

Authors wishing to have papers published in the JOURNAL should communicate them to any one of the persons named above, choosing one in their own country where possible.

Authors are urged to ensure that their papers are written clearly and attractively, in order that their work will be readily accessible to readers.

Manuscripts should be typed in double spacing on one side of the paper only, with references listed at the end in alphabetical order of authors. Drawings should be done on a large scale in Indian ink on tracing cloth or drawing paper, the lettering being shown clearly in pencil for reproduction by the printer; the list of captions should be typed at the end of the manuscript. Proofs of papers from overseas will usually be despatched to authors by airmail. There is no charge for publication. Authors are entitled to receive 50 offprints of a paper in the JOURNAL free of charge, and additional offprints can be purchased if ordered in advance.

SUBSCRIPTIONS

The subscription price for a volume of four parts is £5. 10*s*. net, post free, payable in advance; separate parts 30*s*. net, plus postage. Subscriptions may be sent to any bookseller, or to the Cambridge University Press, Bentley House, 200 Euston Road, London, N.W. 1.

Subscribers in the United States should send their orders to the Cambridge University Press, American Branch, 32 East 57th Street, New York 22, N.Y. The subscription price per volume is $18.50, post free, payable in advance; separate parts $5.00, plus postage.

Quotations for available back volumes and parts may be obtained on application to the Cambridge University Press.

The two-dimensional turbulent wall-jet

By W. H. SCHWARZ AND W. P. COSART

Department of Chemical Engineering, Stanford University, Palo Alto, California

(Received 1 November, 1960)

With the aid of a hot-wire anemometer, the mean velocity distribution of the incompressible, turbulent, plane wall-jet has been examined in some detail. As previously reported, this fully developed boundary layer belongs to the class of self-preserving flows. Over the entire range of experimental conditions, a single velocity scale ($\overline{U}_m$) and a single length scale (δ) seem to correlate all the velocity data. Further, it is shown theoretically that δ must vary as x, and $\overline{U}_m$ must vary as x^a over this range. The exponent a has been empirically determined as $-0{\cdot}555$. Values of the Reynolds shear stress, which are proportional to $\overline{uv}$, the Boussinesq exchange coefficient ϵ, and the shear stress at the wall have been evaluated. The Reynolds number based on the maximum velocity and the thickness of the boundary layer varied from 22,000 to 106,000.

1. Introduction

The wall-jet is described as a jet of fluid which impinges onto a wall at an angle from 0 to 90 degrees. The region of interest is the fully developed boundary layer which occurs after the stagnation flow and the turbulent transition regions, and has both a solid boundary and a free boundary of the same fluid as the jet. The name wall-jet seems to have been ascribed by Glauert (1956), although the terms partially open jet, surface jet, and submerged jet have been used by Förthmann (1934), Zerbe & Selna (1946) and Poreth & Cermak (1959).

Since the boundary conditions on the surface jet are such that the velocity at the wall and also outside the boundary layer are zero, the velocity profile must have a maximum. Further, this flow is of the self-preserving class of shear flows such as jets, wakes, and free-mixing layers. The free and solid boundaries generate considerable interest, since the flow will have both a jet-like property and also be influenced by the wall. A sketch of the tangential wall-jet is shown in figure 1, which includes a fully developed profile.

The earliest known work on the plane wall-jet was done by Förthmann (1934), apparently to complement his investigation of the plane free jet and partially expanding jet. Förthmann observed the self-preserving nature of the wall-jet, and that the boundary-layer thickness varied linearly with x and the maximum velocity varied inversely as the half power of x. Further, he determined from the data that the velocity in the inner layer varied as the one-seventh power of the distance from the wall.

Glauert (1956) has examined theoretically the similarity problem of the laminar and turbulent, radial and plane wall-jets. The velocity distribution of

the turbulent radial wall-jet and the variation of velocity and length scales with downstream position has been measured by Bakke (1957). He found that the velocity scale varied as a power of x with exponent $-1{\cdot}12 \pm 0{\cdot}03$ and the length scale as $0{\cdot}94 \pm 0{\cdot}02$. The velocity profiles showed a self-preserving character in both the inner and outer layers.

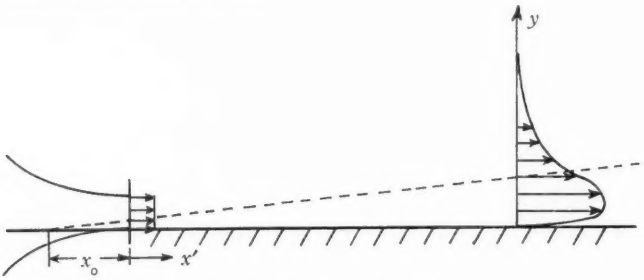

FIGURE 1. Tangential wall-jet.

The measurement of wall shear stress in a tangential jet was done by Sigalla (1958*b*). Data were correlated in a manner analogous to that of a turbulent boundary layer on a flat plate. The boundary-layer thickness was found experimentally to vary linearly, making an angle of 3·7 degrees with the plate and passing approximately through the centre of the outlet nozzle of the jet. Further, it was found that the velocity scale varied as a power of x with an exponent of minus one-half.

2. Theoretical development

The equations of motion for a steady, plane, turbulent, incompressible flow with constant physical properties and negligible energy dissipation may be written as

$$\overline{U}\frac{\partial \overline{U}}{\partial x}+\overline{V}\frac{\partial \overline{U}}{\partial y}=-\frac{1}{\rho}\frac{\partial \overline{p}}{\partial x}+\frac{\partial}{\partial x}\left[\nu\frac{\partial \overline{U}}{\partial x}-\overline{u^2}\right]+\frac{\partial}{\partial y}\left[\nu\frac{\partial \overline{U}}{\partial y}-\overline{uv}\right], \tag{1}$$

$$\overline{U}\frac{\partial \overline{V}}{\partial x}+\overline{V}\frac{\partial \overline{V}}{\partial y}=-\frac{1}{\rho}\frac{\partial \overline{p}}{\partial y}+\frac{\partial}{\partial x}\left[\nu\frac{\partial \overline{V}}{\partial x}-\overline{uv}\right]+\frac{\partial}{\partial y}\left[\nu\frac{\partial \overline{V}}{\partial y}-\overline{v^2}\right], \tag{2}$$

$$0=\frac{\partial \overline{uw}}{\partial x}+\frac{\partial \overline{vw}}{\partial y}. \tag{3}$$

The continuity equation is written

$$\frac{\partial \overline{U}}{\partial x}+\frac{\partial \overline{V}}{\partial y}=0. \tag{4}$$

When the boundary-layer approximations are applied to (1), we obtain

$$\overline{U}\frac{\partial \overline{U}}{\partial x}+\overline{V}\frac{\partial \overline{U}}{\partial y}+\frac{\partial}{\partial x}(\overline{u^2}-\overline{v^2})+\frac{\partial \overline{uv}}{\partial y}=\nu\frac{\partial^2 \overline{U}}{\partial y^2}. \tag{5}$$

Then the following functions may be defined

$$\overline{U}=U_0 f(\eta),\quad \overline{u^2}=U_0^2 g_1(\eta),\quad \overline{v^2}=U_0^2 g_2(\eta),\quad \overline{uv}=U_0^2 g_{12}(\eta),\quad \eta=y/\delta. \tag{6}$$

If (6) are substituted into (5), with suitable rearrangement, the following form is obtained

$$\underset{(a)}{\frac{\delta}{U_0}\frac{\partial U_0}{dx}f(\eta)^2}-\underset{(b)}{\frac{1}{U_0}\frac{d(U_0\delta)}{dx}\frac{df(\eta)}{d\eta}\int_0^\eta f(\eta)\,d\eta}+\underset{(c)}{\frac{2\delta}{U_0}\frac{dU_0}{dx}g_1(\eta)}$$

$$-\underset{(d)}{\frac{d\delta}{dx}\eta\frac{dg_1(\eta)}{d\eta}}+\underset{(e)}{\frac{d\delta}{dx}\eta\frac{dg_2(\eta)}{d\eta}}-\underset{(f)}{2g_2(\eta)\frac{\delta}{U_0}\frac{dU_0}{dx}}+\underset{(g)}{\frac{dg_{12}(\eta)}{d\eta}}=\underset{(h)}{\frac{\nu}{U_0\delta}\frac{d^2f(\eta)}{d\eta^2}}. \quad (7)$$

If the flow is self-preserving, the functions $f(\eta)$, $g_1(\eta)$, $g_{12}(\eta)$, and $g_2(\eta)$ are independent of x, and hence the solution of (7) requires that the coefficients of the universal functions be either non-zero constants or zero. For a non-trivial solution, consider the ratios to be non-zero. The non-repetitive coefficients are

$$\frac{\delta}{U_0}\frac{dU_0}{dx}, \quad \frac{d\delta}{dx} \quad \text{and} \quad \frac{\nu}{U_0\delta}. \quad (8)$$

Each of these coefficients must be equal to a constant, hence

$$\delta = C_2 x \quad \text{and} \quad U_0 = C_0 x^{-1}. \quad (9,10)$$

This result uses the viscous shear stress term (h).

Now it is a well-known fact that in any turbulent flow, the viscous stress is small compared to the turbulent shear stress (term (g)), except very close to a wall. In the present investigation, the viscous shear stress was only 3 % of the turbulent shear stress even at 0·2 mm from the wall, which was the closest point at which the experimental equipment could be used. It seems reasonable therefore to neglect term (h). Then the only non-repetitive constant coefficients are

$$\frac{d\delta}{dx} \quad \text{and} \quad \frac{\delta}{U_0}\frac{dU_0}{dx}. \quad (11)$$

Solving these two equations gives

$$\delta = C_2 \quad U_0 = C_1 x^a, \quad (12)$$

or that the length scale varies linearly with x and the velocity scale varies as a power of the downstream direction. From the above analysis, it is seen that the flow is unlikely to have the same self-preserving character over the entire width of the boundary layer. Very near the wall, the viscous terms will dominate and the velocity scaling factor will have a different x-variation from that of the outer flow. However, for the regions of the flow that were examined, the viscous term was negligible.

If (5) is integrated with respect to y from 0 to ∞, and (4) is used, we find that

$$\frac{\tau_w}{\rho} = -\int_0^\infty \frac{\partial}{\partial x}(\overline{U}^2+\overline{u^2}-\overline{v^2})\,dy. \quad (13)$$

Since $\overline{u^2}-\overline{v^2} \ll \overline{U}^2$, and making use of (6), (13) becomes

$$\frac{\tau_w}{\rho} = -\left(2\delta U_0\frac{dU_0}{dx}+U_0^2\frac{d\delta}{dx}\right)\int_0^\infty f^2(\eta)\,d\eta. \quad (14)$$

Then, with the forms of the x-variation of δ and U_0, this may be written

$$\frac{\tau_w}{\rho} = -C_1^2 C_2 x^{2a}(2a+1)\int_0^\infty f^2(\eta)\,d\eta. \tag{15}$$

A skin friction coefficient may be defined by

$$C_f = \frac{\tau_w}{\frac{1}{2}\rho \bar{U}_m^2}. \tag{16}$$

Then

$$C_f = -2C_2(2a+1)\int_0^\infty f^2(\eta)\,d\eta. \tag{17}$$

From (15), it is apparent that the exponent of the x-variation of the velocity scale must be less than $-\frac{1}{2}$. If it were not, the shear stress on the wall would be either zero or negative, which are both impossible.

	Laminar		Turbulent	
	U_0	δ	U_0	δ
Plane jet	$x^{-\frac{1}{2}}$	$x^{\frac{1}{2}}$	$x^{-\frac{1}{2}}$	x
Plane wall-jet	$x^{-\frac{1}{2}}$	$x^{\frac{1}{2}}$	$x^{-0.555}$*	x
Circular jet	x^{-1}	x	x^{-1}	x
Circular wall-jet	$x^{-\frac{2}{3}}$	$x^{\frac{2}{3}}$	$x^{-1.12}$	$x^{0.94}$†
Flat plate ($dp/dx = 0$)	x^0	$x^{\frac{1}{2}}$	x^0	$x^{\frac{4}{5}}$

* Data of Cosart (1960). † Data of Bakke (1957).

TABLE 1

From the equations of motion, a relationship between the exponents of the x-variation of the length and velocity scales has been obtained. However, a second relation is necessary if a is to be determined uniquely. For a free jet flow, this relation is obtained from the constancy of the flux of momentum. In the Blasius problem, the velocity scale varies as the free stream velocity or is a constant. Similarly, when the potential flow over a solid surface varies as x^m, then the velocity scale will have the same variation. Glauert (1956) has succeeded in obtaining a second relation for the laminar wall-jet by noting that the 'flux of exterior momentum flux' is constant. This approach is not applicable to the turbulent wall-jet. The results of various similar flows are compared in table 1.

Now (7) may be rearranged to give (neglecting the viscous term)

$$g_{12}(\eta) = \left[2\frac{\delta}{U_0}\frac{dU_0}{dx} + \frac{d\delta}{dx}\right]\int_\eta^\infty f^2(\eta)\,d\eta + \left[\frac{\delta}{U_0}\frac{dU_0}{dx} + \frac{d\delta}{dx}\right] f(\eta)\int_0^\eta f(\eta)\,d\eta. \tag{18}$$

Then substituting (12) into (18), we obtain

$$g_{12}(\eta) = C_2(2a+1)\int_\eta^\infty f^2(\eta)\,d\eta + C_2(1+a)f(\eta)\int_0^\eta f(\eta)\,d\eta. \tag{19}$$

The function $g_{12}(\eta)$ is the universal turbulent shear-stress function.

The Boussinesq exchange coefficient may be defined by

$$\epsilon \frac{\partial \overline{U}}{\partial y} = -\overline{uv}. \tag{20}$$

Therefore, from (6) and defining $\bar{\epsilon}$ as $\epsilon/U_0\delta$, we have that

$$\bar{\epsilon} = -g_{12}(\eta)/f'(\eta). \tag{21}$$

3. Experimental method

The wind-tunnel facility used in the investigation consisted of a variable-speed blower, a diffuser section, a plenum chamber or calming section, a contraction and the flat plate. The blower was driven by a variable-speed DC motor and produced a range of velocities at the outlet of the contraction from about 0 to 85 ft./sec. The diffuser and calming section contained a number of screens to reduce turbulence, produce a uniform velocity distribution, and prevent separation in the diffuser. The contraction had an area ratio of 24 to 1 with a 24×1 in. outlet, and further served to produce a uniform and low turbulence velocity distribution at the outlet. The contraction was smoothly joined to a flat plate so that the flow was tangential to the plate. The plate had a smooth aluminium sheet attached to it and was approximately 6 ft. long. Side-boards were attached to the plate to prevent the flow from spilling over the edge and thus interfering with the two-dimensionality of the flow.

All mean velocities of the wall-jet boundary layer were measured with a hot-wire anemometer. The wire element was Wollaston drawn platinum, 0·00025 in. in diameter. The actual position of the wire from the plate was determined with a cathetometer, sensitive to within $\frac{1}{20}$ mm. The wire was easily visible with the telescope and cross-hairs. The actual distance of the wire from the plate was determined by several observations of the wire and its reflected image. The downstream position of the wire from the nozzles was measured with a common pocket tape to within $\frac{1}{8}$ in.

4. Results

A series of velocity tranverses were taken with nozzle speeds of 27, 40, 60, and 83 ft./sec over a range of distance downstream of the outlet from 1·5 to 5·5 ft. A typical set of data is shown in figure 2. The curve drawn through the points is the universal curve which is explained below. For the set of runs, values of the maximum velocity and boundary-layer thickness are listed in table 2.

All the mean velocity data were plotted together in dimensionless form and a single curve drawn through the points. This universal curve is shown in figure 3. From figure 2, typical departures of the data from the universal curve may be seen.

The variation of the boundary-layer thickness with distance has been previously shown to be proportional to the distance from the virtual origin and is of the form given by (12). This equation may be written as

$$\delta = C_2(x' + x_0), \tag{22}$$

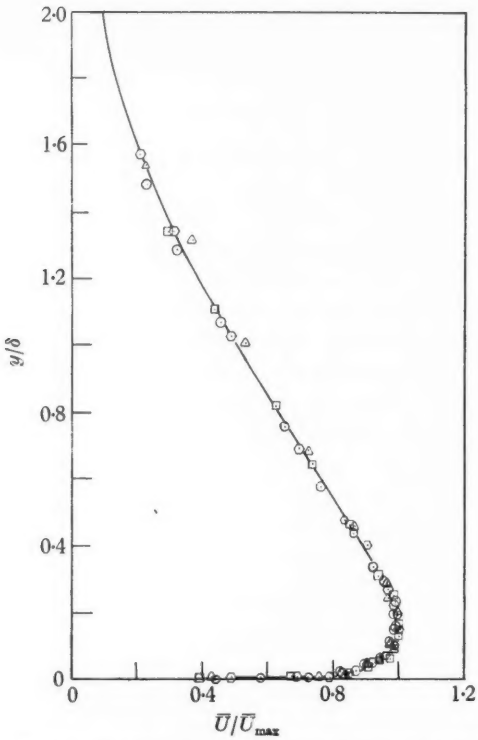

FIGURE 2. Velocity profile: the data points were taken with an outlet nozzle velocity of 83 ft./sec and at four downstream positions. ⊙, $x' = 2{\cdot}0$ ft.; ◇, $x' = 2{\cdot}5$ ft.; △, $x' = 3{\cdot}0$ ft.; ⊡, $x' = 3{\cdot}5$ ft.

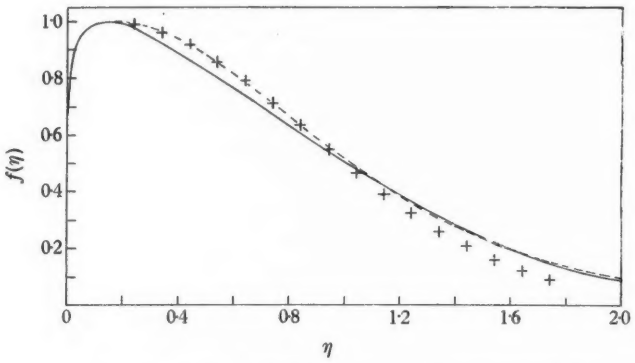

FIGURE 3. Universal velocity profile: ——, experimental data; – – – –, $\mathrm{sech}^2(\eta - 0{\cdot}14)$; +, $\exp[0{\cdot}937(\eta - 0{\cdot}14)^2]$.

where x_0 is the distance from the outlet of the wind tunnel to the point where the turbulence is assumed to originate (the virtual origin). Further, the variation of the maximum velocity with downstream position may be written as

$$\overline{U}_m = C_1(x' + x_0)^a. \tag{23}$$

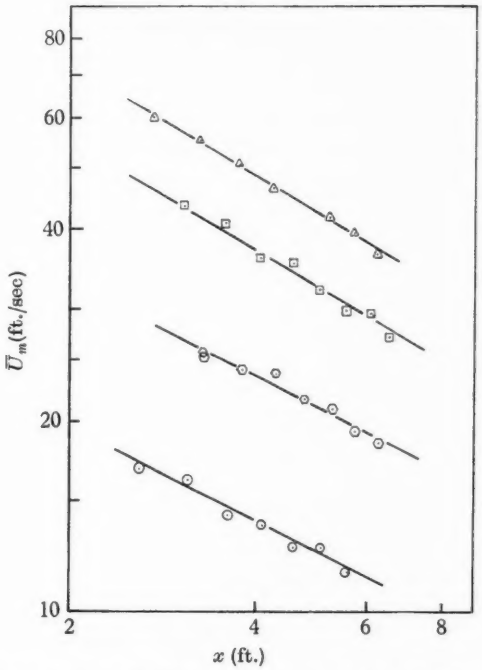

FIGURE 4. Variation of velocity scale: ⊙, $V_0 = 27$ ft./sec.; ⊙, $V_0 = 40$ ft./sec; ⊡, $V_0 = 60$ ft./sec; △, $V_0 = 83$ ft./sec.

V_0 (ft./sec)	x_0 (ft.)	C_1 (ft.$^{1-a}$/sec)	$C_2 = h(R_0)$	a	R_0	$f_1(R_0)$
27	0·60	36·4	0·0851	$-0·50 \pm 0·09$	13,510	4·67
40	1·297	46·8	0·0694	$-0·50 \pm 0·09$	20,100	4·06
60	1·077	88·7	0·0561	$-0·62 \pm 0·08$	30,000	6·90
83	0·748	113·3	0·0607	$-0·60 \pm 0·04$	41,600	5·95
Average value	0·931	—	0·06782	−0·555	—	5·395

TABLE 2

Values for the virtual origin x_0 and the constant C_2 were determined from (22) for each outlet velocity. Then the exponent a and the constant C_1 were obtained from (23) and are given in table 2. These values were obtained by means of a least squares fit of the experimental data and the 95 % confidence intervals were evaluated. A plot of $\overline{U}_m$ versus x is shown in figure 4, for the various outlet velocities.

The inner layer

Some of the velocities measured in the inner layer are presented in figure 5. The plot has logarithmic scales and shows $\overline{U}/U_m$ versus y/δ. It is readily seen that over the whole range of experimental conditions, the data are correlated with the velocity scale $\overline{U}_m$ and the length scale δ. Near the wall, scatter of data was appreciable. This is due to the extremely small distance from the wall (of the order of 0·2 mm). However, from this plot and also a linear plot (not shown), there does not appear to be any systematic variation within the data. It is therefore concluded that the same velocity scale and length scale applies to the whole boundary layer except very close to the wall ($\eta < 0{\cdot}005$).

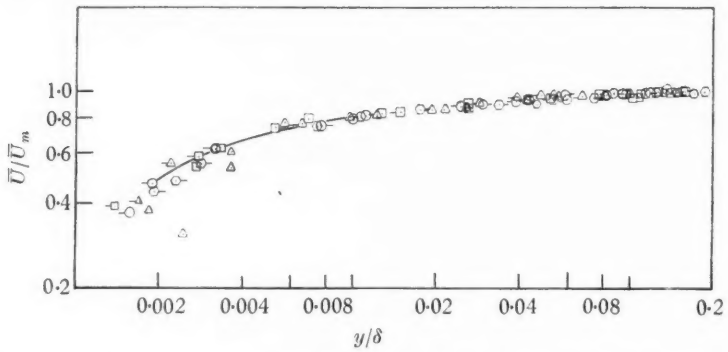

FIGURE 5. The inner layer: the data points shown span the entire outlet velocity range and downstream positions.

V_0	(ft./sec)	x' (ft.)	V_0	(ft./sec)	x' (ft.)
⊙	26·0	2·0	⊔	60·7	5·0
◇	26·2	4·5	△	60·3	5·5
△	34·9	2·5	-⊙	83·4	4·5
□	40·0	2·5	-□	83·1	5·0
⊙-	40·2	3·0	-△	86·1	5·5
◇	40·2	4·5			

The only previous measurements of the velocity distribution in the inner layer of the two-dimensional wall-jet were obtained by Förthmann (1934). He concluded that the velocity profile varied as the classic one-seventh power of the distance from the wall. The present results show the exponent to be $1/(14 \pm 1)$. Nearly 90 % of the inner layer follows this relationship, i.e. for η lying between approximately 0·01 and 0·13. The curve deviates from this relation near the maximum and near the wall.

The one-seventh power law adopted by Förthmann (1934), Glauert (1956), and Sigalla (1958*a*) seems to have been obtained by considering the inner layer of the wall jet to be analogous to the turbulent boundary layer. As a first-order engineering approximation this analogy may be used, if the proper adjustments are made. However, there are certain important dissimilarities between the turbulent boundary layer and the inner layer of the wall-jet. The most important

difference is that of the intermittent nature of the outer part of the turbulent boundary layer. For at least 60% of the thickness of the turbulent boundary layer the flow is characterized by alternate periods of turbulent and non-turbulent flow. Another point of difference lies in the modification of the structure of the inner layer of the wall-jet by the turbulence in the outer layer. Further, the skin-friction coefficient of a turbulent boundary layer varies in a manner different from that of the wall-jet. These factors may lead to serious discrepancies for certain conditions, if the inner layer of the wall-jet is considered to be completely analogous to the turbulent boundary layer.

Dimensional analysis

Since the maximum velocity is a function of the downstream distance from the virtual origin, the outlet velocity, the viscosity and density of the fluid and the width of the nozzle, dimensional analysis shows that

$$\overline{U}_m/V_0 = f(x/d_0, V_0 d_0/\nu). \tag{24}$$

Using (12), (24) may be rewritten as

$$\overline{U}_m/V_0 = (x/d_0)^a f_1(R_0). \tag{25}$$

Hence comparing (12) and (25), it is found that

$$f_1(R_0) = C_1 d_0^a/V_0. \tag{26}$$

The values of $f_1(R_0)$ are listed in table 2 for the several outlet velocities. There is no apparent functional variation with Reynolds number (R_0) of either the virtual origin or the function $f_1(R_0)$. If the average values of $f_1(R_0)$, a, and x_0 are determined for the four outlet conditions, (25) may be written as

$$\overline{U}_m/V_0 = 5{\cdot}395(x'/d_0 + 11{\cdot}2)^{-0{\cdot}555}. \tag{27}$$

Similarly, the boundary-layer thickness is a function of the outlet velocity of the nozzle, the distance from the virtual origin, the viscosity and density of the fluid, and the width of the nozzle. Hence, the dimensionless equation is written

$$\delta/d_0 = h(x/d_0, R_0). \tag{28}$$

From the concept of self-preservation, (28) may be rewritten as

$$\delta/d_0 = (x/d_0)\, h_1(R_0). \tag{29}$$

Therefore comparing (12) and (29),

$$C_2 = h_1(R_0). \tag{30}$$

From the values of C_2 listed in table 2, there does not seem to be any systematic change in $h_1(R_0)$ as the outlet Reynolds number is varied. The average of $h_1(R_0)$ is found to be 0·0678, and the equation (28) is written

$$\delta/d_0 = 0{\cdot}0678(x'/d_0 + 11{\cdot}2). \tag{31}$$

Equations (27) and (31) are approximate formulae and are dependent on the individual system. In particular, the location of the virtual origin is a function of many conditions, such as the free-stream turbulence in the jet, the wall roughness, vibration, sound, and in fact, all the variables which affect the transition

of a laminar flow to a turbulent flow. Hence, each system will have its own specific value for the virtual origin and the virtual origin may vary with the outlet Reynolds number. From these experiments, there is no determinate functional variation of the virtual origin with the outlet Reynolds number, and the average value is used.

If the outlet Reynolds number differs significantly from the range 13,000 to 40,000, the functions $f_1(R_0)$ and $h_1(R_0)$ may change. However these functions at most vary slowly with the outlet Reynolds number.

The angle between the locus of points of the boundary-layer thickness and the plate was computed from (31) and found to be 3·8°. This value may be compared to that of Sigalla (1958*a*) which was 3·7°. Since Sigalla's measurements were in the range of R_0 lying between 20,000 and 50,000, this is not surprising.

Turbulent shear stress

The Reynolds shear stress may be written as

$$\tau_t = -\rho\,\overline{uv}. \tag{32}$$

Also, using (19), (30), the average values of $h_1(R_0)$ and table 2, the dimensionless correlation function becomes

$$g_{12}(\eta) = -0{\cdot}007458\int_{\eta}^{\infty} f^2(\eta)\,d\eta + 0{\cdot}03017 f(\eta)\int_0^{\eta} f(\eta)\,d\eta. \tag{33}$$

This function has been evaluated graphically utilizing the universal velocity function and is shown in figures 6 and 7. Since the contribution to the total shear stress from the viscous terms is very much smaller than the turbulent shear stress (of the order of 3 % very close to the wall), the total shear stress at any η is very closely approximated by (32). A dimensionless shear stress is then defined as

$$c_{f,\eta} = \tau_t / \tfrac{1}{2}\rho \overline{U}_m^2 \tag{34}$$

and hence

$$c_{f,\eta} = -2g_{12}(\eta). \tag{35}$$

From figure 6, it is seen that the correlation function is not equal to zero at η_m which corresponds to the point where the maximum velocity occurs. The two-layer theory becomes suspect since the correlation function $\overline{uv}$ is zero at the outer edge of a turbulent boundary layer and at the centre-line of a symmetrical free jet. These two conditions are not met in the turbulent wall-jet. Further, the shear stress at the point where the maximum velocity occurs is non-zero, at least to the accuracy of the present data. This phenomenon is a consequence of the asymmetrical shape of the velocity distribution.

The Boussinesq exchange coefficient

The dimensionless exchange coefficient or eddy diffusivity has been previously defined in (21). The experimental determination of this quantity involved the graphical differentiation of the universal velocity profile. Also, as previously mentioned, the dimensionless correlation function $g_{12}(\eta)$ was obtained by graphical integration. These numerical techniques, especially the evaluation of the derivative, often produce results which are moderately inaccurate, even when exceptional care is taken with the data.

Values of the exchange coefficient $\tilde{\varepsilon}$, as a function of η, were evaluated as mentioned above, and the smoothed data are plotted in figures 6 and 7 for the outer and inner layers, respectively.

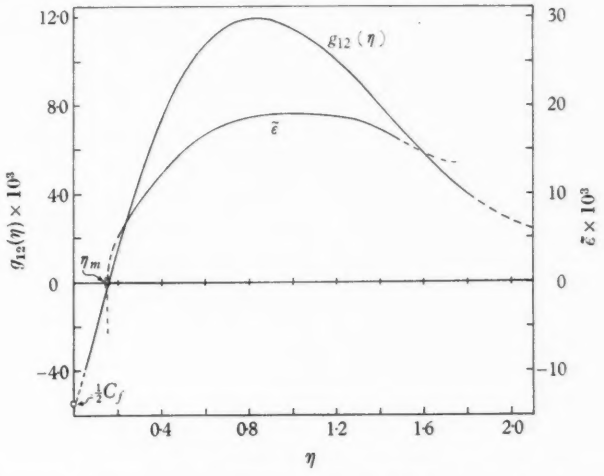

FIGURE 6. Universal correlation function and exchange coefficient.

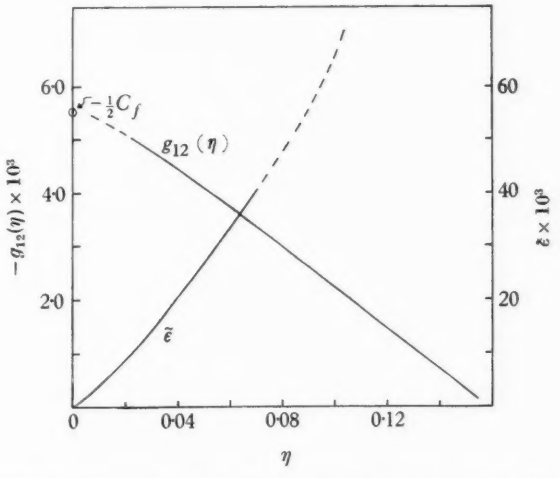

FIGURE 7. Universal correlation function and exchange coefficient for the inner layer.

In the outer layer, the eddy diffusivity shows a similar behaviour to that observed in a two-dimensional free jet. The values of the exchange coefficient are fairly constant in the middle portion and diminish toward the outer edge. However, toward the velocity maximum or where the derivative of the velocity becomes zero, the eddy diffusivity will go to infinity since a finite value is

divided by zero. Also, the eddy diffusivity will change sign near the velocity maximum since $g_{12}(\eta)$ changes sign and hence tends towards minus infinity. This obviously presents some interesting operational difficulties when the concept of an exchange coefficient is employed.

In the inner layer, the functional behaviour of the eddy diffusivity from the wall outward somewhat resembles that of a turbulent boundary layer, except that as η_m is approached, the coefficient tends toward positive infinity. In a turbulent boundary layer or a turbulent pipe flow, the $\overline{uv}$ correlation tends to zero at the outer edge and the centre line, respectively. The form of the exchange coefficient is then indeterminate However, L'Hospital's rule may be applied and it may be shown that the coefficient tends towards a constant if the velocity distribution is parabolic where the derivative goes to zero. For the wall-jet, the $\overline{uv}$ correlation is non-zero, hence the form of $\bar{\epsilon}$ will tend towards infinity.

5. Law of the wall

It has been postulated that near a smooth wall, the velocity profile of an incompressible flow is of the form

$$\overline{U}/U^* = k(yU^*/\nu), \tag{36}$$

where U^* is the friction velocity and is equal to $(\tau_w/\rho)^{\frac{1}{2}}$. Very near the wall, in the laminar sublayer, (36) has the form

$$\overline{U}/U^* = yU^*/\nu. \tag{37}$$

This is obtained from the assumption that the sublayer is so thin that the shear stress is constant across its width and hence the velocity is proportional to y, or conversely this behaviour defines the laminar sublayer.

In the outer layer of a turbulent flow, such as a pipe or boundary layer, the velocity assumes the form

$$(\overline{U}-\overline{U}_m)/U^* = j(y/\delta) \tag{38}$$

which is often called the velocity defect law. Since (36) and (38) overlap, (36) must have the form

$$\frac{\overline{U}}{U^*} = A\log\frac{yU^*}{\nu}+B \tag{39}$$

in the overlap region. The constants A and B have been given by Clauser (1956) as 5·6 and 4·9, respectively, and were obtained from the compilation of data obtained in turbulent boundary layers with and without pressure gradients and in turbulent pipe and channel flows.

The terms in (36) may be rearranged into the forms

$$\frac{\overline{U}}{U^*} = 13{\cdot}41f(\eta) = k\left(\frac{yU^*}{\nu}\right) = k(38{\cdot}5\eta x^{0{\cdot}445}V_0) \tag{40}$$

which are obtained from (15), (6) and (12), and the average values of C_1, C_2 and a. But $f(\eta)$ is a universal function of η and is independent of x and V_0. Therefore, (36) cannot represent the data as long as the universal function applies, i.e. $\overline{U}/\overline{U}_m = f(\eta)$. Now, the velocity defect law may be rewritten as

$$(\overline{U}-\overline{U}_m)/U^* = g(\eta) \tag{41}$$

and from (15)
$$U^* = C_1 x^a \left\{ -C_2(2a+1) \int_0^\infty f^2(\eta)\, d\eta \right\}. \tag{42}$$

Then, defining
$$C_3 = -C_2(2a+1) \int_0^\infty f^2(\eta)\, d\eta, \tag{43}$$

equation (41) may be rewritten

$$\frac{\overline{U}_m[f(\eta)-1]}{C_3 C_1 x^a} = \frac{f(\eta)-1}{C_3} = g(\eta). \tag{44}$$

Hence the velocity defect law is linearly proportional to the present similarity law used to correlate the wall-jet data.

The similarity law correlates the velocity data to the value of η of at least 0·01. If the corresponding value of yU^*/ν is estimated from equation (40), the value is 21·3 for $V_0 = 27$ ft./sec, $x = 5$ ft., and $\nu = 0{\cdot}166 \times 10^{-3}$ ft.^{2}/sec. This value lies well within the logarithmic region of (39), but (39) is not applicable since the similarity law will still correlate the data.

A 'law of the wall' may still apply to the region very near the boundary of the turbulent wall-jet; however, the constants obtained from measurements taken in turbulent boundary layers, pipe and channel flows appear to be inapplicable to the wall-jet flow. Unfortunately the present experimental technique did not allow a study of this inner inner-layer.

6. The skin-friction coefficient

The skin-friction coefficient was evaluated from (17) by graphical integration and using the average value of $h_1(R_0)$. It was found that

$$C_f = 1{\cdot}109 \times 10^{-2}. \tag{45}$$

This is the average value for the present experimental conditions and it is independent of the downstream position and at most a slowly varying function of the outlet Reynolds number, R_0.

This value is in conflict with the work of Sigalla (1958*b*) who has correlated his data in the form
$$C_f = 0{\cdot}0565\,(\overline{U}_m \delta_m/\nu)^{-\frac{1}{4}}. \tag{46}$$

Equation (46) may be rearranged to give

$$C_f = 0{\cdot}0565(R)^{-\frac{1}{4}}(\delta_m/\delta)^{-\frac{1}{4}}. \tag{47}$$

Now since
$$R = \overline{U}_m \delta/\nu = C_1 C_2 x^{a+1}/\nu, \tag{48}$$

$$C_f \propto (x^{0{\cdot}445})^{-\frac{1}{4}} = (x)^{-0{\cdot}111}. \tag{49}$$

This equation gives the variation of the skin-friction coefficient with x according to Sigalla, using the present results for the variation of the length and velocity scales. However, (45) shows that the skin-friction coefficient is constant for the present set of measurements.

In the present work, the Reynolds number of the boundary layer varied from about 22,000 to 106,000. If these extremes are substituted into (46) and δ_m/δ set equal to 0·14, C_f will vary from 0·00743 to 0·00513. These values differ from the present results by about a factor of two. However, it might be mentioned that the absolute value of the skin-friction coefficient that was experimentally

determined is dependent on the quantity $(2a+1)$. Since a is very close to $-\frac{1}{2}$, this quantity can be in error, although the above-mentioned arguments are correct.

The results of Sigalla are based on the analogy of the inner layer of a turbulent wall-jet to that of a turbulent boundary layer. Hence the skin-friction coefficient is considered to have the same functional form as that of the turbulent boundary layer, or the Blasius form. The present results do not indicate that relationship.

Further, the skin-friction coefficients obtained by Sigalla were determined by the method of Preston (1954). It has been shown by Bradshaw (1959) that the Preston tube calibration is not independent of the pressure gradient. Sigalla calibrated his device in a pipe flow, hence in a pressure gradient, and used it in the wall-jet which is without pressure gradient. It is also noted that the primary assumption of the Preston method is that the 'law of the wall' applies to all turbulent flows near a wall. In the previous discussion, it has been shown that this assumption is not true for the turbulent wall-jet.

7. The outer layer

The universal velocity distribution in the outer layer is shown in figure 3. Also shown are curves of $\mathrm{sech}^2\,\eta$ and $\exp[-A(\eta-\eta_m)^2]$. It is seen that a substantial part of the data is not well represented by either functional form. The close fit of the two curves to the data at the outer edge may be purely fortuitous, since no corrections for the effect of intermittency in the outer edge of the wall-jet have been applied.

The velocity distribution for the plane wall-jet has been determined theoretically by Glauert (1956) with the assumptions that the eddy diffusivity varies as $\overline{U}^6$ in the inner layer, and is a constant in the outer layer. The x-wise variation of similarity parameters was considered to be the same for both layers. For the outer layer, a solution of the equations of motion was obtained which deviated only slightly from the square of the hyperbolic secant and the deviation probably lies well within the limits of experimental error. As a matter of fact, the solution of the equations of motion of a plane, turbulent, free jet give this variation, if it is assumed that the exchange coefficient is constant across the flow. It becomes apparent then why the true velocity distribution differs from Glauert's work, by referring to figure 6. It is seen that the dimensionless exchange coefficient deviates markedly from its constant value near the maximum point.

8. Conclusions

All mean velocity data, taken over a three and one-half fold variation in the downstream dimension and a threefold range of nozzle velocities, were found to be reduced to a single universal curve with the length scale δ and the velocity scale $\overline{U}_m$. The correlation seemed to apply over the entire measured range, at least to a minimum value of η equal to 0·005. Further, it was shown with certain assumptions that the length scale must vary as x, the distance downstream from the virtual origin, and the velocity scale must vary as x^a, where a was found equal to $-0{\cdot}555$. The assumptions were that the mean velocity and the statistical

quantities $\overline{u^2}$, $\overline{v^2}$, and $\overline{uv}$ were self-preserving with the same scales, the viscous stresses were negligibly small, and the boundary-layer approximations were applicable.

Empirical expressions were developed to correlate the length and velocity scales with the outlet velocity and widths of the nozzle, and the physical properties of the fluid.

The $\overline{uv}$ correlation as a function of the distance from the wall was computed from the mean velocity data assuming that it had self-preserving characteristics. Since there is a direct relation between the correlation function and the turbulent shear stress, which is practically equivalent to the total shear stress (viscous stresses are negligible), the shear-stress distribution in the turbulent boundary layer was determined. Of interest was the non-zero value of the shear stress or correlation function at the velocity maximum, which is due to the unsymmetrical shape of the velocity distribution. As a consequence, the measured values of the exchange coefficient or eddy diffusivity exhibit peculiar behaviour at this point, since a finite quantity is divided by a quantity which tends to zero in the limit.

It is further concluded that the 'law of the wall' is not applicable to the turbulent wall-jet in the form that was obtained by experimentation in turbulent boundary layers, and turbulent pipe and channel flows. Also, the power-law representation commonly used for turbulent boundary layers to describe the mean velocity is appreciably modified in the wall-jet. Hence, present values of skin-friction coefficients differ from previous work, where the inner layer of the wall-jet was considered to be analogous to a turbulent boundary layer. The inner layer's structure is modified from that of turbulent boundary layer by the presence of the outer layer.

In the outer layer of the wall-jet and near the position of maximum velocity, there is a considerable difference in the velocity profile from that of a free jet or a mixing layer. This is caused primarily by the effect of the inner layer on the outer layer. Further, the square of the hyperbolic secant will not represent the velocity distribution since the value of the eddy viscosity is not constant across the flow, and approaches infinity at the maximum.

REFERENCES

Bakke, P. 1957 *J. Fluid Mech.* **2**, 467.

Bradshaw, P. 1959 *Aero. Res. Coun. Lond.* Rep. no. 20, 889; F.M. 2799.

Clauser, F. H. 1956 Article in *Advances in Applied Mechanics*, **3**. New York: Academic Press Inc.

Cosart, W. P. 1960 M.S. thesis, Stanford Univ., Stanford, Calif.

Förthmann, E. 1934 *Ingenieur Archiv.* **1**, trans.: 1936 *N.A.C.A.* T.M. 789.

Glauert, M. B. 1956 *J. Fluid Mech.* **1**, 625.

Poreth, M. & Cermak, J. E. 1959 *Sixth Midwestern Conference of Fluid Mechanics.* University of Texas, Austin, Texas.

Preston, J. H. 1954 *J. Roy. Aero. Soc.* **58**, 109.

Sigalla, A. 1958*a* *Aircr. Engng.* **30**, 131.

Sigalla, A. 1958*b* *J. Roy. Aero. Soc.* **62**, 873.

Zerbe, J. & Selna, J. 1946 *N.A.C.A.* T.N. 1070.

On the stability of heterogeneous shear flows

By JOHN W. MILES

Department of Engineering and Institute of Geophysics, University of California, Los Angeles

(Received 30 August 1960 and in revised form 21 November 1960)

Small perturbations of a parallel shear flow $U(y)$ in an inviscid, incompressible fluid of variable density $\rho_0(y)$ are considered. It is deduced that dynamic instability of statically stable flows ($\rho_0'(y) < 0$) cannot be other than exponential, in consequence of which it suffices to consider spatially periodic, travelling waves. The general solution of the resulting differential equation is considered in some detail, with special emphasis on the Reynolds stress that transfers energy from the mean flow to the travelling wave. It is proved (as originally conjectured by G. I. Taylor) that sufficient conditions for stability are $U'(y) \neq 0$ and $J(y) > \frac{1}{4}$ throughout the flow, where $J(y) = -g\rho_0'(y)/\rho_0(y)U'^2(y)$ is the local Richardson number. It also is pointed out that the kinetic energy of a normal mode in an ideal fluid may be infinite if $0 < J(y_c) < \frac{1}{4}$, where $U(y_c)$ is the wave speed.

1. Introduction

We shall consider here the stability of a heterogeneous (or stratified) shear flow—namely a parallel shear flow $U(y)$ in an inviscid, non-heat-conducting, incompressible fluid of density $\rho_0(y)$. The principal measure of stability, in so far as the buoyancy effects of the density gradient override its inertial effects, is the Richardson number

$$J(y) = \beta g(dU/dy)^{-2}, \tag{1.1}$$

where

$$\beta(y) = -d/dy \log \rho_0(y) = -\rho_0'(y)/\rho_0(y) \tag{1.2}$$

is a measure of the static stability of the density stratification ($\beta < 0$ implies static instability). The inertial effects of density gradient are measured by βl, where l is a characteristic length; neglecting these effects, as in meteorological and oceanographic problems, implies $|\beta|l \ll 1$.

Analytical studies of heterogeneous shear flow, although finding antecedents in the work of Kelvin and Rayleigh on hydrodynamic stability, may be dated from G. I. Taylor's Adams Prize essay of 1915, which was published concurrently with a closely related investigation by Goldstein (1931). These two papers, dealing primarily with specific flow configurations (see below), were followed closely by Synge's (1933) study of the general boundary-value problem. This important paper appears to have escaped the notice of many later workers,† who have rediscovered several of Synge's results. Subsequent work has been largely in the hands of meteorologists (often in difficult-to-obtain sources),

† Including the present writer, who is indebted to Dr Drazin for bringing Synge's work to his attention.

with special reference to the problems of atmospheric stability and mountain-lee-wave formation (see Hølmboe (1957) for a survey of the latter problem).

The primary goal of the present investigation is a proof that $U'(y) \neq 0$ and $J(y) > \frac{1}{4}$ are sufficient conditions for the stability of a heterogeneous shear flow (Theorem X in §5), as originally conjectured by Taylor (1915/31). We shall follow the usual, normal-mode approach on the ground that dynamic instability of a statically stable ($\beta > 0$) shear flow of an ideal fluid cannot be other than exponential. This is not to say that the normal-mode approach is completely adequate for an ideal fluid, however, and we shall call attention to the striking fact, apparently overlooked by previous workers, that the energies of those modes that are comprised by the neutral-stability boundary *may* be infinite. We also remark that none of the existing investigations of *continuous* shear and density profiles has proved that unstable modes exist and are contiguous to the loci of neutral modes that are asserted to form the stability boundaries. Such a proof is much to be desired, especially in consequence of the aforementioned possibility of infinite energy for the neutral modes. (The energy of an unstable mode is found to be finite at any fixed time, although tending to infinity exponentially in time.)

Throughout our investigation, we shall place special emphasis on the Reynolds stress that transfers energy from the mean flow to the disturbance, following closely the corresponding treatment of homogeneous shear flow (see Lin 1955: this reference will be denoted subsequently by L, followed by the appropriate section or equation number). This is, in some instances, less direct than the application of standard oscillation theorems to the boundary-value problem (as in Synge's paper), but it does throw additional light on the problem and may point the way to further progress in the investigation of unstable modes.

Before proceeding with the mathematical development, we shall outline the known results for a few, representative configurations, assuming $|\beta| l \ll 1$ except as noted.

Taylor (1931) considered a semi-infinite flow, above a horizontal wall, with U' and β constant. He concluded that only neutral waves could exist for $J > \frac{1}{4}$ and that no (harmonic) waves could exist for $0 < J < \frac{1}{4}$. These results were clarified and extended by Eliassen, Høiland & Riis (1953), who considered flow between two parallel walls with U' and β constant. They attacked the initial-value problem and showed that a disturbance originating from arbitrary initial conditions would behave asymptotically like $t^{\frac{1}{2}(\nu-1)}$, $\nu = (1-4J)^{\frac{1}{2}}$, for $-\frac{3}{4} < J < \frac{1}{4}$ (and hence be unstable for $J < 0$) but would be exponentially unstable only for $J < -\frac{3}{4}$; for the semi-infinite case, this asymptotic behaviour holds for $-2 < J < \frac{1}{4}$, with exponential instability for $J < -2$. The initial-value problem for the semi-infinite case also has been solved by Case (1960). His analysis is less general than that of Eliassen *et al.* in considering only $J > 0$, but more general in allowing for the inertial effects of density variation.

Goldstein (1931) considered an imbedded shear layer of thickness $2h$, with both U' and β constant in $|y| < h$ and vanishing in $|y| > h$. He concluded that harmonic perturbations would be stable for $J > \frac{1}{4}$ and unstable for all wavelengths for $0 < J < \frac{1}{4}$.

Drazin (1958*a*) has considered a more realistic model for an imbedded shear layer, with $U(y) = U_0' h \tanh(y/h)$ and $\beta = \text{const}$. He too concluded that harmonic perturbations would be stable for $J_0 = (\beta g/U_0'^2) < \frac{1}{4}$, but predicted instability only for a finite range of wavelengths for $0 < J_0 < \frac{1}{4}$. Drazin concluded that his agreement with Goldstein on the value of the critical Richardson number, namely $J = \frac{1}{4}$, was coincidental (that it is not coincidental follows from Theorem X below, together with the fact that $J(y) \geqslant J_0$ in Drazin's model). Menkes (1959, 1960) has extended Drazin's analysis by including the inertial effects of density variation, which are found to be stabilizing. Hølmboe (1960) has modified Drazin's model by letting $\beta = \beta_0 \operatorname{sech}^2(y/h)$. This leads to the neutral curve $J_0 = \alpha(1-\alpha)$ in place of Drazin's result $J_0 = \alpha^2(1-\alpha^2)$, where $\alpha = kh$ and k is the wave-number.

Neither Drazin's model nor Hølmboe's modification thereof yields instability for $\alpha > 1$, in striking disagreement with Goldstein's result for $0 < J < \frac{1}{4}$. It seems clear that the discontinuities in U' and β at $y = \pm h$ invalidate Goldstein's result for sufficiently small wavelengths (large α), but it is not clear why his model should predict instability for very long wavelengths (small α). Indeed, we should expect the result for sufficiently long wavelengths to resemble that for Kelvin–Helmholtz instability of a vortex sheet. Assuming a small discontinuity $\Delta\rho_0$ ($\ll \rho_0$) in density and a discontinuity ΔU in velocity, the latter model predicts stability for (Lamb 1932, §232)

$$k < 2g\Delta\rho_0/\rho_0(\Delta U)^2, \tag{1.3}$$

or

$$\alpha = kh < g\left(\frac{\Delta\rho_0}{2h\rho_0}\right)\left(\frac{2h}{\Delta U}\right)^2 = J. \tag{1.4}$$

Curiously enough, Goldstein did obtain (1.4), as $\alpha \to 0$, for the somewhat cruder model having U' constant in $|y| < h$ and vanishing in $|y| > h$ and density constant except for equal discontinuities at $y = \pm h$ (in contrast to the continuous density profile for the model described in the penultimate paragraph). Drazin's model predicts stability for $\alpha < J_0^{\frac{1}{2}}$ as $\alpha \to 0$, but Hølmboe's modification leads to (1.4). The anomalous character of Drazin's result evidently must be charged to the evanescence of his density profile as $y \to \infty$.†

2. Equations of motion

The basic equations of motion for our model are the Euler equation

$$\mathbf{q}_t + (\mathbf{q}\cdot\nabla)\mathbf{q} = -\rho^{-1}\nabla p - g\nabla y, \tag{2.1}$$

the condition of incompressibility

$$\rho_t + (\mathbf{q}\cdot\nabla)\rho = 0, \tag{2.2}$$

and the equation of continuity

$$\nabla\cdot\mathbf{q} = 0, \tag{2.3}$$

where $\mathbf{q}$, p and ρ denote vector velocity, pressure and density. We shall consider

† Drazin (private communication) has pointed out that the limiting forms $\alpha \sim J_0^{\frac{1}{2}}$ and $\alpha \sim J_0$, $\alpha \to 0$, for the neutral stability boundaries in his original model and Holmboe's modification thereof may be deduced from dimensional considerations.

only small, two-dimensional disturbances, noting that three-dimensional disturbances of the same wavelength generally are more stable (Yih 1955). Let

$$\mathbf{q} = (U+u, v), \quad \rho = \rho_0 - \rho_0' \eta, \tag{2.4 a, b}$$

where u and v denote the x- and y-components of the perturbation velocity and η denotes the vertical displacement of a particle from its initial position.† Introducing (2.4a, b) in (2.1)–(2.3) and neglecting terms of second order in u, v and η, we obtain the linearized equations

$$\rho_0\left(\frac{Du}{Dt} + U'v\right) = -(p-p_0)_x, \tag{2.5a}$$

$$\rho_0\left(\frac{Dv}{Dt} + \beta g \eta\right) = -(p-p_0)_y, \tag{2.5b}$$

$$\frac{D\eta}{Dt} = v, \tag{2.6}$$

and

$$u_x + v_y = 0, \tag{2.7}$$

where

$$\frac{D}{Dt} = \frac{\partial}{\partial t} + U\frac{\partial}{\partial x},$$

β is defined by (1.2), subscripts denote partial differentiation, and primes denote differentiation with respect to y.

Taking the scalar product of (2.5a, b) with (u, v), substituting v from (2.6) in the product $\beta g v \eta$, multiplying (2.7) by $p-p_0$, adding the results, and integrating over the domain under consideration, say (x_1, x_2) and (y_1, y_2), we obtain the energy-transfer equation

$$\int_{x_1}^{x_2}\int_{y_1}^{y_2} \rho_0 \left[\frac{1}{2}\frac{D}{Dt}(u^2+v^2+\beta g\eta^2) + U'uv\right] dx\,dy$$
$$= -\int_{x_1}^{x_2}\int_{y_1}^{y_2} \{[(p-p_0)u]_x + [(p-p_0)v]_y\}\, dx\,dy. \tag{2.8}$$

Denoting the x-integrals by a bar and assuming either that the disturbance is periodic in x (in which case the bar may be interpreted as implying an average over one wavelength) or that y and v vanish at $x = \pm\infty$ (in which case the bar must be interpreted as implying integration from $x = -\infty$ to $x = +\infty$), we may reduce (2.8) to (cf. Reynolds 1895)

$$\frac{\partial}{\partial t}(T+V) = P+Q, \tag{2.9}$$

where

$$T = \frac{1}{2}\int_{y_1}^{y_2} \rho_0 \overline{(u^2+v^2)}\, dy \tag{2.10}$$

denotes the kinetic energy,

$$V = \tfrac{1}{2} g \int_{y_1}^{y_2} \beta \rho_0 \overline{\eta^2} dy \tag{2.11}$$

† Equation (2.4b) expresses the fact that a particle at the instantaneous elevation y has the density corresponding to its original elevation $y-\eta$. An alternative, and in some ways more fundamental, approach would be to introduce η as the displacement of a streamline in intrinsic co-ordinates *prior* to linearization (cf. Miles, 1959).

the potential energy,

$$P = [-\overline{(p-p_0)v}]_{y_1}^{y_2} \tag{2.12}$$

the rate at which work is done on the perturbation flow by the external pressures at the boundaries y_1 and y_2, and

$$Q = \int_{y_1}^{y_2} \tau U' \, dy \tag{2.13}$$

the rate at which energy is transferred from the mean flow to the perturbation flow by the Reynolds stress

$$\tau = -\rho_0 \overline{uv}. \tag{2.14}$$

We shall restrict the subsequent development to spatially periodic normal modes (see (3.1) below) for which $\beta(y) > 0$. We may regard such motions, in so far as they exist and are either neutrally stable or exponentially unstable, as the dominant components of an asymptotic approximation to the solution of appropriate initial-value problems provided that unstable motions growing more slowly than an exponential cannot exist.† A straightforward extension of the analyses of Eliassen *et al.* (1953) and Case (1960) leads to the conclusion that:

I. The non-exponential growth of a small disturbance in a heterogeneous shear flow cannot be more rapid than $t^{\frac{1}{2}(\nu_m - 1)}$, where ν_m is the maximum value of $[1-4J(y)]^{\frac{1}{2}}$.

It follows that:

II. Dynamic instability of a statically stable, heterogeneous shear flow cannot be other than exponential.

We emphasize, however, that statically unstable flows ($\beta < 0$ in any finite y-interval) may, and generally will, exhibit dynamic instabilities of algebraic growth, even though all spatially periodic wave motions are stable. This last statement is amply illustrated by the results of Eliassen *et al.* as described above.

3. Periodic motions

We now assume the spatially periodic wave motion

$$\eta(x, y, t) = F(y)\, e^{ik(x-ct)}, \tag{3.1}$$

where k is real, but c may be complex. In accordance with the usual convention, we imply that the imaginary part of the right-hand side of (3.1) is to be discarded in the final reckoning; alternatively, we may regard $F(y; k, kc)$ as a double Fourier transform with respect to x and t, the corresponding spectral variables being k and kc. Substituting (3.1) in (2.5)–(2.7), we obtain

$$u = -[(U-c)\eta]', \quad v = ik(U-c)\eta, \quad p - p_0 = \rho_0 (U-c)^2 \eta', \tag{3.2a, b, c}$$

and

$$[\rho_0 (U-c)^2 F']' + \rho_0 [\beta g - k^2 (U-c)^2] F = 0. \tag{3.3}$$

The differential equation (3.3) is especially convenient in the study of non-singular oscillations, but we may proceed more directly to the structure of the

† The importance of aperiodic motions in hydrodynamic stability was recognized and developed by Orr (1907), who solved the initial-value problem for small disturbances of an inviscid, plane Couette flow.

general solution by eliminating the first derivative of the dependent variable through the transformation

$$X(y) = \rho_0^{\frac{1}{2}}(y)[U(y)-c]F(y). \tag{3.4}$$

Substituting (3.4) in (3.3), we may place the resulting differential equation in the standard form

$$X''(y) + h(y)X(y) = 0, \tag{3.5}$$

where $$h = \beta g(U-c)^{-2} - \rho_0^{-1}(\rho_0 U')'(U-c)^{-1} - (k^2 + \tfrac{1}{4}\beta^2 - \tfrac{1}{2}\beta'). \tag{3.6}$$

We note that the stream function is given by

$$\psi(x,y,t) = \rho_0^{-\frac{1}{2}}(y)X(y)e^{ik(x-ct)}, \tag{3.7}$$

and that $X(y)e^{ik(x-ct)}$ may be regarded as a stream function if the inertial effects of density variation are neglected, in which case (3.5) reduces to (the usual meteorological approximation)

$$X''(y) + [\beta g(U-c)^{-2} - U''(U-c)^{-1} - k^2]X = 0. \tag{3.8}$$

Following Synge (1933), we also may reduce the differential equation for the stream function to standard form through the transformation

$$z = \int_0^y \frac{dy}{\rho_0(y)}, \tag{3.9}$$

under which (3.5) goes over to

$$\frac{d^2\psi}{dz^2} + \rho_0^2\left[\frac{\beta g}{(U-c)^2} - \frac{(\rho_0 U')'}{\rho_0(U-c)} - k^2\right]\psi = 0. \tag{3.10}$$

The point $y = y_c$, defined by

$$U(y_c) = c, \quad U_c' = U'(y_c) \neq 0, \tag{3.11 a, b}$$

and designated as the *critical layer* for the shear flow, is a regular singularity for each of the foregoing differential equations.† The exponents of this singularity are $\frac{1}{2}(1 \pm \nu)$, where

$$\nu = i\mu = (1-4J_c)^{\frac{1}{2}}, \tag{3.12}$$

and J_c is the Richardson number of (1.1) evaluated at $y = y_c$. Assuming that ν is not an integer, and that $U(y)$ and $\rho_0(y)$ may be continued analytically into the complex neighbourhood of $y = y_c$, we may apply the method of Frobenius to obtain two, linearly independent solutions to (3.5) in the form

$$X_\pm(y) = (y-y_c)^{\frac{1}{2}(1\pm\nu)}w_\pm(y), \tag{3.13}$$

where $w_\pm$ are analytic functions of y in the neighbourhood of $y = y_c$ having the form

$$w_\pm = 1 + \left[(1+J)\frac{(\rho_0 U')'}{\rho_0 U'} - J\frac{\rho_0''}{\rho_0'}\right]_c \frac{(y-y_c)}{1\pm\nu} + \ldots. \tag{3.14}$$

† The assumption $U_c' \neq 0$ implies a simple zero of $U-c$ at $y = y_c$. The singularity would be irregular if $U_c' = 0$. We shall not consider this possibility, but it clearly may be of considerable importance for jet-type flows. Indeed, Drazin & Howard (personal communication) have found that the most important long-wave instabilities for jet-type shear flows are those for which $c = U_{\max}$, so that $U_c' = 0$.

The Wronskian of these solutions is

$$W\{X_+, X_-\} = X_+X'_- - X'_+X_- = -\nu. \tag{3.15}$$

The solution X_- degenerates if ν is an integer and, except under very special conditions (see below), must be modified to include a component proportional to $X_+(y)\log(y-y_c)$. The only statically stable flow in this category is that for which $J_c = 0$ ($\nu = 1$), and the solutions then are essentially similar to those for homogeneous shear flow. We shall not consider them in any detail here, but we remark that the logarithmic component is proportional to the discontinuity in Reynolds stress at $y = y_c$, as calculated in (5.13) and (5.14) below. The singularity at $y = y_c$ is only apparent if this discontinuity vanishes, and both solutions to the differential equation then are regular.

We may regard the singularity at $y = y_c$ as a consequence of either (*a*) our assumption of the periodic wave motion of (3.1), or (*b*) our neglect of diffusion effects; the branch cut at $y = y_c$ can be determined only after either (*a*) posing an initial-value problem and then determining its asymptotic solution as $t \to \infty$, or (*b*) introducing the dominant diffusion effects and then determining the asymptotic solution as the diffusion parameters tend to zero.† The former approach (cf. Eliassen *et al.* 1953 and Case 1960) implies that the path of integration for the inverse transform in the kc spectral plane must pass above ($kc_i > 0$) the branch point at $kc = kU(y)$ and hence that

$$(U-c) = (c-U)\,e^{\pm i\pi}, \quad k \gtrless 0. \tag{3.16}$$

The latter approach usually has been adopted in considering the stability of homogeneous shear flow (see L 3.4, 3.6, 8.3–8.9), but in the present instance it is necessary to introduce both viscosity and heat conduction to resolve the question. The linearized equations of motion then constitute a system of the sixth order (cf. L 5.2 and 5.3, adding the buoyancy force $(\rho-\rho_0)g$ to the y-component of the perturbation pressure gradient in L 5.2.2 and L(5.3.9)). We shall not present these equations here, but we remark that a boundary-layer analysis in the neighbourhood of $y = y_c$ leads to the conclusion that the order of magnitude of the actual thickness of the critical layer is given by (cf. L 8.8)

$$\delta = O[(\mu/k\rho_0 U')_c^{\frac{1}{3}}(\kappa/\mu R)^{\frac{1}{6}}] \tag{3.17a}$$

$$= O[Re^{-\frac{1}{3}}Pr^{-\frac{1}{6}}(1-\gamma^{-1})^{-\frac{1}{6}}], \tag{3.17b}$$

where μ denotes the viscosity, κ the heat conductivity, R the universal gas constant, Re a Reynolds number based on wavelength, Pr the Prandtl number, and γ the specific heat ratio.

Much of the discussion of the next two sections will be concerned with neutral wave motions, for which $c_i = 0$. We designate such motions as singular or nonsingular as y_c does or does not lie in the open interval (y_1, y_2). In the former case

† We also might regard the singularity at $y = y_c$ as a consequence of linearization, but it is by no means clear that the behaviour of the linear solution in the neighbourhood of $y = y_c$ could be resolved by a consideration of the non-linear, inviscid periodic flow.

we imply that the limit $kc_i = 0$ must be approached through positive values, and (3.16) implies the transition relations (note that $w_+^* = w_-$ for $J_c > \frac{1}{4}$ and y real)

$$X_\pm^*(y) = X_\pm(y) e^{i\pi(1\pm\nu)S(y-y_c)} \quad (J_c < \tfrac{1}{4}), \tag{3.18a}$$

and

$$X_\pm^*(y) = X_\mp(y) e^{\pi(i\pm\mu)S(y-y_c)} \quad (J_c > \tfrac{1}{4}), \tag{3.18b}$$

where the asterisk denotes the complex conjugate and

$$S = 0, \quad y > y_c \tag{3.19a}$$

$$= \pm 1, \quad kU_c' \gtrless 0 \quad (y < y_c). \tag{3.19b}$$

We emphasize that (3.19*a*, *b*) are valid only for real y.

We conclude this discussion by remarking that the singularity in X_- at $y = y_c$ for $0 < J_c < \frac{1}{4}$ (but not for $J_c = 0$) renders both the kinetic and the potential energies of (2.10) and (2.11) infinite for singular neutral modes. A specific example is provided by Drazin's results for singular neutral modes in the range $\frac{1}{2} < \alpha^2 < 1$, where his solution is essentially X_-; for $0 < \alpha^2 < \frac{1}{2}$, on the other hand, his solution is X_+, and the energy is bounded. We observe that these infinite energies are a consequence of our too-idealized model and could be removed by including diffusion effects. It also seems likely that these modes would contribute only a finite amount of energy to the solution of an initial-value problem for an ideal fluid provided that the Fourier transform of the initial disturbance were continuous in k.

4. The eigenvalue problem

We shall consider the eigenvalue problem presented by the assumption of the spatially periodic wave motion (3.1) subject to the boundary conditions

$$\eta_1 = \eta_2 = 0 \quad \text{or} \quad F_1 = F_2 = 0, \tag{4.1a, b}$$

where the subscripts 1 and 2 imply evaluation at $y = y_1$ and $y = y_2$. Many of the subsequent results held for more general boundary conditions, but those of (4.1) hold for the most important cases of horizontal walls at finite values of y_1 or y_2 and/or null conditions at infinity.

Let l be a characteristic length, c_* a characteristic velocity, and β_* a characteristic measure of β (we need not introduce an explicit scale for the density ρ_0 in virtue of the invariance of the eigenvalue problem with respect to changes in this scale). We then may pose the secular equation for our eigenvalue problem in the form

$$\Delta(c/c_*, \alpha, \lambda, \sigma) = 0, \tag{4.2}$$

where

$$\alpha = kl, \quad \lambda = \beta_* g l^2/c_*^2 \equiv J_*, \quad \sigma = \beta_* l \tag{4.3a, b, c}$$

are dimensionless, real parameters but $c = c_r + ic_i$ may be complex. We may assume $\alpha > 0$ without loss of generality. We define a *neutral surface* as a locus of eigenvalues for which $c_i = 0$ in a $(c_r, \alpha, \lambda, \sigma)$-space. Such a surface will be a *stability boundary* if and only if there exist contiguous eigenvalues for which $c_i > 0$ (unstable wave motions).

We shall assume that $U(y)$ and $\rho_0(y)$ are regular functions of y in (y_1, y_2), that these functions may be continued analytically into a neighbourhood of

(y_1, y_2) that includes the singular point $y = y_c$, and that neither $U'(y)$ nor $\beta(y)$ vanishes in this neighbourhood; on the other hand, we do not exclude the end-points y_1 and y_2 as possible singularities of the differential equation. These restrictions, especially the requirements $U' \neq 0$ and $\beta \neq 0$, exclude interesting problems (although several of the following theorems, e.g. V, obviously can be proved under weaker restrictions), but they guarantee that c_i is a continuous function of the remaining parameters, and hence that the trajectory of a complex eigenvalue must terminate on a stability boundary.

We first remark that

$$F_\pm \sim (U-c)^{-1} X_\pm \sim (y-y_c)^{\frac{1}{2}(-1\pm\nu)} \quad (y \to y_c), \tag{4.4}$$

in consequence of which the boundary conditions (4.1*b*) imply that:

III. The phase velocity c cannot be equal to U_1 or U_2.

We observe that this result could not have been inferred from the weaker boundary conditions $v_1 = v_2 = 0$, since $v \sim (U-c)F \sim (y-y_c)^{\frac{1}{2}(1\pm\nu)}$. This paradox is a consequence of linearization, since the approximation $v = ik(U-c)\eta$ is not uniformly valid in the neighbourhood of $U = c$. If $\rho_0'(y_{1,2}) \neq 0$, we may regard the boundary condition $\eta_{1,2} = 0$ as a direct consequence of the physical requirement that a particle at $y = y_{1,2}$ cannot have a density corresponding to an initial position in $y \lesseqgtr y_{1,2}$ (cf. (2.4*b*)); but if $\rho_0'(y_{1,2}) = 0$ the corresponding boundary condition, and hence III, becomes ambiguous as $c \to U_{1,2}$.

Now let us suppose that $c_i > 0$, so that $U(y) \neq c$ in (y_1, y_2) and $F(y)$ is regular there. Then, multiplying both sides of (3.3) by the complex conjugate F^*, integrating between y_1 and y_2, integrating $[\rho_0(U-c)^2 F']' F^*$ by parts, and invoking the boundary conditions (4.1*b*), we obtain (cf. L 8.2)

$$g\int_{y_1}^{y_2} \rho_0 \beta |F|^2 \, dy = \int_{y_1}^{y_2} \rho_0 (U-c)^2 (|F'|^2 + k^2|F|^2)\, dy. \tag{4.5}$$

Equating the real parts of (4.5), we infer that:

IV. Non-singular neutral modes cannot exist if $\beta(y) < 0$ in (y_1, y_2).

Taking the imaginary part of (4.5), we obtain

$$c_i \int_{y_1}^{y_2} (U-c_r)(|F'|^2 + k^2|F|^2)\, dy = 0, \tag{4.6}$$

from which we infer that:

V. The phase velocity c_r for unstable modes ($c_i > 0$) must lie between the maximum and minimum values of $U(y)$ in $[y_1, y_2]$. This implies

$$U_1 < c_r < U_2 \quad \text{if} \quad U' \neq 0 \quad \text{in} \quad (y_1, y_2).$$

We emphasize that this last result is valid for any finite, positive value of c_i. If $c_i \to 0^+$ it also may be inferred from VII below, subject to the restriction that β and $(\rho_0 U')'$ do not vanish simultaneously. This more restricted form of V was proved originally by Synge (1933) and, independently, by Yih (1957). Drazin (1958*b*) proved V as stated above after neglecting the inertial effects of the density gradient.

A direct corollary of III and V, together with the restrictions guaranteeing the continuity of c_i, is:

VI. A stability boundary consists of singular neutral modes—i.e. modes for which $c_i = 0$ and $U(y) = c_r$ in (y_1, y_2).

We remark that the converse of VI is not necessarily true, for we have not demonstrated that unstable modes are contiguous to all singular neutral modes. We also remark that if III were not applicable (as it would not be for homogeneous shear flow), we would have to admit $c = U_1$ and $c = U_2$ as possible end-points for the trajectories of complex eigenvalues and replace (y_1, y_2) by $[y_1, y_2]$ in VI.

5. The Reynolds stress

We may deduce further important results for periodic motions in general, and for the eigenvalue problem of the preceding section in particular, from a consideration of the Reynolds stress defined by (2.14). Expressing u and v in terms of X with the aid of (3.1), (3.2a, b) and (3.4), and substituting the results in (2.14), we obtain (for real y)

$$\tau = \tfrac{1}{2}k(X'X^*)_i e^{2kc_i t}, \tag{5.1}$$

where the subscript i implies the imaginary part. Differentiating (5.1) with respect to y and substituting X'' from (3.5), we obtain

$$\frac{\partial \tau}{\partial y} = \tfrac{1}{2}k(X''X^*)_i e^{2kc_i t} \tag{5.2a}$$

$$= -\tfrac{1}{2}kh_i|X|^2 e^{2kc_i t} \tag{5.2b}$$

$$= -k^{-1}h_i\rho_0\overline{v^2}. \tag{5.2c}$$

Referring to (3.6), we obtain

$$h_i = c_i\left[\frac{2\beta g(U-c_r)}{|U-c|^4} - \frac{(\rho_0 U')'}{\rho_0|U-c|^2}\right]. \tag{5.3}$$

The boundary conditions (4.1) imply

$$\tau_1 = \tau_2 = 0. \tag{5.4}$$

First, let us suppose that $c_i \neq 0$; then, since $\partial\tau/\partial y$ cannot vanish identically, the Reynolds stress must have an extremum and h_i must change sign in (y_1, y_2). This result, which constitutes the extension to heterogeneous shear flows of Rayleigh's theorem on the necessity of a flex ($U'' = 0$) for an unstable mode in a homogeneous shear flow, also follows from the well-known oscillation theorem (Ince 1944, ch. XXI) for the differential equation (3.5) subject to the boundary conditions (5.4). It was proved originally by Synge (1933) and, independently, by Yih (1957) and Drazin (1958b). Synge used it to prove that complex values of c must lie on one of the family of circles (with y as the family parameter)

$$\rho_0^{-1}(\rho_0 U')'[(c_r-U)^2+c_i^2] + 2\beta g(c_r-U) = 0, \tag{5.5}$$

provided that $(\rho_0 U')'$ and β do not vanish simultaneously, and hence that

$$|c_i| \leqslant \max.|\beta g\rho_0/(\rho_0 U')'|. \tag{5.6}$$

This result also was given by Yih (1957) except for an erroneous factor of 2.

Synge also proved that complex values of c must be confined to the interiors of the looped curves

$$\tfrac{1}{2}\pi^2\left[\rho_0\int_{y_1}^{y_2}\rho_0^{-1}dy\right]^{-2}[(c_r-U)^2+c_i^2]^2-\rho_0^{-1}(\rho_0U')'(c_r-U)[(c_r-U)^2+c_i^2]$$
$$-\beta g[(c_r-U)^2-c_i^2]=0, \quad (5.7)$$

which overlap with the circles of (5.5) in a region that cuts the real axis at $c_r = U_{\min}$ and $c_r = U_{\max}$. This region excludes $c_r = U_{\min}$ and includes $c_r = U_{\max}$ for $c_i > 0$, so that Synge's results confine the minimum value of c_r more severely and its maximum value less severely than V above.

We shall restrict the subsequent discussion of this section to neutral wave motions ($c_i = 0$).† The condition $c_i = 0$ implies, through (5.2) and (5.3), that the Reynolds stress τ must be constant except for possible discontinuities at $y = y_c$. No such discontinuities can exist for a non-singular motion, in which case (5.4) implies $\tau \equiv 0$. Only one such discontinuity is possible if $U(y)$ is monotonic in (y_1, y_2), and a necessary condition for a singular neutral mode subject to (5.4) is that this discontinuity vanish to yield $\tau \equiv 0$. We conclude that:

VII. The Reynolds stress for any neutral oscillation vanishes identically for monotonic $U(y)$ if $J_c > 0$.

More than one critical layer may exist if $U(y)$ is not monotonic, however, and then the discontinuities in τ may cancel to satisfy (5.4).

We may calculate rather simple expressions for the Reynolds stress for neutral wave motions by posing a general solution to (3.5) in the form

$$X(y) = AX_+(y)+BX_-(y). \quad (5.8)$$

Substituting (5.8) in (5.1) and setting $c_i = 0+$, we obtain

$$\tau = \tfrac{1}{2}k(|A|^2X'_+X^*_+ + |B|^2X'_-X^*_- + AB^*X'_+X^*_- + A^*BX^*_+X'_-)_i. \quad (5.9)$$

Invoking (3.13) and (3.18a, b), we find that the first two terms in parentheses are real for $J_c < \frac{1}{4}$ (ν real), whereas the last two terms are complex conjugates for $J_c > \frac{1}{4}$ ($\nu = i\mu$ imaginary). In the former case, we have

$$X'_+X^*_- = (X'_+X_-)^*e^{-i\pi(1+\nu)S} \quad (5.10a)$$
$$= (\nu+X_+X'_-)^*e^{-i\pi(1+\nu)S} \quad (5.10b)$$
$$= \nu e^{-i\pi(1+\nu)S}+X_+X'^*_-, \quad (5.10c)$$

with the aid of (3.18a) and (3.15), and we may reduce (5.9) to

$$\tau = \tfrac{1}{2}k\nu\{AB^*e^{-i\pi(1+\nu)S(y-y_c)}\}_i \quad (J_c < \tfrac{1}{4}). \quad (5.11)$$

Similarly, we obtain

$$\tau = \tfrac{1}{4}k\mu\{|A|^2e^{\pi(i+\mu)S(y-y_c)}-|B|^2e^{\pi(i-\mu)S(y-y_c)}\} \quad (J_c > \tfrac{1}{4}). \quad (5.12)$$

If $J_c = 0$, we must distinguish between $\rho'_{oc} = 0$ (heterogeneous flow with an extremum in the density) and $g = 0$ (heterogeneous flow with negligible buoyancy

† A necessary condition for any neutral motion is, from (2.9), $P+Q = 0$. Calculating P through (3.1) (3.2b, c), (3.4) and (2.12), we may express this condition in the form $Q = -P = \tau_2U_2-\tau_1U_1-c(\tau_2-\tau_1)$. This reduces to $P = Q = 0$ under the boundary conditions (5.4).

force). In the former case we may approximate β by $-(\rho_0''/\rho_0 U')_c(U-c)$ and integrate (5.2*c*) between y_c- and y_c+ to obtain (cf. L 4.3)

$$\tau(y_c+)-\tau(y_c-)=\frac{\pi}{k}\left[\left(\rho_0 U''+\frac{\rho_0'' g}{|U'|}\right)\frac{\overline{v^2}}{|U'|}\right]_c \quad (\rho_{0c}'=0), \tag{5.13}$$

whereas in the latter case

$$\tau(y_c+)-\tau(y_c-)=\frac{\pi}{k}\left[(\rho_0 U')'\frac{\overline{v^2}}{|U'|}\right]_c \quad (g=0). \tag{5.14}$$

The results (5.11) to (5.14) hold for any neutral wave motion, independently of the boundary conditions at y_1 and y_2. We shall proceed further on the assumption that $U(y)$ is monotonic ($U'\neq 0$) in (y_1, y_2), so that only a single critical layer can exist and (5.8) to (5.12) remain valid throughout (y_1, y_2) for fixed A and B. Imposing the boundary conditions (5.4) on (5.11), we then obtain $(AB^*)_i=0$ and $AB^*\sin(\pi\nu)=0$, which imply either $A=0$ or $B=0$ (since ν cannot be an integer), whence:

VIII. A singular neutral mode X for which $0<J_c<\frac{1}{4}$ must be simply proportional to either X_+ or X_-.

This theorem, which is illustrated by Drazin's (1958) results, is important in connexion with our previous observation that the modal energy associated with X_- is infinite if $0<J_c<\frac{1}{4}$.

Imposing (5.4) on (5.12), we obtain $A=B=0$, whence:

IX. Singular neutral modes cannot exist for monotonic $U(y)$ if $J(y)>\frac{1}{4}$ in (y_1, y_2).

This result was stated by Synge (1933), who asserted that it follows directly from the fact that neither X_+ nor X_- can be real. This argument appears to overlook the fact that X, as given by (5.8), is real if $B=A^*$, in consequence of which IX can follow only after the invocation of appropriate boundary conditions.† We have not, of course, ruled out non-singular neutral modes for $J(y)>\frac{1}{4}$ in (y_1, y_2).

Now let us consider the possibility of unstable modes for $J(y)>\frac{1}{4}$ in (y_1, y_2). We can approach this question by considering the asymptotic behaviour of c as a function of the parameter λ (see (4.2) and (4.3)), say $c(\lambda)$. We assume that $J(y)$ is positive definite and of prescribed functional form, but that λ may be varied. (It is perhaps simplest, conceptually, to imagine $\beta(y)$ and $U'(y)$ to be prescribed and g varied, but we also may prescribe $\beta(y)/\beta_*$ and $U'(y)\,l/c_*$ and vary any or all of β_*, c_*, l and g.) Let λ_0 be the minimum value of λ for which $J(y)\geqslant\frac{1}{4}$ in (y_1, y_2). Then, from IX, $c(\lambda)$ must either be definitely complex ($|c_i|>0$) or non-singular (real and not in $[U_1, U_2]$) for $\lambda>\lambda_0$. Applying Liouville's method to (3.5), we obtain the asymptotic solutions

$$X_\pm\sim(\beta g)^{-\frac{1}{4}}(U-c)^{\frac{1}{2}}\exp\left[\pm i\int_{y_1}^{y}(\beta g)^{\frac{1}{2}}(U-c)^{-1}dy\right] \quad (\lambda\to\infty). \tag{5.15}$$

Invoking the boundary conditions $X_1=X_2=0$, we obtain

$$\sin\left[\int_{y_1}^{y_2}\frac{(\beta g)^{\frac{1}{2}}dy}{U-c}\right]=0 \quad (\lambda\to\infty), \tag{5.16}$$

† Prof. Synge (private communication) agrees with this statement.

as the asymptotic form of the secular equation. Assuming $U' \neq 0$ in (y_1, y_2), we see that (5.16) can be satisfied only if c is real and not in $[U_1, U_2]$, corresponding to a non-singular neutral mode. It follows that $c_i(\lambda) \equiv 0$ for $\lambda > \lambda_0$ and hence that:

X. Sufficient conditions for the stability of a heterogeneous shear flow are $U'(y) \neq 0$ and $J(y) > \frac{1}{4}$ in (y_1, y_2).

6. Concluding remarks

The most important questions left unresolved by the preceding analysis appear to concern (*a*) the conditions under which a locus of singular neutral modes constitutes a true stability boundary, and (*b*) the significance of singular neutral modes having infinite energies. It appears unlikely that (*a*) could be resolved satisfactorily without first resolving (*b*).

It also would be desirable to give further consideration to non-montonic velocity distributions, but this would appear to raise some difficult mathematical questions.

I am indebted to my colleague Jörgen Hølmboe for several stimulating discussions of the problems considered here and to P. G. Drazin for helpful criticism and for bringing my attention to Synge's work.

This work was supported by the United States Atomic Energy Commission under Contract AT(11-1)-34, Project 34.

REFERENCES

Case, K. M. 1960 *Phys. Fluids*, **3**, 149.

Drazin, P. G. 1958*a* *J. Fluid Mech.* **4**, 214.

Drazin, P. G. 1958*b* On the Dynamics of a Fluid of Variable Density. Ph.D. Thesis, Cambridge University.

Eliassen, A., Høiland, E. & Riis, E. 1953 *Two-Dimensional Perturbation of a Flow with Constant Shear of a Stratified Fluid*, Institute for Weather and Climate Research, Norwegian Academy of Sciences and Letters, Publ. no. 1.

Goldstein, 1931 *Proc. Roy. Soc.* A, **132**, 524.

Hølmboe, J. 1957 *Investigation of Mountain Lee Waves and the Air Flow over the Sierra Nevada*, chap. 12. University of California, Los Angeles.

Hølmboe, J. 1960 Unpublished Lecture Notes, University of California, Los Angeles.

Ince, E. L. 1944. *Ordinary Differential Equations.* New York: Dover.

Lamb, H. 1932. *Hydrodynamics.* Cambridge University Press.

Lin, C. C. 1955 *The Theory of Hydrodynamic Stability.* Cambridge University Press.

Menkes, J. 1959 *J. Fluid Mech.* **4**, 518.

Menkes, J. 1960 *On the Stability of Heterogeneous Shear Layer to a Body Force*, Tech. Report no. 32–12, Jet Propulsion Laboratory, California Institute of Technology, Pasadena; *J. Fluid Mech.* (in the press).

Miles, J. W. 1959 *J. Fluid Mech.* **6**, 583.

Orr, W. McF. 1907 *Proc. Roy. Irish Acad.* **27**, 9.

Reynolds, O. 1895 *Scientific Papers*, **2**, 535. Cambridge University Press (1901).

Synge, J. L. 1933. *Trans. Roy. Soc. Can.* (3), **27**, 1.

Taylor, G. I. 1931. *Proc. Roy. Soc.* A, **132**, 499.

Yih, C. S. 1955 *Quart. Appl. Math.* **12**, 434.

Yih, C. S. 1957 *Tellus*, **9**, 220.

Note on a paper of John W. Miles

By LOUIS N. HOWARD

Mathematics Department, Massachusetts Institute of Technology

(Received 21 March 1961)

The theorem X established by Miles in the preceding paper is here given a simpler and more general proof. Some further theoretical results concerning the stability of heterogeneous shear flows are also presented, in particular a demonstration that the complex wave velocity of any unstable mode must lie in a certain semi-circle.

1. Introduction

In his paper (1961; henceforth referred to as I), Miles has established the conjecture of G. I. Taylor that a sufficient condition for infinitesimal stability in a parallel, stratified, inviscid flow is that the local Richardson number should everywhere exceed $\frac{1}{4}$. Miles assumed in his proof that the velocity profile was monotonic, and that it and the density profile were analytic in a complex neighbourhood of the real flow domain. This note presents a simpler proof of Miles's theorem, which does not require these hypotheses. Some other related results are also given. For a derivation of the basic equations and references to previous work, one may consult Miles's paper.

2. Miles's theorem

To facilitate reference to I, the same notation will be used here. The basic velocity field is $U(y)$, and the density field $\rho(y)$ [$\rho_0(y)$ was used in I, but the subscript will not be needed here]. The stream-function perturbation is

$$(U-c)\,F(y)\,e^{ik(x-ct)},$$

and the linearized equations of motion lead to

$$[\rho(U-c)^2F']' + [\beta g - k^2(U-c)^2]F = 0. \tag{2.1}$$

This is equation (3.3) of I; β is $-\rho'/\rho$, and g is the acceleration of gravity. It is always assumed here that the density stratification is statically stable, i.e. $\beta \geqslant 0$. The boundary conditions are that F vanish on $y = y_1$ and y_2 (rigid walls), which may recede to $\pm\infty$ in limiting cases. The flow is unstable if (2.1) and the boundary conditions have non-trivial solutions with $\operatorname{Im} c > 0$. Set $c = c_r + ic_i$, and for brevity let $W = U - c$. Suppose now that F is such an unstable solution. Since $c_i > 0$, W is never zero and one can select one branch of $W^{\frac{1}{2}}$ to be used consistently throughout (y_1, y_2); it will be as differentiable as U is, say at least piecewise twice continuously differentiable. Now set $G = W^{\frac{1}{2}}F$, and replace the variable F in (2.1) by G. This gives

$$(\rho WG')' - [\tfrac{1}{2}(\rho U')' + k^2\rho W + \rho W^{-1}(\tfrac{1}{4}U'^2 - g\beta)]G = 0, \tag{2.2}$$

and, of course, $G(y_1) = G(y_2) = 0$. Multiplication of (2.2) by the complex conjugate $\overline{G}$ of G and integration over (y_1, y_2) then leads to

$$\int \rho W[|G'|^2 + k^2|G|^2] + \int \tfrac{1}{2}(\rho U')' |G|^2 + \int \rho[\tfrac{1}{4}U'^2 - g\beta]\, \overline{W}\, |G/W|^2 = 0. \tag{2.3}$$

(Here and subsequently $\int$ is used to denote the definite integral over (y_1, y_2).) Recalling that $c_i > 0$, we see that the imaginary part of (2.3) implies

$$\int \rho[|G'|^2 + k^2|G|^2] + \int \rho[g\beta - \tfrac{1}{4}U'^2]\, |G/W|^2 = 0. \tag{2.4}$$

This is clearly impossible if $g\beta - \frac{1}{4}U'^2$ is non-negative throughout, so that a necessary condition for instability is that $g\beta - \frac{1}{4}U'^2$ be somewhere negative, or, as Miles expressed it, a sufficient condition for stability is that $g\beta - \frac{1}{4}U'^2$ should be everywhere non-negative. If the local Richardson number $J(y) = g\beta/U'^2$ is to be well defined everywhere, it is necessary to be cautious about points at which $U' = 0$, so that there is a minor difficulty in converting the dimensional stability condition $g\beta - \frac{1}{4}U'^2 \geqslant 0$ to the dimensionless one $J(y) \geqslant \frac{1}{4}$ if U is not strictly monotonic. This is obviously a trivial difficulty, however; if one prefers the statement $J \geqslant \frac{1}{4}$, it is probably simplest to define J at points at which $U' = 0$ to be its limiting value, $+\infty$ being allowed.

3. The semicircle theorem

Returning for a moment to the original equation (2.1), let us multiply it by $\overline{F}$ and integrate over (y_1, y_2), as in the derivation of (2.3), to get

$$\int \rho W^2[|F'|^2 + k^2|F|^2] - \int g\beta\, |F|^2 = 0, \tag{3.1}$$

or, separating the real and imaginary parts,

$$\int \rho[(U - c_r)^2 - c_i^2][|F'|^2 + k^2|F|^2] - \int g\rho\beta\, |F|^2 = 0, \tag{3.2}$$

$$2ic_i \int \rho(U - c_r)[|F'|^2 + k^2|F|^2] = 0. \tag{3.3}$$

Equation (3.3) gives the result that c_r must lie in the range of U if $c_i > 0$, which goes back to Synge (1933) and has been given under various conditions by several other writers (references are given in I). However, it seems that rather more can be said. Let $Q = [|F'|^2 + k^2|F|^2]$. Then, under the assumption $c_i > 0$, (3.2) and (3.3) can be written

$$\int UQ = c_r \int Q, \tag{3.4}$$

$$\int U^2 Q = (c_r^2 + c_i^2) \int Q + \int g\rho\beta\, |F|^2. \tag{3.5}$$

Suppose now that $a \leqslant U(y) \leqslant b$. Then

$$\begin{aligned} 0 \geqslant \int (U-a)(U-b)Q &= \int U^2 Q - (a+b)\int UQ + ab\int Q \\ &= [c_r^2 + c_i^2 - (a+b)c_r + ab]\int Q + \int g\rho\beta\, |F|^2 \\ &= \{[c_r - \tfrac{1}{2}(a+b)]^2 + c_i^2 - [\tfrac{1}{2}(a-b)]^2\}\int Q + \int g\rho\beta\, |F|^2. \end{aligned}$$

Since $\beta \geqslant 0$ and $Q > 0$, this implies

$$[c_r - \tfrac{1}{2}(a+b)]^2 + c_i^2 \leqslant [\tfrac{1}{2}(a-b)]^2. \tag{3.6}$$

Thus, *the complex wave velocity c for any unstable mode must lie inside the semicircle in the upper half-plane which has the range of U for diameter.*

I have not been able to find that this rather striking extension of the familiar statement 'c_r must lie in the range of U for an unstable wave' has been pointed out before, although it is slightly reminiscent of some results of Synge; unfortunately he started with a different integral relation, which does not give so simple a result.

4. The growth rate

Miles's theorem and the semicircle theorem limit the values of the Richardson number and the complex wave velocity which are accessible to unstable modes. It is of interest to have a similar bound on the growth rate kc_i possible for an unstable wave. A very simple bound of this type can be obtained from (2.4), by observing that $|W|^{-2} \leqslant c_i^{-2}$. Thus (2.4) gives

$$\begin{aligned} k^2 \int \rho |G|^2 &= \int \rho [\tfrac{1}{4} U'^2 - g\rho] |G/W|^2 - \int \rho |G'|^2 \\ &\leqslant \frac{1}{c_i^2} \max [\tfrac{1}{4} U'^2 - g\beta] \int \rho |G|^2, \end{aligned}$$

and so

$$k^2 c_i^2 \leqslant \max [\tfrac{1}{4} U'^2 - g\beta]. \tag{4.1}$$

This estimate is not usually sharp—for example, the Couette flow, with U' constant, is known to be neutrally stable—but in most cases it will probably give the correct order of magnitude of the maximum growth rate. It is sufficient to show that c_i must approach zero as the wavelength decreases to zero, given the boundedness of U'; but there is a likelihood that in fact $kc_i \to 0$ as $k \to \infty$, and with sufficient assumptions the still stronger statement that *all* waves shorter than some critical wavelength are stable is probably true, as illustrated by the examples of Drazin and Hølmboe cited in I.

5. Connexion with Rayleigh's theorem

The proofs of Miles's theorem and the semicircle theorem given above are very similar to the ordinary proof of Rayleigh's theorem on the necessity of an inflection point for instability in homogeneous parallel inviscid flow. Synge (1933) gave a generalization of Rayleigh's theorem for the case of stratified flow. All three results can be obtained in a unified way as follows.

Assuming $c_i > 0$, let $F = W^{-n} H$, some definite branch being selected if n is not an integer. Substituting this in (2.1), one obtains

$$\begin{aligned} [\rho W^{2(1-n)} H']' - [k^2 \rho W^{2(1-n)} + n W^{1-2n} (\rho U')' \\ + \rho W^{-2n} (n(1-n)\, U'^2 - g\beta)] H = 0. \end{aligned} \tag{5.1}$$

Multiplication of this by $\overline{H}$ and integration over (y_1, y_2) gives the integral relation

$$\begin{aligned} \int \rho W^{2(1-n)} [|H'|^2 + k^2 |H|^2] + n \int W^{1-2n} (\rho U')' |H|^2 \\ + \int \rho W^{-2n} [n(1-n)\, U'^2 - g\beta] |H|^2 = 0. \end{aligned} \tag{5.2}$$

Taking $n = 0$ in (5.2) leads to the semicircle theorem, $n = \frac{1}{2}$ gives Miles's theorem, and $n = 1$ gives Synge's generalization of Rayleigh's theorem, which states that a necessary condition for instability is that $(\rho U')' - 2\beta g \rho |W|^{-2} (U - c_r)$ should change sign in (y_1, y_2).

Finally, it should be mentioned that if the rigid upper boundary ($y = y_2$) of the fluid is replaced by a free surface at zero pressure, the boundary condition $H(y_2) = 0$ for (5.1) is replaced by $H' = [nW^{-1}U' + gW^{-2}]H$ at $y = y_2$. Equation (5.2) then becomes

$$\int \rho W^{2(1-n)}[|H'|^2 + k^2|H|^2] + n\int W^{1-2n}(\rho U')'|H|^2 + \int \rho W^{-2n}[n(1-n) - g\beta]|H|^2 - [\rho(nW^{1-2n}U' + gW^{-2n})|H|^2]_{y=y_2} = 0. \quad (5.3)$$

From this equation one can, however, derive Miles's theorem ($n = \frac{1}{2}$) and the semicircle theorem ($n = 0$) by very slight modifications of the arguments given above. The generalization of Rayleigh's theorem does not go through. That this is to be expected is shown by the example $\rho = \text{const.}$, $U = 0$ for $y < 0$, $U = y$ for $0 < y < 1$, $g = 0$, in which the flow is stable if the upper surface ($y = 1$) is rigid, but unstable if it is free.

REFERENCES

MILES, J. W. 1961 On the stability of heterogeneous shear flows. *J. Fluid Mech.* **10**, 496.

SYNGE, J. L. 1933 The stability of heterogeneous liquid. *Trans. Roy. Soc. Can.* (3), **27**, 1.

Diabatic gas flows

By H. MARSH

Engineering Department, Cambridge University

AND J. H. HORLOCK

Department of Mechanical Engineering, Liverpool University

The general equations of motion are developed for a compressible, inviscid flow in which a non-uniform distribution of heat transfer is applied to the fluid or a non-uniform generation of heat per unit volume occurs. In general, vorticity can be created if the cross-products of the temperature and entropy gradients are finite. If the temperature gradients in the flow are small (first-order), then a non-uniform heat addition across the stream will produce a second-order change in vorticity. For this type of flow, solutions are obtained for the variations of velocity and density that occur in a two-dimensional plane flow and an axially symmetric three-dimensional flow. A simple expression is also obtained for the streamline displacement caused by the non-uniform addition of heat.

1. Introduction

The coupling that exists between velocity, vorticity and gradients of stagnation enthalpy and entropy is well known. Tsien (1958) and Vazsonyi (1945) have reviewed the equations of motion for gas flows in which temperature and entropy gradients are present. The work described in this paper deals with the flow which is produced when a non-uniform distribution of heat transfer is applied to a gaseous stream or a non-uniform generation of heat per unit volume occurs. In practice such flows may take place in heat exchangers and nuclear reactors when a local hot spot develops, or in the flow through a flame front in which energy is released non-uniformly across the stream.

The general equations of motion for an inviscid, compressible fluid with vanishing thermal conductivity are first developed, a term allowing for the heat addition being included in the energy equation. The equations for a two-dimensional diabatic flow are next considered, and the equations for the velocity, vorticity and density perturbations are obtained. For the special case in which the temperature gradients are small, two analytical methods of solution and one numerical method are given for subsonic flows. A simple example is given to illustrate two of these methods and to allow a comparison to be made between the two solutions. A brief discussion of an axially symmetric diabatic gas flow then follows, and an example of such a flow is given.

2. The general equations of motion for a diabatic gas flow

The momentum equation for an inviscid flow is

$$-\frac{1}{\rho}\nabla p = (\mathbf{q}.\nabla)\,\mathbf{q} + \frac{\partial \mathbf{q}}{\partial t}, \tag{1}$$

where p is the pressure, ρ the density and $\mathbf{q}$ the velocity vector. Alternatively, using the identity

$$\nabla(\tfrac{1}{2}\mathbf{q}^2) = (\mathbf{q}.\nabla)\,\mathbf{q} + \mathbf{q}\times\mathbf{w},$$

where $\mathbf{w} = \nabla\times\mathbf{q}$ is the vorticity, equation (1) may be written as

$$\frac{1}{\rho}\nabla p + \nabla(\tfrac{1}{2}\mathbf{q}^2) = \mathbf{q}\times\mathbf{w} \tag{2}$$

for a steady flow.

The stagnation enthalpy h_0 is defined in terms of the enthalpy h and the velocity magnitude q by the equation

$$h_0 = h + \tfrac{1}{2}q^2, \tag{3}$$

so that

$$\nabla h_0 = \nabla h + \nabla(\tfrac{1}{2}q^2). \tag{4}$$

From the Gibbs equation relating the properties of the fluid,

$$T\nabla s = \nabla h - \frac{1}{\rho}\nabla p, \tag{5}$$

Crocco's equations is obtained as

$$\nabla h_0 - T\nabla s = \mathbf{q}\times\mathbf{w}, \tag{6}$$

where T is the temperature and s the entropy of the fluid.

If the heat addition to the fluid is $\dot{Q}$ per unit volume per unit time, then the steady-flow energy equation is

$$\dot{Q} = \nabla.(\rho\mathbf{q}h_0). \tag{7}$$

Since the flow is steady, the equation of continuity is

$$\nabla.(\rho\mathbf{q}) = 0, \tag{8}$$

so that (7) may be expressed as

$$\dot{Q} = \rho\mathbf{q}.\nabla h_0. \tag{9}$$

By taking the curl of (6), an equation corresponding to the Helmholtz equation is obtained:

$$\nabla T\times\nabla s = (\mathbf{q}.\nabla)\,\mathbf{w} - (\mathbf{w}.\nabla)\,\mathbf{q} + \mathbf{w}(\nabla.\mathbf{q}). \tag{10}$$

For barotropic flows (e.g. isentropic or isothermal flows), $\nabla T\times\nabla s$ is zero, which is apparent from taking the curl of (5). The usual form of the Helmholtz equation for a barotropic flow then follows from (10).

If the fluid is a perfect gas with $p = R\rho T$ and c_p, the specific heat at constant pressure, a constant, then the steady-flow energy equation is

$$\frac{\dot{Q}}{\rho c_p} = \mathbf{q}.\nabla\left(T + \frac{q^2}{2c_p}\right). \tag{11}$$

From equations (1) and (8), the first term on the right-hand side of (11) is

$$\begin{aligned}\mathbf{q}.\nabla T &= \frac{\mathbf{q}}{R}.\nabla\left(\frac{p}{\rho}\right)\\ &= \frac{\mathbf{q}}{R}.\left(\frac{1}{\rho}\nabla p - \frac{p}{\rho^2}\nabla\rho\right)\\ &= \frac{p}{\rho R}\nabla.\mathbf{q} - \frac{\mathbf{q}}{R}.(\mathbf{q}.\nabla)\,\mathbf{q}.\end{aligned} \tag{12}$$

Using the identity given above (2) along with (12), equation (11) may be written as

$$\left(\frac{k-1}{k}\right)\frac{\dot{Q}}{p} = \nabla.\mathbf{q} - \frac{\mathbf{q}}{kRT}.(\mathbf{q}.\nabla)\,\mathbf{q}, \tag{13}$$

where k is the ratio of the specific heats of the gas. This equation has proved to be the most useful form of the steady-flow energy equation for the purpose of this paper.

3. Two-dimensional flows with heat addition

When a perfect gas flows along a parallel-sided duct, the presence of a non-uniform addition of heat can produce a region in which the streamlines are not parallel to the walls of the duct. By using a perturbation method for a heat addition with only a small degree of non-uniformity, it is possible to demonstrate some of the characteristics of this type of flow. As shown in figure 1, the x-axis is taken along the duct wall, the y-axis lies across the duct and there is no flow normal to the (x, y)-plane. The addition of heat is non-uniformly distributed along and across the duct.

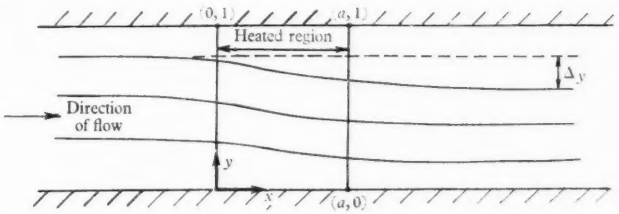

FIGURE 1. Two-dimensional diabatic gas flow.

In a two-dimensional flow where u and v are the x- and y-components of velocity respectively, and η is the only component of vorticity, in a direction normal to the (x, y)-plane, the equations of momentum, continuity and energy are

$$-\frac{1}{\rho}\frac{\partial p}{\partial x} = u\frac{\partial u}{\partial x} + v\frac{\partial u}{\partial y}, \tag{14}$$

$$-\frac{1}{\rho}\frac{\partial p}{\partial y} = u\frac{\partial v}{\partial x} + v\frac{\partial v}{\partial y}, \tag{15}$$

$$0 = \frac{\partial}{\partial x}(\rho u) + \frac{\partial}{\partial y}(\rho v), \tag{16}$$

$$\left(\frac{k-1}{k}\right)\frac{\dot{Q}}{p} = \left[1 - \frac{u^2}{kRT}\right]\frac{\partial u}{\partial x} + \left[1 - \frac{v^2}{kRT}\right]\frac{\partial v}{\partial y} - \frac{uv}{kRT}\left[\frac{\partial u}{\partial y} + \frac{\partial v}{\partial x}\right]. \tag{17}$$

For this two-dimensional flow, equation (10) becomes

$$\frac{\partial T}{\partial x}\frac{\partial s}{\partial y} - \frac{\partial T}{\partial y}\frac{\partial s}{\partial x} = \frac{\partial}{\partial x}(u\eta) + \frac{\partial}{\partial y}(v\eta), \tag{18}$$

which shows the possibility of producing changes in vorticity by the presence of temperature and entropy gradients.

It is assumed that the Mach number of the flow is less than unity, and that far upstream of the region of heat addition the gas has a uniform velocity $\bar{U}$ along the duct and a Mach number $\bar{M}$. The properties of the gas far upstream are also

assumed to be uniform across the duct and are used to make the above equations non-dimensional by writing

$$\left.\begin{aligned} x = bx', \quad y = by', \quad u = \overline{U}u', \quad v = \overline{U}v', \\ \eta = \frac{\overline{U}}{b}\eta', \quad p = \overline{P}p', \quad \rho = \overline{D}\rho', \quad T = \overline{T}\theta, \\ \left(\frac{k-1}{k}\right)\dot{Q} = \frac{\overline{U}\overline{P}}{b}F(x', y'), \end{aligned}\right\} \tag{19}$$

where $\overline{P}$, $\overline{T}$ and $\overline{D}$ are the pressure, temperature and density far upstream and b is the width of the duct. The non-dimensional forms of equations (14) to (17) are then

$$-\frac{1}{\rho}\frac{\partial p}{\partial x} = k\overline{M}^2\left[u\frac{\partial u}{\partial x} + v\frac{\partial u}{\partial y}\right], \tag{20}$$

$$-\frac{1}{\rho}\frac{\partial p}{\partial y} = k\overline{M}^2\left[u\frac{\partial v}{\partial x} + v\frac{\partial v}{\partial y}\right], \tag{21}$$

$$0 = \frac{\partial}{\partial x}(\rho u) + \frac{\partial}{\partial y}(\rho v), \tag{22}$$

$$\frac{1}{p}F(x, y) = \left[1 - \overline{M}^2\frac{u^2}{\theta}\right]\frac{\partial u}{\partial x} + \left[1 - \overline{M}^2\frac{v^2}{\theta}\right]\frac{\partial v}{\partial y} - \overline{M}^2\frac{uv}{\theta}\left[\frac{\partial u}{\partial y} + \frac{\partial v}{\partial x}\right], \tag{23}$$

where, for convenience, the primes have been omitted.

If the heat addition function $F(x, y)$ can be expressed as

$$F(x, y) = F_0(x) + \epsilon f(x, y), \tag{24}$$

where $\epsilon \ll 1$ and $F_0(x)$ and $f(x, y)$ are of the same order of magnitude, then a perturbation method may be applied to the problem. The function $F_0(x)$ represents a heat addition which can vary along the duct, but is uniform across the duct. The second term, $\epsilon f(x, y)$, indicates the presence of a small non-uniform heat addition which can vary both along and across the duct. It is this non-uniform heat addition that produces the displacement of the streamlines and the creation of vorticity.

It is assumed that the variables u, v, η, p, ρ and θ are analytic in ϵ and may be expressed as power series in ϵ, the general form being

$$\left.\begin{aligned} u = u_0 + \epsilon u_1 + \epsilon^2 u_2 + \ldots, \\ v = \epsilon v_1 + \epsilon^2 v_2 + \ldots, \end{aligned}\right\} \tag{25}$$

etc.

If equations (24) and (25) are substituted in equations (20) to (23), then, equating the zero powers of ϵ, we get

$$\left.\begin{aligned} -\frac{1}{\rho_0}\frac{\partial p_0}{\partial x} = k\overline{M}^2 u_0\frac{\partial u_0}{\partial x}, \\ -\frac{1}{\rho_0}\frac{\partial p_0}{\partial y} = 0, \\ 0 = \frac{\partial}{\partial x}(\rho_0 u_0), \\ \frac{1}{p_0}F_0(x) = \left[1 - \overline{M}^2\frac{u_0^2}{\theta_0}\right]\frac{\partial u_0}{\partial x}. \end{aligned}\right\} \tag{26}$$

These are the equations for a one-dimensional Rayleigh-line process, the addition of heat to a one-dimensional steady flow. The solution is well known; the velocity and gas state vary along the duct, but there is no variation across the flow.

By equating the first powers of ϵ in equations (20) to (23), the equations relating the first-order perturbations in velocity, pressure, density and temperature are obtained:

$$\frac{\rho_1}{\rho_0^2}\frac{dp_0}{dx}-\frac{1}{\rho_0}\frac{\partial p_1}{\partial x}=k\bar{M}^2\left[u_0\frac{\partial u_1}{\partial x}+u_1\frac{du_0}{dx}\right], \tag{27}$$

$$-\frac{1}{\rho_0}\frac{\partial p_1}{\partial y}=k\bar{M}^2u_0\frac{\partial v_1}{\partial x}, \tag{28}$$

$$0=\frac{\partial}{\partial x}(u_0\rho_1+u_1\rho_0)+\frac{\partial}{\partial y}(\rho_0 v_1), \tag{29}$$

$$\frac{f(x,y)}{p_0}-\frac{p_1}{p_0^2}F_0(x)=\left[1-\bar{M}^2\frac{u_0^2}{\theta_0}\right]\frac{\partial u_1}{\partial x}+\frac{\partial v_1}{\partial y}-\bar{M}^2\frac{du_0}{dx}\left[\frac{2u_0u_1}{\theta_0}-\frac{\theta_1u_0^2}{\theta_0^2}\right]. \tag{30}$$

The solution of these equations gives the perturbations of velocity and gas state which are superposed on the one-dimensional Rayleigh-line process.

If p_1 and ρ_1 are eliminated from the momentum and continuity equations ((27) to (29)), then an equation connecting the two perturbation velocities is obtained:

$$u_0\frac{\partial}{\partial x}\left[\frac{1}{du_0/dx}\left(\frac{\partial^2v_1}{\partial x^2}-\frac{\partial^2u_1}{\partial x\partial y}\right)\right]+\frac{\partial^2v_1}{\partial y^2}=0. \tag{31}$$

Introducing the vorticity and the uniform heat addition, this equation may be written as

$$u_0\frac{\partial}{\partial x}\left[\frac{p_0}{F_0(x)}\left(1-\bar{M}^2\frac{u_0^2}{\theta_0}\right)\frac{\partial\eta_1}{\partial x}\right]+\frac{\partial^2v_1}{\partial y^2}=0. \tag{32}$$

A further equation relating the two perturbation velocities may be derived by using the equation of state for the gas to eliminate θ_1 from (30), and then differentiating with respect to y to obtain

$$\frac{1}{p_0}\frac{\partial f}{\partial y}(x,y)+\bar{M}^2\frac{u_0}{\theta_0}\frac{du_0}{dx}\left[k\frac{\partial v_1}{\partial x}+\frac{\partial u_1}{\partial y}\right]=\frac{\partial^2u_1}{\partial x\partial y}+\frac{\partial^2v_1}{\partial y^2}-\bar{M}^2\frac{u_0^2}{\theta_0}\frac{\partial^2v_1}{\partial x^2}. \tag{33}$$

The two velocities u_1 and v_1 are therefore determined by (31) and (33), along with the appropriate boundary conditions.

Two of the boundary conditions are those imposed by the duct walls, namely $v=0$ on $y=0$ and $y=1$. It then follows from (32) that in the presence of a heat addition for which $F_0(x)$ is not zero, the vorticity perturbation η_1 can only be zero if the transverse velocity v_1 is also zero throughout the flow. This is the case of the one-dimensional Rayleigh-line process where the flow remains parallel to the walls of the duct and $\epsilon f(x,y)=0$. When $F_0(x)=0$ and only the small non-uniform heat addition is present, the change of vorticity may be shown to be a second- or higher-order perturbation. This case is examined in more detail in the remainder of this paper. In general, if neither $F_0(x)$ nor $\epsilon f(x,y)$ are zero, then there will be a first-order perturbation in vorticity.

4. Two-dimensional flows with $F_0(x) = 0$

No solution has yet been obtained for the general case when both $F_0(x)$ and $\epsilon f(x, y)$ are present. However, it is possible to observe some of the features of two-dimensional diabatic gas flows by considering the special case of $F_0(x) = 0$. The heat addition then consists of the small non-uniform heat addition alone and the temperature gradients are therefore small. For this type of heat addition, a general solution for the first-order velocity perturbations has been derived in the form of an integral, and for a particular distribution of heat addition both a Fourier series solution and a numerical solution have also been obtained.

In the absence of the uniform heat addition $F_0(x)$, the solution of equations (26) for the one-dimensional Rayleigh-line process is that u_0, p_0, ρ_0 and θ_0 are each constant and equal to unity, their value far upstream. The Mach number of the flow is therefore constant and equal to $\bar{M}$, the value far upstream. The first-order perturbations of velocity, pressure and density are then given by

$$-\frac{\partial p_1}{\partial x} = k\bar{M}^2 \frac{\partial u_1}{\partial x}, \tag{34}$$

$$-\frac{\partial p_1}{\partial y} = k\bar{M}^2 \frac{\partial v_1}{\partial x}, \tag{35}$$

$$0 = \frac{\partial}{\partial x}(u_1 + \rho_1) + \frac{\partial v_1}{\partial y}, \tag{36}$$

$$f(x, y) = [1 - \bar{M}^2]\frac{\partial u_1}{\partial x} + \frac{\partial v_1}{\partial y}, \tag{37}$$

which correspond to (27) to (30) of the general analysis.

The elimination of p_1 between (34) and (35) gives

$$\frac{\partial \eta_1}{\partial x} = 0, \tag{38}$$

and since the flow far upstream is uniform, the first-order vorticity perturbation is zero throughout the entire flow. It is therefore possible to define a perturbation velocity potential $\phi(x, y)$ such that

$$u_1 = \frac{\partial \phi}{\partial x}, \quad v_1 = \frac{\partial \phi}{\partial y}. \tag{39}$$

Equation (37) may then be written as

$$[1 - \bar{M}^2]\frac{\partial^2 \phi}{\partial x^2} + \frac{\partial^2 \phi}{\partial y^2} = f(x, y). \tag{40}$$

If the heat addition is confined to a finite length of the duct, say $x = 0$ to $x = a$ in the non-dimensional system, then the boundary conditions for (40) are

$$\left.\begin{aligned} &\frac{\partial \phi}{\partial y} = 0 \quad \text{on} \quad y = 0 \text{ and } y = 1, \\ &\frac{\partial \phi}{\partial x} \to 0, \quad \frac{\partial \phi}{\partial y} \to 0 \quad \text{as} \quad x \to -\infty, \\ &\frac{\partial \phi}{\partial x} \to \alpha^2 \int_0^a \int_0^1 f(x, y)\, dy\, dx \quad \text{as} \quad x \to +\infty, \end{aligned}\right\} \tag{41}$$

where $\alpha^2 = 1/(1-\bar{M}^2)$. The second pair of conditions are necessary to leave the flow far upstream unperturbed and the final boundary condition is obtained from the other conditions by applying Green's Theorem to (40).

Integral solution

The solution of (40) for a unit heat source situated at the point (x_0, y_0) is the Green function $G(x, y; x_0, y_0)$, for the problem. It can be shown that the perturbation velocity potential may then be expressed as

$$\phi(x,y) = \int_0^a \int_0^1 f(x_0,y_0)\, G(x_0,y_0;\, x,y)\, dy_0 dx_0 + C, \tag{42}$$

where C is a constant.

The Green function satisfies the equation

$$[1-\bar{M}^2]\frac{\partial^2 G}{\partial x^2} + \frac{\partial^2 G}{\partial y^2} = \delta(x-x_0)\,\delta(y-y_0), \tag{43}$$

and has the boundary conditions

$$\left.\begin{aligned} &\frac{\partial G}{\partial y} = 0 \quad \text{on} \quad y = 0 \text{ and } y = 1, \\ &\frac{\partial G}{\partial x} \to 0, \quad \frac{\partial G}{\partial y} \to 0 \quad \text{as} \quad x \to -\infty, \\ &\qquad \frac{\partial G}{\partial x} \to \alpha^2 \quad \text{as} \quad x \to +\infty. \end{aligned}\right\} \tag{44}$$

The solution can be obtained by the method of images and takes the form

$$\begin{aligned} G(x_0,y_0;\, x,y) = \frac{\alpha}{4\pi} \log \{ &4[\cosh \pi\alpha(x-x_0) - \cos \pi(y-y_0)] \\ &\times [\cosh \pi\alpha(x-x_0) - \cos \pi(y+y_0)]\} + \tfrac{1}{2}\alpha^2(x+x_0) + \text{const.} \end{aligned} \tag{45}$$

If this expression is substituted in (42), then the two perturbation velocities u_1 and v_1 may be obtained by forming the gradient of $\phi(x, y)$. In practice this method is difficult to apply and an approximate solution is more suitable for estimating the flow pattern.

Fourier series solution

A solution for the perturbation velocity potential has been derived for the case when the heat addition function is given by $f(x, y) = y$. A numerical solution has also been obtained for the transverse velocity v_1 that is produced by this form of heat addition, and this may be compared with the value which is given by the Fourier series solution.

The equation governing the flow outside of the heated region is

$$[1-\bar{M}^2]\frac{\partial^2 \phi}{\partial x^2} + \frac{\partial^2 \phi}{\partial y^2} = 0, \tag{46}$$

and, within the region of heat addition,

$$[1-\bar{M}^2]\frac{\partial^2 \phi}{\partial x^2} + \frac{\partial^2 \phi}{\partial y^2} = y. \tag{47}$$

In order to provide the necessary boundary conditions for these two equations, it is assumed that at the two boundaries of the heated region, $x = 0$ and $x = a$, there is no discontinuity in the gradient of the perturbation velocity potential. The physical interpretation of this requirement is that the two perturbation velocities, u_1 and v_1, are continuous throughout the flow.

If $m = 2n-1$, then the solution of (46) and (47) is that, upstream,

$$\phi(x,y) = \frac{2}{\pi^4}\sum_{n=1}^{\infty}\frac{e^{m\pi\alpha x}}{m^4}[1-e^{-m\pi\alpha a}]\cos(m\pi y), \tag{48}$$

in the heated region,

$$\phi(x,y) = \frac{\alpha^2x^2}{4}+\frac{y^2(2y-3)}{12}-\frac{2}{\pi^4}\sum_{n=1}^{\infty}\left[\frac{e^{-m\pi\alpha x}+e^{m\pi\alpha(x-a)}}{m^4}\right]\cos(m\pi y), \tag{49}$$

and downstream,

$$\phi(x,y) = \frac{\alpha^2 a x}{2}-\frac{2}{\pi^4}\sum_{n=1}^{\infty}\frac{e^{-m\pi\alpha x}}{m^4}[1-e^{m\pi\alpha a}]\cos(m\pi y). \tag{50}$$

The two velocities u_1 and v_1 are then obtained by forming the gradient of $\phi(x,y)$, and it is clear that since the coefficients of the Fourier series for these velocities decrease very rapidly, a good approximation can be obtained by considering only the first terms of the series. The solution also shows that the production of a transverse velocity v_1 is a local effect which does not extend far outside of the region of heat addition.

Numerical solution

The displacement of the streamlines is determined by the transverse velocity v_1 and to the first order in ϵ, the direction of the flow is given by

$$\frac{dy}{dx} = \frac{\epsilon v_1}{u_0} = \epsilon v_1. \tag{51}$$

When considering the characteristics of a diabatic flow, it is useful to know the streamline pattern and the numerical solution was chosen so that the transverse velocity would be calculated directly.

The equation governing the velocity perturbation v_1 is obtained by differentiating (37) with respect to y and eliminating u_1. With $f(x,y) = y$, this equation is

$$\frac{\partial^2 v_1}{\partial z^2}+\frac{\partial^2 v_1}{\partial y^2} = 1 \quad \text{within the heated region,}$$

and

$$\frac{\partial^2 v_1}{\partial z^2}+\frac{\partial^2 v_1}{\partial y^2} = 0 \quad \text{elsewhere,}$$

where $z = \alpha x$. The boundary conditions for these equations are

$$v_1 = 0 \quad \text{on} \quad y = 0 \text{ and } y = 1,$$

and

$$v_1 \to 0 \quad \text{as} \quad z \to \pm\infty.$$

Since the production of a transverse velocity is a local effect, the boundary conditions, as z tends towards infinity, are applied at finite distances upstream and downstream of the heated region which extends from $z = 0$ to $z = 1$. As in the Fourier series solution, it is assumed that the perturbation velocity v_1 is

continuous throughout the region of flow. The mesh size for the difference equation was chosen as $l = \frac{1}{6}$, and the boundary conditions were taken as

$$v_1 = 0 \quad \text{on} \quad y = 0 \text{ and } y = 1, \quad \text{on} \quad z = -2{\cdot}41\dot{6}, \quad \text{and on} \quad z = 3{\cdot}41\dot{6}. \tag{52}$$

If $W^n_{i,j}$ is the nth approximation to $v_1(il, jl)$, then within the heated region the iterative process for solving the difference equation for v_1 is

$$W^{n+1}_{i,j} = W^n_{i,j} + \tfrac{1}{4}[W^n_{i+1,j} + W^n_{i,j+1} + W^{n+1}_{i-1,j} + W^{n+1}_{i,j-1} - 4W^n_{i,j} - \tfrac{1}{36}], \tag{53}$$

and, outside the heated region,

$$W^{n+1}_{i,j} = W^n_{i,j} + \tfrac{1}{4}[W^n_{i+1,j} + W^n_{i,j+1} + W^{n+1}_{i-1,j} + W^{n+1}_{i,j-1} - 4W^n_{i,j}]. \tag{54}$$

z	y	W	v_F
0·4167	0·0000	0·0000	0·0000
0·4167	0·1667	−0·0555	−0·0555
0·4167	0·3333	−0·0871	−0·0870
0·4167	0·5000	−0·0973	−0·0971
0·4167	0·6667	−0·0871	−0·0870
0·4167	0·8333	−0·0555	−0·0555
0·4167	1·0000	0·0000	0·0000

W, numerical solution for v_1. v_F, first term of the Fourier series solution.

TABLE 1

These two equations, along with the boundary conditions given in (52), were solved with the aid of a digital computer, and table 1 shows that there is very close agreement between the values obtained by this method and the values obtained from the first term of the Fourier series solution for v_1 with $a\alpha = 1$.

5. Density perturbations with $F_0(x) = 0$

The non-uniform addition of heat to a perfect gas flow produces both an overall change in the mean density and a density gradient across the duct. From equations (36) and (37), we have

$$\frac{\partial \rho_1}{\partial x} = -f(x,y) - \bar{M}^2 \frac{\partial u_1}{\partial x}. \tag{55}$$

Since both ρ_1 and u_1 are zero far upstream, this equation may be integrated to give

$$\rho_1 = -\int_{-\infty}^{x} f(x,y)\,dx - \bar{M}^2 u_1. \tag{56}$$

If the heat addition is confined to the region $0 \leqslant x \leqslant a$, then, for $x > a$,

$$\rho_1 = -\int_0^a f(x,y)\,dx - \bar{M}^2 u_1,$$

and the density perturbation far downstream is

$$\rho_1 = -\left\{\int_0^a f(x,y)\,dx + \alpha^2 \bar{M}^2 \int_0^a \int_0^1 f(x,y)\,dy\,dx\right\}. \tag{57}$$

This equation shows that the density gradient across the duct is not a local effect like the transverse velocity, but is a feature which is retained in the flow far downstream of the heated region.

6. Streamline displacement with $F_0(x) = 0$

The presence of a transverse velocity causes a displacement of the streamlines, and it has been shown that the flow direction is given by $dy/dx = \epsilon v_1$. The streamline displacement Δy from far upstream to far downstream is then

$$\Delta y = \epsilon \int_{-\infty}^{\infty} v_1 dx, \tag{58}$$

where the integration is performed along the streamline. To the first order in ϵ, this integration may be approximated by an integration parallel to the x-axis. Thus, introducing the perturbation velocity potential, we have

$$\Delta y = \epsilon \int_{-\infty}^{\infty} \frac{\partial \phi}{\partial y} dx. \tag{59}$$

This integral can be evaluated by applying Green's theorem to (40) for the region bounded by the streamline and the duct wall. The streamline displacement can then be expressed as

$$\Delta y = \epsilon \left\{ \int_0^a \int_0^y f(x,y)\, dy\, dx - y \int_0^a \int_0^1 f(x,y)\, dy\, dx \right\}. \tag{60}$$

The same result may also be obtained by considering the continuity of the fluid between the streamline and the duct wall and using the equation for the density perturbation.

Equation (60) is very useful for visualizing the type of flow pattern that is produced by simple heat addition functions such as linear, sinusoidal and step distributions. For the linear distribution $f(x,y) = y$, the displacement is given by

$$\Delta y = \tfrac{1}{2} \epsilon a y (y-1), \tag{61}$$

and when $y = 0{\cdot}5$, $\Delta y = -0{\cdot}125 \epsilon a$. The displacement can also be estimated from the numerical solution by using a summation in place of the integration in (59). The value obtained by this method is $\Delta y = -0{\cdot}12495 \epsilon a$ for $y = 0{\cdot}5$. The very close agreement between these two values and also between those given in table 1 confirms the suitability of the mesh size and the location of the boundary conditions in the numerical solution.

7. Three-dimensional diabatic gas flows with axial symmetry

A similar analysis can be made for the non-uniform addition of heat to an axially symmetric perfect gas flow. The flow, as shown in figure 2, is assumed to take place in a circular duct and the velocity and gas state far upstream of the region of heat addition are assumed to be uniform across the duct. The non-dimensional heating function is expressed as

$$F(x,r) = F_0(x) + \epsilon f(x,r),$$

and the velocity and gas state are written in the form of perturbation series. It can then be shown that the first-order perturbation of vorticity can be zero only if $F_0(x)$ or $\epsilon f(x,r)$ is zero. This corresponds to the result which was deduced from (32) for the two-dimensional flow.

When $F_0(x) = 0$, the first-order vorticity perturbation is zero, and it is possible to define a perturbation velocity potential $\phi(x, r)$ such that

$$u_1 = \frac{\partial \phi}{\partial x}, \quad v_1 = \frac{\partial \phi}{\partial r}, \tag{62}$$

where r is the non-dimensional radius and v_1 is the radial velocity perturbation. The velocity potential $\phi(x, r)$ then satisfies the equation

$$[1 - \bar{M}^2]\frac{\partial^2 \phi}{\partial x^2} + \frac{\partial^2 \phi}{\partial r^2} + \frac{1}{r}\frac{\partial \phi}{\partial r} = f(x, r), \tag{63}$$

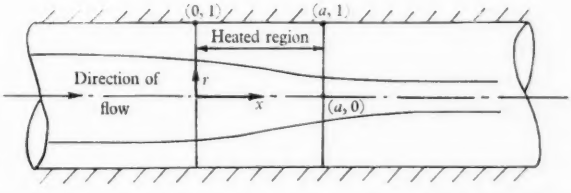

FIGURE 2. Three-dimensional diabatic gas flow with axial symmetry.

which corresponds to (40) of the two-dimensional analysis. The boundary conditions for (63) are

$$\left.\begin{aligned} &\frac{\partial \phi}{\partial r} = 0 \quad \text{on} \quad r = 0 \text{ and } r = 1, \\ &\frac{\partial \phi}{\partial x} \to 0, \quad \frac{\partial \phi}{\partial r} \to 0 \quad \text{as} \quad x \to -\infty, \\ &\frac{\partial \phi}{\partial x} \to 2\alpha^2 \int_0^a \int_0^1 r f(x, r)\, dr\, dx \quad \text{as} \quad x \to +\infty, \end{aligned}\right\} \tag{64}$$

where it is assumed that the heated region extends from $x = 0$ to $x = a$.

For the parabolic distribution of heat addition defined by $f(x, r) = r^2$, a solution for $\phi(x, r)$ has been obtained in terms of zero-order Bessel functions. The flow upstream of the heated region is given by

$$\phi(x, r) = -2 \sum_{n=1}^{\infty} \frac{e^{k_n \alpha x}}{k_n^4} [1 - e^{-k_n \alpha a}] \frac{J_0(k_n r)}{J_0(k_n)}, \tag{65}$$

within the heated region by

$$\phi(x, r) = \frac{\alpha^2 x^2}{4} + \frac{r^2(r^2 - 2)}{16} + 2 \sum_{n=1}^{\infty} \left[\frac{e^{-k_n \alpha x} + e^{k_n \alpha (x-a)}}{k_n^4}\right] \frac{J_0(k_n r)}{J_0(k_n)}, \tag{66}$$

and downstream by

$$\phi(x, r) = \frac{\alpha^2 a x}{2} + 2 \sum_{n=1}^{\infty} \frac{e^{-k_n \alpha x}}{k_n^4} [1 - e^{k_n \alpha a}] \frac{J_0(k_n r)}{J_0(k_n)}, \tag{67}$$

where

$$J_1(k_n) = 0. \tag{68}$$

As with the Fourier series solution, a good approximation may be obtained by taking only the first few terms of the series.

The method for estimating the streamline displacement when $F_0(x) = 0$ can be extended to the three-dimensional axially symmetric flow to give

$$\Delta r = \epsilon\left\{\frac{1}{r}\int_0^a\int_0^r rf(x,r)\,dr\,dx - r\int_0^a\int_0^1 rf(x,r)\,dr\,dx\right\}. \tag{69}$$

For the particular form of heat addition considered above, the displacement is $\Delta r = \frac{1}{4}\epsilon ar(r^2-1)$, which has a maximum value of $\Delta r = -0{\cdot}104\epsilon a$ when $r = 0{\cdot}577$. The general form of this flow is as shown in figure 2.

8. Discussion

For compressible gas flows, vorticity can be created if the cross-products of the temperature and entropy gradients are finite. In particular, for the flow of a perfect gas in a parallel walled duct, it has been shown that except when the temperature gradients are small, a non-uniform heat addition will produce a change in vorticity. A similar result can also be obtained for a three-dimensional flow in a circular duct with axial symmetry. In both cases it has been assumed that far upstream of the heated region, the velocity and gas state are uniform across the duct.

The two solutions given in this paper are for the special case when the temperature gradients are small and the change in vorticity is then a second- or higher-order perturbation. The occurrence of a transverse velocity component may be explained in the following way. Although vorticity cannot be created, a density gradient can be produced by the non-uniform heat addition. The mass flow rate at a point $(+\infty, y)$ far downstream of the heated region differs from that at the corresponding point $(-\infty, y)$ far upstream and the streamline displacement to effect this change requires a transverse velocity perturbation.

It is thought that the study of a few simple cases of non-uniform heat addition, such as the examples given in this paper, may help to illustrate some of the main features of a diabatic flow. Although the two solutions given are for irrotational flows, they do show the presence of a local transverse velocity, an over-all density change, a density gradient across the duct which is retained far downstream and a streamline displacement. A more general form of the heat addition function will show all of these characteristics together with a first-order vorticity perturbation.

The authors are grateful to Dr Sheila Brenner of the Department of Applied Mathematics, Liverpool University, for her advice and discussions on the paper.

REFERENCES

Tsien, H. S. 1958 The equations of gas dynamics, ch. 1 of *Fundamentals of Gas Dynamics*. Oxford University Press.

Vazsonyi, A. 1945 On rotational gas flows. *Quart. Appl. Math.* **3**, 29–37.

Note on the stability of plane parallel flows

By D. H. MICHAEL

Pierce Hall, Harvard University†

(Received 1 July 1960)

The subject of this note is the behaviour of three-dimensional small disturbances to plane parallel flows, which have a variation in the direction normal to the plane of mean flow, in relation to two-dimensional disturbances which vary in the plane of mean flow only. It was pointed out by Squire (1933) that, in linearized theory, the disturbance which is neutrally stable at the critical Reynolds number R_c is two-dimensional in form. More recently interest has turned to the question as to which kind of disturbance is most rapidly amplified at a given Reynolds number above the critical. Jungclaus (1957) pointed out that for certain values of R and of the resolved wavelength in the plane of mean flow, three-dimensional disturbances may be more unstable than plane ones. Recently, Watson (1960) has shown further that a two-dimensional disturbance is the one most rapidly amplified in a certain range of R starting from the critical. In this note we take a slightly different view of the problem which enables us to define specifically the upper end of this range of R, when it exists.

It is clear that when a disturbance consists partly of Fourier components which are propagated obliquely to the plane of the mean motion, each such component interacts only with that component of the mean flow in the direction of propagation of the disturbance. We can illustrate this mathematically by choosing a frame of reference which makes a disturbance in any given direction two-dimensional, say a function of x and y, but not of z. In this frame of reference the mean flow will have a component in the z-direction. If we adopt this point of view and consider the disturbance to a plane parallel incompressible flow bounded by planes $y = \text{const.}$, we can compute the linearized disturbance equations in which the mean velocities $(U(y), O, W(y))$ are disturbed to $(U+u, v, W+w)$, and in which the small disturbance terms are independent of z, and vary with x and t like $e^{i\alpha(x-ct)}$. In the standard notation the linearized equations for the disturbance are

$$i\alpha(U-c)\,u+v\frac{dU}{dy}=-i\frac{\alpha p}{\rho}+\left(\frac{d^2}{dy^2}-\alpha^2\right)u, \tag{1}$$

$$i\alpha(U-c)\,v=-\frac{1}{\rho}\frac{dp}{dy}+\left(\frac{d^2}{dy^2}-\alpha^2\right)v, \tag{2}$$

$$i\alpha(U-c)\,w+v\frac{dW}{dy}=\left(\frac{d^2}{dy^2}-\alpha^2\right)w, \tag{3}$$

$$i\alpha u+\frac{dv}{dy}=0. \tag{4}$$

† Now at Department of Mathematics, University College London, W.C.1.

We see that equations (1), (2) and (4) are not coupled to (3), and with suitable boundary conditions on u and v they provide the characteristic value problem with $U(y)$ the operative component of mean flow. $W(y)$ is only used subsequently in (3), which, when v is established, is an inhomogeneous equation to solve for w with its independent boundary conditions. We may conclude that for a disturbance of wave number α propagated at an angle ϕ to the plane of a mean flow with Reynolds number R, the behaviour is that of a two-dimensional disturbance of wave-number α and reduced Reynolds number $R\cos\phi$. If we know the characteristic curves of constant c_i, where $c = c_r + ic_i$, in the (α, R)-plane, for two-dimensional disturbances of a given velocity profile, this enables us to deduce results simply for three-dimensional disturbances.

It is important in comparing rates of amplification that we should have a correct measure of the amplification rate for different values of α and R. Results of stability calculations are usually given by a plot of curves of constant c_i, in the (α, R)-plane, after these quantities have been made dimensionless. The dimensionless time amplification exponent is αc_i, but the physical exponent is $(V/L)\alpha c_i$, where V and L are the representative velocity and length employed, respectively. Normally we think of varying R for a given fluid by changing V with L fixed. In this case we have to take account of the variation of V in our comparisons by writing the time exponent $(\nu/L^2)(\alpha c_i R)$. With ν the kinematic viscosity and L fixed, it is clear that a correct dimensionless measure of the time amplification is $\alpha c_i R$. If we were to keep V constant and vary L then the measure would be $\alpha c_i/R$, but for the purpose of comparing growth rates of two- and three-dimensional disturbances in a given apparatus the former case is the relevant one here.

If we continue the discussion in terms of the curves $\alpha c_i R = \text{const.}$ in the (α, R)-plane (where α and c_i are now regarded as dimensionless) the point to decide is whether $\alpha c_i R$ has a maximum as a function of α and R; if it has, some of the curves form closed loops about the stationary point. If we assume this behaviour the curves will be of the form given in figure 1, with L the stationary point, at Reynolds number R_L. (The stationary point L may be accompanied by another stationary point at a larger value of R depending on how α and c_i behave as $R \to \infty$. Such a point will be a saddle point if $R \to \infty$ and $\alpha R \to \infty$ for $c_i > \epsilon > 0$.)

If we construct an ordinate MM' at the Reynolds number of the mean flow, the curve through a point of this line, for given α, describes the amplification of a two-dimensional disturbance of that wave-number. All points in the semi-infinite rectangle $M'MO\alpha$ can be reached by three-dimensional disturbances. Whether a two- or three-dimensional disturbance grows fastest will depend on whether all characteristic $(\alpha c_i R)$-lines in the rectangle cut MM'. There will be two distinct cases depending on whether the Reynolds number of the mean flow is greater or less than R_L. If the ordinate is M_1M_1' say, then the disturbance of most rapid growth is a plane one at the wave-number at which M_1M_1' is a tangent to a characteristic $(\alpha c_i R)$-curve. The amplification associated with this curve is greater than at all points inside the rectangle. Hence for $R_c < R \leqslant R_L$ a plane disturbance is amplified fastest. On the other hand, if we have the ordinate M_2M_2', there will be a family of closed characteristic curves enclosing L which

do not intersect M_2M_2' and which provide a higher growth rate than at any point of the line M_2M_2'. Hence for $R > R_L$ a three-dimensional disturbance grows fastest. It may be noted that whereas the maximum amplification rate increases monotonically with R from R_c to R_L, it is constant thereafter, for $R > R_L$, at least up to the next stationary point. In cases where $\alpha c_i R$ does not have a maximum point L we shall know that two-dimensional disturbances will always grow fastest.

Following Watson, we have considered the particular case of plane Poiseuille flow in more detail on the basis of the c_i-curves given by Shen (1954; see also Lin 1955, chap. 3). Figure 2 gives a set of curves $\alpha c_i R = \text{const.}$ obtained by interpolation from Shen's curves (the other details of the figure are explained below).

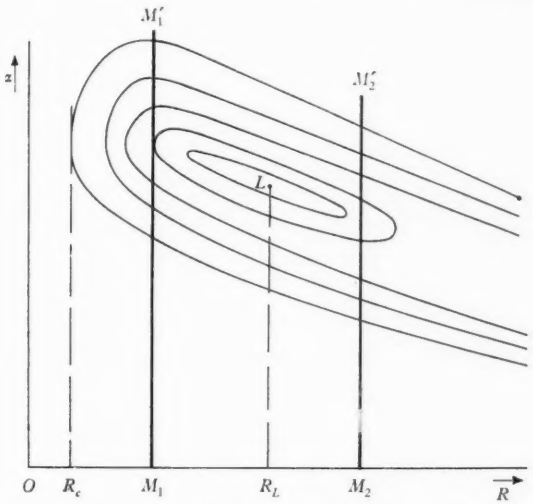

FIGURE 1. Sketch of curves $\alpha c_i R = \text{const.}$

The form of these curves suggests that there is no stationary point L in the range of the Reynolds number covered by the curves, i.e. up to approximately 10^5. This conclusion is in agreement with Watson's conjecture that two-dimensional disturbances grow most rapidly at all values of R.

If we consider Jungclaus's problem in which the resolved component of the wave-number in the plane of mean flow is fixed, the class of disturbance is more restricted. If the resolved wave-number is denoted by β, then the values of α and R for the equivalent plane disturbance are $\beta \sec\phi$ and $R\cos\phi$ respectively. Hence in the (α, R)-plane of figure 1, the locus of three-dimensional disturbances is a branch of a rectangular hyperbola for each pair of values of β and R. In this case, since αR is constant, we can compare amplification rates for different points on any particular hyperbola from the c_i-curves directly, but if we wish to compare points on different hyperbolas the $(\alpha c_i R)$-curves should be used.

Figure 2 also shows a set of curves $\alpha R = \text{const.}$ superposed on the $(\alpha c_i R)$-curves for plane Poiseuille flow.

The line of interest here is PQ, which is the locus of points at which the (αR)-curves are tangential to the $(\alpha c_i R)$-curves. If PS is the (αR)-curve which is tangential to the marginal stability curve PT, on which $\alpha c_i R = 0$, then it is clear that for values of β and R chosen in this plane between PQ and PS there are three-dimensional disturbances which are more rapidly amplified than two-

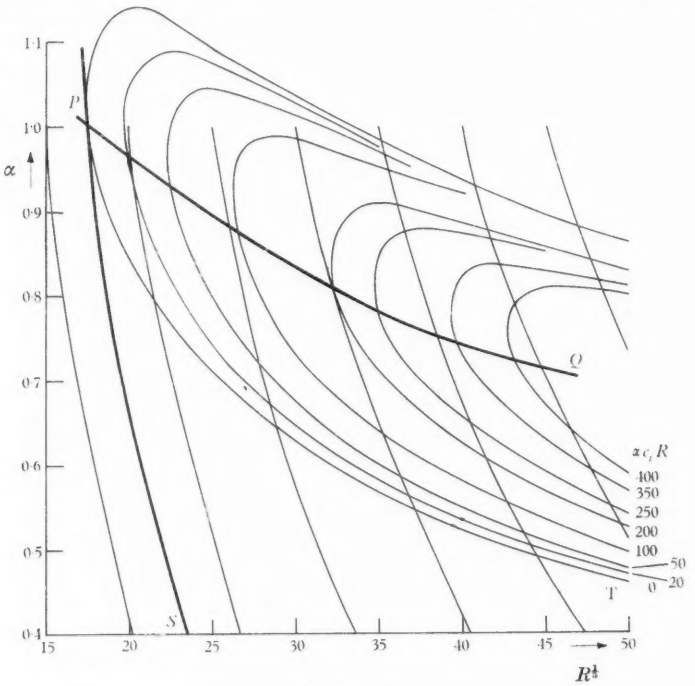

FIGURE 3

FIGURE 2. Curves $\alpha c_i R = \text{const.}$ and $\alpha R = \text{const.}$ (e.g. the curve PS) for plane Poiseuille flow.

dimensional ones. We also note finally that for values of β and R taken between PS and PT, the plane disturbance, and three-dimensional ones up to a certain value of ϕ, are stable.

The author wishes to acknowledge the financial support received under U.S. Navy Contract No. NONR/1866 (34) during the preparation of this paper.

REFERENCES

JUNGCLAUS, G. 1957 Inst. Fluid Dynamics and Appl. Math., University of Maryland, AFOSR, TN 57–577.

LIN, C. C. 1955 *The Theory of Hydrodynamical Stability.* Cambridge University Press.

SHEN, S. F. 1954 *J. Aero. Sci.* **21**, 62.

SQUIRE, H. B. 1933 *Proc. Roy. Soc.* A, **142**, 621.

WATSON, J. 1960 *Proc. Roy. Soc.* A, **254**, 562.

The changes in amplitude of short gravity waves on steady non-uniform currents

By M. S. LONGUET-HIGGINS

National Institute of Oceanography, Wormley, Surrey

AND R. W. STEWART

University of British Columbia, Vancouver

(Received 9 November 1960)

The common assumption that the energy of waves on a non-uniform current $\mathbf{U}$ is propagated with a velocity $(\mathbf{U}+\mathbf{c}_g)$ where $\mathbf{c}_g$ is the group-velocity, and that no further interaction takes place, is shown in this paper to be incorrect. In fact the current does additional work on the waves at a rate $\gamma_{ij}S_{ij}$ where γ_{ij} is the symmetric rate-of-strain tensor associated with the current, and S_{ij} is the radiation stress tensor introduced earlier (Longuet-Higgins & Stewart 1960).

In the present paper we first obtain an asymptotic solution for the combined velocity potential in the simple case (1) when the non-uniform current $\mathbf{U}$ is in the direction of wave propagation and the horizontal variation of $\mathbf{U}$ is compensated by a vertical upwelling from below. The change in wave amplitude is shown to be such as would be found by inclusion of the radiation stress term.

In a second example (2) the current on the x-axis is assumed to be as in (1), but the horizontal variation in $\mathbf{U}$ is compensated by a small horizontal inflow from the sides. It is found that in that case the wave amplitude is also affected by the horizontal advection of wave energy from the sides.

From cases (1) and (2) the general law of interaction between short waves and non-uniform currents is inferred. This is then applied to a third example (3) when waves encounter a current with vertical axis of shear, at an oblique angle. The change in wave amplitude is shown to differ somewhat from the previously accepted value.

The conclusion that non-linear interactions affect the amplification of the waves has some bearing on the theoretical efficiency of hydraulic and pneumatic breakwaters.

1. Introduction

When short surface waves of any kind are propagated over the surface of a medium in steady but non-uniform motion, they tend to undergo refractive changes in length, direction and amplitude. The changes in length and direction depend on kinematical considerations only; a quite general treatment applicable to water waves has been given, for example, by Ursell (1960). But changes in the wave amplitude are less straightforward. Commonly (see Unna 1942; Suthons 1945; Johnson 1947; Evans 1955; Groen & Dorrestein 1958) it has been

assumed without justification that no coupling between the waves and current takes place, and that the wave energy is simply propagated with a velocity equal to $(\mathbf{U}+\mathbf{c}_g)$, where $\mathbf{c}_g$ is the vector group-velocity and $\mathbf{U}$ the local stream velocity. On the contrary, in a recent paper (Longuet-Higgins & Stewart 1960; this paper will be referred to as I), it was found that short gravity waves, riding on the backs of longer waves, are modified to a much greater extent than would be predicted if there were no interchange of energy between the short and the long waves. The discrepancy may be attributed to a term in the equation of energy transfer, called by us the *radiation stress*, and previously overlooked. The stress term occurs quite generally, and must give rise to changes in the wave amplitude in other situations besides the particular one that was considered.

The purpose of the present paper is to study the changes in amplitude of gravity waves riding on steady but non-uniform currents. The subject is of special interest owing to its possible application to bubble-breakwaters, whose action is probably to be ascribed largely to the stopping power of a horizontal current opposing the waves (Taylor 1955; Evans 1955; Straub, Bowers & Tarrapore 1959). Ocean waves entering tidal streams or crossing river flows are known to be subject to a similar effect (Unna 1942; Johnson 1947). The following discussion will be limited to the case of deep currents, that is to say, those for which the change in current velocity in a vertical distance equal to the wavelength is small compared with the wave velocity itself. But quite similar results would apply to waves on shearing currents which penetrated to a depth of only a fraction of a wavelength.

In our first example we consider a system of waves superposed on a current which varies gradually in the x-direction (the direction of wave propagation), and in which the variation in surface current is made up by a vertical upwelling (or downwelling). The modification which the currents produce in the wave form is calculated rigorously by a perturbation method. It is found that, while the variation in the wave-number k is given by the expected formula

$$\frac{1}{k}\frac{\partial k}{\partial x} = -\frac{1}{c+2U}\frac{\partial U}{\partial x}, \tag{1.1}$$

the variation in the wave amplitude, on the other hand, is given by

$$\frac{1}{a}\frac{\partial a}{\partial x} = -\frac{2c+3U}{(c+2U)^2}\frac{\partial U}{\partial x}, \tag{1.2}$$

which is a higher rate of change than if there were no interaction between waves and currents. It is shown that this last result is consistent with the assumption that the equation governing the growth of wave energy E is

$$\frac{\partial}{\partial x}[E(c_g+U)]+S_x\frac{\partial U}{\partial x} = 0, \tag{1.3}$$

where S_x is the radiation stress mentioned earlier. (In deep water, $S_x = \frac{1}{2}E$.) This is to say that in addition to the transport of energy by the group-velocity and stream velocity, the current does work on the waves at a rate $S_x\partial U/\partial x$ per unit distance. In § 4, this conclusion is shown also to be consistent with our earlier

results in I concerning the steepening of surface waves on long waves or tidal streams. Integration of (1.3) leads to the result

$$a \propto [c(c+2U)]^{-\frac{1}{4}}. \tag{1.4}$$

In our second example we consider a situation very similar to the first, but in which the increase in surface current U is made up, not by a vertical upwelling from below, but by a horizontal inflow from the sides. The results are strikingly different. Although the variation in wave-number is the same as in (1.1), the variation in amplitude is now given by

$$\frac{1}{a}\frac{\partial a}{\partial x} = -\frac{c+U}{(c+2U)^2}\frac{\partial U}{\partial x}. \tag{1.5}$$

This is accounted for by including in the energy balance the advection of wave energy by the transverse current V, as well as the work done against the corresponding stress component (equation (6.4)). The amplitude a is now found to be

$$a \propto [(c+2U)/c]^{-\frac{1}{4}}, \tag{1.6}$$

which is a weaker variation than in the previous case.

The appropriate generalization of the equation of energy balance is shown to be

$$\nabla.[E(\mathbf{c}_g+\mathbf{U})]+\tfrac{1}{2}S_{ij}\left(\frac{\partial U_i}{\partial x_j}+\frac{\partial U_j}{\partial x_i}\right) = 0, \tag{1.7}$$

where S_{ij} denotes the radiation stress tensor. In § 8 this is applied to a third example, that of waves crossing a shearing current obliquely. The changes in wavelength and direction of propagation θ are as found by Johnson (1947), but the law governing the wave amplitude is shown to be

$$a \propto (\sin 2\theta)^{-\frac{1}{2}}, \tag{1.8}$$

which differs from Johnson's result.

2. Two-dimensional current: an asymptotic solution

In this section we shall obtain a formal solution for surface waves on a non-uniform current $\mathbf{U}(x)$ which has no transverse component. The solution is to be valid when

$$\sigma^{-1}\frac{\partial U}{\partial x} \ll 1, \tag{2.1}$$

where σ is the wave frequency; in other words, the change in stream velocity U over one wavelength L (that is, $L\partial U/\partial x$) is assumed small compared with the wave velocity $L\sigma/2\pi$.

General equations

It will be supposed that the velocity field $\mathbf{u}$ is irrotational:

$$\mathbf{u} = \nabla\phi; \tag{2.2}$$

that the fluid is incompressible:

$$\nabla.\mathbf{u} = \nabla^2\phi = 0; \tag{2.3}$$

and that viscous effects are negligible. Then we have Bernoulli's integral

$$\frac{p}{\rho}+gz+\tfrac{1}{2}\mathbf{u}^2+\frac{\partial\phi}{\partial t}=C, \tag{2.4}$$

where p, ρ, g denote the pressure, density and acceleration of gravity, and z is the vertical co-ordinate, directed upwards. C is a constant. If $z=\zeta$ is the equation of the free surface, then for the two boundary conditions there are the kinematical condition

$$\frac{\partial\zeta}{\partial t}+\left(\frac{\partial\phi}{\partial x}\frac{\partial\zeta}{\partial x}+\frac{\partial\phi}{\partial y}\frac{\partial\zeta}{\partial y}-\frac{\partial\phi}{\partial z}\right)_{z=\zeta}=0, \tag{2.5}$$

and the condition of constant pressure, which by (2·4) may be written

$$g\zeta+\left(\tfrac{1}{2}\mathbf{u}^2+\frac{\partial\phi}{\partial t}\right)_{z=\zeta}=C. \tag{2.6}$$

It is convenient to replace these last two equations by conditions to be satisfied at the mean surface level $z=0$; this may be done by assuming the potential ϕ to be analytic and by expanding in a Taylor series in z:

$$\left.\begin{aligned}\frac{\partial\zeta}{\partial t}+\left(\frac{\partial\phi}{\partial x}\frac{\partial\zeta}{\partial x}+\frac{\partial\phi}{\partial y}\frac{\partial\zeta}{\partial y}-\frac{\partial\phi}{\partial z}\right)_{z=0}+\zeta\left[\frac{\partial}{\partial z}\left(\frac{\partial\phi}{\partial x}\frac{\partial\zeta}{\partial x}+\frac{\partial\phi}{\partial y}\frac{\partial\zeta}{\partial y}-\frac{\partial\phi}{\partial z}\right)\right]_{z=0}+\ldots=0,\\ g\zeta+\left(\tfrac{1}{2}\mathbf{u}^2+\frac{\partial\phi}{\partial t}\right)_{z=0}+\zeta\left[\frac{\partial}{\partial z}\left(\tfrac{1}{2}\mathbf{u}^2+\frac{\partial\phi}{\partial t}\right)\right]_{z=0}+\ldots=C.\end{aligned}\right\} \tag{2.7}$$

Lastly, we assume that the waves are effectively in deep water, so that as $z\to-\infty$ the periodic part of the motion tends to zero.

Form of the solution

We seek a solution having the character of a time-periodic wave-motion superimposed upon a non-uniform steady flow. Let us then substitute

$$\left.\begin{aligned}\phi&=U_0x+(\alpha\phi_{10}+\beta\phi_{01})+(\alpha^2\phi_{20}+\alpha\beta\phi_{11}+\beta^2\phi_{02})+\ldots,\\ \zeta&=\qquad(\alpha\zeta_{10}+\beta\zeta_{01})+(\alpha^2\zeta_{20}+\alpha\beta\zeta_{11}+\beta^2\zeta_{02})+\ldots,\end{aligned}\right\} \tag{2.8}$$

where U_0 is a steady uniform velocity, the velocity of the stream at $x=0$; ϕ_{01} represents a steady non-uniform current, zero at $x=0$; and ϕ_{10} represents an undisturbed surface wave; α and β are arbitrary small parameters proportional to wave steepness and to the velocity gradient of the current respectively. The terms $\alpha^2\phi_{20}$, etc., are correction terms of higher order, necessary in order to satisfy the boundary conditions at the free surface. We are particularly interested in evaluating the second-order term $\alpha\beta\phi_{11}$, which is the lowest-order interaction potential between the waves and the current.

It may be worth remarking that to eliminate the uniform current U_0 by taking axes moving with velocity U_0 would not be convenient, since in the new frame of reference the motion would no longer be perfectly periodic in time. This is because the modified wavelength is generally a function of x, as will be seen below. Clearly the choice of axes must be made so as to correspond with the physical problem; if the source of the wave-motion is periodic this determines the appropriate frame of reference uniquely.

Retaining terms as far only as $\alpha\beta$, we have from (2.8)

$$\left.\begin{aligned} \nabla\phi &= (U_0, 0, 0) + \alpha\nabla\phi_{10} + \beta\nabla\phi_{01} + \alpha\beta\nabla\phi_{11}, \\ \frac{\partial\phi}{\partial t} &= \alpha\frac{\partial\phi_{10}}{\partial t} + \alpha\beta\frac{\partial\phi_{11}}{\partial t}, \\ \zeta &= \alpha\zeta_{10} + \beta\zeta_{01} + \alpha\beta\zeta_{11}, \end{aligned}\right\} \tag{2.9}$$

and so

$$\left.\begin{aligned} \tfrac{1}{2}\mathbf{u}^2 &= \tfrac{1}{2}U_0^2 + U_0\left(\alpha\frac{\partial\phi_{10}}{\partial x} + \beta\frac{\partial\phi_{01}}{\partial x}\right) \\ &\quad + \alpha\beta\left(U_0\frac{\partial\phi_{11}}{\partial x} + \frac{\partial\phi_{10}}{\partial x}\frac{\partial\phi_{01}}{\partial x} + \frac{\partial\phi_{10}}{\partial y}\frac{\partial\phi_{01}}{\partial y} + \frac{\partial\phi_{10}}{\partial z}\frac{\partial\phi_{01}}{\partial z}\right) + \ldots, \\ \frac{\partial}{\partial z}(\tfrac{1}{2}\mathbf{u}^2) &= U_0\left(\alpha\frac{\partial^2\phi_{10}}{\partial x\,\partial z} + \beta\frac{\partial\phi_{01}}{\partial x\,\partial z}\right) + \ldots. \end{aligned}\right\} \tag{2.10}$$

Substitution in (2.7) shows at once that

$$C = \tfrac{1}{2}U_0^2. \tag{2.11}$$

The terms in α now give

$$\left.\begin{aligned} \left(\frac{\partial}{\partial t} + U_0\frac{\partial}{\partial x}\right)\zeta_{10} - \frac{\partial\phi_{10}}{\partial z} &= 0, \\ g\zeta_{10} + \left(\frac{\partial}{\partial t} + U_0\frac{\partial}{\partial x}\right)\phi_{10} &= 0, \end{aligned}\right\} \tag{2.12}$$

to be satisfied at $z = 0$. On eliminating ζ_{10}, we have

$$\left(\frac{\partial}{\partial t} + U_0\frac{\partial}{\partial x}\right)^2\phi_{10} + g\frac{\partial\phi_{10}}{\partial z} = 0 \quad (z = 0). \tag{2.13}$$

If we choose for ϕ_{10} the wave potential

$$\phi_{10} = A\,e^{k_0 q - i\sigma t}, \tag{2.14}$$

where A and k_0 are constants and

$$q = z + ix, \tag{2.15}$$

then ϕ_{10} satisfies Laplace's equation (2.3), and from (2.13)

$$(\sigma - U_0 k_0)^2 = g k_0. \tag{2.16}$$

Introducing the reference velocity

$$c_0 = \sqrt{(g/k_0)} \tag{2.17}$$

and the non-dimensional parameter

$$\gamma = U_0/c_0 \tag{2.18}$$

we have from (2.16)
$$\sigma = c_0 k_0(1+\gamma). \tag{2.19}$$

(To ensure continuity as γ (or U_0) tends to zero, we have adopted the positive sign in the square root.) From (2.12) and (2.19), we have also

$$\zeta_{10} = -\frac{1}{g}\left[\left(\frac{\partial}{\partial t} + \gamma c_0\frac{\partial}{\partial x}\right)\phi_{10}\right]_{z=0} = \frac{i}{c_0}(\phi_{10})_{z=0}. \tag{2.20}$$

Returning to equation (2.7), we see that the terms in β give equations for ϕ_{01} formally identical with (2.12) except that the time derivatives are now zero:

$$\left.\begin{aligned} U_0 = \frac{\partial \zeta_{01}}{\partial x} - \frac{\partial \phi_{01}}{\partial z} = 0 \\ g\zeta_{01} + U_0 \frac{\partial \phi_{01}}{\partial x} = 0 \end{aligned}\right\} \quad (z = 0), \tag{2.21}$$

whence

$$U_0^2 \frac{\partial^2 \phi_{01}}{\partial x^2} + g \frac{\partial \phi_{01}}{\partial z} = 0 \quad (z = 0). \tag{2.22}$$

We require a potential ϕ_{01} to represent a steady flow having no transverse component $\partial \phi_{01}/\partial y$, which satisfies Laplace's equation, and also the condition $(\partial \phi_{01}/\partial x)_{x=0} = 0$. Such a potential is

$$\phi_{01} = c_0 k_0 (x^2 - z^2) + D c_0 z, \tag{2.23}$$

where D is a constant to be determined. From (2.22),

$$D = -2\gamma^2. \tag{2.24}$$

Therefore

$$\left.\begin{aligned} \phi_{01} &= c_0 k_0 (x^2 - z^2) - 2\gamma^2 c_0 z, \\ \zeta_{01} &= -2\gamma x; \end{aligned}\right\} \tag{2.25}$$

also

$$\frac{\partial U}{\partial x} = \beta \frac{\partial^2 \phi_{01}}{\partial x^2} = 2\beta c_0 k_0 = 2\beta\sigma(1+\gamma)^{-1} \tag{2.26}$$

in accordance with (2.1), since β is assumed small.

The interaction potential

In equations (2.7) the terms in $\alpha\beta$ yield

$$\left.\begin{aligned} \left(\frac{\partial}{\partial t} + U_0 \frac{\partial}{\partial x}\right) \zeta_{11} - \frac{\partial \phi_{11}}{\partial z} + \left(\frac{\partial \phi_{10}}{\partial x}\frac{\partial \zeta_{01}}{\partial x} + \frac{\partial \phi_{01}}{\partial x}\frac{\partial \zeta_{10}}{\partial x}\right) - \left(\zeta_{10}\frac{\partial^2 \phi_{01}}{\partial z^2} + \zeta_{01}\frac{\partial^2 \phi_{10}}{\partial z^2}\right) = 0, \\ g\zeta_{11} + \left(\frac{\partial}{\partial t} + U_0 \frac{\partial}{\partial x}\right) \phi_{11} + \left(\frac{\partial \phi_{10}}{\partial x}\frac{\partial \phi_{01}}{\partial x} + \frac{\partial \phi_{10}}{\partial z}\frac{\partial \phi_{01}}{\partial z}\right) + \zeta_{01}\left(\frac{\partial}{\partial t} + U_0 \frac{\partial}{\partial x}\right)\frac{\partial \phi_{10}}{\partial z} = 0, \end{aligned}\right\} \tag{2.27}$$

to be satisfied when $z = 0$. (Note that $\partial^2 \phi_{01}/\partial t \partial z = \partial^2 \phi_{01}/\partial x \partial z = 0$.) From these equations ζ_{11} may be eliminated by applying the operator $g^{-1}(\partial/\partial t + U_0 \partial/\partial x)$ to the second equation and then subtracting the first. Without substituting explicit expressions for ϕ_{10}, ϕ_{01}, ζ_{10} and ζ_{01} but using (2.12) and (2.21) and the fact that $c\varphi_{10}/\partial z = k_0 \phi_{10}$, we obtain*

$$\begin{aligned} &\frac{1}{g}\left(\frac{\partial}{\partial t} + U_0 \frac{\partial}{\partial x}\right)^2 \phi_{11} + \frac{\partial \phi_{11}}{\partial z} \\ &\quad = 2\left(\frac{\partial \phi_{10}}{\partial x}\frac{\partial \zeta_{01}}{\partial x} + \frac{\partial \phi_{01}}{\partial x}\frac{\partial \zeta_{10}}{\partial x} + k_0 \zeta_{10}\frac{\partial \phi_{01}}{\partial z}\right) - \zeta_{10}\frac{\partial^2 \phi_{01}}{\partial z^2} \quad (z = 0). \end{aligned} \tag{2.28}$$

Now, after substitution from (2.20) and (2.25), the right-hand side of this equation becomes

$$[2ik_0(1 - 2\gamma - 2\gamma^2) - 4k_0^2 x]\,\phi_{10}. \tag{2.29}$$

* In the calculation of ϕ_{11} the complex form of ϕ_{10} can be used, since on the right of (2.28) only products involving ϕ_{10} and ϕ_{01} occur, and ϕ_{01} is real.

As a trial solution let us write

$$\phi_{11} = i(k_1 q + l_1^2 q^2)\,\phi_{10}, \tag{2.30}$$

where $q = z + ix$ and k_1, l_1 are constants to be determined. Then the left-hand side of (2.28), when $z = 0$, reduces to

$$[(1+2\gamma)\,i(k_1 + 2il_1^2 x) - 2i\gamma^2 l_1^2/k_0]\,\phi_{10}. \tag{2.31}$$

On equating coefficients of ϕ_{10} and $x\phi_{10}$ in (2.29) and (2.31) we obtain

$$\left.\begin{aligned} k_1 &= 2k_0\frac{1-4\gamma^2-4\gamma^3}{(1+2\gamma)^2}, \\ l_1^2 &= \tfrac{1}{2}k_0^2\frac{1}{(1+2\gamma)}. \end{aligned}\right\} \tag{2.32}$$

The second of equations (2.27) also gives

$$g\zeta_{11} = [(\gamma k_1 + 2\gamma^2 k_0) - ix(2k_0^2 + 2\gamma k_0^2 - 2\gamma l_1^2 + k_0 k_1) + k_0 l_1^2 x^2]\,c_0\phi_{10}. \tag{2.33}$$

This then is a formal solution of our problem.

Interpretation

Combining (2.33) with (2.20), we have

$$\alpha\zeta_{10} + \alpha\beta\zeta_{11} = \alpha\zeta_{10}\left[1 - i\beta\left(\frac{\gamma k_1}{k_0} + 2\gamma + l_1^2 x^2\right) - 2\beta k_0 x\left(1+\gamma-\frac{\gamma l_1^2}{k_0^2}+\frac{k_1}{2k_0}\right)\right]. \tag{2.34}$$

Correct to order β, this expression may be written

$$\alpha\zeta_{10} + \alpha\beta\zeta_{11} = \alpha i\left(\frac{A}{c_0}\right)\exp\left\{i\left[k_0 x - \beta\left(\frac{\gamma k_1}{k_0} + 2\gamma + l_1^2 x^2\right)\right]\right\} \times\left[1 - 2\beta k_0 x\left(1+\gamma-\frac{\gamma l_1^2}{k_0^2}+\frac{k_1}{2k_0}\right)\right]. \tag{2.35}$$

Now this represents a wave of slowly varying amplitude and wavelength. The local wave-number k is given by the x-derivative of the exponent:

$$k = k_0 - 2\beta l_1^2 x. \tag{2.36}$$

The proportional rate of change of the wave-number at $x = 0$ is therefore

$$\left(\frac{1}{k}\frac{\partial k}{\partial x}\right)_{x=0} = -\frac{2\beta l_1^2}{k_0} = -\frac{4\beta k_0}{1+2\gamma} \tag{2.37}$$

by (2.32). From (2.19) this may be written

$$\left(\frac{1}{k}\frac{\partial k}{\partial x}\right)_{x=0} = -\frac{2}{1+2\gamma}\frac{1}{c_0}\frac{\partial U}{\partial x}. \tag{2.38}$$

The amplitude a of the wave is given by

$$a = \alpha\left(\frac{A}{c_0}\right)\left[1 - 2\beta k_0 x\left(1+\gamma-\frac{\gamma l_1^2}{k_0^2}+\frac{k_1}{2k_0}\right)\right], \tag{2.39}$$

so that the proportional rate of increase is

$$\left(\frac{1}{a}\frac{\partial a}{\partial x}\right)_{x=0} = -2\beta k_0\left(1+\gamma-\frac{\gamma l_1^2}{k_0^2}+\frac{k_1}{2k_0}\right) = -2\beta k_0\frac{2+3\gamma}{(1+2\gamma)^2} \tag{2.40}$$

by equation (2.32), or, from (2.26),

$$\left(\frac{1}{a}\frac{\partial a}{\partial x}\right)_{x=0} = -\frac{2+3\gamma}{(1+2\gamma)^2}\frac{1}{c_0}\frac{\partial U}{\partial x}. \tag{2.41}$$

The mean surface level

Equation (2.25) shows that there is a small change in the mean surface level given by

$$\beta\zeta_{01} = -2\beta\gamma x, \tag{2.42}$$

corresponding to a mean gradient $-2\beta\gamma$, as we should expect in a non-uniform flow. The additional terms $\alpha\zeta_{10}+\alpha\beta\zeta_{11}$ give no change in the mean level. Therefore to order $\alpha\beta$ the mean surface level is unaffected; only at higher approximations is any change apparent.

3. A physical discussion

We have seen that the interaction between the waves and the current can be interpreted as a distortion of the waves, resulting in a change of wavelength and amplitude. In this section we shall try to interpret these changes on the basis of rough physical reasoning.

As before, we denote by σ the angular frequency of the waves (constant over the whole field of motion) and by a, k, U, c the local wave amplitude, wavenumber, stream velocity, and wave velocity relative to the stream. Our object is to obtain a, k and c as functions of U and of their values a_0, k_0, U_0, c_0 in some fixed plane $x = 0$.

The change in wavelength

Consider first the variation in wavelength. Now, the apparent velocity of the waves relative to a fixed plane $x =$ constant is equal to $(c+U)$. The apparent angular frequency of the waves is therefore $k(c+U)$. But by hypothesis this quantity is equal to σ at all points, so that

$$k(c+U) = \sigma = k_0(c_0+U_0). \tag{3.1}$$

Thus

$$\frac{k}{k_0} = \frac{c_0+U_0}{c+U}. \tag{3.2}$$

But the waves being in deep water we expect that their velocities c, c_0 relative to the current will be given by the classical formulae

$$c^2 = g/k, \quad c_0^2 = g/k_0. \tag{3.3}$$

Combining (3.2) and (3.3), we have

$$\frac{c^2}{c_0^2} = \frac{k_0}{k} = \frac{c+U}{c_0+U_0} = \frac{1}{1+\gamma}\left(\frac{c}{c_0}+\frac{U}{c_0}\right), \tag{3.4}$$

where $\gamma = U_0/c_0$ as before. On differentiation with respect to x, we have

$$\frac{2c}{c_0^2}\frac{\partial c}{\partial x} = \frac{1}{1+\gamma}\frac{1}{c_0}\left(\frac{\partial c}{\partial x}+\frac{\partial U}{\partial x}\right), \tag{3.5}$$

and hence at $x = 0$, where $c = c_0$,

$$\frac{\partial c}{\partial x} = \frac{1}{1+2\gamma}\frac{\partial U}{\partial x}. \tag{3.6}$$

Since by (3.4) k varies as c^{-2}, we have (by logarithmic differentiation)

$$\frac{1}{k}\frac{\partial k}{\partial x} = -\frac{2}{c}\frac{\partial c}{\partial x} = -\frac{2}{1+2\gamma}\frac{1}{c}\frac{\partial U}{\partial x} \tag{3.7}$$

in agreement with (2.38).

It will be seen that equation (3.4) is a quadratic in c/c_0, and has the solution

$$\frac{c}{c_0} = \frac{1}{2(1+\gamma)}\left\{1+\sqrt{\left[1+\frac{4(1+\gamma)\,U}{c_0}\right]}\right\} \tag{3·8}$$

(see Unna (1942), for the case $\gamma = 0$). In the square root, the positive sign has been taken to ensure continuity as $x \to 0$. It is interesting to note that no solution can exist when

$$1+\frac{4(1+\gamma)\,U}{c_0} < 0, \tag{3.9}$$

or

$$-U > \frac{c_0}{4(1+\gamma)}, \tag{3.10}$$

that is to say, when the stream velocity is in the opposite direction and exceeds in magnitude about one-quarter of the initial phase velocity of the waves. At the critical point, when the radical vanishes, equation (3·8) shows that

$$\frac{c}{c_0} = \frac{1}{2(1+\gamma)}, \tag{3.11}$$

and so

$$\frac{U}{c} = \frac{U}{c_0}\frac{c_0}{c} = -\tfrac{1}{2}. \tag{3.12}$$

In other words the stream velocity becomes equal and opposite to the local group-velocity $\frac{1}{2}c$; the wave energy can no longer be propagated against the stream. We shall see below that the waves tend to break before this point is reached. From (3.8) we have also

$$\frac{k}{k_0} = \left(\frac{c}{c_0}\right)^{-2} = \left\{\frac{2(1+\gamma)}{1+\sqrt{[1+4(1+\gamma)\,U/c_0]}}\right\}^2. \tag{3.13}$$

The changes in wave amplitude

The change in wave amplitude is interesting, for it enables us to decide between various conflicting hypotheses.

It was shown in I that if waves of amplitude a are propagated over a stream of *uniform* velocity U, the mean rate of energy transfer across a plane $x = \text{const.}$ is given (to order a^2) by

$$\bar{R}_x = E(c_g+U)+S_xU+\tfrac{3}{2}EU^2/c+\tfrac{1}{2}\rho hU^3, \tag{3.14}$$

where E denotes the wave energy per unit horizontal area:

$$E = \tfrac{1}{2}\rho g a^2; \tag{3.15}$$

c_g denotes the group-velocity of the waves; in 'deep' water,

$$c_g = \tfrac{1}{2}c = \tfrac{1}{2}\sigma/k; \tag{3.16}$$

h is the mean depth of the stream, and S_x is defined by

$$S_x = E\left(\frac{2c_g}{c} - \frac{1}{2}\right). \tag{3.17}$$

The first term $E(c_g + U)$ on the right-hand side of (3.14) represents simply the transfer of wave energy by the group-velocity plus the stream velocity, and is to be expected. The last two terms may be written together as $\frac{1}{2}\rho h U'^3$, where

$$U' = U + E/\rho c h \tag{3.18}$$

represents the mean stream velocity modified by the presence of the mass transport. The intermediate term $S_x U$ has been discussed in I. It represents a kind of coupling between the waves and the current. By analogy with the Reynolds stress, S_x has been called the 'radiation stress'.

Now, in the present problem of waves on a non-uniform stream, let us suppose that the transfer of total energy is given with sufficient accuracy by equation (3.14) and further that between the planes $x = 0$ and $x = \text{const.}$ there is no reflexion of wave energy. It follows then that

$$\bar{R}_x = \bar{R}_0 = \text{const.} \tag{3.19}$$

and so

$$\frac{\partial}{\partial x}\bar{R}_x = 0. \tag{3.20}$$

Equation (3.20) is merely an expression of the conservation of the energy, when dissipative mechanisms are ignored. However, it is possible to regard it as the sum of two equations, one representing the balance of wave energy and the other the balance of mean flow energy.

For the exact form of this division, no unique answer is given by physical intuition. (At least *our* initial intuition, as well as that of Unna (1942), Evans (1955), Suthons (1945), Groen & Dorrestein (1958) and Drent (1959) yielded results which sometimes differed from one another but which were all, it as appears, incorrect.) Now, however, we have an arbiter for conflicts of intuition, for the correct division of (3.20) must yield results consistent with § 2.

The first five of the authors just named made the assumption that there was no interchange of energy between waves and current and thus obtained

$$\frac{\partial}{\partial x}[E(c_g + U)] = 0. \tag{3.21}$$

It is clear both from the results of I and from § 2 of the present paper that this assumption cannot be correct.

One might then argue that all the terms dependent on E belong properly to the wave-energy equation, and write

$$\frac{\partial}{\partial x}\left[E(c_g+U)+S_xU+\frac{\frac{3}{2}EU^2}{c}\right]=0, \tag{3.22}$$

or, since the last term may be included with the mean flow,

$$\frac{\partial}{\partial x}[E(c_g+U)+S_xU]=0. \tag{3.23}$$

Each of these equations (3.21), (3.22) and (3.23) yields results in conflict with § 2.

If, on the other hand, it is argued that the effect of the current variation on the wave energy is through the work done by the rate of strain against the radiation stress, then we have

$$\frac{\partial}{\partial x}[E(c_g+U)]+S_x\frac{\partial U}{\partial x}=0. \tag{3.24}$$

Thus, in deep water,

$$\frac{\partial}{\partial x}[E(\tfrac{1}{2}c+U)]+\tfrac{1}{2}E\frac{\partial U}{\partial x}=0. \tag{3.25}$$

Carrying out the differentiation at $x=0$, where $U=\gamma c$, and using equation (3.6), we have

$$\frac{\partial E}{\partial x}[\tfrac{1}{2}c(1+2\gamma)]+E\left[\frac{1}{2(1+2\gamma)}+\frac{3}{2}\right]\frac{\partial U}{\partial x}=0, \tag{3.26}$$

whence

$$\left(\frac{1}{E}\frac{\partial E}{\partial x}\right)_{x=0}=-\frac{4+6\gamma}{(1+2\gamma)^2}\frac{1}{c}\frac{\partial U}{\partial x}, \tag{3.27}$$

or, since E is proportional to a^2,

$$\left(\frac{1}{a}\frac{\partial a}{\partial x}\right)_{x=0}=-\frac{2+3\gamma}{(1+2\gamma)^2}\frac{1}{c}\frac{\partial U}{\partial x} \tag{3.28}$$

in exact agreement with equation (2.41).

It appears then that the correct assumption to make is equation (3.24), rather than the alternatives (3.21) to (3.23). We interpret this as follows:

In a non-uniform current the energy of the waves may be regarded as being transported with the group-velocity plus stream velocity, provided in addition we suppose that the mean stream does work on the waves at a rate $S_x\partial U/\partial x$ per unit distance, where S_x is the radiation stress. Equation (3.24) is then the expression of the energy balance for the waves.

An integral for the wave amplitude

An exact integral of equation (3.25) is

$$E(\tfrac{1}{2}c+U)c=\text{const.}, \tag{3.29}$$

for on differentiating the above and dividing by c, we have

$$\frac{\partial}{\partial x}[E(\tfrac{1}{2}c+U)]+E(\tfrac{1}{2}c+U)\frac{1}{c}\frac{\partial c}{\partial x}=0, \tag{3.30}$$

which by (3.6) is equivalent to (3.25). From equation (3.29) we deduce

$$\frac{E}{E_0} = \frac{c_0(c_0+2U_0)}{c(c+2U)}, \tag{3.31}$$

and thence

$$\frac{a}{a_0} = \left[\frac{c_0(c_0+2U_0)}{c(c+2U)}\right]^{\frac{1}{2}}. \tag{3.32}$$

This law of amplification is illustrated by curve (1) of figure 1. At the critical point, where $U = -\frac{1}{2}c$, the amplification of the waves becomes theoretically infinite. In practice the waves may be expected to break, but the present small-amplitude theory becomes inapplicable before this point is reached.

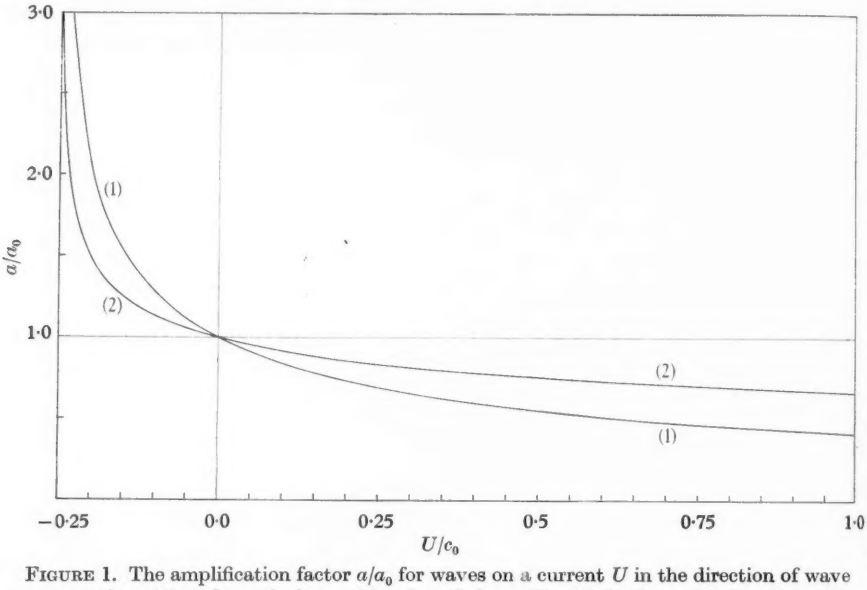

FIGURE 1. The amplification factor a/a_0 for waves on a current U in the direction of wave propagation: (1) with vertical upwelling from below; (2) with horizontal inflow from the sides. [a_0 and c_0 denote the values of a and c when $U = 0$.]

We are indebted to a referee for pointing out that a result similar to (3.29) was derived in an unpublished report by Kreisel (*c.* 1944, pp. 23–24). Kreisel started from the energy integral

$$\overline{\int_{-\infty}^{\zeta} \frac{\partial\phi}{\partial t}\frac{\partial\phi}{\partial x}dz} = \text{const.},$$

and assumed that (in our notation)

$$\phi = Ux - ac\,e^{kz}\cos(kx-\sigma t),$$
$$\zeta = a\sin(kx-\sigma t),$$

where

$$c^2 = gk = (\sigma - kU)^2.$$

Substituting in the integral and treating U, c, a and k as constants during differentiation, one finds eventually

$$\tfrac{1}{2}\sigma a^2 c(c+2U) = \text{const.}$$

(higher powers of a being neglected). Since σ is constant this agrees with (3.29), and indeed provides a physical explanation of that equation. The crux of Kreisel's argument is the assumption that $\partial\phi/\partial t$ contains no constant terms proportional to a^2. This is true for deep water, but not in water of finite depth.

The rules for the variation of wave-number and wave amplitude expressed by (3.13) and (3.32) may be regarded as generalizations of the results found in § 2, the only additional assumptions being that $k^{-1}\partial k/\partial x$ and $a^{-1}\partial a/\partial x$ depend on the local values of U, c and $\partial U/\partial x$ and are linearly proportional to $\partial U/\partial x$.

The analysis of § 2 is correct as far as the first power of $\beta k_0 x$ only. In order to verify that (3.13) and (3.32) are correct to this order we write

$$\frac{U-U_0}{U_0} = \epsilon, \tag{3.33}$$

so that

$$\frac{U}{U_0} = 1+\epsilon, \quad \frac{U}{c_0} = \gamma(1+\epsilon). \tag{3.34}$$

Substituting in equations (3.13) and (3.32) and neglecting ϵ^2 we find, after some reduction,

$$\left.\begin{aligned} \frac{k}{k_0} &= 1-\frac{2\gamma}{1+2\gamma}\epsilon, \\ \frac{a}{a_0} &= 1-\frac{\gamma(2+3\gamma)}{(1+2\gamma)^2}\epsilon, \end{aligned}\right\} \tag{3.35}$$

of which (2.36) and (2.39) will be seen to be special cases.

4. An application to tidal currents

As an example of the application of the general formulae, and as an independent check, we apply the formulae to the case of surface waves on a tidal current, for which a solution was obtained independently in I.

A short wave of mean amplitude a_1, mean wave-number k_1 and frequency σ is assumed to be superposed upon a long (shallow-water) wave of amplitude a_2, wave-number k_2 and frequency σ_2, travelling in the same direction as the first. The conditions of the problem are that

$$\left.\begin{aligned} \sigma_2/\sigma_1 = \lambda \ll 1, \\ k_2 h = \mu \ll 1, \end{aligned}\right\} \tag{4.1}$$

where h is the mean depth of water; also

$$e^{-k_1 h} \ll 1. \tag{4.2}$$

This last assumption ensures that the short waves are effectively in deep water, so that

$$\sigma_1 = (gk_1)^{\frac{1}{2}}, \quad \sigma_2 = (gh)^{\frac{1}{2}}k_2; \quad k_1 h = (\mu/\lambda)^2. \tag{4.3}$$

In the case of tidal currents both λ and μ may be of order 10^{-4} in a typical case, but the ratio μ/λ, $= (k_1 h)^{\frac{1}{2}}$, need not be greater than about 2 in order for the condition (4.2) to be satisfied.

Now let us reduce the long wave to a steady current **U** by superposing on the whole system a uniform stream $-(gh)^{\frac{1}{2}}$. Choosing the origin of x at a node of the longer wave, we have

$$U = -(gh)^{\frac{1}{2}}\left(1-\frac{a_2}{h}\sin k_2 x\right)+O(a^2). \tag{4.4}$$

At $x = 0$ the stream velocity and the velocity of the short waves are given by

$$U_0 = -(gh)^{\frac{1}{2}}; \quad c_0 = (g/k_1)^{\frac{1}{2}}. \tag{4.5}$$

Thus,
$$\gamma = \frac{U_0}{c_0} = -(k_1 h)^{\frac{1}{2}} = -\frac{\mu}{\lambda}. \tag{4.6}$$

Also
$$\epsilon = \frac{U - U_0}{U_0} = -\frac{a_2}{h}\sin k_2 x. \tag{4.7}$$

On substitution in (3.35), we find

$$\left.\begin{aligned} \frac{k}{k_0} &= 1 - \frac{2\mu}{\lambda - 2\mu}\frac{a_2}{h}\sin k_2 x, \\ \frac{a}{a_0} &= 1 - \frac{(2\lambda - 3\mu)}{(\lambda - 2\mu)^2}\frac{\mu}{h}\frac{a_2}{h}\sin k_2 x, \end{aligned}\right\} \tag{4.8}$$

in agreement with equations (2.56) and (2.57) of I.* When μ/λ is sufficiently large, then

$$\left.\begin{aligned} \frac{k}{k_0} &= 1 + \frac{a_2}{h}\sin k_2 x, \\ \frac{a}{a_0} &= 1 + \frac{3}{4}\frac{a_2}{h}\sin k_2 x. \end{aligned}\right\} \tag{4.9}$$

5. Waves on a converging current: no upwelling

In the last three sections we have been concerned with an entirely two-dimensional motion in which the transverse component of the mean current was zero; the increase in the stream velocity with horizontal distance was made up by a compensating current upwelling from below. We now study a somewhat different situation in which the *vertical* component of current vanishes and the increase in the horizontal x-component U is compensated entirely by a horizontal in-flow V from the sides:

$$\frac{\partial U}{\partial x} + \frac{\partial V}{\partial y} = 0. \tag{5.1}$$

The analysis for the asymptotic solution is identical with that in the previous case, § 2, as far as equation (2.22). Now, however, instead of the potential (2.23) we must choose a potential ϕ_{01} to represent a flow having zero vertical component, and satisfying the equation of continuity (5.1). We take

$$\phi_{01} = c_0 k_0 (x^2 - y^2) + D c_0 z, \tag{5.2}$$

and from (2.22) we see that the constant D has to be $-2\gamma^2$ as before. Thus,

$$\left.\begin{aligned} \phi_{01} &= c_0 k_0 (x^2 - y^2) - 2\gamma^2 c_0 z, \\ \zeta_{01} &= -2\gamma x, \end{aligned}\right\} \tag{5.3}$$

and (2.26) still applies.

In the equations (2.27) for the interaction potential, the additional terms all vanish identically, so that (2.28) is still valid; the only difference is that the last term $\zeta_{10}\partial^2\phi_{01}/\partial z^2$ vanishes, and so in place of (2.29) we have

$$[2ik_0(-2\gamma - 2\gamma^2) + 4k_0^2 x]\,\phi_{10}. \tag{5.4}$$

* In equation (2.57) of I, the second term in the curly bracket can be neglected, since $\lambda < \mu \ll 1$.

Now, on equating coefficients between (2.31) and (5.4), we find

$$\left.\begin{aligned} k_1 &= -4k_0\frac{\gamma+2\gamma^2+2\gamma^3}{(1+2\gamma)^2}, \\ l_1^2 &= 2k_0^2\frac{1}{1+2\gamma}. \end{aligned}\right\} \tag{5.5}$$

Since the value of l_1^2 is still the same, equations (2.34) to (2.38) are still applicable and in particular (2.38) shows that we have the same rate of change of the wave-number k as in the previous case.

But, since k_1 has a different value, equation (2.41) must now be replaced by

$$\left(\frac{1}{a}\frac{\partial a}{\partial x}\right)_{x=0} = -\frac{1+\gamma}{(1+2\gamma)^2}\frac{1}{c_0}\frac{\partial U}{\partial x}, \tag{5.6}$$

showing that the change in *amplitude* of the waves is different from the previous case.

6. Physical interpretation

The current U along the x-axis being as in § 3, the changes in wave velocity and wave-number which were derived in that section (by arguments depending only on kinematical considerations) are still given by (3.6) and (3.7). This confirms what was found in § 5 concerning the change in wave-number.

The change in wave amplitude, however, must be related to the equation of energy transfer. Now it was found in I that in the presence of a horizontal stream $\mathbf{U} = (U, V, 0)$ not necessarily in the x-direction, the mean transfer of energy across a vertical plane whose normal is $\mathbf{n} = (l, m, 0)$ is given by

$$\bar{R} = E(\mathbf{c}_g + \mathbf{U}).\mathbf{n} + \mathbf{U}.\mathbf{S}.\mathbf{n} + \tfrac{1}{2}\rho h\mathbf{U}'^2(\mathbf{U}'.\mathbf{n}), \tag{6.1}$$

where $\mathbf{c}_g$ denotes the vector group-velocity, $\mathbf{U}'$ denotes the stream velocity as modified by the mass-transport and $\mathbf{S}$ is a stress tensor. If the x-direction is the direction of wave propagation, then $\mathbf{c}_g = (c_g, 0, 0)$, $\mathbf{U}' = \mathbf{U} + (E/\rho ch, 0, 0)$, and

$$\mathbf{S} = \begin{pmatrix} S_x & 0 & 0 \\ 0 & S_y & 0 \\ 0 & 0 & 0 \end{pmatrix}, \tag{6.2}$$

where S_x is given by (3.17) and

$$S_y = E\left(\frac{c_g}{c} - \frac{1}{2}\right). \tag{6.3}$$

Therefore a natural generalization of equation (3.14) is to assume

$$\nabla.[E(\mathbf{c}_g + \mathbf{U})] + \left[S_x\frac{\partial U}{\partial x} + S_y\frac{\partial V}{\partial y}\right] = 0. \tag{6.4}$$

In other words, the divergence of the energy flux is exactly compensated by work done by the mean current against the radiation stress. In deep water this becomes

$$\frac{\partial}{\partial x}[E(\tfrac{1}{2}c + U)] + \frac{\partial}{\partial y}[EV] + \tfrac{1}{2}E\frac{\partial U}{\partial x} = 0. \tag{6.5}$$

By the symmetry of the flow about the plane $y = 0$, we see that, on the x-axis, $\partial E/\partial y$ vanishes identically, and so making use of (5.1) we have

$$\frac{\partial E}{\partial x}(\tfrac{1}{2}c+U)+\tfrac{1}{2}E\left(\frac{\partial c}{\partial x}+\frac{\partial U}{\partial x}\right)=0. \tag{6.6}$$

On substituting for $\partial c/\partial x$ from (3.6), we find

$$\left(\frac{1}{E}\frac{\partial E}{\partial x}\right)_{x=0}=-\frac{2(1+\gamma)}{(1+2\gamma)^2}\frac{1}{c}\frac{\partial U}{\partial x}, \tag{6.7}$$

from which follows

$$\left(\frac{1}{a}\frac{\partial x}{\partial x}\right)_{x=0}=-\frac{1+\gamma}{(1+2\gamma)^2}\frac{1}{c}\frac{\partial U}{\partial x}, \tag{6.8}$$

in exact agreement with (5.7).

Equation (6.5) may also be written as

$$\frac{\partial}{\partial x}[E(\tfrac{1}{2}c+U)]-\tfrac{1}{2}E\frac{\partial U}{\partial x}=0, \tag{6.9}$$

which has the integral

$$E(\tfrac{1}{2}c+U)/c=\text{const.}, \tag{6.10}$$

as may be verified in the same way as (3.28). Hence, in the present situation,

$$\frac{E}{E_0}=\frac{c(c_0+2U_0)}{c_0(c+2U)}, \tag{6.11}$$

and

$$\frac{a}{a_0}=\left[\frac{c(c_0+2U_0)}{c_0(c+2U)}\right]^{\frac{1}{2}}. \tag{6.12}$$

It will be seen that as the critical point is approached, $a/a_0 \to \infty$ as before.

The amplitude variation corresponding to equation (6.12) is shown in figure 1, curve (2), compared with the corresponding variation in the case of no lateral flow.

7. Waves on currents of arbitrary form

To generalize our previous results, we note that $\mathbf{S}$ is a Cartesian tensor of rank 2, which we may write S_{ij}; equation (6.2) gives S_{ij} in diagonal form, when referred to axes perpendicular and parallel to the local wave front.

The velocity gradients $\partial U/\partial x$ and $\partial V/\partial y$ are also components of the symmetric rate-of-strain tensor

$$\gamma_{ij}=\frac{1}{2}\left(\frac{\partial U_i}{\partial x_j}+\frac{\partial U_j}{\partial x_i}\right), \tag{7.1}$$

and the generalization of the interaction term in the wave-energy equation is $S_{ij}\gamma_{ij}$, which is, of course, an invariant.

Hence the correct generalization of equation (6.4) for steady currents of arbitrary form is

$$\nabla.[E(\mathbf{c}_g+\mathbf{U})]+\tfrac{1}{2}S_{ij}\left(\frac{\partial U_i}{\partial x_j}+\frac{\partial U_j}{\partial x_i}\right)=0. \tag{7.2}$$

For time-varying currents we assume

$$\frac{\partial E}{\partial t}+\nabla.[E(\mathbf{c}_g+\mathbf{U})]+\tfrac{1}{2}S_{ij}\left(\frac{\partial U_i}{\partial x_j}+\frac{\partial U_j}{\partial x_i}\right)=0. \tag{7.3}$$

In the case of purely two-dimensional motion ($\partial/\partial y = 0$), this reduces to

$$\frac{\partial E}{\partial t} + \frac{\partial}{\partial x}[E(\mathbf{c}_g + \mathbf{U})] + S_x \frac{\partial U}{\partial x} = 0, \tag{7.4}$$

an equation that was verified approximately in § 5 of I. In that paper it was not possible to distinguish between equation (7.4) and the same equation with $\partial(S_x U)/\partial x$ replacing $S_x \partial U/\partial x$, since the difference, $(\partial S_x/\partial x)\, U$, was negligibly small. However, the technique adopted in § 4 of the present paper, whereby the long wave was reduced to rest by superposing a finite negative velocity, removes the ambiguity in the final term.

Given the appropriate boundary conditions, equation (7.3) is generally sufficient to determine the variation in the wave-energy density E. From this the variation in wave amplitude may be deduced on the assumption that the relation between amplitude and energy-density is

$$E = \tfrac{1}{2}\rho g a^2 (1 + \dot{W}/2g), \tag{7.5}$$

where $\dot{W}$ denotes the vertical acceleration of a particle carried by the mean current.* (See § 4 of I.) For steady currents we have

$$\dot{W} = \kappa(U^2 + V^2), \tag{7.6}$$

where κ is the curvature of the path of the particle. If $\dot{W}$ is small compared with g then we may take

$$E = \tfrac{1}{2}\rho g a^2, \tag{7.7}$$

as has been assumed throughout this paper.

It may be mentioned that some experiments have recently been performed by Hughes (1960) on the interaction of waves and shear flows. These he has analysed using an assumption equivalent to (7.2), and his results tend to confirm the theory.

8. Waves on a shearing current

As a final example we shall apply the general equation (7.2) to the interesting case of waves traversing a simple horizontal current with vertical axis of shear. This was previously considered by Johnson (1947) without taking into account the transfer of energy between the waves and the current.†

The stream velocity $(0, V, 0)$ is supposed to be everywhere parallel to the y-axis, and also

$$\frac{\partial V}{\partial y} = \frac{\partial V}{\partial z} = 0. \tag{8.1}$$

The wavelength and amplitude of the waves are supposed also to be independent of y. The angle which the waves make locally with the x-axis is denoted by θ (see figure 2).

Purely kinematical considerations yield the following: since the wave-number in the y-direction ($k \sin\theta$) must be independent of x, we have

$$k \sin\theta = m, \tag{8.2}$$

* It is assumed that the current is nearly horizontal.

† Some of the results of this section were obtained by Drent (1959) who, adopting a different approach, was led to make an assumption equivalent to (7.2) in this case.

a constant. Since the apparent velocity of the waves at right-angles normal to their crests is $(c+V\sin\theta)$ and their wave-number is k, the apparent angular frequency of the waves relative to a fixed point is

$$k(c+V\sin\theta)=\sigma, \tag{8.3}$$

also a constant. Thirdly, we have the relation connecting local wave-number and velocity:

$$kc^2=g. \tag{8.4}$$

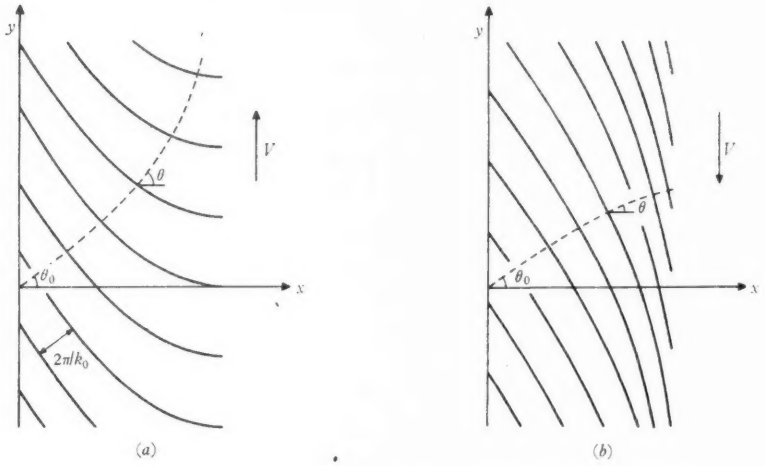

FIGURE 2. Definition diagram for waves on a shearing current, showing the qualitative effect of the current (*a*) when $V>0$, (*b*) when $V<0$.

From equation (8.3), by use of (8.4) and (8.2), it follows that

$$\frac{g}{c}+mV=\sigma, \tag{8.5}$$

or

$$c=\frac{g}{\sigma-mV}. \tag{8.6}$$

Then, from (7.4),

$$k=\frac{(\sigma-mV)^2}{g}, \tag{8.7}$$

and, from (7.2),

$$\sin\theta=\frac{mg}{(\sigma-mV)^2}. \tag{8.8}$$

If c_0, k_0, θ_0 denote the values of c, k, θ when the transverse velocity V vanishes, then we have

$$\left.\begin{aligned}\frac{c}{c_0}&=\frac{1}{1-(V/c_0)\sin\theta_0},\\ \frac{k}{k_0}&=[1-(V/c_0)\sin\theta_0]^2,\\ \sin\theta&=\frac{\sin\theta_0}{[1-(V/c_0)\sin\theta_0]^2}.\end{aligned}\right\} \tag{8.9}$$

Since $\sin\theta$ cannot exceed unity, there is clearly an upper limit to V for which a solution exists:

$$V/c_0 \leqslant \frac{1-(\sin\theta_0)^{\frac{1}{2}}}{\sin\theta_0}. \tag{8.10}$$

At this upper limit θ becomes equal to $\frac{1}{2}\pi$, and the waves are totally reflected by the current.

On the other hand, for negative currents $V < 0$, there is no kinematic limit to V. However, as $V \to -\infty$, k becomes very large, that is to say the wavelength becomes very small (figure 2(*b*)). The angle θ approaches zero, that is, the direction of propagation becomes nearly normal to the current.

Now the vector group-velocity is given by

$$\mathbf{c}_g = \tfrac{1}{2}\mathbf{c} = (\tfrac{1}{2}c\cos\theta,\ \tfrac{1}{2}c\sin\theta). \tag{8.11}$$

Hence equation (7.2) becomes in this case

$$\frac{\partial}{\partial x}[E.\tfrac{1}{2}c\cos\theta] + \frac{\partial}{\partial y}[E(\tfrac{1}{2}c\sin\theta + V)] + \tfrac{1}{2}E\frac{\partial V}{\partial x}\cos\theta\sin\theta = 0. \tag{8.12}$$

Since all derivatives with respect to y vanish identically, we find, on substitution from (8.6) and (8.8),

$$\frac{\partial}{\partial x}\left(\frac{E\cos\theta}{\sigma - mV}\right) + \frac{Em\cos\theta}{(\sigma - mV)^2}\frac{\partial V}{\partial x} = 0, \tag{8.13}$$

of which the integral is

$$\frac{E\cos\theta}{(\sigma - mV)^2} = \text{const.}, \tag{8.14}$$

or, from (8.8),

$$E\cos\theta\sin\theta = \text{const.} \tag{8.15}$$

The relative amplification of the waves is therefore given by

$$\frac{a}{a_0} = \left(\frac{E}{E_0}\right)^{\frac{1}{2}} = \left(\frac{\sin 2\theta_0}{\sin 2\theta}\right)^{\frac{1}{2}}. \tag{8.16}$$

This ratio is shown graphically in figure 3 as a function of V/c_0, for various values of the initial angle θ_0.

Evidently the amplification of the waves becomes infinite both when $\theta \to 90°$ and when $\theta \to 0$. In the first case the infinity is not significant: it is due to the fact that the ray-paths intersect, and the corresponding line $x = \text{const.}$ is a caustic. To the left of this line there are essentially two systems of waves, the incident and transmitted systems, while to the right of it there is a 'shadow zone'. In the neighbourhood of such a line the ordinary approximations of ray optics do not apply; a higher-order theory, generally involving Airy functions, must be used. One may expect that the wave amplitude in fact remains finite even in the neighbourhood of the critical line.

The second case, when $\theta \to 0$, corresponds to the limit $V \to -\infty$. In that case the infinity is genuine and is due mainly to the fact that the wavelength and wave velocity are so much reduced that, in order to maintain the energy flux in the x-direction, the amplitude must increase. In practice the waves may break; but for no finite velocity $V < 0$ is the ratio a/a_0 theoretically infinite.

We may note that it is possible for the component of stream velocity opposite to the waves to exceed the group-velocity:

$$\tfrac{1}{2}c + V\sin\theta < 0. \tag{8.17}$$

The waves are not thereby stopped, for the wave amplitude tends to be diminished by a lateral stretching of the wave crests.

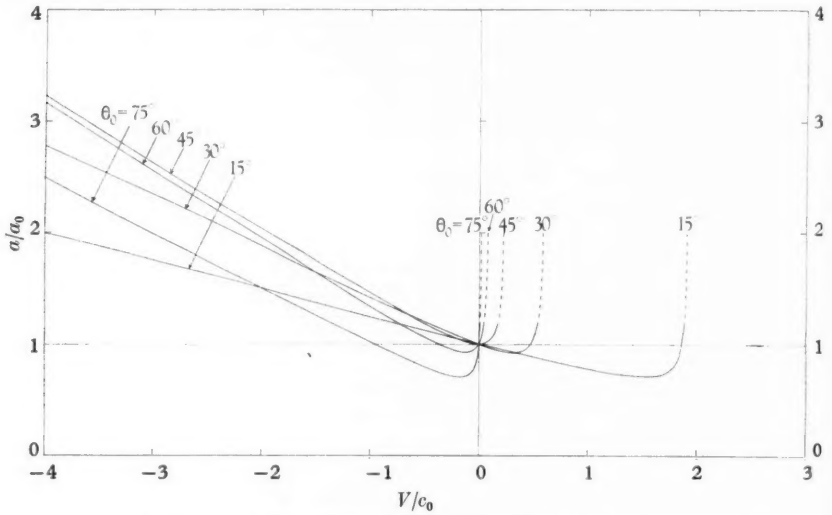

FIGURE 3. The amplification factor for waves crossing a shearing current V at an oblique angle θ, for various angles of entry θ_0.

9. Conclusions

The amplitude of surface waves on non-uniform currents is affected by a non-linear interaction between the waves and the components of the currents; the coupling terms are proportional to the radiation stresses, and the general equation governing the transfer of wave energy is equation (7.3).

Waves travelling on a non-uniform current U that varies in the direction of wave propagation undergo an amplification that is greater than previously supposed, and is dependent on whether the variation in current is made up by a small vertical upwelling from below or by a small horizontal inflow from the sides; this difference is illustrated by the two curves in figure 1.

The amplification of waves on a transverse shearing current has also been calculated. Here the interaction between waves and current also produces an amplification different from that obtained by neglecting the interaction terms.

The results show that the efficiency of a hydraulic or pneumatic breakwater should be affected not only by the surface currents directly opposing the waves but also by the transverse or vertical components of the secondary circulating flow, for these produce different effects on the wave steepening. The absolute limits to the wavelengths that can be transmitted are still set by Taylor's kinematical theory (1955). But for waves longer than the critical wavelength,

whether breaking occurs must depend on the amplification factor. We suggest that differences in the secondary circulation may account for some of the anomalies in past experimental work, both on models and on prototypes.

Since the currents have been seen to do work on the waves, then we would expect the waves also to react on the currents. From (6.1), by conservation of the total energy, one would expect for steady currents

$$\nabla.[E(\mathbf{c}_g+\mathbf{U})+\mathbf{S}.\mathbf{U}+(\tfrac{1}{2}\rho h\mathbf{U}'^2)\,\mathbf{U}'] = 0. \tag{9.1}$$

Hence, on subtracting (7.2) and using the fact that S_{ij} is symmetric, we have

$$\nabla.[(\tfrac{1}{2}\rho h\mathbf{U}'^2)\,\mathbf{U}'] + U_i\frac{\partial S_{ij}}{\partial x_j} = 0. \tag{9.2}$$

A fuller account of equation (9.2) will be given subsequently.

REFERENCES

Drent, J. 1959 A study of waves in the open ocean and of waves on shear currents. Ph.D. Thesis, University of British Columbia, Vancouver.

Evans, J. T. 1955 Pneumatic and similar breakwaters. *Proc. Roy. Soc.* A, **231**, 457–66.

Groen, P. & Dorrestein, R. 1958 Zeegolven. *Kon. Ned. Met. Inst.* Publ. 111–11.

Hughes, B. A. 1960 Interaction of waves and a shear flow. M.A. Thesis, University of British Columbia, Vancouver.

Johnson, J. W. 1947 The refraction of surface waves by currents. *Trans. Amer. Geophys. Un.* **28**, 867–74.

Kreisel, G. *c.* 1944 Surface waves. *Admiralty Report SRE/Wave/*1.

Longuet-Higgins, M. S. & Stewart, R. W. 1960 Changes in the form of short gravity waves on long waves and tidal currents. *J. Fluid Mech.* **8**, 565–83.

Straub, L. G., Bowers, C. E. & Tarrapore, Z. S. 1959 Experimental studies of pneumatic and hydraulic breakwaters. *Univ. Minnesota, St Anthony Falls Lab., Tech. Papers*, no. 25, Ser. B.

Suthons, C. T. 1945 (revised 1950) Forecasting of sea and swell waves. *Admiralty, Naval Weather Service Dep.*, Memo. no. 135/45. Also *N.W.S. Memos.* nos. 180/52 and 135B/58.

Taylor, G. I. 1955 The action of a surface current used as a breakwater. *Proc. Roy. Soc.* A, **231**, 466–78.

Unna, P. J. H. 1942 Waves and tidal streams. *Nature, Lond.*, **149**, 219–20.

Ursell, F. 1960 Steady wave patterns on a non-uniform steady fluid flow. *J. Fluid Mech.* **9**, 333–46.

Wind tunnel measurements of sphere drag at supersonic speeds and low Reynolds numbers

By PETER P. WEGENER† AND HARRY ASHKENAS

Jet Propulsion Laboratory, California Institute of Technology, Pasadena, California

(Received 23 January 1961)

Sphere drag has been measured in a low-density supersonic wind tunnel by a simple displacement technique. A conical nozzle of fixed geometry, operated at a constant supply temperature of about 300 °K was used. Test section Mach numbers ranged between 3·8 and 4·3 depending on supply pressure. The Reynolds number and Knudsen number range, based on free-stream conditions and sphere diameter, were $50 < Re_\infty < 1000$ and $0{\cdot}106 < Kn_\infty < 0{\cdot}006$, respectively. This range was achieved by varying sphere size and supply pressure. The drag coefficient was found to increase from a value of $C_D = 1{\cdot}17$ at $Re_\infty = 1000$ to $C_D = 1{\cdot}73$ at $Re_\infty = 50$.

1. Introduction

The determination of sphere drag has long been a classical problem in aerodynamics. Unfortunately, few reliable experimental results are available at supersonic speeds and at Reynolds numbers below about 2000. We find in the literature the pioneering low density supersonic wind tunnel experiments by Kane (1951), Sherman (1951), and Jensen (1951) of the University of California at Berkeley covering a Reynolds number range from $Re_\infty = 10$ to that characteristic of the continuum regime for $2 < M < 2{\cdot}8$. In the early days of low-density experiments, however, incomplete knowledge of the flow structure in the test section with resulting uncertainties about the sphere wake (and hence the base drag) cast some doubt on the results reported in Kane (1951), Sherman (1951), and Jensen (1951).‡ Other results have been obtained in firing ranges by May (1957) and May & Witt (1953), of the U.S. Naval Ordnance Laboratory down to $Re_\infty = 1140$ and $Re_\infty = 485$, respectively, for $0{\cdot}82 < M < 4{\cdot}69$. The scatter of firing range data obtained at low Reynolds numbers is relatively large because of the small decrease of flight speed in the range at the low densities. The sphere surface temperature of the Berkeley wind tunnel experiments may be taken to be constant and equal to a mean recovery temperature close to the supply temperature. The range data surface temperatures are undetermined, and, depending on the sphere material, the time of flight, and the ambient density, they range from room temperature to flight temperatures.

There are no complete calculations of sphere drag in the transitional flight régime between continuum and free-molecule flows. Free-molecule results are

† Now at Yale University, New Haven, Connecticut.

‡ Private communication from Prof. F. Sherman, University of California, Berkeley, California.

available from the analytical work of Heineman (1948), who considered the limiting cases of diffuse and specular reflexion in supersonic flow, arriving at values of the drag coefficient, much above the continuum value ($C_D \simeq 1$) for supersonic speeds.

In order to resolve this unsatisfactory state of affairs and to gain a basis for comparison with future theoretical work, it was decided to measure again sphere drag in the transitional flow régime. In particular, a simple method not involving a balance system appeared appropriate to determine the very low values of the drag. This technique consisted of measuring the deflexion of a sphere of known weight and diameter in the supersonic air stream of a low-density tunnel.

2. Experimental methods

The experiments were conducted in the low-density gas dynamics facility, illustrated in figure 1, at the Jet Propulsion Laboratory. Continuous flow in a Mach number range of 3·8–4·3 for free-stream static pressures of 30–100 μ can

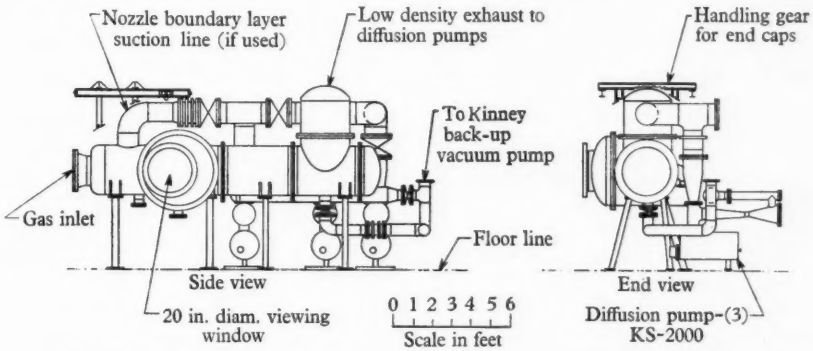
Nozzle boundary layer suction line (if used)
Low density exhaust to diffusion pumps
Handling gear for end caps
To Kinney back-up vacuum pump
Gas inlet
Floor line
Side view
End view
20 in. diam. viewing window
0 1 2 3 4 5 6
Scale in feet
Diffusion pump-(3) KS-2000

FIGURE 1. Jet propulsion laboratory low-density gas dynamics facility.

be achieved for dry air initially at room temperature. The nozzle exit and the traversing mechanism with a Pitot pressure probe installed are shown in figure 2, plate 1. This system allows traversing in three mutually perpendicular directions; 10 in. of travel are available in the horizontal and vertical cross-flow directions for a fixed position of the base of the system. The device is equipped with reversing motors and two-speed magnetically engaged transmissions; counters on the precision lead screws may be used to determine position to the nearest 0·001 in., or, alternatively, an analog position signal is provided by linear potentiometers.

A simple conical supersonic nozzle with an exit diameter of 2·28 in. was used for the experiments. The usable width of the isentropic core of the flow and, correspondingly, the flow Mach number depend on the supply pressure as seen in the pitot pressure profiles taken at right angles to the flow and 0·5 in. downstream from the nozzle exit (figure 3). The pitot pressure p_0' was measured with a U-tube silicone-oil manometer in the tunnel (figure 2); the fluid level height was determined with an external cathetometer. The pitot tube diameter was chosen to

be large enough to ensure the absence of viscous effects according to the criteria established by Sherman (1955). The supply pressure p_0 was determined with a Betz manometer filled with silicone oil, and the flow Mach number of the isentropic core was found from the ratio p_0'/p_0, using an isentropic flow table. All other required flow parameters were also found from the flow table and the measured supply conditions. Since the conical nozzle does not produce uniform flow in the test section, the Mach number increases with distance in the x-direction. In figure 4, the variation of centreline Mach number with supply pressure is seen clearly. The calibration data of figures 3 and 4 are used to determine all flow conditions shown subsequently, and a given free-stream value was assigned to the stagnation point of the sphere.

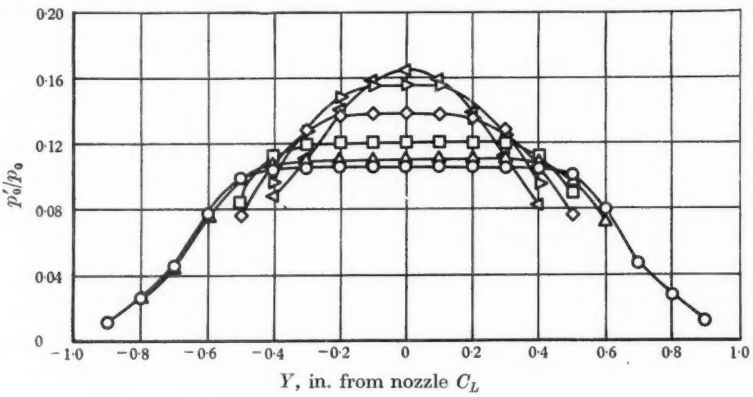

FIGURE 3. Pitot pressure profiles; horizontal traverse across jet; $\frac{1}{2}$ in. downstream from nozzle exit. $T_0 = 300$ °K.

	p_0 mm Hg	p_∞ μ Hg	$M_\infty(p_0'/p_0)$
○	15·81	93	4·322
△	13·76	85	4·279
□	10·34	73	4·171
◇	6·89	61	4·008
▷	5·16	51	3·869
◁	3·46	48	3·784

The method of drag determination is shown schematically in figure 5. A steel or bronze ball-bearing is suspended from the traversing mechanism on a fine (0·00015 to 0·001 in. diameter) tungsten wire; the sphere stagnation point is located $\frac{1}{2}$ in. downstream from the nozzle exit on the nozzle centreline. The air is then turned on and the sphere is blown downstream until an equilibrium position, determined by the drag and weight, is reached. The traversing mechanism is used next to return the sphere to its original, undeflected position, and the distance travelled is found on the traverse counter as Δx in figure 5.

The sphere is stabilized in the airstream by suspending a second damping sphere immersed in an oil bath outside the airstream below the model. In order to specify the geometry completely, the length of the suspension wire, L, is measured

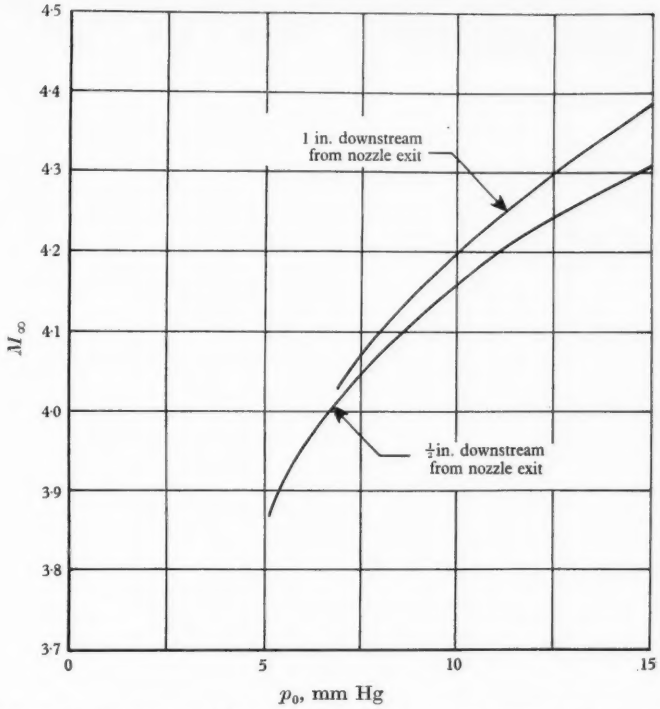

FIGURE 4. Free-stream Mach number dependence on stagnation pressure. 295 °K $\leqslant T_0 \leqslant$ 300 °K.

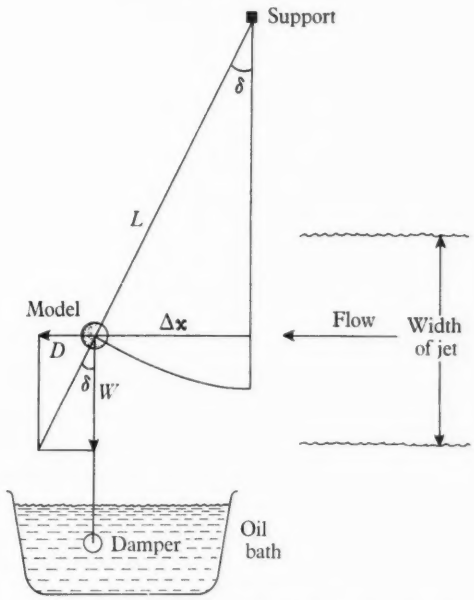

FIGURE 5. Geometry of sphere-drag measurement.

with a cathetometer. The total drag of the sphere and suspension wire D_T is determined from the measured geometry and the measured weight of model plus damper, W.

Thus, we have

$$D_T = (W - b)\tan(\sin^{-1}\Delta x/L), \tag{1}$$

where $D_T = D_{\text{wire}} + D_{\text{sphere}}$ and b = buoyancy force on damper-sphere $= V_d \rho_{\text{oil}}\, g$ = (damper-sphere volume) (density of oil) (acceleration of gravity).

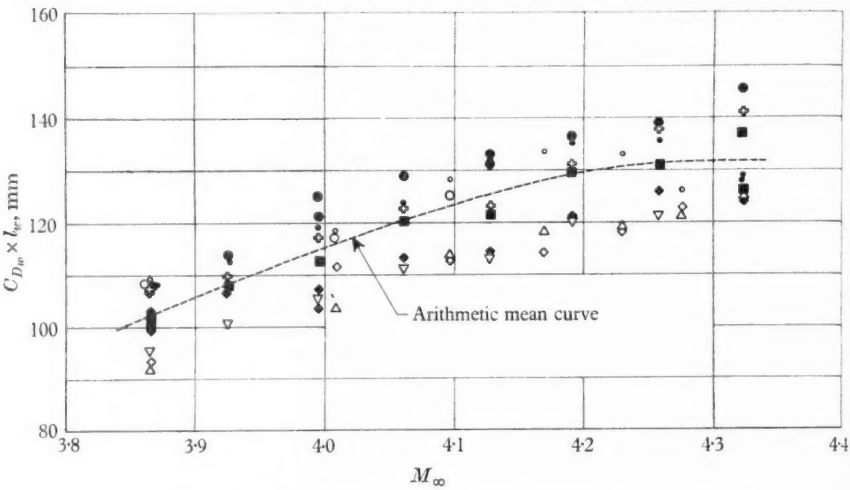

FIGURE 7. Support-wire drag coefficient. Wire diameter, in.: ◇, ◆, 0·001; ○, ●, 0·00068; △, ▽, 0·0005; ○, ●, 0·0003; ✣, 0·00015; □, ■, 0·0002.

In order to separate the wire drag from that of the sphere, measurements of the wire drag alone were made, as illustrated in figure 6, plate 2. The wire was suspended from the traversing mechanism, and a nylon sphere was used to damp the motion of the wire. As the photograph shows, the wire is blown by the airstream to some equilibrium position; the balance of forces on the wire is determined by the angle assumed by the upper straight portion of the wire and the measured weight of wire and damper. An optical comparator is used to determine the angular position from a photographic negative by reference to the plumb bob shown. The wire-drag data were reduced to the wire-drag coefficient shown as a function of Mach number in figure 7. The wire-drag coefficient is defined by

$$C_{D_w} = D_w/(q_\infty\, l_w d_w), \tag{2}$$

where l_w = wire length, d_w = wire diameter, D_w = wire drag, and q_∞ = free-stream dynamic pressure. The scatter in these data is of the order of $\pm 10\,\%$, thus in order to minimize the effect of wire-drag uncertainty on the sphere-drag results, the wire size was reduced as sphere size decreased; in any case, for the results reported here, the wire drag never exceeded 15 % of the total drag D_T. The Knudsen number of the wires, based on free-stream conditions, ranged from 6 to

43; therefore, in principle, wire drag may be computed from free-molecule theory, e.g. for adiabatic surface conditions and diffuse reflexion. Such a comparison was, however, unsuccessful at the lower Mach numbers with the correspondingly large boundary-layer thicknesses through which the wire extended; therefore the current corrections are purely empirical.

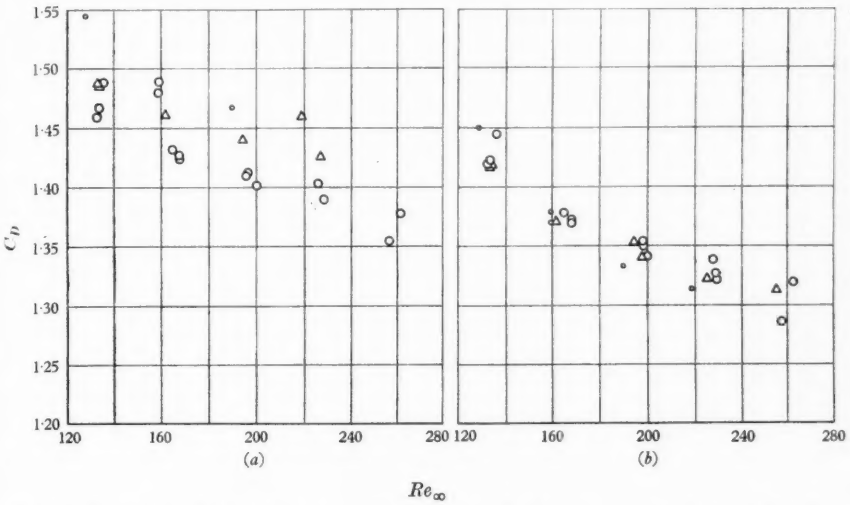

FIGURE 8. Effect of wire-drag correction on drag of $\frac{5}{32}$ in. diameter sphere. Wire diameter, in.: ○, 0·00068; △, 0·0005; ○, 0·0003. (*a*) Uncorrected for wire drag. (*b*) Corrected for wire drag; wire drag obtained by direct measurement.

The drag coefficient of the sphere is defined by

$$C_D = \frac{D_s}{q_\infty A_s}, \tag{3}$$

where A_s is the cross-sectional area of the sphere. Combining (1) and (3) and including the correction for the drag of the supporting wire, the drag coefficient becomes

$$C_D = \frac{4}{\pi d_s^2}\left[\frac{(W-b)\tan(\sin^{-1}\Delta x/L)}{q} - C_{D_w} l_w d_w \left(\frac{l_w - d_s}{l_w}\right)\right], \tag{4}$$

where d_s is the diameter of the sphere, and the correction for finite support drag is modified by the masking effect of the sphere on the wire; l_w is taken arbitrarily as the jet width where the dimensionless pitot-pressure plotted in figure 3 had dropped to 90 % of its centreline value.

The magnitude of the wire-drag correction in a restricted Reynolds number range is shown in figure 8, where a comparison is made between corrected and uncorrected drag data.

3. Results and discussion

Excerpts of the results for the series of experiments reported here are shown in table 1. In addition to the final corrected drag coefficient C_D, the free-stream Mach number M_∞, the supply temperature T_0, the free-stream Reynolds number Re_∞, the free-stream Knudsen number Kn_∞, the Reynolds number based on conditions behind the shock wave Re_s, and the Knudsen number behind the shock wave Kn_s are presented. For the calculation of Re_s, the viscosity was based on

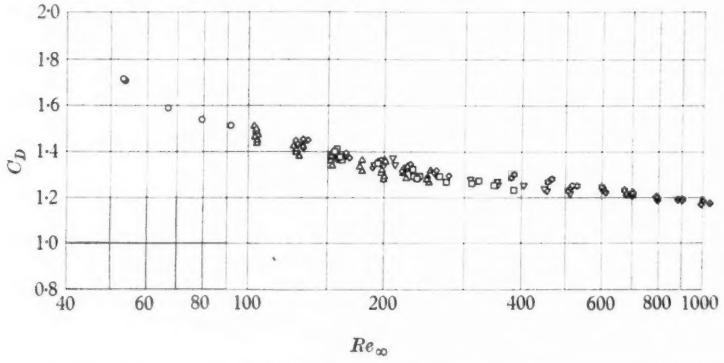

FIGURE 9. Sphere drag; $3{\cdot}8 \leqslant M_\infty \leqslant 4{\cdot}3$; $0{\cdot}013 \leqslant Kn \leqslant 0{\cdot}200$. Sphere diameter in.: ○, $\frac{1}{16}$; △, $\frac{1}{8}$; ◇, $\frac{5}{32}$; □, $\frac{3}{16}$; ▽, $\frac{1}{4}$; ✲, $\frac{3}{8}$; ✣, $\frac{1}{2}$.

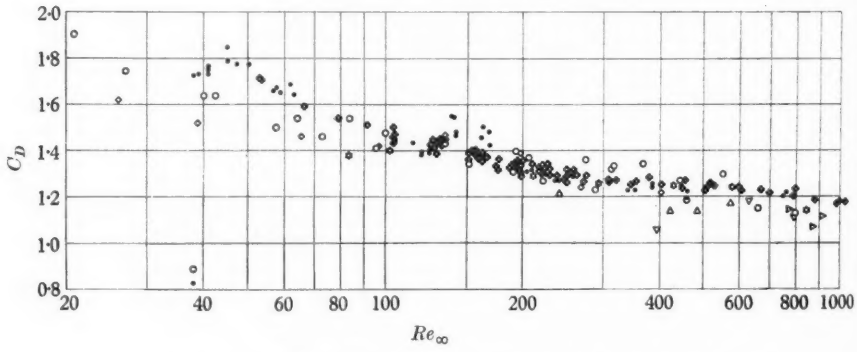

FIGURE 10. Sphere drag; present data compared with earlier investigations.

	M_∞	
○	$2{\cdot}0 < M < 2{\cdot}99$	Wind tunnel data
∘	$2{\cdot}0 < M < 2{\cdot}99$	
◇	$2{\cdot}0 < M < 2{\cdot}99$	
✲	$3{\cdot}0 < M < 3{\cdot}99$	
△	$1{\cdot}0 < M < 1{\cdot}99$	Range data
▽	$2{\cdot}0 < M < 2{\cdot}99$	
▷	$3{\cdot}0 < M < 3{\cdot}99$	
✣	$3{\cdot}8 < M < 4{\cdot}30$	This report: wind tunnel data.

Sphere diameter d_s, in.	T_0, °C	M_∞	Re_∞	Re_s	Kn_∞	Kn_s	C_D
$\frac{1}{16}$	20·1	3·865	53·4	15·5	0·1071	0·0419	1·713
	19·1	3·865	53·6	15·5	0·0167	0·0419	1·709
	19·3	4·007	66·3	18·2	0·0894	0·0354	1·593
	19·6	4·097	79·0	21·0	0·0767	0·0305	1·543
	19·8	4·170	91·3	23·6	0·0675	0·0270	1·508
$\frac{1}{8}$	24·9	3·865	104	30·3	0·0550	0·0214	1·506
	24·9	3·865	104	30·3	0·0550	0·0214	1·498
	24·3	3·862	104	30·3	0·0550	0·0214	1·463
	24·0	3·864	104	30·3	0·0550	0·0214	1·450
	24·2	3·867	105	30·6	0·0545	0·0212	1·511
	22·4	3·866	105	30·4	0·0545	0·0214	1·473
	22·5	3·860	105	30·6	0·0544	0·0212	1·438
	24·8	4·007	127	35·0	0·0467	0·0184	1·428
	24·0	4·008	128	35·2	0·0463	0·0183	1·415
	24·3	4·008	128	35·3	0·0463	0·0182	1·402
	22·5	4·008	130	35·8	0·0456	0·0180	1·383
	24·0	4·096	152	40·6	0·0399	0·0158	1·361
	24·0	4·096	152	40·6	0·0399	0·0158	1·350
	24·9	4·096	154	41·1	0·0394	0·0156	1·396
	22·5	4·097	154	41·0	0·0394	0·0156	1·343
	24·1	4·169	176	45·4	0·0350	0·0140	1·337
	22·5	4·170	177	45·7	0·0349	0·0139	1·316
	24·8	4·169	178	46·1	0·0347	0·0138	1·373
	24·1	4·230	199	50·3	0·0314	0·0123	1·324
	24·1	4·299	199	50·3	0·0314	0·0126	1·316
	24·8	4·230	201	50·8	0·0311	0·0125	1·359
	22·5	4·230	201	50·6	0·0311	0·0126	1·300
	22·5	4·230	201	50·6	0·0311	0·0126	1·292
	24·3	4·276	221	54·8	0·0286	0·0116	1·312
	22·5	4·276	223	55·3	0·0284	0·0114	1·288
	24·9	4·276	225	56·0	0·0281	0·0113	1·343
	24·3	4·323	248	60·5	0·0258	0·0104	1·281
	22·7	4·325	250	61·0	0·0256	0·0104	1·267
	24·9	4·323	252	61·5	0·0254	0·0103	1·324
$3\frac{5}{32}$	26·8	3·863	128	37·4	0·0447	0·0174	1·452
	26·1	3·864	129	37·7	0·0443	0·0172	1·430
	20·6	3·866	133	38·6	0·0430	0·0168	1·446
	20·8	3·866	133	38·6	0·0430	0·0168	1·425
	20·1	3·866	134	38·9	0·0427	0·0167	1·452
	18·6	3·867	134	38·9	0·0427	0·0167	1·418
	17·4	3·867	136	39·3	0·0421	0·0165	1·447
	26·5	4·007	159	43·9	0·0373	0·0146	1·370
	20·7	4·008	165	45·4	0·0360	0·0142	1·394
	21·0	4·008	165	45·4	0·0360	0·0142	1·380
	17·6	4·010	168	46·0	0·0353	0·0140	1·371
	26·6	4·096	190	50·7	0·0319	0·0126	1·336
	19·1	4·098	195	51·7	0·0311	0·0124	1·355
	21·2	4·097	196	52·1	0·0309	0·0123	1·353
	17·8	4·098	200	53·0	0·0303	0·0121	1·342
	26·7	4·169	220	57·0	0·0280	0·0112	1·328

TABLE 1. Sphere drag data

Sphere diameter d_s, in.	T_0, °C	M_∞	Re_∞	Re_s	Kn_∞	Kn_s	C_D
$\frac{5}{32}$	19·1	4·171	225	57·8	0·0274	0·0110	1·324
	21·3	4·170	226	58·3	0·0273	0·0109	1·340
	20·8	4·170	228	58·8	3·0271	0·0108	1·344
	26·7	4·229	249	63·0	0·0251	0·0101	1·290
	18·1	4·231	262	66·0	0·0239	0·00962	1·321
	26·7	4·275	278	69·2	0·0228	0·00915	1·298
	27·0	4·322	312	76·4	0·0203	0·00827	1·275
$\frac{3}{16}$	24·2	3·866	157	45·7	0·0364	0·0142	1·399
	21·8	3·865	158	46·0	0·0362	0·0141	1·398
	17·8	3·867	162	46·8	0·0353	0·0139	1·360
	24·3	4·007	194	53·5	0·0306	0·0120	1·345
	18·1	4·009	201	55·1	0·0295	0·0117	1·304
	24·4	4·097	232	61·9	0·0261	0·0103	1·391
	24·4	4·097	232	61·9	0·0261	0·0103	1·317
	18·8	4·098	239	63·3	0·0254	0·0101	1·282
	18·3	4·098	240	63·6	0·0253	0·0101	1·289
	24·4	4·169	265	68·4	0·0233	0·0093	1·293
	18·6	4·171	276	70·9	0·0224	0·0089	1·270
	18·6	4·231	313	78·9	0·0200	0·0080	1·264
	18·8	4·231	313	78·9	0·0200	0·0080	1·258
	18·6	4·277	350	86·8	0·0181	0·0073	1·248
	19·0	4·324	392	95·2	0·0163	0·0066	1·229
$\frac{1}{4}$	23·7	3·865	209	60·8	0·0274	0·01067	1·374
	22·3	3·867	212	61·5	0·0270	0·01055	1·342
	23·8	4·009	255	70·1	0·0233	0·00917	1·306
	22·3	4·009	262	72·0	0·0226	0·00893	1·301
	23·8	4·097	310	82·8	0·0196	0·00773	1·277
	23·7	4·169	358	92·4	0·0172	0·00689	1·265
	22·6	4·171	361	93·1	0·0171	0·00684	1·259
	23·7	4·230	406	102	0·0154	0·00623	1·252
	23·5	4·276	453	112	0·0140	0·00566	1·235
	22·6	4·276	456	113	0·0139	0·00561	1·229
	22·7	4·323	506	123	0·0126	0·00514	1·218
$\frac{3}{8}$	25·6	4·007	385	106	0·0154	0·00607	1·287
	25·6	4·096	460	123	0·0132	0·00520	1·269
	24·9	4·096	462	123	0·0131	0·00520	1·267
	25·6	4·169	532	138	0·0116	0·00462	1·254
	24·8	4·170	534	138	0·0116	0·00462	1·249
	25·6	4·229	602	152	0·0104	0·00418	1·244
	24·6	4·230	605	153	0·0103	0·00415	1·241
	25·5	4·275	672	167	0·0094	0·00379	1·227
	24·6	4·275	676	168	0·0094	0·00377	1·227
$\frac{1}{2}$	26·5	4·007	509	140	0·0116	0·00460	1·254
	26·2	4·007	512	141	0·0116	0·00456	1·247
	26·2	4·096	612	163	0·0099	0·00393	1·226
	26·5	4·169	704	182	0·0088	0·00350	1·220
	26·2	4·169	707	183	0·0087	0·00348	1·213
	27·5	4·229	794	202	0·0079	0·00314	1·206
	26·2	4·228	800	202	0·0078	0·00314	1·197
	26·1	4·275	894	223	0·0071	0·00284	1·190
	26·1	4·322	1004	246	0·0064	0·00257	1·177

TABLE 1 (*cont.*)

T_s, the free-stream temperature behind the normal shock wave. Viscosity, where it enters the above parameters, was determined as a function of temperature from Sutherland's law for $T > 110{\cdot}4\,^{\circ}\mathrm{K}$. For temperatures below $110{\cdot}4\,^{\circ}\mathrm{K}$, Van Driest's approximation (1954), in which the viscosity-temperature relation is taken to be the tangent to the Sutherland curve at $110{\cdot}4\,^{\circ}\mathrm{K}$, was used. The sphere-drag coefficient is shown in figure 9 as a function of free-stream Reynolds number for spheres of different sizes. In figure 10 these results are compared with those previously cited. It is seen that the scatter of the current experiments is generally satisfactory and that the results for $Re_\infty > 100$ agree with the range of the older experimental findings. At the low Reynolds numbers, the present results appear to give an upper bound of the data.

There clearly exists the need for further data at even lower Reynolds numbers. The data of table 1 have been plotted with the drag coefficient as a function of free-stream Knudsen number and of Reynolds and Knudsen numbers based on conditions behind the shock. These curves are not shown here, as no improvement in the correlation is to be noted. However, the flow state was known well enough to permit the calculation of these variables, and they are included for later use when comparisons with results obtained in high-temperature facilities become available. Such results ought to be correlated on the basis of conditions behind the shock-wave.

Finally, several practical points concerning these experiments must be noted.

1. The pull on the damper sphere wire due to surface tension in the oil at the oil surface may be neglected.

2. The Mach number gradient in the tunnel airstream of 0·1/in. has no noticeable effect on the drag of the smaller diameter spheres, as evidenced by the complete overlap of the drag data for these models as seen in figure 9. The larger models (e.g. those of $\frac{1}{2}$ and $\frac{3}{8}$ in. diameter) exhibit a small but definite deviation in the overlapping ranges. This may be partially due to the Mach number gradient; additionally, the model size approaches the core diameter of the stream, and this also gives rise to error. No jet boundary interference corrections have been applied to the present data.

3. Drag measurements obtained after several hours of continuous tunnel operation showed no sensible deviation from values obtained after only 10 minutes of operation. Therefore it is presumed that all the measurements presented represent the equilibrium wall temperature drag, although no attempts were made to measure the surface temperature of the model.

This paper presents the results of one phase of research carried out at the Jet Propulsion Laboratory, California Institute of Technology, under joint sponsorship of the Department of the Army, Ordnance Corps (under contract no. Da-04-495-Ord 18), and the Department of the Air Force.

The authors wish to acknowledge the work of H. N. Riise, who provided the nozzle calibration data, S. B. Wheeler, whose painstaking construction of the model suspensions is in large measure responsible for the success of the experiments, and A. C. Bouck, whose operation of the tunnel and assistance in the measurements is greatly appreciated.

REFERENCES

HEINEMAN, M. 1948 Theory of drag in highly rarefied gases. *Comm. Appl. Math.* **1**, 259–73.

JENSEN, N. A. 1951 Supplementary data on sphere drag tests. Part 2. *Univ. Calif., Inst. Engng. Res.* HE-150-92.

KANE, E. D. 1951 Sphere drag data at supersonic speeds and low Reynolds numbers. *J. Aero. Sci.* **18**, 259–70.

MAY, A. 1957 Supersonic drag of spheres at low Reynolds numbers in free flight. *J. Appl. Phys.* **28**, 910–12.

MAY, A. & WITT, W. R. 1953 Free flight determinations of the drag coefficients of spheres. *J. Aero. Sci.* **20**, 635–38.

SHERMAN, F. S. 1951 Note on sphere drag data. *J. Aero. Sci.* **18**, 566.

SHERMAN, F. S. 1955 New experiments on impact pressure interpretation in supersonic and subsonic rarefied airstreams. *NACA TN* 2995.

VAN DRIEST, E. R. 1954 The laminar boundary layer with variable fluid properties. *Report AL-1866, North American Aviation Co., Downey, California.*

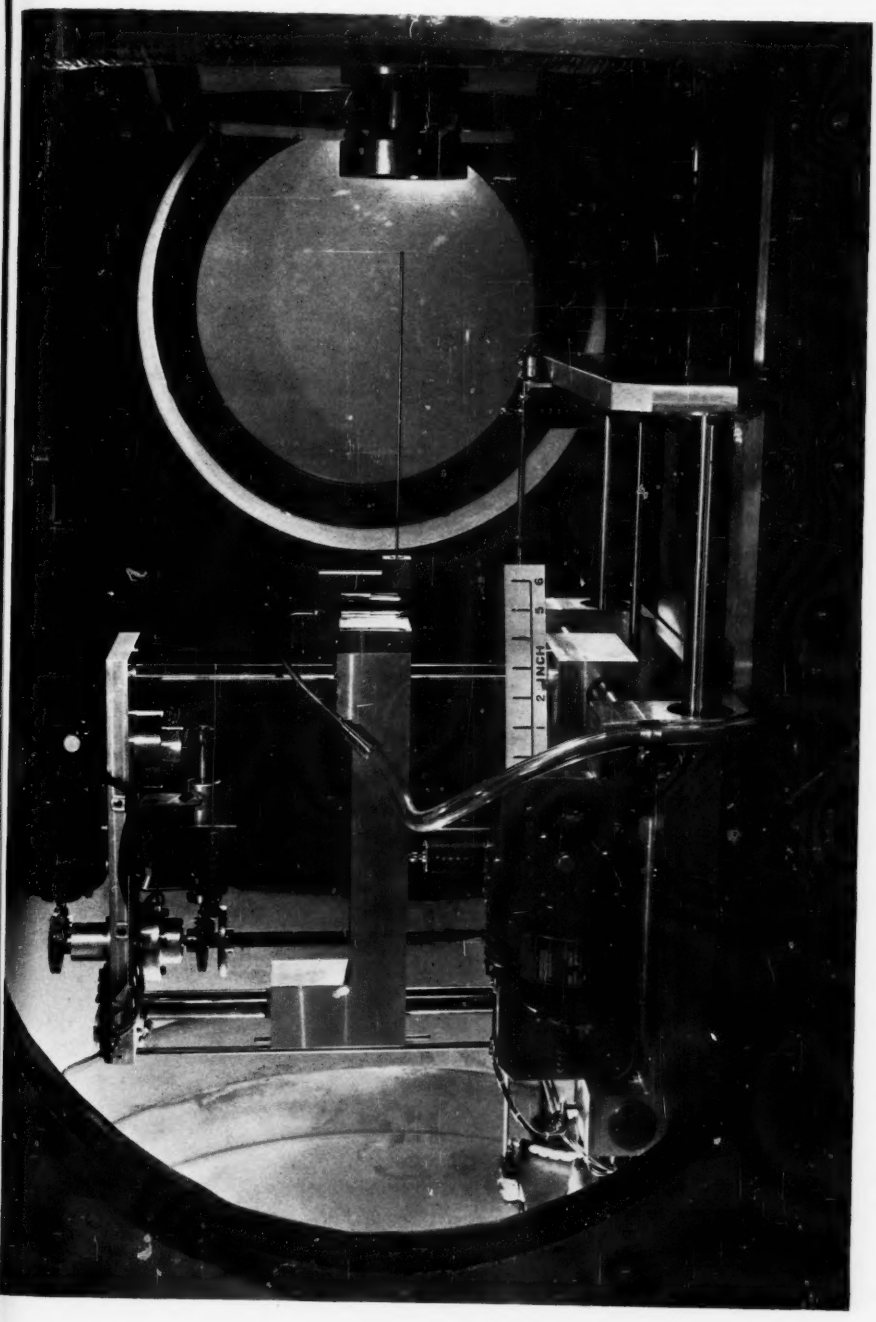

FIGURE 2. Traversing mechanism with instrumentation for tunnel calibration; $M = 4$ (nominal) nozzle at right.

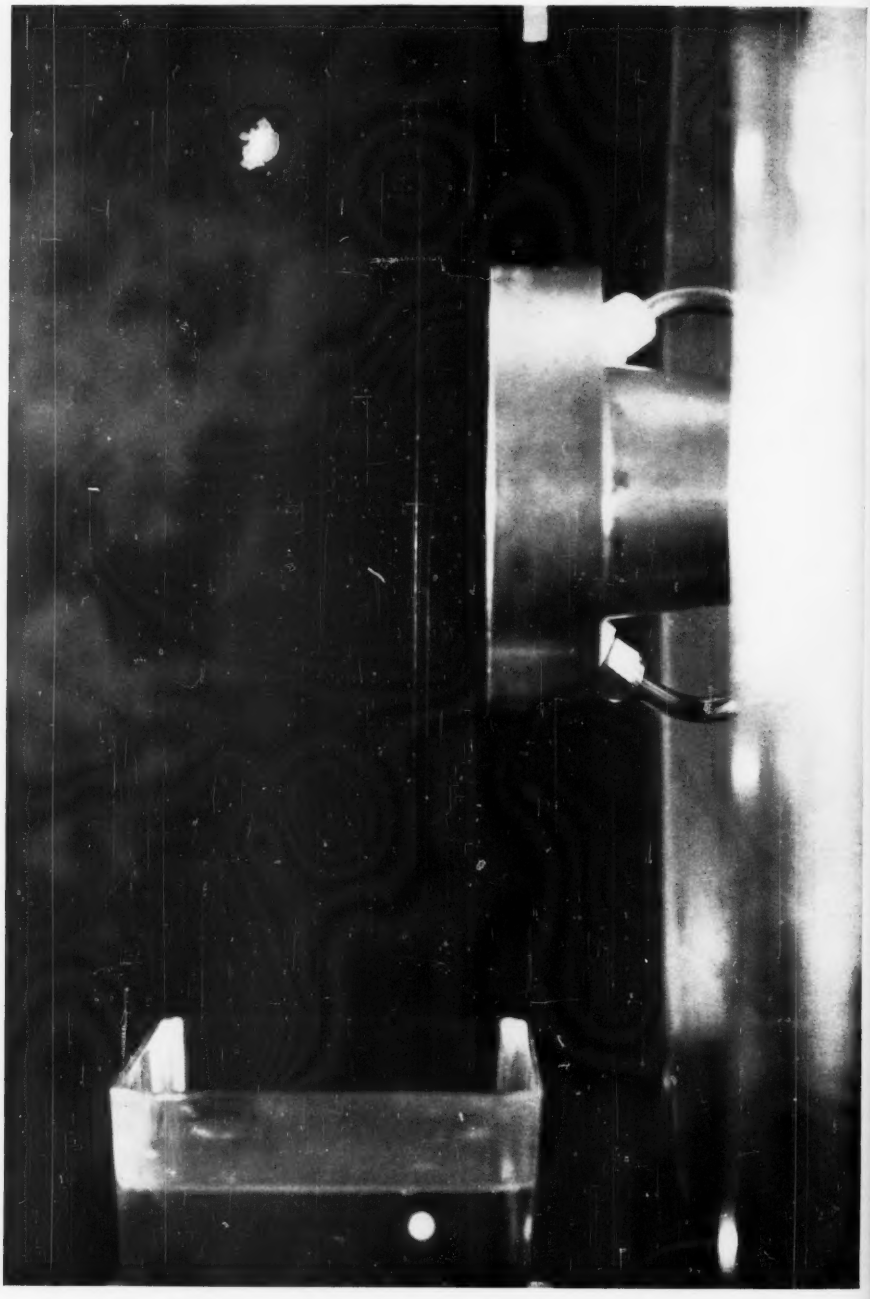

FIGURE 6. Support-wire drag determination.

The motion of single immiscible drops through a liquid

By R. SATAPATHY

Shri Ram Institute for Industrial Research, Delhi

AND W. SMITH

D.S.I.R. Warren Spring Laboratory, Stevenage, Herts.

(Received 21 October 1960)

The motion of drops of liquid through an immiscible field liquid has been observed and drag coefficients have been measured at Reynolds numbers from 0·01 to 1500. Several kinds of motion have been distinguished and it has been noticed that a change in the motion is always preceded by an increase in the drag coefficient and is usually followed by a return to the drag coefficient for solid spheres. When the drop is deformed, the drag coefficient and the form of the motion is not determined solely by the Reynolds number. The effect of the walls of a containing vessel on the motion is computed for low Reynolds numbers.

Introduction

Bringing into contact two immiscible phases and transferring a mutually soluble component from one phase to the other is a process frequently encountered in the chemical industry. Usually, one phase is dispersed in the other in the form of bubbles of gas or vapour, drops of liquid or particles of solid in such a way as to give a high interfacial area and a good rate of mass or heat transfer. The mechanics of the motion of the dispersed phase through the continuous phase is important in all these cases for two reasons: first, the velocity of the particles of the dispersed phase determines the capacity of the equipment; and secondly, the motion near the interface between the phases determines the convective rate of transfer of mass or heat between the particles and the continuous phase.

The capacity of industrial equipment can be related to the terminal velocity of single particles in an extended fluid. The terminal velocity (or drag coefficient) of single particles of solid or bubbles of gas has been measured by many workers, but liquid drops have until recently received less attention (Hughes & Gilliland 1952; Hu & Kintner 1955; Licht & Narasimhamurty 1955; Klee & Treybal 1956; Krishna, Venkateswarlu & Narasimhamurty 1959; Warshay, Bogusz, Johnson & Kintner 1959). These, like gas bubbles, have a more complicated motion than solids, for they are able to deform and oscillate, and owing to the difficulty of obtaining accurate data there is some conflict between the measurements of different workers. Although the scatter in values of drag coefficient is small, there is uncertainty about those values of the Reynolds number at which the character of bubble motion changes; for instance, when oscillation starts, or when vortices

are detached. As will be shown, under conditions where the drop is deformed, changes in the state of the motion are not decided by the value of the Reynolds number alone. It is important to know what kind of motion the drop has for this critically affects the rate of mass or heat transfer between the phases. For this reason careful measurements were made, during this work, of the drag coefficient of drops of liquid as a function of Reynolds number, and these values were correlated with the kind of motion observed.

Experimental equipment used for solvent extraction is often designed to give a long contact time between the two liquids and the Reynolds number of drops moving through the equipment is therefore low. The drops are sometimes in viscous flow (Stokes region) or move with a stable single-ring vortex at the rear; that is, below the Reynolds number at which vortices detach or at which there is much deformation. This region especially has been examined and the effect of containing walls on the motion has been calculated approximately. Also, since at low Reynolds numbers accurate measurements can be compared with theory, it is possible to decide whether the surface viscosity of Boussinesq (1913) plays an important part in determining the motion of the drop. Surface viscosity has been invoked recently to explain several phenomena noticed in liquid–liquid extraction (Sternling & Scriven 1959).

Experimental technique

The drag coefficient is given by

$$C_D = \frac{W}{\frac{1}{2}\rho U^2 \pi a^2}. \tag{1}$$

U, the steady terminal velocity of the drop, is measured directly; W, the effective weight of the drop in the field liquid, is found from the volume of the drop; and a is the apparent radius of the drop as seen from the direction of its motion.

Photographs were taken by a ciné-camera of drops moving (usually falling) through a square column of 6 in. side and filled with the field liquid to a height of 6 ft. Drops were formed and released beneath the surface of the field liquid from nozzles with a straight bore and a flat face. Several sizes of nozzle were used to give a range of drop sizes. The nozzle was fed with drop liquid from a container giving a constant head at the tip of the nozzle. In this way, as the photographs showed, drops of constant size were obtained and at a fixed frequency. The interval between drops was regulated to be long enough for the disturbance of the field liquid by the previous drop to have decayed. The velocity of the drop was determined either from the ciné-film, that is, from the position of the drop in successive frames, or by measuring with a stop-watch the time taken by the drop to move through a height of 70 cm. Each result registered was the average of 20 determinations. It was found that a distance of about 50 cm was sufficient to allow all drops to attain their steady velocity, and all readings were taken at least 70 cm from the nozzle. All drops had a diameter less than 1 cm: at this ratio of container to drop size (about 15 to 1) the effect of the walls of the container on the terminal velocity of the drop is small (Uno & Kintner 1956). The volume of liquid accumulated at the end of the column by about 20 of the

same drops was measured; this gave the volume of each drop. The projected area of the drops as seen from the direction of their motion was measured from the photographs, assuming that the drops have a circular cross-section in a horizontal plane. The drop and field liquids were mutually saturated with each other in order to eliminate mass transfer between the phases during the experiments. The viscosity and density of the mutually saturated liquids were measured and these were used in all calculations.

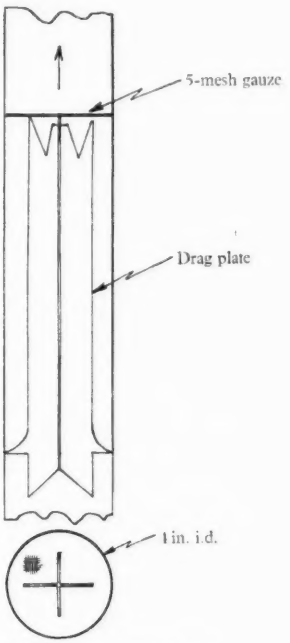

FIGURE 1. Drag plate.

At Reynolds numbers less than 40 the terminal velocity of solid spheres was measured in the same way as described above, except that the sphere was released from a hemispherical cup, to which it was initially attached by vacuum. The main purpose of these measurements was to check the experimental technique, and in the Stokes region ($R < 1$), the measured drag coefficient was within $\frac{1}{4}\%$ of the theoretical value, $24/R$ ($R = \rho U d/\mu$, ρ and μ being the density and viscosity of the field liquid, d being the maximum diameter of the drop in a horizontal plane).

Some experiments were carried out in which aluminium particles were added to the drop liquid, or dyestuff soluble in the field liquid was injected near the surface of the drop. This served to show up circulation of liquid within the drop or the vortex at the rear of the drop.

An apparatus was built in which it was possible to keep a drop stationary in a moving field liquid. This was effected by 'inverting' the velocity profile of the field liquid by placing a solid surface, a cruciform drag plate, along the axis

of the containing column and smoothing the disturbance so caused by a wire mesh (figure 1). It was possible by this means to keep the drop in the same horizontal plane in the centre of the column, and to observe oscillation of the drop or circulation within the drop. But quantitative measurement of the position of streamlines, shown up by injecting dyestuff in fine streams, was not accurate owing to uncertainty about the distribution of velocity in the liquid outside the drop. An alternative way of suspending the drops is to pass the field fluid vertically through a divergent conduit. This technique was used by Garner & Kendrick (1959) for suspending liquid drops in a gas stream, but was found here to be unsuitable for suspending liquid drops in a liquid.

Drag coefficient and drop motion

Drag coefficients, calculated by using equation (1), are plotted in figure 2 as a function of the Reynolds number. Glycerol, water and glycerol–water solutions (85, 65, 50 and 35 % by weight) were used as field liquids: these and the liquids forming the drops were all Newtonian in behaviour. Figure 2 is divided according to differences observed in the motion of the drops, which were as follows.

A. *R less than* 4

This is the viscous flow or Stokes region: the drops appear to be spherical and move steadily along a vertical straight line. At low Reynolds numbers (less than about 1) the streamlines at the front and rear of the drop appear to be distributed symmetrically. As the Reynolds number approaches 4 streamlines at the rear of the drop diverge, but no vortex is formed. The results shown are for drops having a size much greater than the critical value of Bond (1927, 1928); that is, liquid within the drop circulates in a symmetrical, stable ring vortex. Small drops which move as if they are solid spheres have been extensively studied before (Garner & Haycock 1959) and were not examined here. In order to obtain a low Reynolds number with a drop of a diameter of about $\frac{1}{2}$ cm, the field liquid must be very viscous (pure glycerol). Consequently most of the results plotted are close to the theoretical line predicted by Hadamard (1911) for the case where the viscosity of the drop liquid is zero ($16/R$).

B. *R from* 4 *to* 10

Above a Reynolds number of 4 the drag coefficient is higher than is predicted by Hadamard, and at a Reynolds number of 10 the drag coefficient attains the same value as is measured for solid spheres. A single-ring vortex, moving with the drop, forms at the rear; the stagnation point, that is the point where the outer boundary of this vortex returns to the axis of the motion, first moving from the drop at a Reynolds number of 4. At a Reynolds number of 10 the vortex has a total width of about $\frac{3}{4}$ of the diameter of the drop. Below a Reynolds number of 8 there is little deformation of the drop, but above a Reynolds number of 8 the rear of the drop progressively becomes flatter (figure 3). Inside the drop the liquid circulates, the centre of this motion appearing to move towards the front of the drop as the Reynolds number increases.

C. *R from* 10 *to* 45

As may be seen from figure 2 there appears to be a discontinuity in the slope of the curve of drag coefficient against Reynolds number at a Reynolds number of 10, and at Reynolds numbers between 10 and 40 the drag coefficient has the value found for solid spheres. As the Reynolds number approaches 40, the deformation of the drop becomes more pronounced and the vortex at the rear

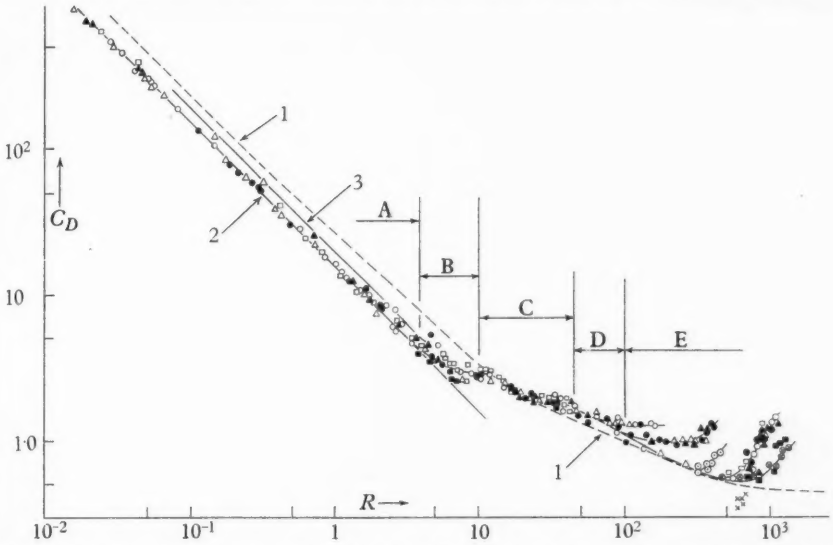

FIGURE 2. Drag coefficients. 1, solid spheres; 2, Hadamard ($\sigma = \infty$); 3, $\sigma = 7{\cdot}5$. Experimental: ○, tetrachloroethylene; ●, carbon tetrachloride; △, chloroform; ▲, bromobenzene; □, ethyl bromide; ■, carbon disulphide; ⊗, chlorobenzene; ⊙, benzyl alcohol; ×, aniline.

suddenly increases in length, but never has a width greater than the equatorial diameter of the drop (figure 3). The way in which liquid within the drop moves becomes complicated and difficult to observe. Above a Reynolds number of 40 the drop moves unsteadily; the vortex stays attached to the rear of the drop, but attains its maximum size and moves from side to side about the axis of the motion. Between Reynolds numbers of 40 and 45 the drag coefficient is higher than the value measured for solid spheres.

D. *R from* 45 *to* 100

The vortex at the rear of the drop begins to break up once the Reynolds number is greater than 45. In turn each side of the vortex grows in size, the other side remaining small and stable, until it is greater in length than about $1\frac{1}{2}$ drop diameters when a part of the elongated vortex detaches itself (figure 3). The drop is deformed but again moves steadily, the drag coefficient remaining a little higher than the value measured for solid spheres. There appears to be little or no internal circulation.

E. *R greater than* 100

In this region vortices are detached from alternate sides of the drop, as described above, but the drop no longer moves steadily. In some cases the drop fluctuates in shape as shown in figure 3, while in other cases there is no axial symmetry in the shape of the drop. Circulation of liquid inside the drop appears to stop when oscillation of the surface commences. Above a Reynolds number of 300 the drop no longer moves in a vertical plane but follows the line of a helical spiral: this

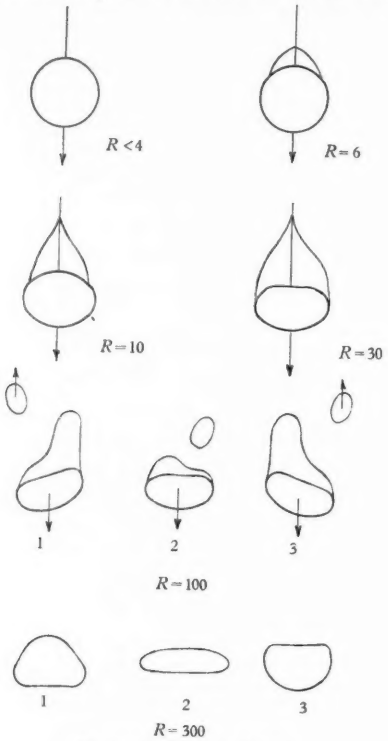

FIGURE 3. Drop shapes.

appears to be induced by the alternate detachment of vortices at the rear of the drop. Deviation from a vertical path is less with larger drops (see Margarvey & Bishop 1960). Drops formed from different liquids but moving in the same field liquid have different drag coefficients, the value (except for aniline) being greater than that for solid spheres. Evidently, under conditions where the surface of the drop is expanded and contracted, the drag coefficient will depend upon the interfacial tension (γ) as well as the Reynolds number. This is indicated by the fact that these results are correlated by the Weber number ($\rho U^2 a/\gamma$) by the method proposed by Hu & Kintner (1955). The various lines of the plot of drag coefficient against Reynolds number each terminate below a Reynolds number of 1500, at the condition where a drop breaks up before attaining a dynamically steady motion.

Analysis for low Reynolds numbers

In experimental equipment used to study mass transfer in solvent extraction processes, often single drops are allowed to move under the action of gravity in relatively narrow tubes and at low Reynolds numbers. The effect of the confining walls of the vessel on the position of the streamlines near the surface of the drop and on the drag coefficient can be calculated in the simple although approximate way suggested by Williams (1915): that is, by putting the disturbance caused by the drop as zero at a concentric spherical boundary moving with the drop. Less accurately, the influence on the motion of the presence of other drops can be estimated in the same way. It is possible to fit boundary conditions at a cylindrical surface coaxial with the axis of drop motion (Bohlin 1960), but this gives an answer which is too complicated for straightforward use.

Stokes's solution of the equations of motion in spherical polar co-ordinates for a viscous fluid is, in terms of the stream function,

$$\psi = (A/r + Br + Cr^2 + Dr^4)\sin^2\theta; \tag{2}$$

r is the distance from the centre of the sphere and θ is the latitude. It is assumed that there is symmetry in planes through the axis of the motion. This solution can be used both for fluid outside and inside the drop (quantities referring only to the fluid inside the drop will be distinguished by primes). The component velocities are

$$u_r = \frac{1}{r^2\sin\theta}\frac{\partial\psi}{\partial\theta}, \quad u_\theta = -\frac{1}{r\sin\theta}\frac{\partial\psi}{\partial r}. \tag{3}$$

All quantities are made dimensionless and are related to the dimensional quantities in terms of U, the steady terminal velocity and a, the radius of the drop. We apply the following boundary conditions which lead to the necessary number of relationships between the coefficients of r in equation (2).

(*a*) For a stationary drop with the field fluid moving at the outer, concentric, spherical boundary (of radius σ) at a dimensional velocity of U (or a dimensionless velocity of unity), we have

$$r = \sigma, \quad u_r = \cos\theta, \quad u_\theta = -\sin\theta.$$

This gives, by equations (3),

$$\frac{2A}{\sigma^3} + \frac{2B}{\sigma} + 2C + 2D\sigma^2 = 1, \tag{4}$$

$$-\frac{A}{\sigma^3} + \frac{B}{\sigma} + 2C + 4D\sigma^2 = 1. \tag{5}$$

(*b*) On the spherical surface of the stationary drop, since there is no deformation we must have the normal velocities of both fluids zero and the tangential velocities equal. For

$$r = 1, \quad u_r = u_r' = 0, \quad u_\theta = u_\theta'.$$

This leads to

$$A + B + C + D = 0, \tag{6}$$

$$A' + B' + C' + D' = 0, \tag{7}$$

$$A - B - 2C - 4D = A' - B' - 2C' - 4D'. \tag{8}$$

(*c*) The velocity of fluid inside the drop at $r = 0$ must remain finite, which dictates that

$$A' = B' = 0. \tag{9}$$

(*d*) At the surface of the drop the tangential stresses must be equal

$$r = 1, \quad p_{r\theta} = p'_{r\theta},$$

where

$$p_{r\theta} = \frac{2}{R}\left(\frac{\partial u_\theta}{\partial r} + \frac{1}{r}\frac{\partial u_r}{\partial \theta} - \frac{u_\theta}{r}\right).$$

This gives

$$(A' + D') = v(A + D), \tag{10}$$

where

$$v = \mu/\mu'.$$

Solution of equations (4) to (10) leads to

$$B = -\frac{3\sigma^6 - 3\sigma + 2\sigma^6 v + 3\sigma v}{4\sigma^6 - 9\sigma^5 + 10\sigma^3 - 9\sigma + 4\sigma^6 v - 6\sigma^5 v + 6\sigma v + 4v},$$

$$D = \frac{2B\sigma^3 + 4B - 6B\sigma - 3\sigma}{4\sigma^6 - 10\sigma^3 + 6\sigma},$$

$$C = \frac{1}{2} - \frac{2B}{3\sigma} - \frac{5D\sigma^2}{3}. \tag{11}$$

A is then given by equation (6), D' by equation (10) and C' by equation (7).

The total of the forces acting at the surface of the drop in the direction of its motion is the drag force, which in steady motion is equal to the effective weight of the drop. The drag coefficient is given by

$$C_D = 4\int_0^\pi (p_{rr}\cos\theta - p_{r\theta}\sin\theta)_{r=1}\sin\theta\, d\theta, \tag{12}$$

where

$$p_{rr} = -p + \frac{4}{R}\frac{\partial u_r}{\partial r}, \tag{13}$$

and p is obtained from the equations of motion as a function of θ. Equations (12) and (13) give

$$C_D = -16\frac{\mu}{\rho U a}B = -\frac{32}{R}B. \tag{14}$$

Equation (14) can also be obtained by finding the dissipation of energy by viscous motion of fluid inside and outside the drop. If the totals of the normal stresses on each side of the interface are calculated, it is now found that they are equal; that is, the sum of the dynamic pressure, hydrostatic head and viscous stress outside the drop equals the sum of the dynamic pressure, viscous stress and the normal stress owing to interfacial tension inside the drop.

Comparison with experiment

In equation (11), if σ is put equal to infinity, we get

$$B = -\frac{3}{4}\frac{2\mu + 3\mu'}{3\mu + 3\mu'}.$$

By equation (14), the drag coefficient is

$$C_D = \frac{24}{R}\frac{2\mu + 3\mu'}{3\mu + 3\mu'}. \tag{15}$$

This is Hadamard's solution. In our experiments σ had a high value of about 15. Even so, there is an appreciable difference between the drag coefficient given by equation (14) and that given by equation (15). For instance, for a drop of tetrachloro-ethylene ($\mu' = 0{\cdot}00851$ poise) in 85 % by weight glycerol ($\mu = 0{\cdot}5495$ poise), when $\sigma = 15$, $B = -0{\cdot}560$ and by equation (14), $C_D = 17{\cdot}9/R$; and when $\sigma = 7{\cdot}5$, $B = -0{\cdot}631$ and $C_D = 20{\cdot}2/R$ (see figure 2). By equation (15) Hadamard's solution gives for the same liquids $C_D = 16{\cdot}1/R$.

The maximum velocity at which fluid moves inside the drop (V_c) occurs at the origin along the axis of motion, and this is the same in magnitude as the tangential velocity at the surface at the equator of the drop. By equations (2) and (3)

$$V_c = -2C'.$$

For the liquids considered above and for $\sigma = 15$, $C' = -0{\cdot}258$. So $V_c = +0{\cdot}516$; that is, 52 % of the velocity with which the drop is moving. An internal circulation of this magnitude should be readily observable even in small drops. But the observation of Bond (1927) (and more recently of Garner & Haycock 1959) is that there is a specific size of drop below which there is no circulation. Thus, with small drops there must be tangential stresses other than the viscous stress which restrict the transmission of motion from the field to the drop liquid.

According to Boussinesq (1913) the dynamic value of interfacial tension is different from the static value (γ). In dimensionless terms the difference in normal stress is

$$2\left[\frac{1}{We}+\frac{1}{R_s}\left(\frac{\partial u_\theta}{\partial \theta}\right)_{r=1}\right],$$

and in tangential stress is $(u_\theta/R_s)_{r=1}$, where $R_s = \rho U a^2/\mu_s$ and μ_s is called the surface viscosity. Applying these relations, in the normal stress the first term $(2/We)$ merely increases the mean normal pressure inside the drop by the static value of the interfacial tension and has no effect on the solution. If the remaining terms owing to surface viscosity are accounted for we find, after Boussinesq,

$$C_D = \frac{24}{R}\left(\frac{2\mu+3\mu'+e}{3\mu+3\mu'+e}\right), \tag{16}$$

for $\sigma = \infty$. The experimental results obey equation (15) rather than equation (16) and show that the surface viscosity is small.

We should like to thank Professor D. M. Newitt for his guidance and for providing facilities for this work, which was done at the Department of Chemical Engineering, Imperial College. One of the authors (R. S.) wishes to acknowledge the award of the Assam Oil Co. scholarship.

REFERENCES

Bohlin, T. 1960 *Trans. Roy. Inst. Tech., Stockholm*, no. 155.

Bond, W. N. 1927 *Phil. Mag.* **4**, 889.

Bond, W. N. & Newton, D. R. 1928 *Phil. Mag.* **5**, 794.

Boussinesq, J. 1913 *Ann. Chem. Phys.* **29**, 349.

Garner, F. H. & Haycock, P. J. 1959 *Proc. Roy. Soc.* A, **252**, 457.

Garner, F. H. & Kendrick, P. 1959 *Trans. Inst. Chem. Engrs*, **37**, 155.

HADAMARD, J. 1911 *C.R. Acad. Sci., Paris*, **152**, 1735.

HU, S. & KINTNER, R. C. 1955 *J. Amer. Inst. Chem. Engrs*, **1**, 42.

HUGHES, R. R. & GILLILAND, E. R. 1952 *Chem. Engng Prog.* **48**, 497.

KLEE, A. J. & TREYBAL, R. E. 1956 *J. Amer. Inst. Chem. Engrs*, **2**, 444.

KRISHNA, P. M., VENKATESWARLU, D. & NARASIMHAMURTY, G. S. R. 1959 *J. Chem. Engng Data*, **4**, 336.

LICHT, W. & NARASIMHAMURTY, G. S. R. 1955 *J. Amer. Inst. Chem. Engrs*, **1**, 366.

MARGARVEY, R. H. & BISHOP, R. L. 1960 *Nature, Lond.*, **188**, 735.

STERNLING, C. V. & SCRIVEN, L. E. 1959 *J. Amer. Inst. Chem. Engrs*, **5**, 514.

UNO, S. & KINTNER, R. C. 1956 *J. Amer. Inst. Chem. Engrs*, **2**, 420.

WARSHAY, M., BOGUSZ, E., JOHNSON, M. & KINTNER, R. C. 1959 *Canad. J. Chem. Engng*, **37**, 29.

WILLIAMS, W. E. 1915 *Phil. Mag.* **29**, 526.

Discontinuous velocity profiles for the Orr–Sommerfeld equation

By P. G. DRAZIN

Department of Mathematics, University of Bristol

(Received 6 December 1960)

Simple ideas of dimensional analysis and of limiting cases are used to elucidate the stability characteristics of a steady basic parallel flow of a viscous incompressible fluid. The principal result is that the stability characteristics of a smoothly varying velocity profile for wave disturbances of small wave-number can be found by use of a *discontinuous* velocity profile. The boundary conditions for a disturbance at a discontinuity of the basic flow are derived, and are used to find the stability characteristics of broken-line representations of the half-jet and jet. These findings are in agreement with previous ones.

1. Introduction

Most work on the Orr–Sommerfeld equation involves elaborate analysis (cf. Lin 1955). It seems desirable to devise simpler, though possibly less informative, methods in order to understand the nature of instability more directly, to teach the analysis to graduate classes, and to make it accessible to specialists in other fields. Such methods could aid new calculations of stability characteristics when the influence of variation of density or viscosity, of magnetic fields, or of rotating systems is considered. In this paper dimensional analysis and limiting cases of small Reynolds number or small wave-number will be used. The principal result is an interpretation and justification of the use of *discontinuous* velocity profiles for finding stability characteristics of a parallel flow of a viscous incompressible fluid.

Recently, the stability characteristics of an unbounded jet (Tatsumi & Kakutani 1958; Howard 1959) and half-jet (Tatsumi & Gotoh 1960) have been found by use of expansions in the wave-number, valid when that number is small. In these papers the growth rate of a small wave disturbance was expressed essentially as an explicit algebraic function of integrals of the velocity distribution function of the basic flow. Because only integrals of the velocity distribution are involved, these methods could be used for discontinuous velocity distributions. For example, a piecewise-constant distribution could be used to approximate the growth rate of a smoothly varying distribution as closely as desired. The apparent physical absurdity of a discontinuity of velocity in a viscous fluid will be shown in this paper to arise from a misinterpretation of a mathematical method of approximation valid for small wave-numbers. In fact, Esch (1957) has already used the basic velocity distribution

$$w_*(y_*) = \begin{cases} Vy_*/|y_*| & (|y_*| > L), \\ Vy_*/L & (|y_*| < L), \end{cases} \tag{1}$$

with two discontinuities of viscous stress to represent the half-jet. He assumed three, and then proved the fourth, of the boundary conditions at each of the discontinuities $y_* = \pm L$. These conditions were used to join up the solutions in the regions $y_* > L$, $L > y_* > -L$, $-L > y_*$ and get the eigenvalue relation for the growth rate. In § 2 we shall prove Esch's four conditions at a discontinuity of basic velocity as well as stress. In §§ 3, 4 these conditions will be applied to broken-line representations of the velocity profiles of the half-jet and jet. The results are in agreement with those of Tatsumi & Gotoh (1960) and of Tatsumi & Kakutani (1958, 1960).

First, we shall summarize the eigenvalue problem used to derive the stability characteristics, and introduce some ideas of dimensional analysis and of limiting cases. When a basic flow with velocity $w_*(y_*)$ in the x_*-direction is bounded by rigid walls at $y_* = y_{*1}, y_{*2}$ (where y_{*1} and/or y_{*2} may be infinite if the flow is unbounded), it is known (cf. Lin 1955) that the stability characteristics can be found from the eigenvalues of the Orr–Sommerfeld equation

$$(D_*^2 - \alpha_*^2)^2 \phi_* = (i\alpha_*/\nu)\{(w_* - c_*)(D_*^2 - \alpha_*^2)\phi_* - (D_*^2 w_*)\phi_*\} \tag{2}$$

and the boundary conditions

$$\alpha_* \phi_* = 0 = D_* \phi_* \quad \text{for} \quad y_* = y_{*1}, y_{*2}. \tag{3}$$

An asterisk is used as a subscript to denote dimensional parameters and variables; $D_* \equiv d/dy_*$; and ν is the kinematic viscosity of the fluid. The solution of the eigenvalue problem gives the stream function of a perturbation of the basic flow, assumed to be of the form

$$\psi'_* = \phi_*(y_*) \exp\{i\alpha_*(x_* - c_* t_*)\}. \tag{4}$$

Thus, the flow is stable or unstable to small disturbances of positive wave-number α_* accordingly as the imaginary part c_{*i} of the complex velocity $c_*(\alpha_*)$ is negative or positive, respectively.

If the velocity distribution $w_*(y_*)$ is dimensionally characterized by some length scale L and velocity scale V, the Reynolds number may be defined as

$$R = VL/\nu. \tag{5}$$

With dimensionless variables $y \equiv y_*/L$, $w(y) \equiv V^{-1} w_*(y_*)$, $\phi(y) \equiv V^{-1}L^{-1}\phi_*(y_*)$ and parameters $\alpha \equiv \alpha_* L$, $c \equiv V^{-1} c_*$, the Orr–Sommerfeld equation becomes

$$(D^2 - \alpha^2)^2 \phi = i\alpha R\{(w - c)(D^2 - \alpha^2)\phi - (D^2 w)\phi\}, \tag{6}$$

and the boundary conditions become

$$\alpha\phi = 0 = D\phi \quad \text{for} \quad y = y_1, y_2. \tag{7}$$

The solutions of the equation are integral functions of y, c, α^2 and αR (or R/α). This leads to an eigenvalue relation of the form $F(c, \alpha^2, R/\alpha) = 0$, where F is an integral function of c, α^2, R/α. This may be written as

$$c = c(\alpha, R/\alpha), \tag{8}$$

which function may be multi- or single-valued or undefined for given values of α, R/α.

We shall now take the argument applied by Drazin & Howard (1961) to stability of an inviscid fluid and generalize it for a viscous fluid. Let us consider unbounded flows only, with derivatives of the velocity distribution function tending to zero at infinity. These flows are of two basic types. For the half-jet type, $w_*(-\infty) \neq w_*(\infty)$. We may choose the origin of velocity (by making a Galilean transformation if necessary) so that $w_*(-\infty) = -w_*(\infty)$. This may change c_r, but not c_i, and hence not the growth rate of the disturbance. We then take $V = w_*(\infty)$. For the jet type, $w_*(-\infty) = w_*(\infty)$; and we choose the origin of velocity so that $w_*(\infty) = 0$. We shall not specify V for this case generally. These choices give

$$w(y) \to \begin{cases} y/|y| & \text{(half-jet type),} \\ 0 & \text{(jet type),} \end{cases} \tag{9}$$

as $y \to \pm\infty$.

Let us suppose $L \to 0$ for a fixed function $w(y)$. Then

$$\begin{aligned} w_*(y_*) &= Vw(y) = Vw(y_*/L) \\ &\to \begin{cases} Vy_*/|y_*| & \text{(half-jet type),} \\ 0 & \text{(jet type),} \end{cases} \end{aligned} \tag{10}$$

because $y_*/L \to \pm\infty$ accordingly as $\pm y_* > 0$, respectively. Also $\alpha \to 0$, $R/\alpha = \text{const.}$ as $L \to 0$ for fixed α_*. Therefore $c \to c(0, R/\alpha) \equiv f(V/\alpha_*\nu)$, say, and

$$c_* \to Vf(V/\alpha_*\nu). \tag{11}$$

(We have assumed that the model is physically reasonable so that these limits may exist.)

Consider the two limits: (*a*) $\alpha_* \to 0$ for fixed $R/\alpha = V/\alpha_*\nu$ and L; (*b*) $L \to 0$ for fixed α_* and V/ν. Each limit, (*a*) or (*b*), gives $\alpha \to 0$ for fixed R/α. Therefore each limit for fixed $w(y)$ gives the same limiting form $f(R/\alpha)$ of $c(\alpha, R/\alpha)$ as $\alpha \to 0$ for fixed R/α. Therefore the stability characteristics $c_* \to Vf(V/\alpha_*\nu)$ are valid for both the limiting profile w_* when $L \to 0$ and the original w_* when $\alpha_* \to 0$. The limiting profile w_* when $L \to 0$ may have discontinuities or discontinuities of its derivatives. It will be shown that such profiles may be used to find the stability characteristics of smoothly varying profiles as $\alpha_* \to 0$ in this way.

These arguments show that all profiles of the half-jet type have the same stability characteristics as $\alpha \to 0$. These characteristics will be found directly in § 3 by use of the profile $w_* = Vy_*/|y_*|$ to determine $f(V/\alpha_*\nu)$. Our results agree with those of Tatsumi & Gotoh (1960).

For profiles of the jet type, $w_* \to 0$ as $L \to 0$. If $w_* = 0$, there is no non-zero eigensolution of the Orr–Sommerfeld equation which vanishes at infinity. However,

$$\phi_* = \text{const.}, \quad c_* = -i\alpha_*\nu \tag{12}$$

is a solution bounded at infinity. If this is an acceptable limit of the eigensolution, then

$$c \to -i\alpha/R \quad \text{as} \quad \alpha \to 0 \quad \text{for fixed } R/\alpha. \tag{13}$$

(Tatsumi & Kakutani (1958, equations (5.3), (5.8), (6.9)) show that in fact this is the proper limit, with $\phi \sim \text{const.} \times \exp\{-[\alpha^2 + i\alpha R(w-c)]^{\frac{1}{2}}\,|y|\}$ as $\alpha \to 0$, the

square-root having non-negative real part.) In § 4 we use the broken-line representation

$$w_* = \begin{cases} 0 & (|y_*| > H), \\ V & (|y_*| < H), \end{cases} \tag{14}$$

of the jet to find a better approximation than (13). A lower branch of the curve of neutral stability $c_i(\alpha, R/\alpha) = 0$ is found; it is of the same form as found by Tatsumi & Kakutani (1958) and Howard (1959) for the smoothly varying jet with $w_* = V \operatorname{sech}^2(y_*/L)$. A second branch of similar form also is found.

The above arguments are as valid for flows with one finite boundary as for flows with none. However, for flows with two finite boundaries there is an imposed length scale, namely, the distance between the boundaries, which cannot tend to zero without removing the field of flow.

If we let $V \to 0$ for a fixed function $w(y)$, then $w_* \to 0$. Therefore

$$c_* \to \alpha_* \nu g(\alpha_* L)$$

by dimensional analysis. Therefore $c \sim (\alpha/R)\, g(\alpha)$ as $R \to 0$ for fixed α. If we may suppose that the shape of the profile w_* is unimportant as $V \to 0$, we may deduce from equation (12) that $g(\alpha) = -i$, and

$$c \sim -i\alpha/R \tag{15}$$

as $R \to 0$ for fixed α.

Having examined the limit $\alpha_* \to 0$, let us put $\alpha_* = 0$. Then the stream function of the disturbance $\psi'_* = \phi_*(y_*) \exp(-\sigma_* t_*)$, for $\sigma_* \equiv i\alpha_* c_*$ need not vanish as $\alpha_* \to 0$. Then the longitudinal and lateral velocity components of the disturbance are respectively

$$u'_* = \partial\psi'_*/\partial y_* = (D_*\phi_*) \exp(-\sigma_* t_*), \quad v'_* = -\partial\psi'_*/\partial x_* = 0;$$

it can be seen that the velocity of the disturbance is parallel to the basic flow.

In this case with $\alpha_* = 0$ the Orr–Sommerfeld equation is

$$-\sigma_* D_*^2 \phi_* = \nu D_*^4 \phi_*.$$

Therefore

$$\phi_* \propto \begin{cases} 1,\ y_*,\ \exp[\pm i y_* (\sigma_*/\nu)^{\frac{1}{2}}] & (\sigma_* \neq 0), \\ 1,\ y_*,\ y_*^2,\ y_*^3 & (\sigma_* = 0). \end{cases}$$

If $y_{*1} = -L$, $y_{*2} = L$, the eigensolution satisfying boundary conditions (7) is either

$$\phi_* \propto \sin[(\sigma_*/\nu)^{\frac{1}{2}} y_*], \quad \alpha_* = 0, \quad \sigma_*/\nu = (n\pi/L)^2 \quad (n = 0, \pm 1, \pm 2, \ldots), \tag{16}$$

or

$$\phi_* = \text{const.}, \quad \alpha_* = 0, \quad \sigma_* \text{ indeterminate}. \tag{17}$$

For the former mode (16), $c = -i(n\pi)^2 R/\alpha$. If y_{*1} and/or y_{*2} is infinite, the only eigensolution is (17).

In contrast to this, the Navier–Stokes equations for parallel flow reduce to the diffusion equation $\partial u_*/\partial t_* = \nu \partial^2 u_*/\partial y_*^2$,

whose solution for bounded flow is

$$u_*(y_*, t_*) = \sum_{n=1}^{\infty} b_{*n} \sin(n\pi y_*/L) \exp(-n^2\pi^2 t_* \nu/L^2),$$

where

$$b_{*n} \equiv \frac{1}{2\pi} \int_{-L}^{L} u_*(y_*, 0) \sin(n\pi y_*/L)\, dy_*;$$

and for unbounded flow the solution is

$$u_*(y_*, t_*) = \int_{-\infty}^{\infty} b_*(n_*) \exp(in_* y_* - n_*^2 t_* \nu)\, dn_*,$$

where

$$b_*(n_*) \equiv \frac{1}{2\pi} \int_{-\infty}^{\infty} u_*(y_*, 0) \exp(-in_* y_*)\, dy_*.$$

However, the above solutions of the Orr–Sommerfeld and Navier–Stokes equations differ when the flow is unbounded (or semi-bounded, similarly). The difference occurs because no enumerable set of eigenfunctions of the Orr–Sommerfeld equation can form a base for solutions of the Navier–Stokes equations. In fact, a Fourier integral of solutions of the Orr–Sommerfeld can satisfy the boundary conditions though no single solution can.

In our search for simplicity we shall not comment further on the relation of the initial-value problem to that of separate wave components. We have considered the special case $\alpha_* = 0$ to see if it can shed some light on the solution of the Orr–Sommerfeld equation. Now all solutions of the diffusion equation are stable, so it might be concluded that those of the Orr–Sommerfeld equation give $c_{*i} \leqslant 0$ as $\alpha_* \to 0$ for fixed ν. This conclusion contradicts a result of Tatsumi & Gotoh (1960). The discrepancy appears to be due to the breakdown of the assumption of the existence of a steady parallel flow $w_*(y_*)$, made in the derivation of the Orr–Sommerfeld equation. As Tatsumi & Gotoh pointed out, when R or α is small, no unbounded steady flow is even approximately parallel in a characteristic length α^{-1}. We may add that the characteristic rate of change ν/L^2 of unbounded parallel flow is not very much less than the change $\alpha_* c_*$ of a small disturbance if R or α is small. In that case, the Orr–Sommerfeld equation has no physical relevance. However, mathematical knowledge of the limiting forms of the eigensolutions is nonetheless useful as a means to find the eigensolutions at greater values of R, α_* for which the Orr–Sommerfeld equation does describe approximately a real perturbation.

2. The boundary conditions for the disturbance at a discontinuity of the basic flow

In deducing the Orr–Sommerfeld equation (cf. Lin 1955), it is found that the equations of motion give

$$u'_* = (D_* \phi_*) \exp\{i\alpha_*(x_* - c_* t_*)\}, \quad v'_* = -i\alpha_* \phi_* \exp\{i\alpha_*(x_* - c_* t_*)\},$$

and, for the pressure of the disturbance,

$$p'_* = \rho\{(D_* w_*)\phi_* - (w_* - c_*) D_* \phi_* - i\nu\alpha_*^{-1}(D_*^2 - \alpha_*^2) D_* \phi_*\} \times \exp\{i\alpha_*(x_* - c_* t_*)\},$$

where ρ is the density of the fluid. Therefore the components of the stress tensor of the basic flow and the disturbance superposed are

$$p_{*xx} = \rho\{(w_* - c_*) D_* \phi_* - (D_* w_*)\phi_* + i\nu\alpha_*^{-1}(D_*^2 + \alpha_*^2) D_* \phi_*\} \times \exp\{i\alpha_*(x_* - c_* t_*)\},$$

$$p_{*xy} = p_{*yx} = \rho\nu D_* w_* + \rho\nu\{(D_*^2 + \alpha_*^2)\phi_*\} \exp\{i\alpha_*(x_* - c_* t_*)\},$$

$$p_{*yy} = \rho\{(w_* - c_*) D_* \phi_* - (D_* w_*)\phi_* + i\nu\alpha_*^{-1}(D_*^2 - 3\alpha_*^2) D_* \phi_*\} \times \exp\{i\alpha_*(x_* - c_* t_*)\}.$$

For stability of fluid at rest under the influence of gravity, Harrison (1908) supposed that these velocity and stress components were continuous at an interface where the density and viscosity were discontinuous. This method has also been used by Lock (1954) to deal with a basic flow under gravity with discontinuous viscosity and density distributions but continuous velocity and stress. For a basic flow (not under gravity) with continuous velocity but discontinuous stress, Esch (1957) implicitly assumed that ϕ_*, $D_*\phi_*$, $D_*^2\phi_*$ were continuous, and then deduced the 'jump' of $D_*^3\phi_*$ at the discontinuity of basic stress as follows. If the Orr–Sommerfeld equation is integrated from $y_{*0}-\epsilon$ to $y_{*0}+\epsilon$ across the discontinuity of D_*w_* at $y_*=y_{*0}$, we find

$$\left[D_*^3\phi_*-2\alpha_*^2D_*\phi_*\right]_{y_{*0}-\epsilon}^{y_{*0}+\epsilon}+\alpha_*^4\left[D_*^{-1}\phi_*\right]_{y_{*0}-\epsilon}^{y_{*0}+\epsilon}$$
$$=i\alpha_*\nu^{-1}\left[(w_*-c_*)D_*\phi_*-(D_*w_*)\phi_*\right]_{y_{*0}-\epsilon}^{y_{*0}+\epsilon}-\left[D_*^{-1}(w_*-c_*)\phi_*\right]_{y_{*0}-\epsilon}^{y_{*0}+\epsilon}.$$

Therefore

$$[D_*^3\phi_*+i\alpha_*\nu^{-1}(D_*w_*)\phi_*]=0 \tag{18}$$

as $\epsilon\to 0$, where square brackets are used to denote the 'jump', or difference across the discontinuity, of their contents. We shall develop this argument by showing that ϕ_*, $D_*\phi_*$ are continuous if w_* is piecewise continuously differentiable, and that discontinuous profiles may be used to approximate the eigenvalue c_* for a smoothly varying velocity profile at small wave-numbers. In view of the unphysical nature of the use of the discontinuous profiles, it seems wisest to abandon consideration of continuity of velocity or stress when seeking the approximate solution of the Orr–Sommerfeld equation. (Another reason is that that equation itself is derived by the approximation that the basic flow is an exact solution of the Navier–Stokes equations.) The Orr–Sommerfeld equation has solutions in simple terms of known functions in two cases: the solutions are exponential if $w_*(y_*)$ is constant, and involve Airy and exponential functions if $w_*(y_*)$ is linear. Our aim is merely to use these simple solutions to compute approximate values of c_* for curved profiles, as Rayleigh did in1880 (cf. Rayleigh 1945, ch. 21) for an inviscid fluid.

Successive integrals of the Orr–Sommerfeld equation are

$$D_*^3\phi_*-i\alpha_*\nu^{-1}\{(w_*-c_*)D_*\phi_*-(D_*w_*)\phi_*\}$$
$$=2\alpha_*^2D_*\phi_*-\alpha_*^4D_*^{-1}\phi_*-i\alpha_*^3\nu^{-1}D_*^{-1}(w_*-c_*)\phi_*, \tag{19}$$

$$D_*^2\phi_*+i\alpha_*\nu^{-1}(w_*-c_*)\phi_*=2\alpha_*^2\phi_*-\alpha_*^4D_*^{-2}\phi_*$$
$$+i\alpha_*\nu^{-1}\{2D_*^{-1}(w_*-c_*)D_*\phi_*-\alpha_*^2D_*^{-2}(w_*-c_*)\phi_*\}, \tag{20}$$

$$D_*\phi_*=2\alpha_*^2D_*^{-1}\phi_*-\alpha_*^4D_*^{-3}\phi_*+i\alpha_*\nu^{-1}\{2D_*^{-2}w_*D_*\phi_*$$
$$-2c_*D_*^{-1}\phi_*-\alpha_*^2D_*^{-2}(w_*-c_*)\phi_*\}. \tag{21}$$

These equations suggest that $D_*^4\phi_*$, $D_*^3\phi_*$, $D_*^2\phi_*$ become discontinuous when a smoothly varying function $w_*(y_*)$ tends to a discontinuous one for a fixed function $w(y)$, because these differentials equal sums involving $D_*^2w_*$, D_*w_*

and w_*. However, $D_*\phi_*$, ϕ_* should be continuous, because they depend on w_* through its integrals only.

To prove this, suppose parameters α_*^2, $\alpha_*\nu^{-1}$ and the function $w(y)$ are fixed and non-zero as $L \to 0$. Further, if the flow is unbounded, suppose that all derivatives of $w(y)$ vanish at infinity, so that w is bounded.

Integrability or boundedness (though not continuity or differentiability) of a function of y implies the same of the corresponding function of y_* in the limit $L \to 0$. Therefore $\phi_*(y_*)$, like $\phi(y)$, is bounded. It follows that all terms, except $D_*^{-2} w_* D_* \phi_*$ possibly, of the right-hand side of equation (21) are continuous functions of y_* in the limit $L \to 0$. To show that this term also is continuous, we need only note that

$$|D_*^{-1} w_* D_* \phi_*| = V\,|D^{-1} w D\phi| \leqslant V D^{-1}\,|w|\,|D\phi| \leqslant V\left[D^{-1}\,|w|\,|D\phi|\right]_{y_1}^{y_2},$$

which is bounded, because $|w|$ and $\left[D^{-1}\,|D\phi|\right]_{y_1}^{y_2}$ are. Thus, the right-hand side of equation (21), and therefore $D_*\phi_*$, is continuous. The integral of equation (21) shows that ϕ_* is continuous. Finally, the right-hand sides of equations (19) and (20) give the jumps of $D_*^3\phi_*$ and $D_*^2\phi_*$ as $L \to 0$. Thus,

$$[\phi_*] = 0,$$

$$[D_*\phi_*] = 0,$$

$$[D_*^2\phi_* + i\alpha_*\nu^{-1}(w_* - c_*)\,\phi_*] = 0,$$

$$[D_*^3\phi_* - i\alpha_*\nu^{-1}\{(w_* - c_*)\,D_*\phi_* - (D_* w_*)\,\phi_*\}] = 0.$$

These conditions are valid as $L \to 0$ for bounded α_*, $\alpha_*\nu^{-1}$, in the sense that the resultant limiting profile $w_*(y_*)$ will give the same stability characteristics as the smoothly varying profile $w(y)$ does for small α.

These conditions may be applied to any flow, bounded, semi-bounded or unbounded, with only one length scale. However, bounded flows have an imposed length scale, $y_{*2} - y_{*1}$, which cannot tend to zero without the field of flow vanishing. When the basic flow has two length scales, we may suppose H is characteristic of distances between regions of shear of order V/L; in particular, we may take $H \equiv y_{*2} - y_{*1}$ for bounded flows. Then the above boundary conditions are still valid as $L \to 0$ in the above sense. Note that ν only occurs in the combination $\alpha_*\nu^{-1}$, so that it is possible to let $\alpha_* H \to 0$ for fixed $\alpha_* H^2 V \nu^{-1}$ in this case.

It is known (cf. Lin 1955) that bounded flows are stable as $\alpha \to 0$ for bounded αR, and that their mechanism of instability is associated with the singularity of the critical layer where $w_*(y_*) = c_*$ when $\alpha R \to \infty$ for fixed α. This mechanism can never be described by our conditions derived for small L, i.e. for small α. Thus we shall apply our conditions to unbounded flows only, for which instability occurs at small α and finite αR, and not bother to verify the stability of bounded flows for this range of α and R.

We shall not consider the smoothly varying profile further in our analysis, so it is convenient to redefine dimensionless variables with H as length scale after

taking the limit $L \to 0$. Thus, with $\alpha \equiv \alpha_* H$, $R \equiv VH/\nu$, $w(y) \equiv V^{-1} w_*(y_*/H)$, etc., henceforth, we get dimensionless conditions

$$[\phi] = 0, \tag{22}$$

$$[D\phi] = 0, \tag{23}$$

$$[D^2\phi + i\alpha R(w-c)\phi] = 0, \tag{24}$$

$$[D^3\phi - i\alpha R\{(w-c)D\phi - (Dw)\phi\}] = 0, \tag{25}$$

for bounded α, αR at a discontinuity of w and/or Dw.

Rayleigh's use (1945, ch. 21) of broken-line profiles for the stability equation

$$(w-c)(D^2-\alpha^2)\phi - (D^2 w)\phi = 0 \tag{26}$$

of an inviscid fluid can be justified similarly from the integrals

$$(w-c)D\phi - (Dw)\phi = \alpha^2 D^{-1}(w-c)\phi,$$

$$\phi/(w-c) = \alpha^2 D^{-1}(w-c)^{-2} D^{-1}(w-c)\phi.$$

It can be seen that

$$[(w-c)D\phi - (Dw)\phi] = 0, \tag{27}$$

$$[\phi/(w-c)] = 0 \tag{28}$$

at a discontinuity of w or Dw. In fact, these are the familiar conditions that pressure and normal velocity respectively are continuous at an interface. (Critical reviews of the validity of these conditions are given by Lin (1945, pp. 121, 221) and by Drazin & Howard (1961).)

3. Broken-line half-jet

If $w(y)$ is piecewise constant, the Orr–Sommerfeld equation has solutions

$$\phi = e^{\pm\alpha y}, \quad e^{\pm\beta y}, \tag{29}$$

where

$$\beta \equiv +\{\alpha^2 - i\alpha R(c-w)\}^{\frac{1}{2}} \tag{30}$$

has non-negative real part for definiteness. In this case the boundary conditions (22) to (25) become

$$[\phi] = 0, \tag{31}$$

$$[D\phi] = 0, \tag{32}$$

$$[(D^2+\beta^2)\phi] = 0, \tag{33}$$

$$[(D^2-\beta^2)D\phi] = 0. \tag{34}$$

The simplest flow is that in which w has one jump; this is the Helmholtz flow or broken-line half-jet with

$$w = y/|y| \quad (-\infty < y < \infty). \tag{35}$$

(In this case the basic flow has only one length scale L, but we may choose H arbitrarily for use in the dimensionless equations.) The most general solution of the Orr–Sommerfeld equation satisfying the boundary conditions at infinity is of the form

$$\phi = \begin{cases} A\,e^{-\alpha y} + B\,e^{-\beta_1 y} & (y > 0), \\ D\,e^{\alpha y} + E\,e^{\beta_2 y} & (y < 0), \end{cases} \tag{36}$$

for some constants A, B, D, E where

$$\beta_1 \equiv +\{\alpha^2 - i\alpha R(c-1)\}^{\frac{1}{2}}, \quad \beta_2 \equiv +\{\alpha^2 - i\alpha R(c+1)\}^{\frac{1}{2}}. \tag{37}$$

The boundary conditions (31) to (34) at $y = 0$ give four homogeneous linear equations in A, B, D, E. A non-zero solution exists if and only if their discriminant is zero; thus the eigenvalue relation is

$$0 = \begin{vmatrix} 1 & 1 & 1 & 1 \\ -\alpha & -\beta_1 & \alpha & \beta_2 \\ \beta_1^2+\alpha^2 & 2\beta_1^2 & \beta_2^2+\alpha^2 & 2\beta_2^2 \\ \alpha(\beta_1^2-\alpha^2) & 0 & -\alpha(\beta_2^2-\alpha^2) & 0 \end{vmatrix}$$

$$= \begin{vmatrix} 1 & 1 & 1 & 1 \\ -\alpha & -\beta_1 & \alpha & \beta_2 \\ 0 & \beta_1^2-\alpha^2 & \beta_2^2-\beta_1^2 & 2\beta_2^2-\beta_1^2-\alpha^2 \\ 0 & -\beta_1(\beta_1^2-\alpha^2) & \alpha(\beta_1^2-\beta_2^2) & \beta_2(\beta_1^2-\alpha^2) \end{vmatrix}. \tag{38}$$

This last equation is $E_{0000} = 0$ in equation (4.2) of Tatsumi & Gotoh (1960). On evaluation of that determinant, they found

$$2\alpha(\beta_1-\alpha)(\beta_2-\alpha)(\beta_1+\beta_2)\{\beta_1^2+\beta_2^2-\beta_1\beta_2+\alpha(\beta_1+\beta_2)+\alpha^2\} = 0.$$

The only roots relevant to the flow are those of

$$\beta_1^2+\beta_2^2-\beta_1\beta_2+\alpha(\beta_1+\beta_2)+\alpha^2 = 0, \tag{39}$$

which is equation (4.8) of Tatsumi & Gotoh (1960). On division by α^2 it can be seen that this equation is reducible to the form (11), viz. $c = f(R/\alpha)$. On squaring (39) twice to eliminate radicals, we find a quadratic in R/α whose roots are

$$R/\alpha = -4i(c \pm 3^{\frac{1}{2}}i)/(3^{\frac{1}{2}}c \pm i)^2. \tag{40}$$

Therefore

$$c = \tfrac{1}{3} - 2i(\alpha/R) \pm 3^{\frac{1}{2}}i \pm 2\{-(\alpha/R)^2 \pm 2.3^{\frac{1}{2}}(\alpha/R)\}^{\frac{1}{2}}. \tag{41}$$

The first and third $\pm$ signs are ordered as those in the previous equation; the second is independent. It can be shown from equation (39) that the appropriate solution with $\mathrm{Re}\,\beta_1, \mathrm{Re}\,\beta_2 \geqslant 0$ is given by

$$c_r = 0, \tag{42}$$

and

$$c_i = \tfrac{1}{3}[3^{\frac{1}{2}} - 2(\alpha/R) - 2\{(\alpha/R)^2 + 2.3^{\frac{1}{2}}(\alpha/R)\}^{\frac{1}{2}}], \tag{43}$$

or

$$\alpha/R = (1-3^{\frac{1}{2}}c_i)^2/4(3^{\frac{1}{2}}-c_i). \tag{44}$$

This is the solution of Tatsumi & Gotoh.

It follows that

$$c \sim -4i\alpha/3R \quad \text{as} \quad R/\alpha \to 0, \tag{45}$$

and

$$c \to 3^{-\frac{1}{2}}i \quad \text{as} \quad R/\alpha \to \infty. \tag{46}$$

Also the curve of neutral stability ($c_i = 0$) is

$$R = 4.3^{\frac{1}{2}}\alpha, \tag{47}$$

as found by Esch (1957) and Tatsumi & Gotoh (1960).

4. Broken-line jet

Suppose
$$w = \begin{cases} 0 & (|y| > 1), \\ 1 & (|y| < 1). \end{cases} \tag{48}$$

The anti-symmetric disturbance with even $\phi(y)$ is thought (cf. Tatsumi & Kakutani 1958; Howard 1959; Clenshaw & Elliott 1960; Drazin & Howard 1961) to be the least stable for even profiles, so we shall take the most general even solution

$$\phi = \begin{cases} A\exp\{-\alpha(|y|-1)\} + B\exp\{-\beta_0(|y|-1)\} & (|y|>1), \\ D\dfrac{\cosh\alpha y}{\cosh\alpha} + E\dfrac{\cosh\beta_1 y}{\cosh\beta_1} & (|y|<1), \end{cases} \tag{49}$$

where
$$\beta_0 \equiv +\{\alpha^2 - i\alpha R c\}^{\frac{1}{2}}, \tag{50}$$

satisfying the Orr–Sommerfeld equation and the boundary conditions at infinity.

On elimination of A, B, D, E from the boundary conditions (31) to (34) at $y = \pm 1$, we find

$$\begin{vmatrix} 1 & 1 & 1 & 1 \\ -\alpha & -\beta_0 & \alpha\tanh\alpha & \beta_1\tanh\beta_1 \\ \beta_0^2+\alpha^2 & 2\beta_0^2 & \beta_1^2+\alpha^2 & 2\beta_1^2 \\ \alpha(\beta_0^2-\alpha^2) & 0 & -\alpha(\beta_1^2-\alpha^2)\tanh\alpha & 0 \end{vmatrix} = 0. \tag{51}$$

If $H \to \infty$, we see that the jet has the same stability characteristics as two distantly separated half-jets, each with velocity difference unity, because equation (51) becomes (38) with β_0 for β_1 and β_1 for β_2 in the limits $\alpha, R \to \infty$.

In general, after discarding the trivial factors $\alpha(\beta_0-\alpha)(\beta_1^2-\alpha^2)$, we can reduce equation (51) to

$$\begin{aligned} \beta_0(\beta_0+\alpha) + (2\beta_1^2-\beta_0^2+2\alpha\beta_0+\alpha^2)\tanh\alpha + \alpha(\beta_0+\alpha)\tanh^2\alpha \\ + (\beta_0+\alpha)(\beta_1^2-\alpha^2)^{-1}(\beta_1\tanh\beta_1 - \alpha\tanh\alpha) \\ \times\{2\beta_0^2-\beta_1^2-\alpha^2+(\beta_1^2-\alpha^2)\tanh\alpha\} = 0. \end{aligned} \tag{52}$$

When $\alpha R \to \infty$ for fixed α, the inviscid limit of equation (52) gives

$$3(1+\tanh\alpha)^2c^2 + (1+\tanh\alpha)(1-7\tanh\alpha)c + 4\tanh^2\alpha = 0.$$

This gives complex conjugate roots c when $7-4.3^{\frac{1}{2}} < \tanh\alpha < 7+4.3^{\frac{1}{2}}$; therefore there is instability only when $\alpha > \tanh^{-1}(7-4.3^{\frac{1}{2}})$. This differs from Rayleigh's result that $c = \{1 \pm i(\coth\alpha)^{\frac{1}{2}}\}/(1+\coth\alpha)$ when $\alpha R \to \infty$ in the Orr–Sommerfeld equation before the broken-line profile is taken, i.e. when the broken-line profile is used with equation (26). It will be shown in § 5 that Rayleigh's result is the physically meaningful one, and that the result of this paragraph is useful only to elucidate the roots of equation (52) for finite αR and small α.

When $\alpha \to 0$ for fixed R/α in equation (52), it can be shown that

$$c = -i(\alpha/R)\{1 + R^2 + 4R^2(\alpha+iR) + O(\alpha^4)\}.$$

This gives stability near the origin in the (α, R)-plane, in agreement with our heuristic conclusion (13).

When $R \to \infty$ for fixed $X \equiv \alpha R^2$, equation (52) gives

$$c = \alpha^2\{4(X^{-1} - \tfrac{1}{3}) - 4iX^{-1}R^{-1}(\tfrac{4}{45}X^2 - 3X + 4) + O(R^{-2})\}. \tag{53}$$

Therefore $c_i(\alpha, R) = 0$ has asymptotes

$$\tfrac{4}{45}X^2 - 3X + 4 = 0. \tag{54}$$

Thus, there are branches of the curve of neutral stability on which $\alpha R^2 \to 1{\cdot}34$ or $32{\cdot}4$ and $c \sim 1{\cdot}54\alpha^2$ or $-1{\cdot}21\alpha^2$, respectively, as $\alpha \to 0$. The relation (53) has been found by Tatsumi & Kakutani (1960)†, and is similar to that for the smoothly varying jet $w = \operatorname{sech}^2 y$.

If symmetric disturbances with odd $\phi(y)$ are considered instead of antisymmetric disturbances (49), it can be seen that the eigenvalue equation is the same as (52) except that hyperbolic cotangents replace hyperbolic tangents. Thus, in the limit $\alpha R \to \infty$ for fixed α, c has complex conjugate values and the flow is unstable if $\alpha > \coth^{-1}(7 + 4.3^{\frac{1}{2}})$. As $\alpha \to 0$ for fixed αR, equation (52), modified for symmetric disturbances, gives

$$\beta_0\beta_1 + (2\beta_1^2 - \beta_0^2)\tanh\beta_1 = O(\alpha).$$

This has limiting solution

$$c = 1 + 2n^2\pi^2/\alpha R,$$

$$\alpha R = 2n^2\pi^2/[1 - \tfrac{3}{2}\cosh^2(n\pi)\{1 - (1 - \tfrac{8}{9}\operatorname{sech}^2(n\pi))^{\frac{1}{2}}\}] \quad (n = 1, 2, 3, \ldots). \tag{55}$$

This type of behaviour, viz. $c \to$ const., $\alpha R \to$ const. on the lower branch of the curve of neutral stability, has already been found by Clenshaw & Elliott (1960) for symmetric disturbances of the jet $w = \operatorname{sech}^2 y$. The precise result (55) for the broken-line jet is new. It may be noted that these results confirm the greater instability of antisymmetric disturbances.

5. Discussion

The use of discontinuous profiles is suitable for small wave-numbers, for which variations of velocity of a smoothly varying profile occur in a small fraction of a wavelength. This use is the antithesis of the W.K.B. approximation, in which it is assumed that the coefficients of an ordinary differential equation are slowly varying. We shall not pursue the W.K.B. approximation because it is valid only for large wave-numbers, for which it is already known that flows are stable.

The stability characteristics (43) of a vortex-sheet or broken-line half-jet give $c_i = 3^{-\frac{1}{2}}$, and therefore instability, when $R \to \infty$. It might be thought that the wavelength was the only length-scale in instability of a vortex-sheet, and that therefore this result should agree with Helmholtz's that $c_i = \pm 1$ for all

† In this unpublished letter the authors pointed out that they had recently found that terms of order $(\alpha R)^3$ should be included in equation (6.4) of their paper of 1958 for the calculation of the proper limit of c for a jet-like profile as $\alpha \to 0$. The term

$$i(\alpha R)^3\{-\tfrac{1}{2}(6\alpha - 13\beta) - 3\beta\log 2 + \tfrac{1}{6}\pi^2(3\alpha - 4\beta) - \tfrac{9}{2}(\alpha - \beta)(\log 2)^2\}$$

should be added to equation (7.3) of their paper of 1958 on the stability of the Bickley jet $w = \operatorname{sech}^2 y$. This gives $c/\alpha^2 \to 2(2X^{-1} - 1)$ as $\alpha \to 0$, when $(\frac{1}{6}\pi^2 - 1)X^2 - 9X + 8 = 0$, the result first found by Howard (1959). It gives $\alpha R^2 \to 0{\cdot}954$ and $c \sim 2{\cdot}19\alpha^2$ as $\alpha \to 0$ on the lower branch of the curve of neutral stability. They also extended their results of 1958 to other jet-like profiles. In particular they found the stability characteristics of the broken-line jet for small α; our equation (53) agrees with these.

wave disturbances of a vortex-sheet in an inviscid fluid. This superficial contradiction can be resolved by remembering that our results are not for a vortex-sheet but for a smoothly varying half-jet in a certain limit of small wave-number. We took $\alpha \to 0$ for fixed R/α and then let $R \to \infty$, and Helmholtz's result comes from taking $\alpha R \to \infty$ first. The former corresponds to the origin and the latter to infinity in the (α, R)-plane. For similar reasons we cannot expect our eigenvalues (53) for the broken-line jet to be related to Rayleigh's eigenvalues for the same jet in an inviscid fluid.

The use of discontinuous profiles in §§ 2–4 is a simple tool to find stability characteristics for bounded αR and small α, but cannot be used for more. This limitation means that the method is not suitable for bounded or semi-bounded flows, which are already known to be stable in that region of the (α, R)-plane.

Tatsumi & Kakutani (1960) have given our approximation (53) to the eigenvalue of an antisymmetric disturbance of the broken-line jet by their series in αR (Tatsumi & Kakutani 1958). We presume that the complete power series can be shown to give our eigenvalue relation (52). Our result (55) for the symmetric disturbance is in qualitative agreement with that of Clenshaw & Elliott (1960) for the Bickley jet $w = \operatorname{sech}^2 y$.

Equation (53) shows that there is instability between the two branches of the curve of neutral stability on which $\alpha R^2 \to 1{\cdot}54$ and $32{\cdot}4$ as $\alpha \to 0$, i.e. the flow is unstable for values of (α, R) between these two branches. This strange result is not due to the broken-line profile, because similar behaviour can be found for the smoothly varying jet $w = \operatorname{sech}^2 y$. Howard's (1959) results imply that

$$c_i = -2\alpha R^{-3}\{(\tfrac{1}{6}\pi^2 - 1)\,(\alpha R^2)^2 - 9(\alpha R^2) + 8 + O(R^{-2})\}$$

as $\alpha \to 0$. Again, this gives instability as $R \to \infty$ if $0{\cdot}954 < \alpha R^2 < 13{\cdot}0$ and stability if αR^2 lies outside that interval. The significance of these two roots does not appear to have been recognized by previous authors.

We have found three branches of the curve (or curves) of neutral stability for the broken-line jet as $R \to \infty$. On the lowest $\alpha R^2 \to 1{\cdot}54$, on the middle $\alpha R^2 \to 32{\cdot}4$, on the highest $\alpha \to \tanh^{-1}(7 - 4.3^{\frac{1}{2}})$. The flow is unstable above the highest branch and between the lower pair. There do not appear to be any other branches as $R \to \infty$, and it may be concluded that the middle joins up with the highest, and that $\alpha \to \infty$ on the other end of the lowest branch. This gives two curves of neutral stability, between which there is instability. However, the broken-line jet can tell us little of the analogous behaviour of the smoothly varying jet, because they do not have similar stability characteristics when $\alpha R \to \infty$ or α is not small. This discrepancy was anticipated in § 2, where it was pointed out that the proof of conditions (22)–(25) was invalid for infinite αR.

For the jet $w = \operatorname{sech}^2 y$, three branches of the curve of neutral stability are known at large Reynolds numbers. On the highest, $\alpha \to 2$ and $\phi \to \operatorname{sech}^2 y$ as $R \to \infty$. On the lower pair, $\alpha R^2 \to 0{\cdot}954$ or $13{\cdot}0$. There is instability directly below the highest branch and between the lower pair. I am indebted to Dr J. T. Stuart, who in a private letter conjectured the synthesis of the above properties shown schematically in figure 1. The lowest branch joins with the highest, as supposed by Tatsumi & Kakutani (1958), Howard (1959) and Clenshaw & Elliott (1960). However, the middle branch may return to infinity with asymp-

totic behaviour $\alpha R^p \to$ constant as $R \to \infty$ for $0 < p < 1$. This gives a 'minor' curve of neutral stability inside the 'major' curve found by previous authors, the region of instability being between the two curves. On the upper branch of the minor curve $\alpha R \to \infty$, so it might be expected that $\phi \to w$, $c \to 0$, the 'trivial' eigensolution of the stability equation (26) for an inviscid fluid when $\alpha = 0$. If this were so, the argument Howard (1959, p. 285) suggested as plausible would be false. He made the explicit assumption that an integration and the limit

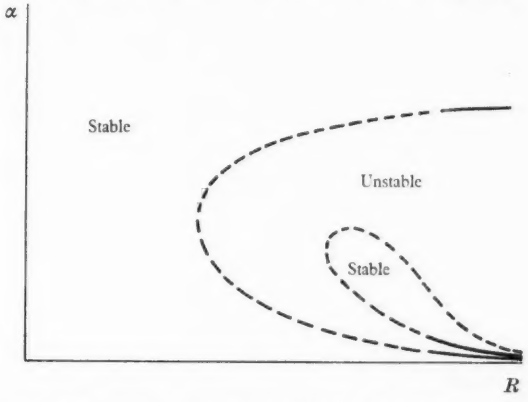

FIGURE 1. Sketch of the curve of neutral stability of the anti-symmetrical disturbance of a symmetrical smoothly varying jet. Conjectured parts of the curve are denoted by broken lines.

$R \to \infty$ could be inverted in order to show that the trivial solution was not a limit of the viscous eigensolution for unbounded flow; this inversion would be invalid if, for example, $\phi \sim w + R^{-1}\exp(-y^2/R^2)$ as $R \to \infty$, and now seems so for the actual eigensolution.

This conjecture of Stuart might be confirmed by the asymptotic theory of the Orr–Sommerfeld equation for large αR. However, the work of Tatsumi & Kakutani (1958), Howard (1959), and Clenshaw & Elliott (1960) shows clearly the occurrence and form of the most unstable disturbances of a jet, which will dominate the less unstable ones represented by points inside the 'minor' curve.

REFERENCES

CLENSHAW, C. W. & ELLIOTT, D. 1960 *Quart. J. Mech. Appl. Math.* **13**, 300–13.
DRAZIN, P. G. & HOWARD, L. N. 1961 (To be published.)
ESCH, R. E. 1957 *J. Fluid Mech.* **3**, 289–303.
HARRISON, W. J. 1908 *Proc. Lond. Math. Soc.* (2), **6**, 396–405.
HOWARD, L. N. 1959 *J. Math. Phys.* **37**, 283–98.
LIN, C. C. 1945 *Quart. Appl. Math.* **3**, 117–42, 218–34, 277–301.
LIN, C. C. 1955 *The Theory of Hydrodynamic Stability.* Cambridge University Press.
LOCK, R. C. 1954 *Proc. Camb. Phil. Soc.* **50**, 105–24.
RAYLEIGH, LORD 1945 *The Theory of Sound.* New York: Dover.
TATSUMI, T. & GOTOH, K. 1960 *J. Fluid Mech.* **7**, 433–41.
TATSUMI, T. & KAKUTANI, T. 1958 *J. Fluid Mech.* **4**, 261–75.
TATSUMI, T. & KAKUTANI, T. 1960 Private letter.

A stationary-phase approximation to the ship-wave pattern

By F. W. G. WARREN

Department of Mathematics, University of Sheffield

(Received 12 September 1960 and in revised form 8 February 1961)

Scorer (1950) has described an extension of the method of stationary phase. This method is used to derive an approximation to the wave pattern at large distances from the ship in a simple manner. The approximation is valid in the vicinity of the critical angle and the nature of the disturbance in this region is readily seen. The divergent and transverse wave systems in a critical region are shown, together with their variation of amplitude and phase.

1. Introduction

The pattern of gravity waves set up behind a ship on a steady course has been discussed by many writers. Hogner (1923) has given a first approximation to this pattern, and recently Ursell (1960) has given an asymptotic series solution for the critical region for a point disturbance. In this paper a first approximation is derived in a simpler manner.

An integral expression for the wave motion caused by a ship in deep water has been given, for example, by Hogner (1923, equation (51)). The form which we will use here is

$$\zeta = \mathrm{Im} \int_{-\rho}^{\infty} \psi(k)\, e^{ix\phi(k)}\, dk,$$

where $\phi(k) = \cosh k + \frac{1}{2}\tan\theta \sinh 2k$, and where $\psi(k)$ is some function which depends on the shape of the ship. For the present purpose we may assume that ρ is infinite. ζ is the surface displacement at a point with Cartesian co-ordinates (x, y) or polar co-ordinates (r, θ), where the x-axis ($\theta = 0$) is drawn on the surface against the direction of motion. The unit of distance is U^2/g, where U is the steady velocity of the ship. Terms of order r^{-1} have been omitted in this representation.

The usual method of stationary phase gives a first approximation of ζ in the region $|\theta| < \tan^{-1}(1/2\sqrt{2}) = \theta_c$, but it fails in the vicinity of $\theta = \theta_c$ since $\phi'(k)$ and $\phi''(k)$ vanish together along this line. (The dashes denote differentiation with respect to k.) Scorer's method overcomes this difficulty by replacing $\phi(k)$ with parabolas of the third order applied at the stationary values of ϕ. This leads to an approximation in terms of the Airy integral $\mathrm{Ai}(z)$ and the conjugate integral $\mathrm{Gi}(z)$:

$$\mathrm{Ai}(z) + i\,\mathrm{Gi}(z) = \frac{1}{\pi}\int_0^{\infty} \exp\{i(zu + \tfrac{1}{3}u^3)\}\, du.$$

$\mathrm{Ai}(z)$ has been tabulated by Miller (1946). Scorer (1950) tabulates $\mathrm{Gi}(z)$ for $|z| \leqslant 10$, and for larger values there is an asymptotic expression valid to the accuracy of the tables.

2. The approximation

For this purpose the range of integration is suitably divided at k_I, where $\phi''(k_I) = 0$. The function $\phi(k)$ has two turning points when $|\theta| < \theta_c$ and these are denoted by the suffixes T and D, where $k_D < k_I < k_T$. The approximation to $\phi(k)$ is then as follows:

(i) $\phi(k) \doteq \phi_T + \frac{1}{2}\phi''_T(k-k_T)^2 + \frac{1}{6}\phi'''_T(k-k_T)^3$, if $k > k_I$,

and (ii) $\phi(k) \doteq \phi_D + \frac{1}{2}\phi''_D(k-k_D)^2 + \frac{1}{6}\phi'''_D(k-k_D)^3$, if $k < k_I$.

Figure 1 illustrates this. The expression for ζ is written $\zeta = \zeta_T + \zeta_D$, where

$$\zeta_T = \int_{k_I}^{\infty} \quad \text{and} \quad \zeta_D = \int_{-\infty}^{k_I}.$$

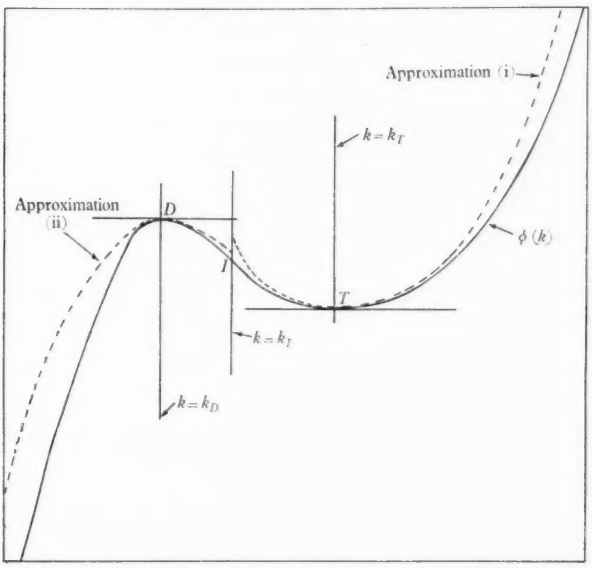

FIGURE 1. An illustration of the approximation to $\phi(k)$ when $|\theta| < \theta_c$. The approximation is most accurate where the rate of change of phase is zero.

It is assumed that $\psi(k)$ is sensibly constant in the region of stationary phase, and we have for large values of x

$$\zeta_T = \mathrm{Im} \int_{k_I}^{\infty} \psi(k)\, e^{ix\phi(k)}\, dk$$

$$= \mathrm{Im}\, \psi_T\, e^{i\phi_T x} \int_{k_I - k_T}^{\infty} \exp\{ix(\tfrac{1}{2}\phi''_T k^2 + \tfrac{1}{6}\phi'''_T k^3)\}\, dk.$$

Following Scorer (1950), we now replace the lower limit of integration by $-\phi''_T/\phi'''_T$. This does not effect the result because the contribution from the

interval $(k_I - k_T, -\phi_T''/\phi_T''')$ is negligible when x is large. We may now write ζ in the form

$$\zeta_S \sim \operatorname{Im} \pi\psi_S \left(\frac{2}{\phi_S''' x}\right)^{\frac{1}{3}} \exp\left[ix\left(\phi_S + \frac{1}{3}\frac{(\phi_S'')^3}{(\phi_S''')^2}\right)\right]\{\operatorname{Ai}(-q_S) \pm i \operatorname{Gi}(-q_S)\},$$

where $q_S = (\phi_S'')^2 [x/2(\phi_S''')^2]^{\frac{2}{3}}$. Here and after where an alternative sign is attached to a symbol the upper and lower sign correspond to $S = T, D$ respectively. This approximation also holds when T, I and D coincide for when $|\theta| = \theta_c$. The expression is simplified if we write

$$\psi(k) = A(k)\, e^{i\alpha(k)},$$

and

$$\operatorname{Ai}(z) + i \operatorname{Gi}(z) = K(z)\, e^{i\kappa(z)}.$$

Scorer has tabulated $K(z)$ and $\kappa(z)$ for $|z| \leqslant 6$. We may then write

$$\zeta_S \sim A_S \left(\frac{2}{\phi_S''' x}\right)^{\frac{1}{3}} K(-q_S) \sin\{\phi_S x \pm \tfrac{2}{3} q_S^{\frac{3}{2}} \pm \kappa(-q_S) + a_S\}. \tag{1}$$

As usual, ζ_T and ζ_D are called the transverse and divergent wave systems respectively. If the stationary phase approximations to $K(-q_S)$ and $\kappa(-q_S)$ are substituted in this formula, the usual stationary-phase approximations to ζ_T and ζ_D are obtained. For $K(-q_S) \sim (\pi^2 q_S)^{-\frac{1}{4}}$ and $\kappa(-q_S) \sim -\frac{2}{3} q_S^{\frac{3}{2}} + \frac{1}{4}\pi$ as $q_S \to \infty$. By (1) we then have

$$\zeta_S \sim A_S \left(\frac{2\pi}{x|\phi_S''|}\right)^{\frac{1}{2}} \sin(\phi_S x \pm \tfrac{1}{4}\pi + a_S)$$

for large values of q_S.

The method may be justified briefly as follows. One of two conditions is to be satisfied. The first is that the ϕ_S'' should be sufficiently small, so that both

$$\exp\left[ix\left\{\frac{\phi_S^{\mathrm{iv}}}{4!}\left(-\frac{\phi_S''}{\phi_S'''}\right)^4 + \frac{\phi_S^{\mathrm{v}}}{5!}\left(-\frac{\phi_S''}{\phi_S'''}\right)^5 + \ldots\right\}\right] \doteqdot 1, \tag{2}$$

and

$$\left|(k_I - k_S) + \frac{\phi_S''}{\phi_S'''}\right| \ll \{|\phi_S'' x|^{-\frac{1}{2}}, |\phi_S''' x|^{-\frac{1}{3}}\}_{\min} \tag{3}$$

hold. Here (2) expresses the condition that the cubic approximation to ϕ is sufficiently accurate in the neighbourhood of stationary phase, and (3) expresses the condition that the contribution from the intervals $(k_I - k_S, -\phi_S''/\phi_S''')$ are negligible. It is easily found that the length of this interval is $O(\phi_S'')^2$ when the ϕ_S'' are small, so that condition (3) is weaker than (2). Hence the first condition may be written

$$(\phi_S'')^4 x \ll 1. \tag{4}$$

The alternative, which is the condition for the validity of the usual method of stationary phase, is that the ϕ_S'' should be sufficiently large so that

$$|\phi_S''|^3 x \gg 1. \tag{5}$$

The regions in which the alternatives (4) and (5) hold overlap if x is sufficiently large, and the approximation (1) is then valid for all $|\theta| \leqslant \theta_c$.

For values of $|\theta| > \theta_c$, $\phi(k)$ has no turning point and we write

$$\phi(k) \sim \phi_I + \phi_I'(k - k_I) + \tfrac{1}{6}\phi_I'''(k - k_I)^3,$$

for all values of k. Figure 2 shows this (cf. Hogner 1923, equation (33)). This approximation may be regarded as a further extension of the principle of stationary phase. For although here no turning point exists, the rate of change of phase is sufficiently small if θ is sufficiently close to θ_c. We have

$$\begin{aligned}\zeta_T &= \operatorname{Im}\int_{k_I}^{\infty}\psi(k)\,e^{ix\phi(k)}\,dk\\ &\sim \operatorname{Im}\psi_I\,e^{ix\phi_I}\int_0^{\infty}\exp\{i(\phi_I'k+\tfrac{1}{6}\phi_I'''k^3)\}\,dk\\ &= \operatorname{Im}\pi\psi_I\left(\frac{2}{\phi_I'''x}\right)^{\frac{1}{3}}e^{i\phi_I x}\{\mathrm{Ai}\,(p)+i\,\mathrm{Gi}\,(p)\},\end{aligned}$$

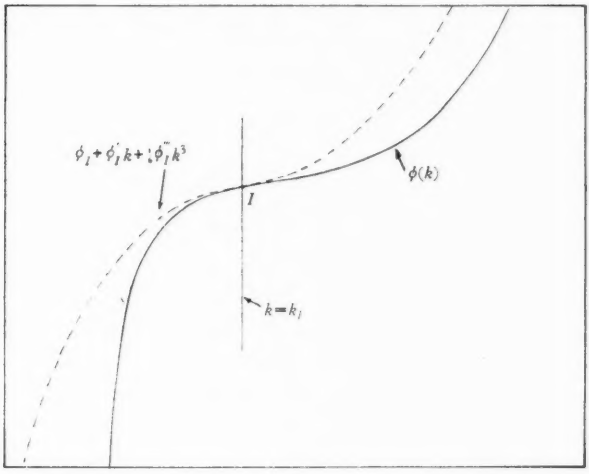

FIGURE 2. The approximation to $\phi(k)$ when $|\theta| > \theta_c$. The approximation is most accurate where the rate of change of phase is least.

where $p = \phi_I'(2x^2/\phi_I''')^{\frac{1}{3}}$. A similar expression for ζ_D holds except that the term in $\mathrm{Gi}\,(p)$ is prefixed by a minus sign. These results for ζ_T and ζ_D may be added to eliminate the term in $\mathrm{Gi}\,(p)$, and we obtain

$$\zeta = 2\pi A_I\left(\frac{2}{\phi_I'''x}\right)^{\frac{1}{3}}\mathrm{Ai}\,(p)\sin\{\phi_I x+a_I\}.$$

This expression rapidly tends to zero as the angle θ increases. However, it is of interest to extend the two wave systems beyond the critical line, so that the manner in which the transverse and divergent wave system interfere with each other may be seen. The expressions for ζ_T and ζ_D when $|\theta| > \theta_c$ may be written

$$\zeta_S \doteq \pi A_I\left(\frac{2}{\phi_I'''x}\right)^{\frac{1}{3}}K(p)\sin\{\phi_I x\pm\kappa(p)+a_I\}. \tag{6}$$

3. The wave pattern

The surface displacement given by (1) and (6) is calculated in the vicinity of $\theta = \theta_c$ with $x \doteqdot 10^4$. It is assumed that $\psi(k)$ in the region is a constant, which for convenience we take to be π^{-1}. The parameter used for the calculations is Δ, where $\Delta^2 = 1 - 8\tan^2\theta$. This gives

$$\phi_S = \tfrac{3}{4}(\tfrac{3}{2})^{\frac{1}{3}}(1 \pm \tfrac{1}{3}\Delta)\left(\frac{1 \pm \frac{1}{3}\Delta}{1 \pm \Delta}\right)^{\frac{1}{2}}, \quad \phi_S'' = \pm\frac{3\Delta}{2^{\frac{1}{2}}}\left(\frac{1 \mp \Delta}{1 \pm \Delta}\right)^{\frac{1}{2}},$$

$$\phi_I = \tfrac{3}{4}(\tfrac{3}{2})^{\frac{1}{3}}\left(\frac{1 - \frac{2}{3}\Delta^2}{1 - \Delta^2}\right)^{\frac{1}{2}}, \quad \phi_I' = -\frac{1}{2^{\frac{1}{2}}2}\frac{\Delta^2}{(1-\Delta^2)^{\frac{1}{2}}},$$

$$q_S x^{-\frac{2}{3}} = \frac{\Delta^2}{2.3^{\frac{1}{3}}}\frac{1 \pm \frac{1}{3}\Delta}{1 \mp \Delta}\left(\frac{1 \mp \Delta}{1 \pm \Delta}\right)^{\frac{1}{2}}, \quad px^{-\frac{2}{3}} = \frac{-\Delta^2}{2.3^{\frac{1}{3}}\{(1 - \frac{2}{3}\Delta^2)(1-\Delta^2)\}^{\frac{1}{3}}}.$$

The substitution $y = (x/2\sqrt{2}) - \eta$ is also made, so that for small Δ,

$$\eta/x = \Delta^2(1 + \tfrac{1}{4}\Delta^2)/4\sqrt{2},$$

and for small η, p and q_S are proportional to $x^{-\frac{1}{3}}\eta$. It is interesting that although there is an optimum choice of axes by which the approximation is most accurate, a change of origin shows that the critical line is fixed only in direction. This is illustrated by the extent of the region where the surface displacement is $O(x^{-\frac{1}{3}})$. Ursell (1960, pp. 429, 430) has shown that this region extends to a distance $O(x^{\frac{1}{3}})$ on both sides of the critical line. Here it is shown by the form of p and q. For example, outside the critical line, for values of p less than about 1 (or for values of η in the range $0 > \eta > -\frac{1}{2}x^{\frac{1}{3}}$), ζ_T, ζ_D and ζ are comparable with ζ_c. For small values of Δ a series expansion is made; and for points just within the critical angle, we have

$$\zeta_S \simeq x^{-\frac{1}{3}}\left(1 \pm \Delta + \frac{\Delta^2}{18}\right) K\left[\frac{\Delta^2 x^{\frac{2}{3}}}{2.3^{\frac{1}{3}}}(1 \pm \tfrac{2}{3}\Delta + \tfrac{2}{3}\Delta^2)\right]$$
$$\times \sin\left\{(\tfrac{3}{2})^{\frac{2}{3}}\left(1 + \frac{\Delta^2}{6} + \frac{61}{216}\Delta^4\right)x \pm \kappa\left[\frac{\Delta^2 x^{\frac{2}{3}}}{2.3^{\frac{1}{3}}}(1 \pm \tfrac{2}{3}\Delta + \tfrac{2}{3}\Delta^2)\right]\right\}.$$

The variation of amplitude and phase with η for the divergent and transverse wave systems is shown in figure 3. ζ_T, ζ_D and ζ may be written in the forms

$$\zeta_S \propto B_S \sin\{\tfrac{1}{2}(\phi_T + \phi_D)x \pm \epsilon_S\},$$

and

$$\zeta \propto B \sin\{\tfrac{1}{2}(\phi_T + \phi_D)x + \epsilon\},$$

so that ϵ is the phase of the combined wave system with respect to the curve $\phi_T + \phi_D = \text{const.}$ B has a maximum of about 1·09 at $\eta \doteqdot 13$, a minimum of about 0·06 at $\eta \doteqdot 28$, and at $\eta = 0$, $B \doteqdot 0{\cdot}71$. Since the amplitude B_S and the phases ϵ_S of the two wave systems are comparable with each other in the vicinity of θ_c, the phase of the resultant wave system changes rapidly in regions where ζ_T and ζ_D are opposed, that is, in regions where $\epsilon_T + \epsilon_D = \pi$. Ursell (1960, figures 2–4 and p. 431) shows this and explains this in terms of the zeros of the Airy integral. Here in figure 4 it is shown by a bend in the curve of zero surface displacement in the region of $\eta = 28$. Figure 4 also shows the two wave systems extended beyond

the critical line. Here the amplitudes of both waves steadily decrease and the crests of one system rapidly approach the troughs of the other.

The general character of the results is similar to those of Hogner (1923) and Ursell (1960). However, differences in detail are to be expected since a different form of ϕ is used here. There is a corresponding difference in ψ, but this is not taken into account since the nature of ψ depends on the ship, as does the nature of the waves. This partly accounts for the difference between Hogner's curves of

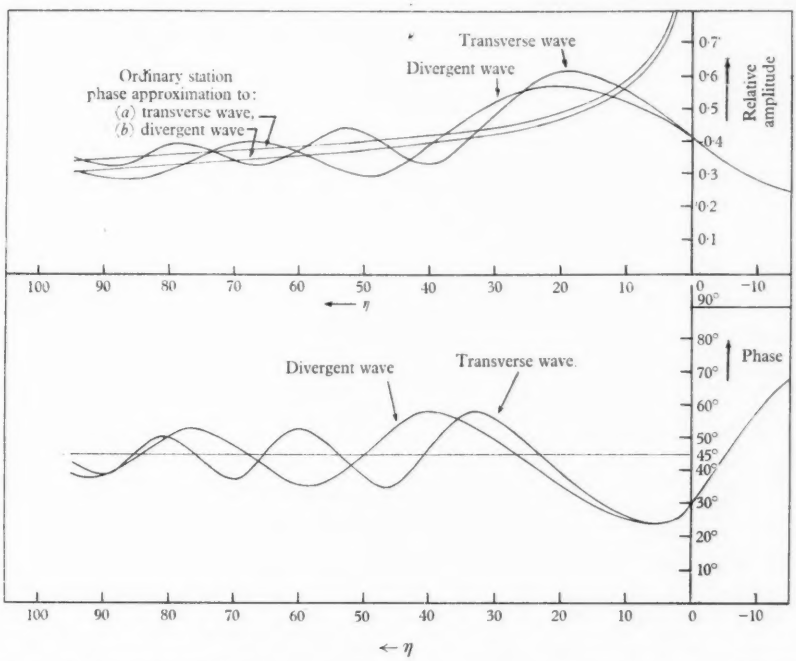

FIGURE 3. Curves of amplitude and phase for the divergent and transverse wave systems in the critical region for $x = 10^4$. The amplitude of both systems are comparable with each other, but the variation of amplitude and phase is more rapid for the transverse waves.

the divergent and transverse wave amplitudes and those shown in figure 3. There is also another reason for this difference. Hogner defines ζ_1 and ζ_2 differently from their counterparts in this paper. In effect the values ζ_T and ζ_D are augmented and diminished respectively by an integral taken along a path in the complex k-plane from the point k_I on the real axis to $-i\infty$. The contours of the system, not shown here, are similar to those given by Ursell (1960, figure 4). Ursell derives for ζ a full asymptotic development whose form remains unchanged across the critical line. However, the simplicity and directness of the method described here have obvious advantages if a first approximation is required.

Further, when $\psi(k)$ is variable the method quickly gives an idea of the magnitude of the transverse and divergent waves over the whole wave pattern. Thus, for ships of broad beam moving at slow speeds, the transverse waves dominate

the pattern, but for slender high-speed craft the divergent waves are most prominent. For example,

$$\psi = \exp\left[-\frac{ag}{U^2}\cosh k - \frac{bg}{U^2}\cosh k \sinh |k|\right] \tag{7}$$

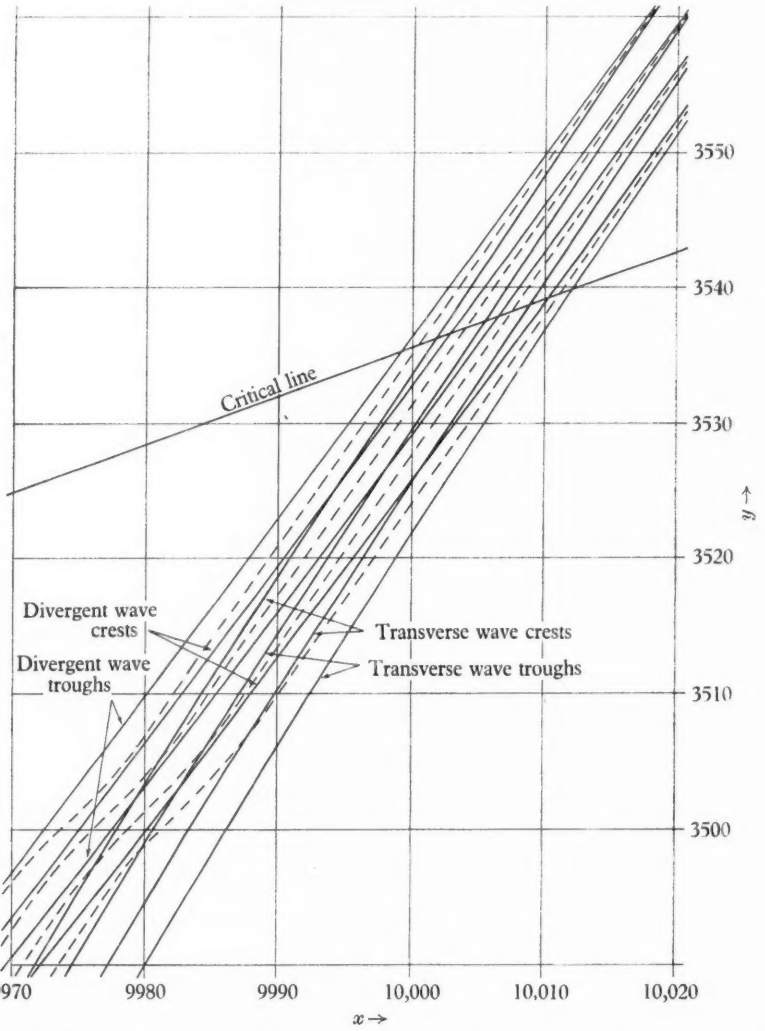

FIGURE 4. Crests and troughs of the two wave systems in a critical region in the vicinity of $x = 10^4$. Curve of zero surface displacement are shown as broken lines. These curves turn sharply in the region of $\eta = 28$, where the two wave systems are opposed, because the two systems have nearly equal amplitudes. Beyond the critical line the amplitudes of both systems are equal and decrease like η^{-1}. Here the troughs of one system rapidly approach the crests of the other and the resultant surface displacement dies away extremely rapidly, like $(\eta x)^{-\frac{1}{4}} \exp(-c\eta^{\frac{1}{2}}x^{-\frac{1}{4}})$, where c is a constant; but for values of η in the range $0 > \eta > -\frac{1}{2}x^{\frac{1}{2}}$, ζ_T, ζ_D and ζ are comparable with ζ_c ($= \zeta$ for $\theta = \theta_c$).

represents a 'forcive' whose strength at any point is proportional to

$$(a^2+x^2)^{-1}\,(b^2+y^2)^{-1}.$$

This forcive is of infinite extent, but beyond certain points its effect is negligible, and expression (7) therefore represents a disturbance whose beam–length ratio is b/a. If the ship is moving at an angle of yaw β, (7) becomes

$$\psi(k) = \exp\left[-\frac{ag}{U^2}\cosh k\,|\cos\beta - \sin\beta\,\sinh k|\right] \times \exp\left[-\frac{bg}{U^2}\cosh k\,|\sin\beta + \cos\beta\,\sinh k|\right].$$

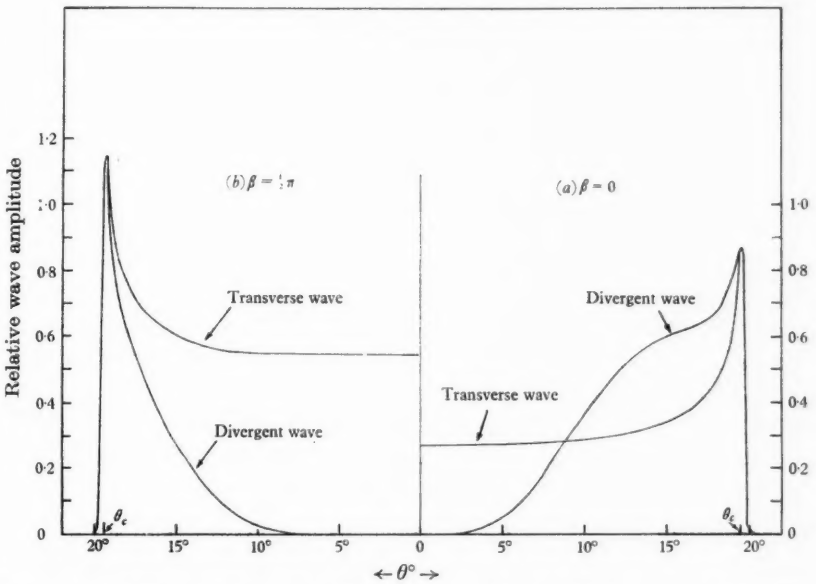

FIGURE 5. Variation of the amplitude of the transverse and divergent waves for a slender high-speed craft, whose beam–length ratio is 1:10. (*a*) For no yaw, $\beta = 0$. (*b*) Lateral motion, $\beta = \frac{1}{2}\pi$. This also illustrates the nature of the relative wave amplitudes for a slow moving broad-beamed ship.

In particular for points at θ ($\theta > 0$) well within the critical angle, this gives expressions for the amplitudes of the transverse and divergent waves which are proportional to

$$\exp\left[-a'\left(\frac{1\pm\frac{1}{3}\Delta}{1\pm\Delta}\right)^{\frac{1}{2}}\left|\cos\beta+\frac{1}{2^{\frac{1}{2}}}\sin\beta\left(\frac{1\mp\Delta}{1\pm\Delta}\right)^{\frac{1}{2}}\right|\right]\exp\left[-b'\left(\frac{1\pm\frac{1}{3}\Delta}{1\pm\Delta}\right)^{\frac{1}{2}}\left|\sin\beta - \frac{1}{2^{\frac{1}{2}}}\cos\beta\left(\frac{1\mp\Delta}{1\pm\Delta}\right)^{\frac{1}{2}}\right|\right]\left(\frac{1\pm\frac{1}{3}\Delta}{1\pm\Delta}\right)^{\frac{5}{4}}(\Delta x)^{-\frac{1}{2}},$$

where

$$a' = \frac{ag}{U^2}\left(\frac{3}{2}\right)^{\frac{1}{2}}, \quad b' = \frac{bg}{U^2}\left(\frac{3}{2}\right)^{\frac{1}{2}}.$$

For corresponding points at $-\theta$, we obtain the same expressions for the wave amplitudes except that β is replaced by $-\beta$. The relative amplitudes for $\beta = 0$,

$\beta = \frac{1}{2}\pi$ are shown in figure 5, where values of $a' = 1$ and $b' = 0{\cdot}1$ have been taken. It shows that for such a craft moving ahead at high speed, the divergent waves are most prominent, whereas a broadside current produces mostly transverse waves.

An interesting case arises when $\beta = \tan^{-1}\sqrt{2} \doteqdot 54\frac{3}{4}°$, i.e. when the ship lies parallel to the wave crests at the critical line, for then the largest wave amplitudes occur. For negative θ, very large divergent waves occur which dominate the pattern. When $|\theta|$ is smaller or when θ is positive, however, transverse waves of

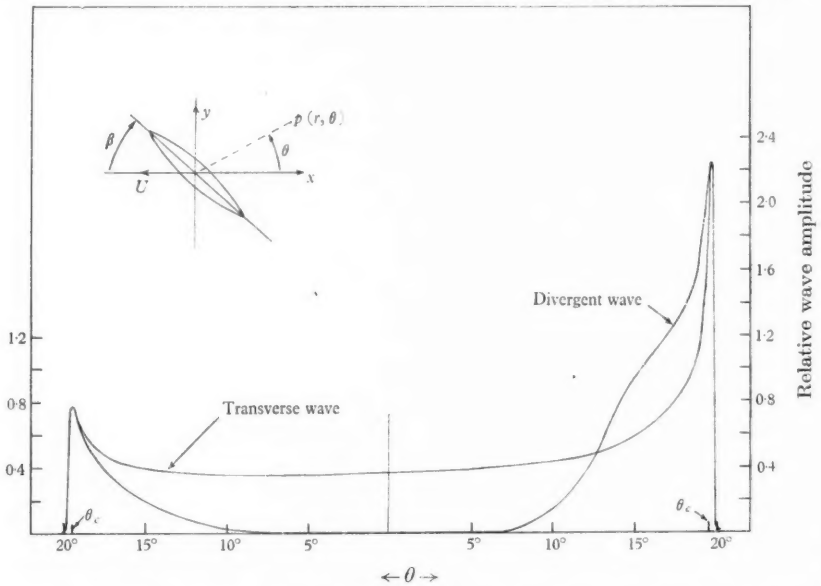

FIGURE 6. Variation of the amplitude of the transverse and divergent waves for a slender high-speed craft whose beam–length ratio is 1:10, for an angle of yaw $\beta = \tan^{-1}\sqrt{2} \doteqdot 54\frac{3}{4}°$ and $x = 10^4$. Here the centre-line of the ship is parallel to the wave crests at the critical line on the after port side.

smaller amplitude are most apparent. Figure 6 illustrates this. These results are similar to those of Scorer (1956*a*, *b*), where lee waves caused by direct and oblique airflow over an isolated hill are discussed.

I would like to express my warmest thanks to Dr Scorer for suggesting this problem and for his very valuable help and encouragement during all stages of this work.

REFERENCES

HOGNER, E. 1923 *Ark. Mat. Astr. Fys.* **17**, 1–50.
MILLER, J. C. P. 1946 *Brit. Ass. Math. Tables*, vol. B. *The Airy Integral.*
SCORER, R. S. 1950 *Quart. J. Math. Appl. Math.* **3**, 107–112.
SCORER, R. S. 1956*a* *Quart. J. Roy. Met. Soc.* **82**, 75–81.
SCORER, R. S. 1956*b* *Quart. J. Roy. Met. Soc.* **82**, 419, 427.
URSELL, F. 1960 *J. Fluid Mech.* **8**, 418–31.

Boundary-layer flow at a saddle point of attachment

By A. DAVEY

Department of Mathematics, University of Manchester

(Received 5 December 1960)

This paper is a study of the flow of a viscous incompressible fluid in the immediate neighbourhood of a saddle point of attachment, near which the external flow is irrotational with components $\{ax, by, -(a+b)z\}$, where $a > 0 > b$. It is shown that the flow is of a boundary-layer character, and that part of the boundary-layer flow is reversed when $b/a < -0{\cdot}4294$.

On the assumption that such flows are physically plausible, the problem may be solved for all values of $b/a \geqslant -1$. Even in the limiting case $b/a = -1$, an effect of the boundary layer is everywhere to draw fluid towards the wall, so that vorticity is still convected towards the wall.

Numerical solutions have been computed, and some of the results are presented in the tables and diagrams.

1. Introduction

When a viscous fluid flows past a body which is simply connected and has a smooth surface, the fluid velocity at a small distance z from the surface is $\boldsymbol{\epsilon} z + O(z^2)$, where $\boldsymbol{\epsilon}$ is tangential to the surface S of the body. In fact $\mu\boldsymbol{\epsilon}$ denotes the skin-friction vector, that is the tangential component of the stress acting on S, where μ is the coefficient of viscosity. A point of the surface at which $\boldsymbol{\epsilon} = 0$ is a stagnation point of the flow and is a 'singular' point of the system of skin friction and vortex lines on S. Such points may be classified into two types, nodal points and saddle points. Moreover, these points are said to be points of attachment or separation according as the fluid near the stagnation streamline is moving towards or away from the surface.

The range of possible patterns of skin friction and vortex lines on such a surface is subject to a topological law, namely, that the number of nodal points must exceed the number of saddle points by 2. A proof of this theorem is given in the Appendix to this paper, together with definitions of the different types of singular points.

It suffices to say here that for a stagnation point of attachment P of a streamline from far upstream, where the flow is irrotational, we may express $\boldsymbol{\epsilon}$ in the form (ax, by), where $P(x, y)$ is the tangent plane at P and x, y are Cartesian co-ordinates. Points P such that both a and b are positive are nodal points of attachment, points P such that one (and only one) of a, b is negative are saddle points of attachment, provided $a+b > 0$. Saddle points of the flow may in some cases be related to the geometrical saddle points of the surface of the body, as will be discussed later. In general boundary-layer theory is not applicable at stagnation

points of separation, since at these points vorticity is not convected towards the body's surface.

In the neighbourhood of a stagnation point of attachment, however, the flow of a viscous fluid is of a boundary-layer character even for moderate Reynolds numbers. Solutions for the flow at two-dimensional and axially symmetrical stagnation points of attachment indicate that the additional terms in the full Navier–Stokes equations are identically zero, provided that the curvature of the body is so small that the surface may be taken to be plane. For the flow at a three-dimensional nodal point of attachment (Howarth 1951) it is also known that the boundary-layer equations yield similarly solutions which are full solutions of the Navier–Stokes equations.

The work of Howarth is important here in that he shows that with a suitable choice of orthogonal axes (x, y, z) the mathematical solution is the same as if the surface were plane, with the x- and y-axes in the plane, and with the external flow given by $\{ax, by, -(a+b)z\}$, where a and b are positive constants.

The purpose of this paper is to discuss the flow near a stagnation point which is a saddle point of attachment. Here again the solution, with suitable choice of axes, is the same as for the problem with a plane surface, in which lie the x and y axes, with the external flow given by $\{ax, by, -(a+b)z\}$, but where now $-a \leqslant b < 0$. The case $b < -a$ would correspond to a saddle point of separation, but it will be shown in § 5 that the equations cannot then be solved.

Saddle points of attachment will occur on suitably shaped bodies placed in a uniform stream or, more practically, may occur for instance between the wing of an aeroplane and an engine mounting, the flow at which may affect separation of the laminary boundary layer over a larger area of the wing.

The present work and that of Howarth only holds near stagnation points for which the external flow is irrotational. It is hoped to extend the treatment in a later paper to discuss cases when the external flow possesses vorticity.

2. The flow past a wavy cylinder

As mentioned in the Introduction of this paper, it is possible for the inviscid flow at a stagnation point to be a saddle point of attachment. For an example of such a case let us consider the flow of an inviscid uniform stream past the cylinder

$$r = r_0(1 + \epsilon \cos \lambda z),$$

as shown in figure 1. We choose ϵ very small and use z to measure distance parallel to the axis of the cylinder, the uniform stream being perpendicular to this axis.

The potential ϕ of the inviscid flow satisfies Laplace's equation $\nabla^2\phi = 0$. We seek a solution of the form $\phi = \phi_0 + \epsilon\phi_1 + O(\epsilon^2)$, where ϕ_0 and ϕ_1 are independent of ϵ. Now ϕ_0 is the potential for flow past the cylinder $r = r_0$, so that

$$\phi_0 = -U\left(r + \frac{r_0^2}{r}\right)\cos\theta. \tag{2.1}$$

Now

$$\nabla^2\phi_1 = 0, \tag{2.2}$$

and on the wall we require

$$\frac{\partial\phi}{\partial r}\cos\gamma + \frac{\partial\phi}{\partial z}\sin\gamma = 0,$$

where γ is the angle between the normal to the surface and the radial direction, since the component of velocity normal to the wall vanishes.

Since $\gamma = O(\epsilon)$, we have

$$\frac{\partial \phi_0}{\partial r} + \epsilon \frac{\partial \phi_1}{\partial r} = O(\epsilon^2) \tag{2.3}$$

when $r = r_0(1 + \epsilon \cos \lambda z)$. Thus

$$-U\{1 - (1 + \epsilon \cos \lambda z)^{-2}\} \cos \theta + \epsilon \frac{\partial \phi_1}{\partial r} = O(\epsilon^2),$$

whence

$$\left[\frac{\partial \phi_1}{\partial r}\right]_{r=r_0} = 2U \cos \lambda z \cos \theta. \tag{2.4}$$

Hence we seek a solution of (2.2) of the form $\phi_1 = \Phi(r) \cos \lambda z \cos \theta$, and we obtain

$$\phi_1 = \{AI_1(\lambda r) + BK_1(\lambda r)\} \cos \lambda z \cos \theta.$$

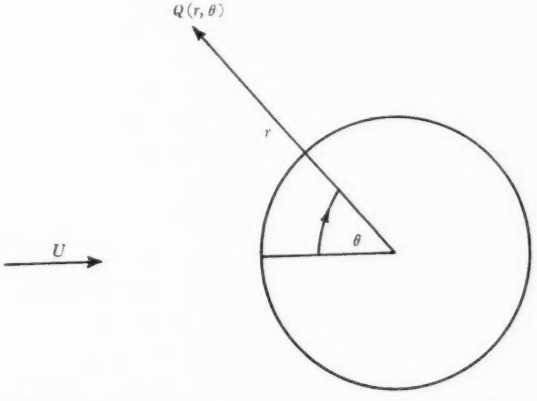

FIGURE 1. Flow past the cylinder $r = r_0(1 + \epsilon \cos \lambda z)$.

Since $I_1(\lambda r) \sim \dfrac{e^{\lambda r}}{(2\pi\lambda r)^{\frac{1}{2}}}$ we take $A = 0$ so that the outer boundary condition may be satisfied. Then (2.4) gives $B = 2U/\{\lambda K_1'(\lambda r_0)\}$, so that

$$\phi_1 = \frac{2UK_1(\lambda r)}{\lambda K_1'(\lambda r_0)} \cos \lambda z \cos \theta.$$

Thus the velocity components (u_z, u_r, u_θ) are given by

$$u_z = -\frac{2U\epsilon K_1(\lambda r)}{K_1'(\lambda r_0)} \sin \lambda z \cos \theta,$$

$$u_r = -U\left\{1 - \frac{r_0^2}{r^2}\right\} \cos \theta + \frac{2U\epsilon K_1'(\lambda r)}{K_1'(\lambda r_0)} \cos \lambda z \cos \theta,$$

$$u_\theta = +U\left\{1 + \frac{r_0^2}{r^2}\right\} \sin \theta - \frac{2U\epsilon K_1(\lambda r)}{\lambda r K_1'(\lambda r_0)} \cos \lambda z \sin \theta.$$

Now set $z = \pi/\lambda + \hat{z}$ and $r = r_0(1-\epsilon) + \hat{r}$ where, for given ϵ, $\hat{z}$ and $\hat{r}$ are arbitrarily small, so that to the first order in $\hat{z}$ and $\hat{r}$ the flow near the geometrical saddle point $z = \pi/\lambda$, $r = r_0(1-\epsilon)$, $\theta = 0$ is given by

$$u_z = \frac{2U\lambda\epsilon K_1(\lambda r_0)}{K_1'(\lambda r_0)}\hat{z}, \tag{2.5}$$

$$u_r = -\left\{\frac{U}{r_0}(2+6\epsilon) + \frac{2U\lambda\epsilon K_1''(\lambda r_0)}{K_1'(\lambda r_0)}\right\}\hat{r}, \tag{2.6}$$

$$u_\theta = \left\{\frac{U}{r_0}(2+4\epsilon) + \frac{2U\epsilon K_1(\lambda r_0)}{\lambda r_0^2 K_1'(\lambda r_0)}\right\}\theta. \tag{2·7}$$

Since $K_1(\lambda r_0) > 0$ and $K_1'(\lambda r_0) < 0$ for $\lambda r_0 > 0$, these equations show that the flow has a saddle point of attachment at the geometrical saddle point

$$\hat{z} = \hat{r} = \theta = 0.$$

3. The flow near a singular point

Howarth (1951) obtained equations for the boundary-layer flow over a general curved surface S. He used a triply-orthogonal co-ordinate system (ξ, θ, ζ), such that $\xi =$ constant and $\theta =$ constant represent developable surfaces formed by the normals to the lines of curvature of S, and $\zeta =$ constant represents a surface parallel to S.

In fact the restriction to lines of curvature is unnecessary, as Howarth's equations are valid for any orthogonal system of curves $\xi =$ constant, $\theta =$ constant on S, as shown by Squire (1957).

Let us choose such an arbitrary system (ξ, θ, ζ) and suppose that the length elements are $h_1 d\xi$, $h_2 d\theta$, $h_3 d\zeta$ in the ξ, θ, ζ directions. Here h_3 is by definition a function of ζ alone, so that we may set $h_3 = 1$ and use ζ to measure distance from S.

If u, v, w are the velocity components in the ξ, θ, ζ directions, respectively, the boundary-layer equations (assuming that h_1, h_2 and all their first derivatives are not large) are as follows:

$$\frac{\partial u}{\partial t} + \frac{u}{h_1}\frac{\partial u}{\partial \xi} + \frac{v}{h_2}\frac{\partial u}{\partial \theta} + w\frac{\partial u}{\partial \zeta} - K_2 uv + K_1 v^2 = -\frac{1}{\rho h_1}\frac{\partial p}{\partial \xi} + \nu\frac{\partial^2 u}{\partial \zeta^2}, \tag{3.1}$$

$$\frac{\partial v}{\partial t} + \frac{u}{h_1}\frac{\partial v}{\partial \xi} + \frac{v}{h_2}\frac{\partial v}{\partial \theta} + w\frac{\partial v}{\partial \zeta} + K_2 u^2 - K_1 uv = -\frac{1}{\rho h_2}\frac{\partial p}{\partial \theta} + \nu\frac{\partial^2 v}{\partial \zeta^2}, \tag{3.2}$$

$$\frac{1}{h_1}\frac{\partial u}{\partial \xi} + \frac{1}{h_2}\frac{\partial v}{\partial \theta} + \frac{\partial w}{\partial \zeta} - K_1 u - K_2 v = 0. \tag{3.3}$$

Here $$K_1 = -\frac{1}{h_1 h_2}\frac{\partial h_2}{\partial \xi} \quad \text{and} \quad K_2 = -\frac{1}{h_1 h_2}\frac{\partial h_1}{\partial \theta}$$

are respectively the geodesic curvatures of the curves $\xi =$ constant and $\theta =$ constant.

In equations (3.1), (3.2) and (3.3) the values of h_1, h_2, K_1 and K_2 may, to the orders of approximation involved, be taken in the surface S. The pressure p is supposed to be prescribed by the inviscid flow, as its variation across the boundary layer is negligible.

Now let P be a stagnation point of attachment of the flow over S. Choose the co-ordinates (ξ, θ, ζ) such that at P, $\xi = \theta = \zeta = 0$ and $h_1 = h_2 = 1$, and such that the boundary-layer equations hold in the form (3.1) to (3.3) near P.

If the mainstream has velocity components U, V, then, by irrotationality,

$$h_2 \frac{\partial V}{\partial \xi} - h_1 \frac{\partial U}{\partial \theta} + V \frac{\partial h_2}{\partial \xi} - U \frac{\partial h_1}{\partial \theta} = 0, \tag{3.4}$$

so that near P, neglecting terms of $O(\xi, \theta)$,

$$\frac{\partial V}{\partial \xi} - \frac{\partial U}{\partial \theta} = 0. \tag{3.5}$$

Thus, if we choose our co-ordinate system (ξ, θ) on the surface so that near P, $U = A\xi$, then also $V = B\theta$, where A and B are constants. In equations (3.1) to (3.3), the terms of lowest order near P are obtained by neglecting the curvature terms and replacing h_1 and h_2 by 1. Moreover, to the same order of approximation, we may suppose the surface to be plane at P with ζ measured normal to the surface so that in the neighbourhood of P the ξ-, θ-, ζ-axes are rectangular.

We now re-name these axes—$P(\xi, \theta, \zeta)$ becoming $P(x, y, z)$—and set $A\xi = ax$ and $B\theta = by$. Hence, as might have been expected, we see that a first solution to the problem is the flow bounded by the plane $z = 0$ with an external velocity $\{ax, by, -(a+b)z\}$, where $P(x, y, z)$ are rectangular cartesian co-ordinates. We do not consider the case when a and b are both negative, which would be appropriate for a nodal point of separation. Hence one of a and b is positive and we shall take the greater of these to be $a > 0$.

Howarth (1951) showed that the velocity components (u, v, w) referred to the axes $P(x, y, z)$ may be taken in the form

$$u = axf'(\eta), \quad v = byg'(\eta), \quad w = -\nu^{\frac{1}{2}}\{af(\eta) + bg(\eta)\}/a^{\frac{1}{2}}, \tag{3.6}$$

where $\eta = a^{\frac{1}{2}}z/\nu^{\frac{1}{2}}$ is the dimensionless distance from the surface. Equation (3.3) is then satisfied, and equations (3.1) and (3.2) become

$$f''' + (f + cg)f'' + (1 - f'^2) = 0, \tag{3.7}$$

$$g''' + (f + cg)g'' + c(1 - g'^2) = 0, \tag{3.8}$$

where $c = b/a$.

The boundary conditions for (3.7) and (3.8) are

$$\left.\begin{aligned} &f = g = f' = g' = 0 \quad \text{when} \quad \eta = 0, \\ &f' \to 1, \; g' \to 1 \quad \text{as} \quad \eta \to \infty. \end{aligned}\right\} \tag{3.9}$$

The solution given above leads to a solution of the full Navier–Stokes equations of motion, as the variation of pressure across the boundary layer can be determined from the z-momentum equation. When $c = 1$ we have $f = g$, and this gives the flow at an axi-symmetrical stagnation point. When $c = 0$, we have $b = 0$ and the flow is that in the neighbourhood of a two-dimensional stagnation point, as on a cylinder in a uniform stream perpendicular to its axis.

For intermediate values of c the velocity profiles given by $f'(\eta)$ and $g'(\eta)$ are of a boundary-layer type, as shown by Howarth who, in his paper, calculated these profiles for $c = 0{\cdot}25$, $0{\cdot}50$ and $0{\cdot}75$, besides giving the already known solutions for $c = 0$ and $c = 1$.

4. The flow near a saddle point of attachment

In his paper Howarth (1951) stated that the solutions of $f'(\eta)$ and $g'(\eta)$ for $c < 0$ may be found from

$$f(\eta, -c) = f(\eta, c), \quad g(\eta, -c) = -g(\eta, c),$$

but these equations are incorrect since they do not satisfy the boundary condition at infinity. Thus solutions with $c < 0$ cannot be found from Howarth's results.

The component of velocity normal to the surface near the stagnation point is $\{-a(1+c)z\}$, which is negative when $c > -1$; in the corresponding viscous flows the vorticity is therefore being convected inwards at the edge of the boundary layer. Thus it is likely that the conditions at infinity can be satisfied only when $c > -1$, and that equations (3.7) and (3.8) will then have solutions of a boundary-layer form. Values of c between 0 and -1 correspond to saddle points of attachment.

A flow with $0 > c > -1$ can occur when an otherwise uniform stream flows past a suitably shaped body, as was shown in §2. It is desirable therefore to obtain quantitative results from equations (3.7) and (3.8) when $c < 0$, with the boundary conditions (3.9). These equations were integrated using the Manchester Mercury Computer. To solve the two-point boundary-value problem a special integration programme was written and solutions for $f(\eta)$ and $g(\eta)$ and their derivatives were obtained, for different negative values of c, correct to three decimal places.

For a certain range of integration the programme evaluated the dependent variables at specified subintervals of the range and an auxiliary routine was used to tabulate the results. The integration programme used the Runge–Kutta process with an error per step of order h^5, where h is a step length. To ensure a given accuracy in each subinterval of size d say, the results of using first p substeps and then $p+1$ substeps were compared. If these differed by less than a preassigned small quantity the machine proceeded to the next subinterval. Otherwise p was increased until agreement was obtained or until there was no further improvement.

For each value of the parameter c the corresponding values of $s = f''(0)$ and $t = g''(0)$ had to be determined so that when the equations were integrated outwards from the origin the solutions had the correct asymptotic behaviour.

It was found that for each specific value of c there existed a line of points (s, t) all of which gave solutions satisfying the outer boundary conditions. Thus the solution is not unique and it was found that the end-point of the line, which was semi-infinite in extent, was the one that made $f'(\eta)$ and $g'(\eta)$ approach unity from below more quickly than any other solution without either ever becoming equal to unity. These solutions (for different c) were taken to be the correct ones as they gave most rapid approach to the outer boundary condition, minimizing the boundary-layer thickness. These solutions are the ones whose asymptotes are derived solely from exponential terms.

Let us determine for large values of η the asymptotic solutions of equations (3.7) and (3.8).

Let $$\alpha = \lim_{\eta\to\infty}(\eta - f), \quad \beta = \lim_{\eta\to\infty}(\eta - g),$$

and put $f = \eta - \alpha - H$, $g = \eta - \beta - K$. Then if

$$F = H'(\eta) = 1 - f' \quad \text{and} \quad G = K'(\eta) = 1 - g',$$

the result of linearizing (3.7) and (3.8) is

$$F'' - \{(\alpha + \beta c) - \eta(1+c)\}F' - 2F = 0, \tag{4.1}$$

$$G'' - \{(\alpha + \beta c) - \eta(1+c)\}G' - 2cG = 0, \tag{4.2}$$

where primes denote differentiation with respect to η.

Now choose a new independent variable

$$\chi = k\left\{\eta - \left(\frac{\alpha + \beta c}{1+c}\right)\right\} \quad (c > -1),$$

where $k = (1+c)^{\frac{1}{2}}$ which is > 0, and (4.1), (4.2) become respectively

$$F'' + \chi F' - \frac{2}{1+c}F = 0, \tag{4.3}$$

$$G'' + \chi G' - \frac{2c}{1+c}G = 0. \tag{4.4}$$

The asymptotic solutions of (4.3) and (4.4) then give

$$1 - f' \sim A_1 e^{-\frac{1}{2}\chi^2}\chi^{\{2/(1+c)+1\}}\{1 + o(1)\} + B_1\chi^{2/(1+c)}\{1 + o(1)\} \tag{4·5}$$

$$1 - g' \sim A_2 e^{-\frac{1}{2}\chi^2}\chi^{\{2c/(1+c)+1\}}\{1 + o(1)\} + B_2\chi^{2c/(1+c)}\{1 + o(1)\}. \tag{4.6}$$

The values of A_1, A_2, B_1, B_2 will depend upon the position of the point (s, t). In order to satisfy the boundary conditions at infinity, we must have $B_1 = 0$ but (since $-1 < c < 0$) B_2 is left arbitrary.

Thus there will be a curve in the (s, t)-plane given by $B_1 = 0$ and the solution which approaches its asymptote most rapidly will be obtained from that point (s^*, t^*) of the curve which makes $B_2 = 0$. The solutions which arise from points of the curve $B_1 = 0$ on one side of (s^*, t^*) will make $B_2 < 0$, and so g' would approach its limit from above, whereas those on the other side will make $B_2 > 0$, so that g' remains < 1. Thus, for each value of c the required point (s^*, t^*) is the intersection of the curves $B_1(s, t) = 0$ and $B_2(s, t) = 0$.

A special subprogramme was written for the Mercury Computer to determine the appropriate points (s^*, t^*) as accurately as possible. For each case s^* was determined to 8 places of decimals and t^* to 5 places.

When c is slightly negative the solutions for f and g resemble those with $c > 0$. As c decreases $g''(0)$ decreases so that the skin-friction along the y-axis is reduced as c becomes more negative. When $c = -0{\cdot}4294$ one finds that $g''(0) = 0$, indicating that there is a tendency for some of the flow to reverse its direction. When $c < -0{\cdot}4294$ reversal of the v-component of flow does in fact occur. However, the velocity profiles given by $f'(\eta)$ and $g'(\eta)$ are still of the same character as velocity profiles in two-dimensional boundary-layer flows with separation.

When $c = -1$ solutions satisfying the outer boundary condition are still obtainable, the amount of reversed flow is greatest and the greatest value of

$-g'(\eta)$, the backflow velocity, is roughly 0·33. For this case ($c = -1$) equations (4.1) and (4.2) take the form

$$F''+(\beta-\alpha)F'-2F=0, \tag{4.7}$$

$$G''+(\beta-\alpha)G'+2G=0. \tag{4.8}$$

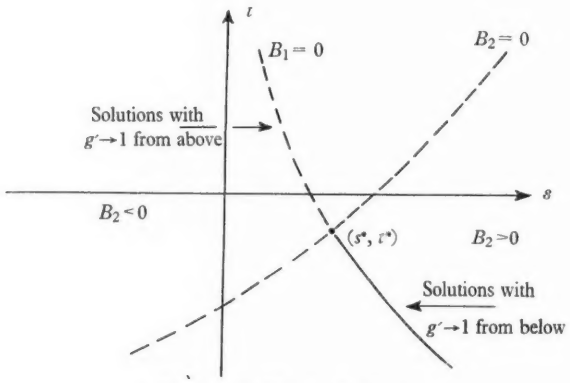

FIGURE 2. The (s, t)-plane.

Moreover, it was found from the numerical integration of (3.7) and (3.8) that when $c = -1$, $\beta-\alpha = 2\sqrt{2}$ to 5 decimals. Hence the asymptotic solutions are

$$1-f' \sim A_1 e^{-(2+\sqrt{2})\eta}\{1+o(1)\}+B_1 e^{(2-\sqrt{2})\eta}\{1+o(1)\}, \tag{4.9}$$

$$1-g' \sim A_2 e^{-\sqrt{2}\eta}\{1+o(1)\}+B_2\eta e^{-\sqrt{2}\eta}\{1+o(1)\}, \tag{4.10}$$

and the appropriate ones, for the same reasons as before, are given by $B_1 = B_2 = 0$.

Thus even when $c = -1$ equations (3.7) and (3.8) still yield solutions which satisfy the Navier–Stokes equations for the flow over an infinite plane with an external flow $(ax, -ay, 0)$. The three-dimensional boundary-layer displacement thickness which we define, in accordance with Lighthill (1958), to be the thickness of that layer which when attached to the original surface modifies the inviscid flow outside it by the same amount as the boundary layer, is now infinite and for large values of η we have $w = -2(2a\nu)^{\frac{1}{2}}$. When η is small

$$w \sim -\nu^{\frac{1}{2}}a^{\frac{1}{2}}\{f''(0)-g''(0)\}\eta^2,$$

so that the negative value of $g''(0)$, which indicates a reversal of flow, contributes to the flow towards the surface and so opposes the spreading of vorticity away from the surface. Thus a boundary-layer type of flow is still possible.

Solutions of equations (3.7) and (3.8) with the boundary conditions (3.9) were obtained for thirteen different negative values of $c \geqslant -1$ and some of these results are given in §7, which contains the numerical results.

Finally we give the appropriate formulae for the various boundary-layer displacement thicknesses for general c. Since $w = -\nu^{\frac{1}{2}}(af+bg)/a^{\frac{1}{2}}$, we have for large η

$$w = -\nu^{\frac{1}{2}}\{a(\eta-\alpha)+b(\eta-\beta)+o(1)\}/a^{\frac{1}{2}},$$

where α and β are as defined earlier. Hence the three-dimensional boundary-layer displacement thickness δ_1 at the saddle point is given by

$$\delta_1 = \frac{\nu^{\frac{1}{2}}}{a^{\frac{1}{2}}}\left\{\frac{\alpha+c\beta}{1+c}\right\}. \tag{4.11}$$

The two-dimensional boundary-layer displacement thicknesses δ_x, δ_y in the x-, y-directions respectively are given by

$$\frac{a^{\frac{1}{2}}}{\nu^{\frac{1}{2}}}\delta_x = \int_0^\infty (1-f')\,d\eta = \lim_{\eta\to\infty}(\eta-f) = \alpha,$$

$$\frac{a^{\frac{1}{2}}}{\nu^{\frac{1}{2}}}\delta_y = \int_0^\infty (1-g')\,d\eta = \lim_{\eta\to\infty}(\eta-g) = \beta.$$

Some values of δ_1, δ_x, and δ_y, are tabulated for different values of c in table 1 of §7.

5. Insolubility of the case $c < -1$

When $c < -1$ the external flow has $w = -a(1+c)z$ so that $w > 0$. Hence in the corresponding viscous flow it seems likely that vorticity will beconvected away from the surface into the mainstream. Because of this we expect conditions at infinity to be upset, and we prove below that no solutions of (3.7) and (3.8) exist which satisfy all the boundary conditions (3.9). We restrict our attention to the existence of solutions f and g which possess derivatives of every order at all points in the range $0 \leqslant \eta \leqslant \infty$.

Lemma 1. No solution $g'(\eta)$ exists which has a stationary value of 1 for finite η.

Proof. Equation (3.8) may be re-arranged in the form

$$g''' = c(g'^2-1) - (f+cg)g''. \tag{5.1}$$

Suppose for $\eta = \eta_1$ we have $g'(\eta_1) = 1$ and $g''(\eta_1) = 0$. Then it follows from (5.1) and the derivatives of this equation that g''' and all higher derivatives are zero when $\eta = \eta_1$, hence $g' \equiv 1$. The boundary condition $g'(0) = 0$ is thus not satisfied and the Lemma is proved.

Lemma 2. When $c < 0$ and g' has a stationary value then if $|g'| < 1$ it is a minimum and if $|g'| > 1$ it must be a maximum.

Proof. If g' has a stationary value, then $g'' = 0$ at this point and $g''' = c(g'^2-1)$ by equation (5.1).

Thus if $c < 0$ and $|g'| < 1$, $g''' > 0$ so that g' is a minimum. If $c < 0$ and $|g'| > 1$, $g''' < 0$ and g' is a maximum.

Theorem 1. There is no solution $g'(\eta)$ when $c < -1$ such that $g' \to 1$ as $\eta \to \infty$, with $|g'| < 1$ for all $\eta > \eta_0$.

Proof. Suppose if possible that such a solution $g'(\eta)$ exists. By lemma 2, since $|g'| < 1$, g' has for $\eta > \eta_0$ at most one stationary value because one cannot have two consecutive stationary values which are both minima.

Also since $g' \to 1$ as $\eta \to \infty$ and $|g'| < 1$ for all $\eta > \eta_0$ then g'' must be positive for all sufficiently large η.

Moreover $f+cg \sim (1+c)\eta$ will, for $c < -1$, be negative for all sufficiently large η. Hence (5.1) gives $g''' > 0$ for all sufficiently large η. Since $g'' > 0$ this contradicts the assumption that $g' \to 1$ and so no such solutions exists.

Theorem 2. There is no solution $g'(\eta)$ when $c < -1$ such that $g' \to 1$ as $\eta \to \infty$, with $g' > 1$ for all $\eta > \eta_0$.

Proof. Similar to that given in theorem 1.

Lemma 3. If, when $c < -1$, $f+cg < 0$ for all $\eta > \eta_0$ and $g''(\eta)$ vanishes for $\eta = \eta_1, \eta_2, \ldots$ with $\eta_0 < \eta_1 < \eta_2 < \ldots$, then the sequence $g'(\eta_i)$ does not tend to 1 as $i \to \infty$.

Proof. Multiply (5.1) throughout by $g''(\eta)$ and integrate between η_r and η_s, where $g''(\eta_r) = g''(\eta_s) = 0$ with $\eta_0 < \eta_r < \eta_s$.

Then
$$[\tfrac{1}{2}g''^2]_{\eta_r}^{\eta_s} = \tfrac{1}{3}c[(g'^3 - 3g')]_{\eta_r}^{\eta_s} - \lambda, \tag{5.2}$$
where $\lambda = \int_{\eta_r}^{\eta_s} (f+cg)\, g''^2 d\eta$.

Since $f+cg < 0$ for all $\eta > \eta_0$, λ is negative and (5.2) gives
$$(g'^3 - 3g')_{\eta_s} > (g'^3 - 3g')_{\eta_r}.$$

As $g' = 1$ makes $(g'^3 - 3g')$ a minimum when regarded as a function of g', we therefore cannot have $g'(\eta_i) \to 1$ as $i \to \infty$.

Theorem 3. Equation (5.1) or (3.8) has no solution satisfying $g'(\eta) \to 1$ as $\eta \to \infty$ when $c < -1$.

Proof. Suppose if possible such a solution $g'(\eta)$ exists. Then it follows from theorems 1 and 2 that g' must take values on both sides of 1 as $\eta \to \infty$. Hence there must be a distinct sequence η_i with $\eta_{i+1} > \eta_i$ and $\lim_{i\to\infty} \eta_i = \infty$ at which g' has stationary values. Since $f' + cg' \to 1 + c < 0$ we can choose η_0 such that $f+cg < 0$ for all $\eta > \eta_0$. Then by lemma 3 the sequence $g'(\eta_i)$ does not tend to 1, contrary to hypothesis.

We might note that theorem 3 disproves the existence of mathematical solutions of equations (3.7) and (3.8) with the boundary conditions (3.9), whereas lemma 1 and theorem 1 in themselves are sufficient to disprove the existence of solutions which are physically plausible.

6. Physical interpretation of the results

To what extent does one have fluid flows with saddle points of attachment which may be quantitatively explained by our results? Also, how useful a guide are our solutions, when it is remembered that we used a mainflow which was a linear function of the co-ordinates, so that our solutions are only applicable in the immediate neighbourhood of the stagnation point?

The possibility of saddle points of attachment occurring in inviscid flows was demonstrated in §2. Consider now a body, symmetrical about the planes $x = 0$, $y = 0$, possessing two protuberances as shown in figure 3. Here the z-axis is normal to the body at Z_3 and the (x, y)-plane is the tangent plane at Z_3, the y-axis lying in the plane of the paper.

When this body is placed in a uniform stream U_∞ parallel to the z-direction there will be nodal points of attachment at the protuberances if the rest of the body is slenderly swept back. If the curve C, the intersection of the surface of the body with the (y, z)-plane is indented only slightly between the nodes, there will be a saddle point of attachment at Z_3. The flow in the neighbourhood of Z_3 will be given by the solution of equation (3.7) and (3.8) for some value of c between 0 and $-0{\cdot}4294$.

In figure 4 the full lines give the mainflow in the y-direction near the nodes and the saddle point, where it depends linearly on y. It is reasonable to suppose

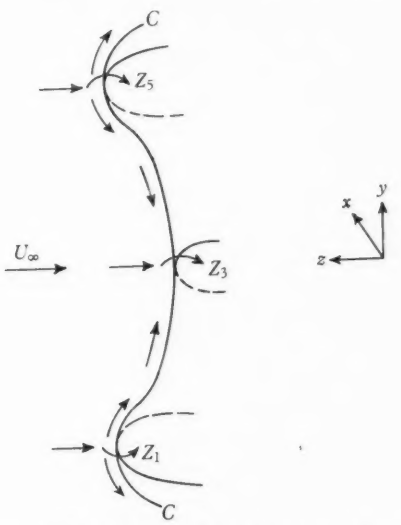

FIGURE 3. Flow past a body with two protuberances.

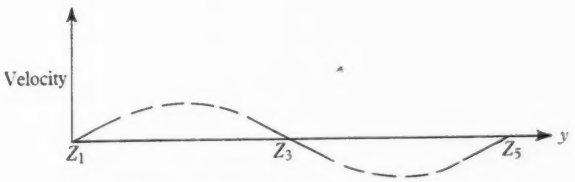

FIGURE 4. The external velocity in the y-direction.

that between these points the mainflow may be extrapolated via the dashed lines. These would not cross the axis, for if so, we would have more nodes and saddles but we are explicitly considering a saddle point of the flow and its two adjacent nodes. In this case, where the flow near Z_3 is given by equations (3.7) and (3.8) for some value of c between 0 and $-0{\cdot}4294$, the pattern of the skin-friction lines on the surface of the body is as shown in figure 5.

Two cases are possible according as to which direction the skin-friction lines at Z_1 and Z_5 are tangential. A general guide is that they will be tangential to the

direction of greatest principal curvature at these points, which direction will depend on the shape of the protuberances. The topography for the two cases is, however, essentially unchanged save near these points, and we illustrate the case when the protuberances extend more in the x-direction than in the y-direction.

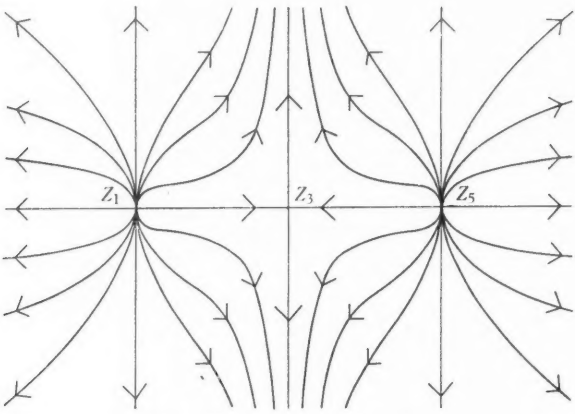

FIGURE 5. The pattern of skin-friction lines when the flow near Z_3 is given by equations (3.7) and (3.8) for a value of $c > -0{\cdot}4294$.

Now suppose we bend the curve C in figure 3 further inwards at Z_3 so as to increase the inflow in the y-direction towards Z_3. Then the corresponding value of c, appropriate to the flow near Z_3, will diminish and if the inflow towards Z_3 is great enough the flow would reverse its direction along and near to the y-axis. It is possible that if this happened the backflow would spread causing additional saddle points of attachment Z_2 and Z_4 (at which there was no reversed flow) in the flow very close to the surface and in the skin-friction lines, the original saddle point having changed into a node so that the new pattern is as in figure 6. Note that in the region shown here the excess number of nodal points over saddle points is unchanged as required (see Appendix).

Since streamlines from far upstream now attach themselves at Z_2 and Z_4, the surface flow near Z_3 is considerably altered, however, the general structure of the flow is readily inferred on examining figure 6. The lines SS through Z_2 and Z_4 will be lines of separation of limiting streamlines and the line AA through Z_3 will be a line of attachment. One infers that fluid separates, in the form of bubbles from the lines SS, the surfaces of separation curling over as fluid falls down the 'back' of the saddle and attaching themselves to the line AA. This means that mainstream fluid which approaches the body between the streamline surfaces through say the stagnation streamlines which attach themselves to Z_2 and Z_3, falls off the 'back' of the saddle, rotates, and stretched away like a vortex in a clockwise direction viewed from figure 7. Similarly another vortex rolls away on the other side of Z_3 in an anti-clockwise direction.

The presence of the vortex bubble may invalidate the assumption that the flow near Z_3 is of boundary-layer nature, and so solutions of equations (3.7)

and (3.8) for values of c less than $-0{\cdot}4294$ may be only of theoretical interest. When one has flow over a semi-infinite plane, the only singularity being the saddle point, backflow may be said to occur where

$$\mathbf{v}_e . \mathbf{v}_s < 0. \tag{6.1}$$

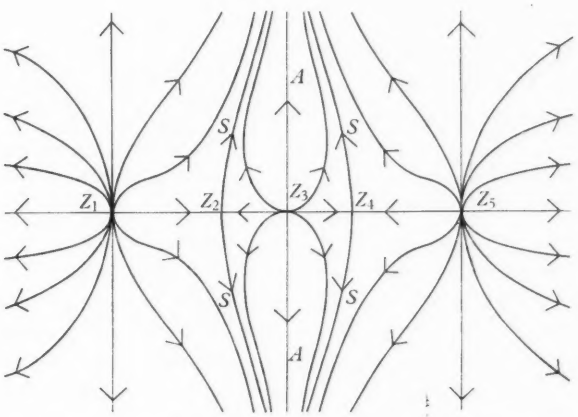

FIGURE 6. The pattern of skin-friction lines when reverse flow occurs in the boundary layer near Z_3.

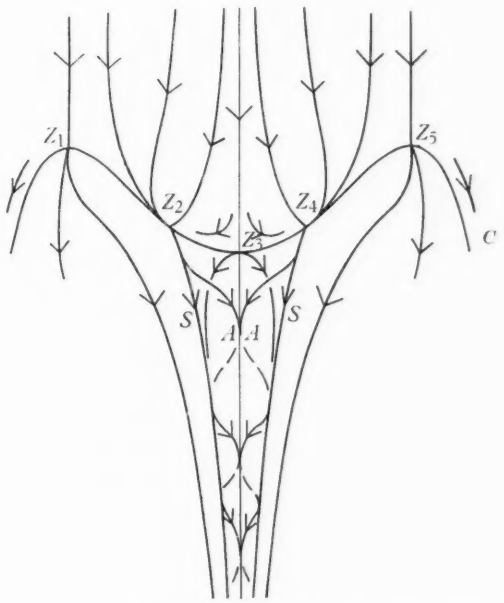

FIGURE 7. The 'twin vortex bubble' which rolls away from Z_3 down the back of the saddle.

Here $\mathbf{v}_e$ is the external mainflow and $\mathbf{v}_s$ is the velocity within the boundary layer. Near the saddle point Z_3 then there is backflow where

$$a^2x^2f'(\eta)+b^2y^2g'(\eta)+\frac{\nu}{a}(a+b)\,\eta\{af(\eta)+bg(\eta)\}<0. \tag{6.2}$$

For fixed η this is the region contained by a hyperbola whose asymptotes L_1, L_2 are the lines

$$a^2x^2f'(\eta)+b^2y^2g'(\eta)=0. \tag{6.3}$$

Velocities normal to the surface $\eta = 0$ are small even for a moderate Reynolds number, so that such hyperbolae lie close to their asymptotes. In fact as $\eta \to 0$ the associated hyperbola reduces to its asymptotes which then pass through the origin. For fixed η the region of backflow diminishes as η increases until it becomes zero at $\eta = \bar{\eta}$, where $g'(\eta) = 0$ again, when the two lines L_1, L_2 coincide.

7. Numerical results

Solutions of equations (3.7) and (3.8) subject to the boundary conditions (3.9) were obtained for thirteen negative values of c and in particular for $c = 0$, $-0{\cdot}25$, $-0{\cdot}4294$, $-0{\cdot}50$, $-0{\cdot}75$ and -1. The initial values $f''(0)$ and $g''(0)$, together with the three boundary-layer displacement thicknesses, are given in

c	$f''(0)$	$g''(0)$	$\frac{a^{\frac{1}{2}}}{\nu^{\frac{1}{2}}}\delta_1$	$\frac{a^{\frac{1}{2}}}{\nu^{\frac{1}{2}}}\delta_x$	$\frac{a^{\frac{1}{2}}}{\nu^{\frac{1}{2}}}\delta_y$
0·0	1·2326	0·5705	0·648	0·648	1·026
−0·1	1·2284	0·4594	0·600	0·654	1·141
−0·2	1·2258	0·3353	0·501	0·658	1·287
−0·25	1·2251	0·2680	0·421	0·659	1·375
−0·3	1·2250	0·1970	0·311	0·660	1·474
−0·4	1·2265	0·0460	−0·036	0·659	1·702
−0·4294	1·2273	0	−0·183	0·658	1·776
−0·5	1·2302	−0·1115	−0·652	0·655	1·962
−0·6	1·2359	−0·2666	−1·726	0·649	2·232
−0·7	1·2432	−0·4130	−3·688	0·641	2·497
−0·75	1·2473	−0·4821	−5·330	0·637	2·625
−0·8	1·2517	−0·5488	−7·852	0·632	2·753
−0·9	1·2612	−0·6761	−20·96	0·622	3·018
−1·0	1·2729	−0·8112	$-\infty$	0·610	3·438

TABLE 1

table 1 for all thirteen cases considered and the corresponding quantities for $c = 0$ are also given for comparison. Quantities in this table are correct to the number of decimal places given. One may note from this table that δ_1, the three-dimensional displacement thickness, is negative for a range of c for which reverse flow does not occur. As c approaches -1 then δ_1 becomes large and negative. When $c = -1$ we have $\delta_1 = -\infty$ and $\delta_y - \delta_x = 2{\cdot}828$. This last figure was evaluated more accurately and found to be equal to $2\sqrt{2}$ to five decimal places.

Table 2 contains, for the six values of c mentioned in the text, the functions f' and g' correct to three decimal places.†

As Howarth found for his range of c, it is also the case here that for $-1 \leqslant c \leqslant 0$ changes with c are small for the velocity in the x-direction, though much greater in the y-direction, the direction in which backflow occurs. This is indicated by the growing difference between δ_x and δ_y as c becomes more negative. For negative values of c, $f''(0)$ reaches a minimum value of 1·225 near $c = -0{\cdot}3$ and then rises to 1·273 when $c = -1$ so that over the whole range from $c = 1$, when $f''(0) = 1{\cdot}312$, to $c = -1$, $f''(0)$ varies very little. However $g''(0)$, which is also

	$c = 0$		$c = -0{\cdot}25$		$c = -0{\cdot}4294$	
η	f'	g'	f'	g'	f'	g'
0·0	0·000	0·000	0·000	0·000	0·000	0·000
0·1	0·118	0·057	0·118	0·028	0·118	0·002
0·2	0·227	0·114	0·225	0·059	0·226	0·009
0·3	0·325	0·171	0·323	0·092	0·324	0·019
0·4	0·414	0·227	0·412	0·127	0·412	0·034
0·5	0·495	0·284	0·491	0·164	0·492	0·053
0·6	0·566	0·339	0·562	0·204	0·563	0·076
0·7	0·630	0·393	0·625	0·245	0·626	0·103
0·8	0·686	0·446	0·681	0·287	0·682	0·134
0·9	0·735	0·498	0·729	0·331	0·731	0·167
1·0	0·778	0·547	0·772	0·375	0·773	0·204
1·1	0·815	0·594	0·809	0·419	0·810	0·243
1·2	0·847	0·639	0·841	0·464	0·841	0·284
1·3	0·874	0·681	0·868	0·508	0·868	0·327
1·4	0·897	0·720	0·891	0·551	0·891	0·371
1·5	0·916	0·756	0·910	0·593	0·911	0·415
1·6	0·932	0·789	0·927	0·633	0·927	0·460
1·7	0·946	0·819	0·941	0·672	0·941	0·504
1·8	0·957	0·846	0·952	0·708	0·952	0·547
1·9	0·966	0·870	0·961	0·742	0·961	0·589
2·0	0·973	0·891	0·969	0·774	0·969	0·629
2·2	0·984	0·926	0·981	0·829	0·980	0·703
2·4	0·991	0·951	0·988	0·875	0·988	0·769
2·6	0·995	0·969	0·993	0·911	0·993	0·824
2·8	0·997	0·981	0·996	0·938	0·996	0·869
3·0	0·998	0·989	0·998	0·958	0·997	0·905
3·2	0·999	0·993	0·999	0·973	0·998	0·933
3·4	1·000	0·996	0·999	0·983	0·999	0·954
3·6	—	0·998	1·000	0·989	1·000	0·969
3·8	—	0·999	—	0·994	—	0·979
4·0	—	1·000	—	0·996	—	0·987
4·5	—	—	—	0·999	—	0·996
5·0	—	—	—	1·000	—	0·999
6·0	—	—	—	—	—	1·000

TABLE 2

† A table of values of f and g and their first and second derivatives for these same values of c has been lodged with the Editor of the *Journal of Fluid Mechanics* and may be consulted by readers on application to the Editor.

	$c = -0{\cdot}50$		$c = -0{\cdot}75$		$c = -1$	
η	f'	g'	f'	g'	f'	g'
0·0	0·000	0·000	0·000	0·000	0·000	0·000
0·1	0·118	−0·009	0·120	−0·044	0·122	−0·076
0·2	0·226	−0·012	0·230	−0·081	0·235	−0·142
0·3	0·325	−0·011	0·330	−0·111	0·337	−0·198
0·4	0·413	−0·005	0·420	−0·133	0·430	−0·244
0·5	0·493	0·007	0·501	−0·147	0·513	−0·280
0·6	0·565	0·023	0·574	−0·154	0·588	−0·307
0·7	0·628	0·043	0·638	−0·153	0·653	−0·323
0·8	0·684	0·069	0·695	−0·145	0·711	−0·330
0·9	0·733	0·098	0·744	−0·130	0·760	−0·328
1·0	0·775	0·131	0·786	−0·109	0·803	−0·318
1·1	0·812	0·167	0·823	−0·082	0·840	−0·299
1·2	0·843	0·207	0·854	−0·049	0·870	−0·273
1·3	0·870	0·248	0·881	−0·011	0·896	−0·241
1·4	0·893	0·292	0·903	0·031	0·917	−0·203
1·5	0·912	0·337	0·922	0·076	0·935	−0·160
1·6	0·928	0·382	0·937	0·124	0·949	−0·114
1·7	0·942	0·428	0·950	0·175	0·960	−0·064
1·8	0·953	0·473	0·960	0·226	0·969	−0·012
1·9	0·962	0·518	0·968	0·279	0·976	0·042
2·0	0·970	0·562	0·975	0·331	0·982	0·097
2·2	0·981	0·644	0·985	0·433	0·990	0·206
2·4	0·988	0·717	0·991	0·529	0·994	0·311
2·6	0·993	0·780	0·995	0·617	0·997	0·410
2·8	0·996	0·833	0·997	0·694	0·998	0·500
3·0	0·997	0·876	0·998	0·759	0·999	0·581
3·2	0·999	0·911	0·999	0·814	1·000	0·651
3·4	0·999	0·937	0·999	0·859	—	0·712
3·6	1·000	0·956	1·000	0·895	—	0·764
3·8	—	0·970	—	0·923	—	0·807
4·0	—	0·980	—	0·944	—	0·844
4·5	—	0·994	—	0·977	—	0·909
5·0	—	0·998	—	0·991	—	0·948
6·0	—	1·000	—	0·999	—	0·984
7·0	—	—	—	1·000	—	0·995
9·0	—	—	—	—	—	1·000

TABLE 2 (*cont.*)

1·312 when $c = 1$, is zero when $c = -0{\cdot}4294$ and becomes negative attaining a minimum value of $-0{\cdot}811$ when $c = -1$. The function $\bar{\eta} = \bar{\eta}(c)$ mentioned at the end of the previous section, which measures, when $c < -0{\cdot}4294$, the height of the back-flow region, has a maximum value of 1·82 when $c = -1$.

I wish to thank Professor M. J. Lighthill and Mr E. J. Watson for their guidance and inspiration throughout the preparation of this paper, Mr R. A. Brooker for his tuition in writing programmes for a Mercury Computer and the Department of Scientific and Industrial Research for a maintenance grant.

Appendix: singular points

If, as in the Introduction, we have viscous fluid flowing past a body which is topologically equivalent to a sphere and which has a smooth surface, the fluid velocity at a small distance z from the surface is $\boldsymbol{\epsilon}z+O(z^2)$, where $\boldsymbol{\epsilon}$, a function of position of a point P on the surface S, lies in the tangent plane to S at P. Let $\mathbf{n}$ denote the unit vector along the outward normal to S at P and let $\boldsymbol{\omega}$ denote the fluid vorticity in the tangent plane to S at P so that $\boldsymbol{\epsilon} = \boldsymbol{\omega} \wedge \mathbf{n}$. Then the system of lines $\boldsymbol{\epsilon}$ parallel to $\mathbf{dr}$ and $\boldsymbol{\omega}$ parallel to $\mathbf{dr}$, where $\mathbf{dr}$ is the relative position of two adjacent points on a curve, form an orthogonal net on S, the latter being the vortex lines on the surface.

A point of S at which $\boldsymbol{\epsilon} = \boldsymbol{\omega} = 0$ is a stagnation point of the flow and is a singular point of the differential equations of both systems of curves which map S. Let P be such a singular point and take rectangular Cartesian co-ordinates $P(x, y, z)$ such that Pz is along the outward normal to the surface and $P(x, y)$ is the tangent plane to S at P.

By continuity of the flow the normal component of velocity w is given by

$$w = -\tfrac{1}{2}\Delta z^2 + O(z^3),$$

where $\Delta = \operatorname{div} \boldsymbol{\epsilon}$ is the two-dimensional divergence of $\boldsymbol{\epsilon}$.

According as to whether $\Delta > 0$ or $\Delta < 0$ we say that P is a stagnation point of attachment or separation, respectively.

Now suppose $\boldsymbol{\epsilon}$ has components ϵ_x, ϵ_y with respect to the x, y-axes and define

$$J = \frac{\partial \epsilon_x}{\partial x}\frac{\partial \epsilon_y}{\partial y} - \frac{\partial \epsilon_x}{\partial y}\frac{\partial \epsilon_y}{\partial x}.$$

J is invariant with respect to a rotation about P of the x, y-axes in the tangent plane at P and according as $J > 0$ or $J < 0$ we say that P is a nodal point or a saddle point, respectively.

Also, the vorticity normal to the surface is

$$\left(\frac{\partial \epsilon_y}{\partial x} - \frac{\partial \epsilon_x}{\partial y}\right) z + O(z^2),$$

and at a stagnation point of attachment of a streamline from far upstream where the flow is irrotational we must have

$$\frac{\partial \epsilon_y}{\partial x} - \frac{\partial \epsilon_x}{\partial y} = 0,$$

since fluid very close to the stagnation streamline can in no way acquire vorticity. This means that by suitably choosing our x- and y-axis $\boldsymbol{\epsilon}$ takes to first order in x and y the form (ax, by) near P.

This is the case which covers the stagnation point flows discussed in the present paper. For this case we have $\Delta = a + b$ and $J = ab$. Since $\Delta > 0$, one of a, b must be positive and we choose the greater to be $a > 0$. Hence $J = a^2(b/a)$, so that for $b > 0$ we have a nodal point and for $b < 0$ we have a saddle point.

We now give a proof that the number of nodal points on S exceeds the number of saddle points by 2. We assume that the skin-friction lines on S have a finite

number of distinct nodes and saddles at which $\boldsymbol{\epsilon} = 0$, where we say the vector field has an isolated singularity.

Let A be a non-intersecting polygon on S whose sides $C_1, C_2 \ldots, C_n$ are geodesics which do not pass through a singularity of $\boldsymbol{\epsilon}$. Define an integer

$$\Delta(A) = \frac{1}{2\pi}\left(\sum_i [\theta]_{C_i} + \int_A K\, d\sigma\right),$$

where $[\theta]_{C_i}$ is the variation along C_i in a counter-clockwise direction of the angle θ between the tangent $\mathbf{t}$ to C_i and the vector $\boldsymbol{\epsilon}$, and K is the Gaussian curvature of S.

In the case of a small (almost plane) polygon enclosing a singularity of $\boldsymbol{\epsilon}$, $\int_A K\, d\sigma \doteqdot 0$ and $\Delta(A)$ coincides with the index of the singularity, defined to be the variation of θ round the polygon.

In general $\int_A K\, d\sigma$ is a correction term to make $\Delta(A)$ an integer, and is the measure of the non-Euclidean nature of S, for

$$\int_A K\, d\sigma = 2\pi - \Sigma\,(\text{exterior angles of } A);$$

this is the content of the Gauss–Bonnet Theorem (Eisenhart 1940). It is easily shown that if A, B are polygons overlapping only on their edges, then

$$\Delta(A) + \Delta(B) = \Delta(A + B),$$

also if A is small and contains at most one singularity of $\boldsymbol{\epsilon}$, then $\Delta(A) = 1, -1, 0$ according as A contains a node, a saddle point, or no singularity of $\boldsymbol{\epsilon}$. Thus for any A, $\Delta(A) = n_A - s_A$ where A contains n_A nodes and s_A saddle points of $\boldsymbol{\epsilon}$.

Thus if S contains n nodes and s saddle points, then

$$n - s = \Delta(A) + \Delta(S - A) = \frac{1}{2\pi}\int_S K\, d\sigma,$$

since the terms $[\theta]_{C_i}$ cancel in the sum. The expression on the right is the Euler–Poincaré characteristic of S, and is 2 for a sphere. Thus we have for S that $n - s = 2$ as required.

If, for instance, $s = 0$ there will be just one nodal point of attachment on the body. The surface streamlines will diverge therefrom and then converge to leave the body at one nodal point of separation, If, however, there are two nodal points of attachment the surface streamlines from each must divide somewhere at a saddle point of the surface flow. Similarly, if one has two nodal points of separation these will also have associated with them a saddle point, the streamlines from which will diverge to one or other of these nodal points of separation. Thus, over and above the two original nodal points, one of attachment and one of separation, for each additional nodal point there will be an additional saddle point so that $n - s = 2$ in all possible cases.

REFERENCES

Eisenhart, L. P. 1940 *Introduction to Differential Geometry*. Princeton University Press.

Howarth, L. 1951 *Phil. Mag.* **42**, 239, 1422.

Lighthill, M. J. 1958 *J. Fluid Mech.* **4**, 383.

Squire, L. C. 1957 *Aero. Res. Counc., Lond., Rep. Mem.*, 3006.

Solution of the non-linear equations of cellular convection and heat transport

By H. L. KUO

Massachusetts Institute of Technology†

(Received 23 August 1960 and in revised form 30 December 1960)

By expanding the dependent variables in series of orthogonal functions on the one hand, and expanding the coefficients of these functions in power series of a parameter η on the other hand, a solution has been obtained for the system of non-linear equations of cellular convection. The expansion parameter η is chosen in such a way as to make it remain less than 1 for all finite values of the Rayleigh number. The solution so obtained is found to be valid for a large range of the imposed temperature difference, and converges rapidly. This solution provides a quantitative theory for the convective heat transport as a function of the temperature difference in the range of laminar flow.

The solution also reveals that when the actual Rayleigh number is greater than twice the critical Rayleigh number, a layer of isothermal (adiabatic lapse-rate in a gas medium) mean temperature develops in the middle of the fluid layer. The thickness of this layer increases as the actual Rayleigh number increases, and at the same time the temperature gradient increases in the boundary layer so that an increase in the heat transport is accomplished.

The solution reveals further that the large temperature gradients are concentrated in the region where the cold descending current approaches the lower boundary and where the warm ascending current approaches the upper boundary. It is also shown that these ascending and descending currents spread out in mushroom-like patterns, a feature characteristic of the convection of isolated hot bubbles, but one which never has been considered as the form for finite cellular convection. Recent optical observations indicate that this is the most common form of the temperature field.

The heat transport given by this solution fits a power law of exponent 1·24, which is very close to the observed power law of exponent 1·25 for laminar flow.

1. Introduction

When a layer of fluid is heated uniformly from below and cooled from above, cellular convection starts to set in as the Rayleigh number R reaches its critical value R_0. This starting convection has a definite form and a definite scale, which are given by the solutions of the linearized equations in accordance with the boundary conditions (Rayleigh 1916; Pellew & Southwell 1940).

† The research reported in this paper has been sponsored in part by the Geophysics Research Directorate of the Air Force Cambridge Research Laboratories, Air Research and Development Command, under Contract No. AF 19(604)-6108.

When R is raised above R_0, the motion increases its intensity but remains laminar and steady for a large range of values of R, followed by unsteady, turbulent convection at a much higher temperature difference.

Formal solutions of the non-linear equations for thermal convection have been obtained in the works of Malkus & Veronis (1958) and Kuo & Platzman (1960), under the tacit assumptions that the motion is steady and that all the higher modes of convection are created by the non-linear interactions. However, the solutions obtained so far are valid only for small values of $(R - R_0)$, and therefore cannot be used for larger temperature differences.

It should be mentioned that by assuming a steady state we are considering the final equilibrium state between the temperature field and the motion field. If this equilibrium state is stable, it must be reached asymptotically. On the other hand, if it is unstable, it will be replaced by another state which is stable but is more likely to be unsteady.

In the work presented here a different solution of the steady non-linear equations is obtained. This new solution converges more rapidly and is valid for a much larger range of the imposed temperature difference. Because of these features, this solution provides a quantitative theory for the convective heat transport as a function of the temperature difference for a large range of the laminar flows. It also sheds some light on the problem of transition to turbulent convection, which occurs at a much higher temperature difference.

The method of solution adopted here is that of double expansions. In this method, the dependent variables are first expressed as infinite series of a set of orthogonal space functions, and second, the amplitudes of these functions are expressed as infinite series of an expansion parameter η which is a function of R.

For the case of two free boundaries the space functions of all modes are simple sine and cosine functions, and therefore the dependent variables can be represented directly by double Fourier trigonometric series. The non-linear equations are then reduced to spectral equations and the solutions can be obtained more readily by induction, as has been already done by Kuo & Platzman (1960). In the present paper, the same method will be used in obtaining the new solution for two free boundaries, and it will be developed to higher approximations.

For the cases of two rigid boundaries and of one rigid and one free boundary, these orthogonal functions must be obtained in a consecutive manner, as solutions of a set of linear but inhomogeneous equations, with the inhomogeneous terms containing functions of the lower modes. Therefore the method of solution for these cases is similar to that employed by Malkus & Veronis (1958), but differs from theirs in detail.

In this paper, we shall choose the expansion parameter η in such a way as to make it remain less than 1 for all finite values of R. The solution so obtained will be valid for a much larger range of temperature difference and will converge more rapidly.

Because of the difference in the methods of solution employed, only the solution for the case of two free boundaries will be presented in this paper, while those for the case of two rigid boundaries and of one rigid and one free boundary will be presented in another paper.

2. The governing equations

Consider a horizontal layer of fluid of depth h, confined between two parallel planes at $z = 0$ and $z = h$, the upper and lower planes being maintained at temperatures T_a and T_0 respectively. In the undisturbed state the temperature T is constant over a horizontal plane and decreases linearly with z and is given by

$$T = T_0 + \beta z, \tag{2.1}$$

where $\beta = (T_a - T_0)/h$ is the constant initial temperature gradient. The relation between the temperature T and the density ρ is given by

$$\rho = \rho_0\{1 - \alpha(T - T_0)\}, \tag{2.2}$$

where ρ_0 is the density corresponding to the temperature T_0 and α is the thermal expansion coefficient.

To investigate the convection problem, it is only necessary to take into consideration the variation of density when it is multiplied by the gravity g, whereby it introduces a buoyancy force $g\alpha T'$, where T' is the departure of the temperature from its horizontal average. At all other places, such as in the inertia terms of the equations of motion and in the continuity equation, the effect of the variations of ρ is quite small and can be neglected. Therefore we shall replace ρ by its mean value ρ_m after introducing the buoyancy force in the vertical equation of motion. This is the principal feature of the so-called Boussinesq approximation.

On making use of the Boussinesq approximation, the equations of motion, the thermal energy equation and the continuity equation may be written as

$$\frac{d\mathbf{v}}{dt} = -\frac{1}{\rho_0}\nabla p + g\alpha T'\mathbf{k} + \nu\nabla^2\mathbf{v}, \tag{2.3}$$

$$\frac{dT'}{dt} = \kappa\nabla^2 T', \tag{2.4}$$

$$\nabla . \mathbf{v} = 0, \tag{2.5}$$

where $\mathbf{v}$ is the vector velocity, $\mathbf{k}$ is the unit vector along the vertical, p is the departure of pressure from the hydrostatic pressure $\bar{p}(z)$, T' is the departure of temperature from the horizontal average $\bar{T}(z)$, ν is the kinematic viscosity coefficient, κ is the thermometric conductivity and α is the thermal expansion coefficient.

As in the previous study, we shall restrict our consideration in this paper to the simplest model of cellular convection: the infinite roll in a steady state, such that $\partial/\partial y = 0$ and $\partial/\partial t = 0$. It is then more convenient to introduce a stream function ψ to represent the field of motion, given by

$$u = -\frac{\partial\psi}{\partial z}, \quad w = \frac{\partial\psi}{\partial x}. \tag{2.6}$$

The fundamental equations (2.3) to (2.5) can be reduced to non-dimensional forms by the following choice of the units of length, time, and temperature, respectively

$$h, \quad h^2/\kappa, \quad \kappa\nu/g\alpha h^3. \tag{2.7}$$

Henceforth the symbols u, ψ, T, p, etc., will represent the physical values they have had heretofore divided by the relevant dimensional quantities from (2.7).

Eliminating p from the equation of motion (2.3) by applying the curl-operator and expressing in terms of the non-dimensional stream function ψ we obtain the following steady-state vorticity equation

$$\nabla^4\psi + \frac{\partial\theta}{\partial x} = \frac{1}{\sigma}B, \quad B \equiv \frac{\partial(\psi, \nabla^2\psi)}{\partial(x,z)}, \quad \sigma = \frac{\nu}{\kappa}. \tag{2.8}$$

where θ is defined below.

Expressing the temperature as the sum of the undisturbed mean temperature and the departure (θ) from this mean, then the total non-dimensional temperature T is given by

$$T = T_0 - Rz + \theta, \quad R \equiv \frac{g\alpha(\Delta T')}{\kappa\nu}h^3, \tag{2.9}$$

where $\Delta T'$ is the dimensional temperature difference between the bottom and the top, and therefore R is the Rayleigh number.

The non-dimensional steady-state thermal energy equation is given by

$$\nabla^2\theta + R\frac{\partial\psi}{\partial x} = H, \quad H \equiv \frac{\partial(\psi,\theta)}{\partial(x,z)}. \tag{2.10}$$

The equations (2.8) and (2.10) form a closed system for the two dependent variables ψ and θ.

The boundary conditions with respect to which these equations must be solved depend on whether the bounding surface is free or rigid. On a free surface, the vertical velocity and the tangential stress must vanish. Since the temperature of the boundary is being kept constant, we shall then have for a free surface,

$$\psi = \nabla^2\psi = \theta = 0. \tag{2.11}$$

On the other hand, if the surface is rigid, then both the vertical and the tangential velocities must vanish, and therefore we must have

$$\psi = \frac{\partial\psi}{\partial z} = \theta = 0. \tag{2.12}$$

An important consequence of these conditions is that both the vorticity advection Jacobian B and the heat advection Jacobian H vanish at the lower and upper boundaries.

3. Spectral equations

For the case of two free boundaries, all the space functions of the various modes $\psi(l,n)$ and $\theta(l,n)$ are sine and cosine functions,

$$\psi(l,n) \sim \sin(lk\pi x)\sin(n\pi z), \quad \theta(l,n) \sim \cos(lk\pi x)\sin(n\pi z), \tag{3.1}$$

where l and n are integers and k is the horizontal wave-number of the first mode ($l = n = 1$), which is geometrically unrestricted when the fluid extends to infinity in the horizontal direction. However, since convection is assumed to set in when R reaches its critical value R_0, which is a function of k, we must choose k so as

to make R_0 a minimum. Solutions corresponding to other k-values represent unstable situations and therefore cannot persist.

Since all the functions (3.1) satisfy the boundary conditions (2.11) we may represent ψ and θ by the following double Fourier expansions

$$\left.\begin{aligned}\psi &= \sum_{l=0}^{\infty}\sum_{n=0}^{\infty}\hat{\psi}_{l,n}\sin(lk\pi x)\sin(n\pi z),\\ \theta &= \sum_{l=0}^{\infty}\sum_{n=0}^{\infty}\hat{\theta}_{l,n}\cos(lk\pi x)\sin(n\pi z),\end{aligned}\right\} \tag{3.2}$$

where $\hat{\psi}_{l,n}$ and $\hat{\theta}_{l,n}$ are functions of R.

In order to transform the basic non-linear differential equations (2.8) and (2.10) into spectral forms, it is more convenient to express ψ and θ in the following complex forms in place of (3.2)

$$\left.\begin{aligned}\psi &= -\sum_{l=-\infty}^{\infty}\sum_{n=-\infty}^{\infty}\psi_{l,n}\exp(lkx+nz)\pi i,\\ \theta &= -\pi^3 i\sum_{l=-\infty}^{\infty}\sum_{n=-\infty}^{\infty}\theta_{l,n}\exp(lkx+nz)\pi i.\end{aligned}\right\} \tag{3.3}$$

We note that (3.2) is equivalent to (3.3) provided

$$\left.\begin{aligned}\psi_{l,n} &= -\psi_{-l,n} = -\psi_{l,-n} = \psi_{-l,-n} = \tfrac{1}{4}\hat{\psi}_{l,n},\\ \theta_{l,n} &= \theta_{-l,n} = -\theta_{l,-n} = -\theta_{-l,-n} = \frac{1}{4\pi^3}\hat{\theta}_{l,n},\end{aligned}\right\} \tag{3.4}$$

where the range of z has been extended to $-1 \leqslant z \leqslant 1$. Furthermore, all the coefficients $\psi_{l,n}$ and $\theta_{l,n}$ are real.

A simplification of notation will be introduced by regarding the pair of integers l, n as the components of a vector γ. We may then replace the double subscripts l, n, by a single subscript γ. The summation over γ is then understood to stand for summation over the components l and n.

The problem now is to determine the coefficients $\psi_{l,n}$ and $\theta_{l,n}$ so as to make (3.3) satisfy the two equations (2.8) and (2.10). Substituting (3.3) into these equations and equating to zero the coefficient of the individual components $\exp(lkx+nz)\pi i$ we obtain the following two systems of spectral equations

$$\alpha_\gamma^4\psi_\gamma - lk\theta_\gamma = -\sigma^{-1}kB_\gamma, \tag{3.5a}$$

$$\alpha_\gamma^2\theta_\gamma - lk\lambda\psi_\gamma = -kH_\gamma, \tag{3.5b}$$

where $\alpha_\gamma^2 \equiv l^2k^2+n^2$, $\lambda \equiv R/\pi^4$, and B_γ and H_γ are the vorticity–advection spectrum and the heat–advection spectrum, which represent the contribution to the γ-component by the non-linear interactions between the various wave-number vector pairs γ_1 and γ_2 in the equations (2.8) and (2.10). These two spectral functions are given by

$$B_\gamma = \sum_{\gamma_1}\sum_{\gamma_2}(l_1n_2 - l_2n_1)\,\alpha_{\gamma_2}^2\psi_{\gamma_1}\psi_{\gamma_2}, \tag{3.6a}$$

$$H_\gamma = \sum_{\gamma_1}\sum_{\gamma_2}(l_1n_2 - l_2n_1)\,\psi_{\gamma_1}\theta_{\gamma_2}, \tag{3.6b}$$

where the wave number pairs γ_1 and γ_2 satisfy the selection rule

$$\gamma_1+\gamma_2=\gamma, \quad \text{i.e.} \quad l_1+l_2=l, \quad n_1+n_2=n. \tag{3.7}$$

Because of this relation, we may replace γ_1 by $\gamma-\gamma_2$ and write the sum over γ_2 only, which is from $-\infty$ to $+\infty$ for both l and n. However, for each interacting pair γ_1, γ_2 there is a corresponding pair γ_2, γ_1. Both of these interacting pairs must be included in these advection spectral functions. Therefore we may write (3.6a and b) in the following non-redundant forms

$$B_\gamma = \sum_{\gamma_2} (ln_2-l_2n)(\alpha^2_{\gamma_2}-\alpha^2_{\gamma-\gamma_2})\psi_{\gamma-\gamma_2}\psi_{\gamma_2}, \tag{3.8a}$$

$$H_\gamma = \sum_{\gamma_2} (ln_2-l_2n)(\psi_{\gamma-\gamma_2}\theta_{\gamma_2}-\psi_{\gamma_2}\theta_{\gamma-\gamma_2}), \tag{3.8b}$$

where the relation (3.7) has been used.

The two equations (3.5a and b) together with the relations (3.8a and b) form a closed system for the joint determination of ψ_γ and θ_γ.

It may be mentioned that the perturbation temperature θ defined by (2.9) includes a part $\overline{\theta}(z)$ which is independent of x. This part represents the modification of the mean temperature distribution by convection, and is given by the components with $l=0$ in (3.3). On the other hand, no mean wind is produced by the convention, therefore $\psi_\gamma=0$ when $l=0$.

In solving the two sets of equations (3.5a and b) for $l\neq 0$, we may eliminate θ_γ and obtain

$$(\lambda-\lambda_\gamma)\psi_\gamma=(1/l)H_\gamma+(\alpha^2_\gamma/l^2k\sigma)B_\gamma \quad (l\neq 0), \quad \lambda_\gamma\equiv\alpha^6_\gamma/l^2k^2. \tag{3.9}$$

Denoting θ_γ by θ_{0n} and H_γ by H_{0n} when $l=0$ and substituting θ_γ from (3.5a) we find

$$n\theta_{0n}=-(k/n)H_{0n}=\sum_{\gamma_1} l_1k\psi_{n-\gamma_1}\theta_{\gamma_1}. \tag{3.10}$$

It appears easier to enumerate the the terms of H_γ by using (3.5a) and (3.10) as auxiliary equations, rather than to eliminate θ_γ completely.

4. The advection spectra B_γ and H_γ

Since B_γ and H_γ are given by the sums of infinite numbers of non-linear interactions, the first step toward solving the infinite sets of equations (3.9) and (3.10) is to find the most important terms of these advection spectra.

As has been discussed before, the spectral equations (3.9) and (3.10) are to be solved by expanding ψ_γ and the other quantities into power series of a parameter η, of the form

$$\psi_{l,n}(\eta)=\psi_{l,n,r}\eta^r+\psi_{l,n,r+2}\eta^{r+2}+\ldots, \tag{4.1}$$

where $\psi_{l,n,r+2j}$ represents a numerical coefficient. We define the order of magnitude r of ψ_r and θ_γ as the lowest power of η in their expansions. Since convection starts in the form $\psi_{1,1}$, it will be taken as a first-order quantity so that $r=1$ for $\psi_{1,1}$. On the other hand, all the functions of the higher modes must be of higher order by definition because they are produced by non-linear interactions represented by B_γ and H_γ.

In the calculations which are presented in this paper, the expansions are not carried out beyond the eighth order, the components l, n, and the power $p = r+2j$ used are all less than the integer 9. Consequently, only one digit is required to represent l, n, and p. Therefore we shall omit the comma between these indices. This simplification of notation also applies to the coefficients in (4.1). It will be understood in the following that whenever a three-digit subscript is attached to a quantity, the first two digits represent the components l and n of the wave-number vector γ while the third digit p indicates that it is the coefficient of η^p in the power-series expansion. For example, ψ_{111} and ψ_{113} stand for the coefficients of η and of η^3 of the expansion of $\psi_{11}(\eta)$, respectively.

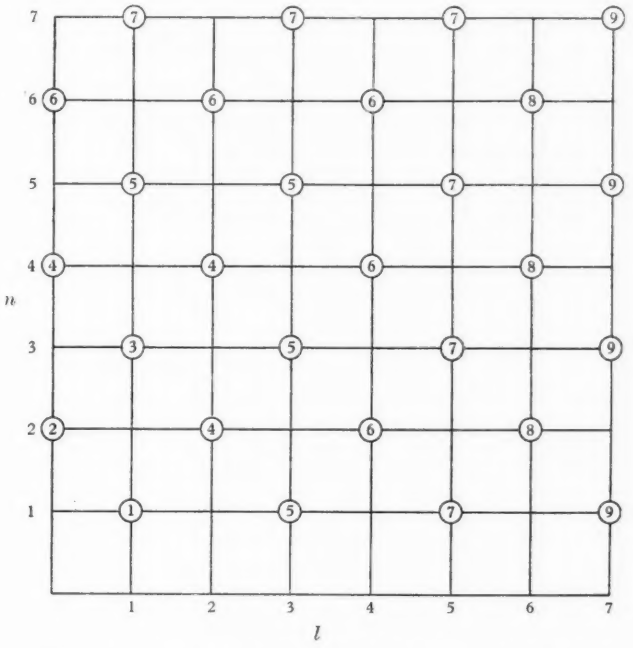

FIGURE 1. The order of magnitude of the spectral elements ψ_{ln}, θ_{ln} that occur in the non-linear solution as a function of the wave-numbers l, n.

The various components that are created by the non-linear interactions beginning with the initial convection ψ_{11}, θ_{11} are shown in figure 1, with their respective order of magnitude indicated by the numbers inside the circles. We note that for this case odd l occurs with odd n and even l occurs with even n, so that for every mode (l, n), $l+n$ is always even. We also note that for the modes with odd l and odd n, the power-series expansion is odd in η, while those modes with even l and even n are even functions of η. Therefore in the expansions represented by (4.1) the powers of η of two consecutive terms increase by 2.

As has been mentioned before, the first step toward solving the infinite sets of equations (3.9) and (3.10) is to find the most important terms of the advection

spectral functions B_γ and H_γ. That is to say, our first task is to find the interacting pairs (γ_1, γ_2) that contribute to the lower-order terms of B_γ and H_γ.

The result of this portion of the work is given in Appendix I, where all the interacting pairs (γ_1, γ_2) that contribute to the γ-mode spectral functions B_γ and H_γ up to their η^7 or η^8 terms have been listed. In order to facilitate the reading, this table is given as an appendix at the end of this paper.

With the help of this table, it is a simple matter to express $\theta_{0,2n}$, B_γ and H_γ in terms of ψ_γ and θ_γ. Some of these non-linear spectral functions used in this study are given in Appendix II.

5. Expansion of spectral functions

In the paper by Kuo & Platzman referred to before, the spectral functions ψ_γ were expressed as infinite power series of a parameter $\Delta = (\lambda - \lambda_0)^{\frac{1}{2}}$. The function ψ_{11} so obtained is an alternating series whose rate of convergence is very slow and whose first four partial sums behave divergingly for $\lambda > 3\lambda_0$ (see figure 2*b*). However the oscillatory nature of this expansion suggests that an asymptotic solution which is valid for a larger range of values of λ can be obtained by choosing a more suitable parameter. In this paper we shall choose an expansion parameter η defined by

$$\eta = \left(\frac{\lambda - \lambda_0}{\lambda}\right)^{\frac{1}{2}}, \tag{5.1}$$

where λ_0 is the critical value of λ above which convection exists. We note that this expansion parameter η remains less than 1 for all finite values of λ. The advantage of using such an expansion parameter is to bring out the most important part of the solution in the lower-order terms and thereby to eliminate the oscillation of the solution.

The procedure of solving the spectral equation (3.9) is to expand ψ_γ, B_γ and H_γ in power series of η in the form shown in (4.1). In order to determine the various coefficients $\psi_{l,n,p}$ from the system of equations (3.9), we must also expand λ in power series of η. According to the definition (5.1) we have

$$\lambda = \frac{\lambda_0}{1-\eta^2} = \lambda_0\left(1 + \sum_{j=1}^{\infty} \eta^{2j}\right), \tag{5.2}$$

which shows that an infinite number of terms are required to represent λ. To overcome this difficulty we rewrite (5.2) in the form of a finite series by introducing a quantity λ_{0s}.† Thus

$$\lambda = \lambda_0 + \lambda_{0s}(\eta^2 + \eta^4 + \ldots + \eta^{2s}), \tag{5.3}$$

$$\lambda_{0s} = \frac{\lambda_0}{1-\eta^{2s}}, \tag{5.3a}$$

where the integer s stands for the number of terms of the expansion. Since only powers of η lower than $2s$ occur in the formal expansion, the quantity λ_{0s} may be

† As will be seen from the subsequent development, we must take the first term of (5.3) as λ_0, not λ_{0s}. That is to say, we represent $(\lambda - \lambda_0)$ by a finite power series in η^2. Note that when s approaches infinity, λ_{0s} approaches λ_0.

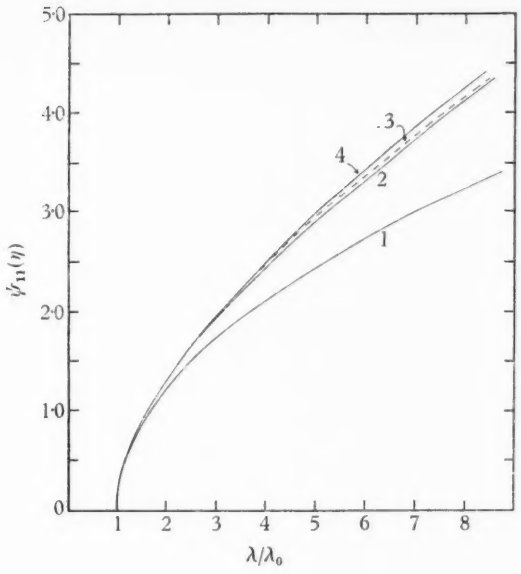

(*a*)

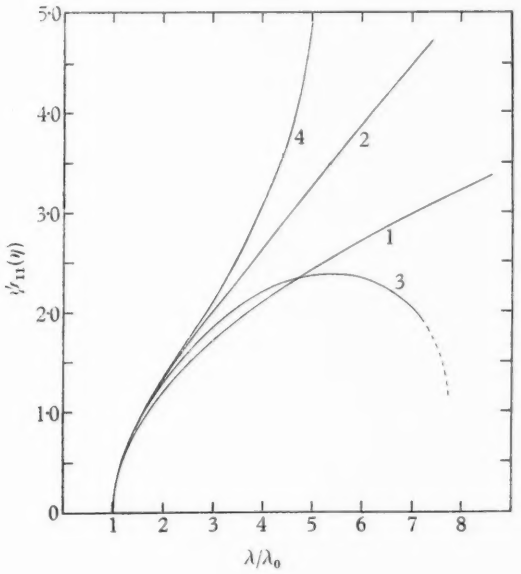

(*b*)

FIGURE 2. (*a*) Variation of the amplitude of the fundamental mode ψ_{11} as a function of λ/λ_0.

(*b*) Variation of ψ_{11} as a function of λ/λ_0 given by the η_1-expansion. [$\eta_1^2 \equiv \epsilon = (\lambda/\lambda_0) - 1$.]

treated as a constant without affecting the expansion. On the other hand, in computation λ_{0s} is to be evaluated directly from the definition (5.3a) for any chosen value of s so that the representation of λ by (5.3) is exact.

The convergence of the expansion is to be tested by increasing s and observing the behaviour of the results.

Substituting (4.1) and (5.3) into (3.9) and equating to zero the coefficients of the individual powers of η we obtain the following set of equations

$$(\lambda_\gamma - \lambda_0)\psi_{\gamma, r+2j} = -\frac{1}{l} H_{\gamma, r+2j} - \frac{\alpha_\gamma^2}{l^2 k\sigma} B_{\gamma, r+2j} + \lambda_{0s} \sum_{p=0}^{j-1} \psi_{\gamma, r+2p}, \tag{5.4}$$

where $j = 0, 1, 2, \ldots$, $\lambda_\gamma \equiv (l^2k^2 + n^2)^3/l^2k^2$, and λ_{0s} is given by (5.3a), which depends upon the number of terms s of the expansion of the individual ψ_γ. The coefficient $\theta_{\gamma, r+2j}$ of the θ_γ-expansion is given by

$$lk\theta_{\gamma, r+2j} = \alpha_\gamma^4 \psi_{\gamma, r+2j} + kB_{\gamma, r+2j}/\sigma. \tag{5.4a}$$

The expansion coefficients $H_{\gamma, r+2j}$ and $B_{\gamma, r+2j}$ are expressed in terms of the expansion coefficients ψ_γ and θ_γ through the equations (3.8a and b).

To solve the system of equations (5.4) we at first put $\gamma = 1, 1, r = 1$ and $j = 0$ in (5.4). Since $B_{111} = H_{111} = 0$ and $\psi_{111} \neq 0$, the first result obtained from this equation is

$$\lambda_0 = \lambda_{11} \equiv (k^2 + 1)^3/k^2, \tag{5.5}$$

which gives the critical value λ_0 as a function of k^2. The minimum value of λ_0 is 6·75, corresponding to $k^2 = \frac{1}{2}$.

It may be pointed out that even though the solution can be developed for arbitrary values of k with the exception of some discrete values, only that solution corresponding to $k^2 = \frac{1}{2}$, or its neighbourhood, can be stable. However, in order to examine whether some slight change of the horizontal scale of convection will occur at a later stage, the solution has been carried out to the third approximation for the arbitrary k.

Because of the result (5.5) the term on the left of equation (5.4) disappears for $\gamma = 1, 1$. Therefore for the first mode this equation degenerates into the following

$$\lambda_{0s} \sum_{j=1}^{p} \psi_{11, 2j-1} = H_{11, 2p+1} + \frac{\alpha_{11}^2}{k\sigma} B_{11, 2p+1} \quad (p = 1, 2, 3, \ldots). \tag{5.6}$$

The expansion coefficients of the first mode must be obtained from this equation while those of the higher modes are given by (5.4).

We shall demonstrate the way of development of the solution by obtaining the first few expansion coefficients.

Putting $p = 1$ in (5.6) gives

$$\lambda_{0s}\psi_{111} = H_{113} + (\alpha_{11}^2/k\sigma) B_{113}. \tag{5.7}$$

From the equations (3.8a and b) and (3.10), or from equation (A.4) in Appendix II we find

$$B_{113} = 0, \quad H_{113} = -2\psi_{111}\theta_{022}, \quad \theta_{022} = -\alpha_{11}^4 \psi_{111}^2.$$

Therefore (5.7) yields the results

$$\theta_{022} = -\tfrac{1}{2}\lambda_{0s}, \tag{5.8}$$

$$\psi_{111} = (\tfrac{1}{2}\lambda_{0s})^{\frac{1}{2}}/\alpha_{11}^2, \quad k\theta_{111} = \alpha_{11}^4 \psi_{111}. \tag{5.9}$$

By taking the plus sign here, we have chosen $x = 0$ at the point where there is ascending motion.

With $\gamma = 1, 3$ and $r = 3, j = 0$, equation (5.4) reduces to

$$(\lambda_{13} - \lambda_{11})\,\psi_{133} = -H_{133} - (\alpha_{13}^2/k\sigma)\,B_{133}. \tag{5.10}$$

From (A. 5) and (5.8) we find

$$B_{133} = 0, \quad H_{133} = -\lambda_{0s}\psi_{111}.$$

Substituting in (5.10) and (5.4a) then yields the results

$$\psi_{133} = \frac{\lambda_{0s}}{\lambda_{13} - \lambda_{11}}\psi_{111}, \quad k\theta_{133} = \alpha_{13}^4\psi_{133}. \tag{5.11}$$

To obtain ψ_{113} we put $p = 2$ in (5.6). It then gives

$$\psi_{113} + \psi_{111} = \frac{1}{\lambda_{0s}}\left(H_{115} + \frac{\alpha_{11}^2}{k\sigma}B_{115}\right). \tag{5.12}$$

From equations (A. 1) and (A. 4) in Appendix II we find

$$\theta_{024} = -2\alpha_{11}^4\psi_{111}\psi_{113} + (\alpha_{11}^4 + \alpha_{13}^4)\,\psi_{111}\psi_{133},$$
$$B_{115} = 0, \quad H_{115} = 3\lambda_{0s}\psi_{113} - \{2 + (\alpha_{13}^4/\alpha_{11}^4)\}\,\lambda_{0s}\psi_{133}.$$

Substituting into (5.12) and making use of (5.11) and (5.4a) we obtain

$$\psi_{113} = \tfrac{1}{2}\psi_{111}\left\{1 + \frac{\lambda_{0s}}{\lambda_{13} - \lambda_{11}}\left(2 + \frac{\alpha_{13}^4}{\alpha_{11}^4}\right)\right\}, \tag{5.13}$$

$$\theta_{024} = -\tfrac{1}{2}\lambda_{0s}\left(1 + \frac{\lambda_{0s}}{\lambda_{13} - \lambda_{11}}\right). \tag{5.14}$$

At this stage the coefficient θ_{044} can be determined also. From the equations (A.2). (5.9) and (5.11) we find

$$\theta_{044} = -\frac{\lambda_{0s}^2}{4(\lambda_{13} - \lambda_{11})}\left(1 + \frac{\alpha_{13}^4}{\alpha_{11}^4}\right). \tag{5.15}$$

From the above developments we see that the coefficients $\psi_{11,r}$ and $\theta_{02,r+1}$ must be determined simultaneously.

The higher-order coefficients can be obtained in the same manner. However, the calculation becomes more tedious as the order increases, especially when k is being kept arbitrary. In reality, one k value must be selected by the fluid according to certain physical principles. The purpose of using an arbitrary k is that it enables us to investigate the probability of a change of scale of the convection at some later stage of the development, for example, by applying a certain selection principle to our non-linear solution which contains an arbitrary k. From the theoretical point of view, a comparison of the relative stability of the solutions will provide the proper selection rule. However, an analysis of the relative stability of the non-linear solutions is very difficult to carry out, and we are therefore forced to make use of more heuristic principles. One such principle is to maximize the total kinetic energy. This is based on the consideration that the final equilibrium state is arrived at through steps of development, each of which is represented by a maximum rate of increase of the kinetic energy, and therefore the end result should be characterized by a maximum of the total kinetic energy.

Another heuristic selection principle is the maximization of the heat transport, which has been used by Malkus & Veronis (1958).

As has been mentioned earlier, the cell scale which is selected on the basis of the linear theory (minimum λ_0) for two free boundaries is $k^2 = \frac{1}{2}$. This value of k, or some near-by value, must be taken as the starting scale of convection because other values of k represent unstable conditions. On the other hand, when λ is well above the lowest critical value, a change of the horizontal scale may occur. However, no such shift is found by either one of the two selection principles mentioned above for $\lambda \leqslant 1{\cdot}5\lambda_0$. For still higher values of λ the determination of the most preferred scale is very difficult because of the extreme flatness of the heat transfer and kinetic energy functions around $k^2 = \frac{1}{2}$. At any event, such slight shift of the horizontal scale is insignificant for the energetics of the system. We shall therefore restrict the higher-order expansions and the subsequent developments to $k^2 = \frac{1}{2}$ only.†

The expansion has been carried out to the η^7- and the η^8-order terms. Since the higher-order coefficients are polynomials of both $q\,(\equiv \lambda_{0s}/\lambda_0 = 1/1-\eta^{2s})$ and σ, their forms are very complex. We have therefore listed them in Appendix III. However, in order to illustrate the nature of our expansion, here we shall give the expansions of the two most important and also most interesting spectral functions ψ_{11} and θ_{02}:

$$\begin{aligned}\psi_{11} = {} & 1{\cdot}2247q^{\frac{1}{2}}(\eta+\tfrac{1}{2}\eta^3+\tfrac{3}{8}\eta^5+\tfrac{5}{16}\eta^7)\\ & +0{\cdot}1019q^{\frac{3}{2}}(\eta^3+\tfrac{3}{2}\eta^5+\tfrac{15}{8}\eta^7)-0{\cdot}0117q^{\frac{5}{2}}\eta^7\\ & -10^{-3}q^{\frac{5}{2}}(27{\cdot}5+3{\cdot}4\sigma^{-1}+0{\cdot}85\sigma^{-2})(\eta^5+2{\cdot}088\eta^7)\\ & +10^{-4}q^{\frac{7}{2}}(153+42\sigma^{-1}+31\sigma^{-2}+15\sigma^{-3}+4\sigma^{-4})\eta^7+\ldots, \qquad (5.16)\\ \theta_{02} = {} & -3{\cdot}375q(\eta^2+\eta^4+\eta^6+\eta^8)-0{\cdot}013338q^2(\eta^4+2\eta^6+3\eta^8)\\ & -10^{-3}q^3\eta^6(10{\cdot}28-3{\cdot}97\sigma^{-1}-2{\cdot}30\sigma^{-2})\\ & -10^{-3}\eta^8[(3{\cdot}085-4{\cdot}73\sigma^{-1}-5{\cdot}00\sigma^{-2})q^3\\ & -(1{\cdot}40+1{\cdot}86\sigma^{-1}+1{\cdot}11\sigma^{-2}+2{\cdot}18\sigma^{-3}+1{\cdot}01\sigma^{-4})q^4]+\ldots. \qquad (5.17)\end{aligned}$$

We mention again that if these equations are to be used up to the η^7 and the η^8 terms, we must then put $s = 4$ in q. On the other hand, if equation (5.16) is used only up to the η^5 terms, we should then put $s = 3$ in q.

We note that in the present problem, the Prandtl number σ appears only in the higher-order coefficients with $r \geqslant 4$, and that its direct effect on ψ is small when σ is not much smaller than unity. The effect of σ on the temperature field is even smaller.

6. Variations of the spectral functions with λ

The values of the spectral coefficients ψ_γ and θ_γ have been computed from the fourth approximations of the η-expansion for $\sigma = 10$ and for different values of λ, up to $\lambda = 8\lambda_0$. Within this range, the solutions for ψ_{11} and θ_{11} converge rapidly,

† Expansion coefficients for an arbitrary k have been obtained up to the η^5 and η^6 terms and are given in Scientific Report No. 3 of the M.I.T. Planetary Circulation Project, October 1960.

as can be seen from figure 2*a*, where the values of ψ_{11} computed from the first four approximations (corresponding to $s = 1, 2, 3, 4$) have been plotted. In fact, the values of ψ_{11} given by the third approximation are correct to the third significant figure for $\lambda \leqslant 3\lambda_0$, and the differences between the third and the fourth approximations remain less than 3 % in the whole range of computation.

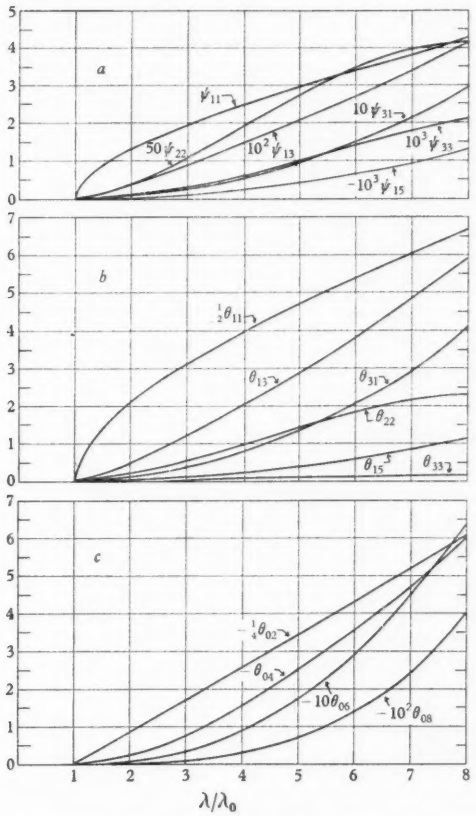

FIGURE 3. The variations of the spectral functions ψ_γ and θ_γ as functions of λ/λ_0.

For comparison, the values of ψ_{11} given by the first four approximations of the Δ-expansion ($\Delta^2 \equiv \lambda - \lambda_0$) obtained in the paper by Kuo & Platzman (1960) have been plotted in figure 2*b*. It is seen that the first four partial sums so obtained converge only for $\lambda < 2\lambda_0$, whereas for $\lambda > 3\lambda_0$ they behave divergently. A similar behaviour has been exhibited by the solutions of Malkus & Veronis (1958).

The second quantity that converges rapidly in the present solution is θ_{02}. The differences between the first four approximations remain less than 3 % within the whole range of computation. Its values also agree well with the values obtained directly from (A. 1) by making use of the values of ψ_γ and θ_γ, which

shows that the solution is self-consistent to a relatively high degree of accuracy. On the other hand, the rates of convergence for the coefficients of the higher modes are much slower for larger λ.

The values of the various spectral functions as given by their respective fourth approximations have been plotted in figure 3 for different values of λ/λ_0, where some proper constant factors have been introduced so as to make them have the same order of magnitude.

From the results in the figures 3*a* and *b* we see that just a little above the critical point the various components are arranged according to their order of expansion. The intensity of the first mode increases very rapidly near $\lambda = \lambda_0$ whereas those of the higher modes increase only very slowly. However, this is not true for larger values of λ.

One significant result of the computation is that for larger values of λ, the magnitudes of the higher-order coefficients ψ_γ and θ_γ are not arranged according to their degrees in η. The curves in figure 3 show that some of these coefficients increase more rapidly than the others. For example, even though ψ_{31} is a fifth-order quantity, it becomes the largest higher mode of the ψ-field for $\lambda > 3\lambda_0$. The next largest is ψ_{22} while ψ_{13} ranks third. This is also true in the kinetic energy spectrum, which is given by $\alpha_\gamma^2 \psi_\gamma^2$.

In the temperature spectrum, θ_{31} also increases more rapidly than the other components even though θ_{13} remains the largest higher mode in the range of computation. As a result of the rapid growth of the (3, 1)-mode of convection, it becomes the second largest contributor to the heat transfer for $\lambda > 2\lambda_0$. We also mention that at $\lambda = 8\lambda_0$, θ_{31} and θ_{13} are of the same order of magnitude as θ_{11}. The rapid rate of growth of ψ_{31} and θ_{31} for large values of λ is due to their large expansion coefficients in equation (5.4), which are proportional to $(\lambda_\gamma - \lambda_{11})$. Judging from equation (5.4) which holds for all the higher modes γ, we may expect that at larger values of λ, the magnitudes of ψ_γ will be roughly proportional to $(\lambda_\gamma - \lambda_{11})^{-1}$ while the contribution from the (l, n)-mode to the heat transfer is likely to become proportional to $\alpha_{ln}^4 (\lambda_{ln} - \lambda_{11})^{-2}$.

7. Convective heat transport and mean temperature distribution

In the results obtainable from the non-linear solution, the dependence of the rate of heat transfer upon the imposed temperature difference is of primary interest. This dependence can most conveniently be expressed by the functional relation between the Nusselt number N and the Rayleigh number, or between the heat transfer ratio S and the Rayleigh number.

The Nusselt number is the ratio of the actual heat transport rate to the rate at which heat would be transported by conduction for the given temperature difference between the hot and cold reservoirs were convection absent. Thus, according to this definition N is given by

$$N = -\frac{h}{\Delta T}\left(\frac{d\bar{T}}{dz}\right)_{z=0} = -\frac{1}{R}\left(\frac{d\bar{T}}{dz}\right)_{z=0},$$

where $\bar{T}$ is the horizontally averaged temperature.

On the other hand, the heat transport ratio S is defined as the ratio between the actual heat transport to the rate at which heat would be transported conductively at the critical Rayleigh number, therefore it is given by

$$S \equiv \frac{R}{R_0} N = -\frac{1}{R_0}\left(\frac{d\overline{T}}{dz}\right)_{z=0}.$$

According to the equations (2.9) and (3.2), $\overline{T}$ is given by

$$\overline{T} = T_0 - Rz + \sum_{n=1}^{\infty} \hat{\theta}_{0,2n} \sin(2\pi n z).$$

Substituting $\theta_{0,2n}$ from (3.4) we obtain

$$\begin{aligned}\overline{\Theta} &\equiv (\overline{T} - T_0)/R \\ &= -z + \frac{2}{\pi\lambda} \sum_{n=1}^{\infty} \theta_{0,2n} \sin(2\pi n z). \end{aligned} \tag{7.1}$$

Therefore the heat transport ratio S is given by

$$S = \frac{\lambda}{\lambda_0} - \frac{4}{\lambda_0} \sum_{n=1}^{\infty} n\theta_{0,2n}. \tag{7.2a}$$

The values of the first four $\theta_{0,2n}$ have been obtained from their η^8-approximations and are plotted in figure 3*c*. According to equation (3.10), $\theta_{0,2n}$ is produced by the non-linear interactions between the various modes. However, it can be seen from the equations following (A. 1) that only the non-linear interaction between ψ_γ and θ_γ of the individual modes themselves contributes to the heat transport, while the non-linear interactions between different modes cancel out in equation (7.2*a*). Thus, in terms of ψ_γ and θ_γ, S is given by

$$S = \frac{\lambda}{\lambda_0} + \frac{4k}{\lambda_0} \sum_{\gamma} l\psi_\gamma \theta_\gamma. \tag{7.2b}$$

Thus there are two different ways of computing S (or N). One method is by taking the sum of the various $n\theta_{0,2n}$ as given by their respective expansions (figure 3). The other method is to compute S directly from the second expression (7.2*b*) with the values of ψ_γ and θ_γ obtained from the solution. This method represents a higher approximation than the first, but not completely in accordance with the order of the η-expansion.

The variations of S with λ as given by the second-order and the eighth-order expansions are represented in figure 4 by the curves $S^{(1)}$ and $S^{(4)}$, respectively, while $S^{(d)}$ is obtained from the second expression (7.2*b*) and the ψ_γ and θ_γ functions given in figure 3. It is seen that for larger λ/λ_0, $S^{(4)}$ is much higher than $S^{(1)}$. On the other hand, the fourth-order and the sixth-order approximations of S are nearly the same as $S^{(4)}$, therefore they are not plotted in these graphs.

It may be mentioned that the Δ-expansion ($\Delta^2 = \lambda - \lambda_0$) of the Nusselt number obtained by Kuo & Platzman (1960) also diverges for $\lambda > 3\lambda_0$.

On examining the various terms of $S^{(d)}$ it is found that the (3.1) mode makes an appreciable contribution to the heat transport when λ is greater than $4\lambda_0$. Since this transport is of the tenth order in η, its effect is not included in the eighth-

order approximation $S^{(4)}$. Thus, the difference between $S^{(d)}$ and $S^{(4)}$ is mainly due to the transport by the (3, 1)-mode.

It may be mentioned that the second-order approximation to S in this η-expansion is identical with the corresponding second-order approximation of the Δ-expansion. This approximation gives a linear dependence of the convective heat transport on the Rayleigh number. On the other hand, the results given by the higher approximations obtained in this study definitely show that the heat transport increases faster than the first power of λ.

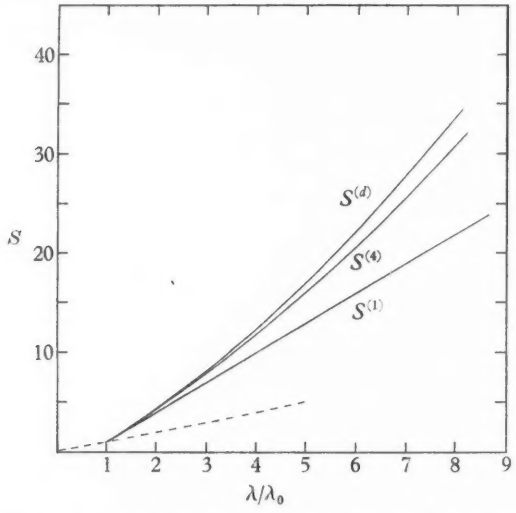

FIGURE 4. The variation of the heat transport function S as a function of λ/λ_0.

On plotting the quantity $\log(S-1)$ against $\log\{(\lambda/\lambda_0)-1\}$, we find that for $\lambda > 4\lambda_0$, the $S^{(d)}$ and $S^{(4)}$ obtained above may also be represented by the formula

$$S = 1 + c\{(\lambda/\lambda_0)-1\}^{\alpha}. \tag{7.3}$$

The value of the exponent α as given by $S^{(d)}$ is $\alpha = 1{\cdot}24$ while that given by $S^{(4)}$ is $\alpha = 1{\cdot}19$. These values are very close to the observational result $S \sim (\lambda/\lambda_0)^{\frac{5}{4}}$ for laminar convection (see Jakob 1949).

We mention that the convection heat transfer given by Nakagawa's heuristic theory (1960) is the same as that given by the second-order approximation obtained in the present paper. Evidently that approximation greatly underestimates the convective heat transfer except when λ is only slightly above its critical value.

Besides the heat transport, the next most interesting quantity obtainable from the non-linear solution is the modified mean temperature distribution, which is given by (7.1). The mean temperature profile has been computed from this equation for six different values of λ, by making use of the $\theta_{0,2n}$ values given in figure 3. The results of those computations are represented in figure 5 by the six curves, where the numbers attached to these curves indicate the values of λ/λ_0.

These curves show clearly the effect of convective heat transfer on the mean temperature distribution. The most striking feature of this effect, as revealed by the solution, is that for $\lambda > 2\lambda_0$ a region of isothermal stratification is produced by convection in the middle of the fluid layer.† The thickness of the isothermal layer increases as λ increases, so that when the imposed temperature difference

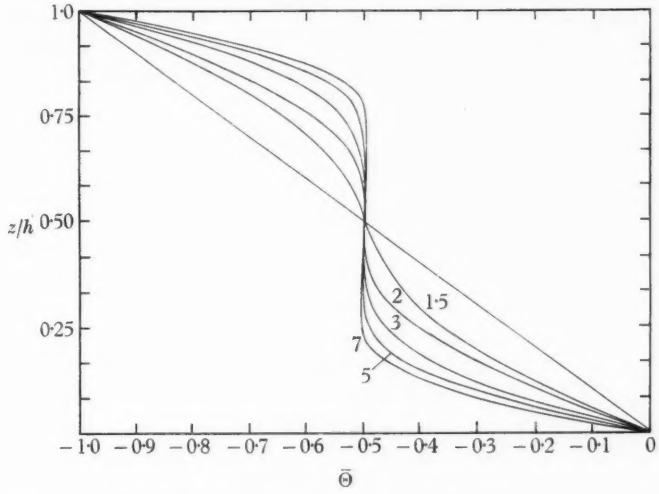

FIGURE 5. Distribution of the mean temperature for different values of λ/λ_0.

between the hot and cold sources is very large, the main body of the fluid will become isothermal (or adiabatic if the medium is a gas) in the mean, while large mean temperature gradients will be confined to the boundary layers adjacent to the hot and cold reservoirs thus providing a higher rate of heat transport. This feature of the development must persist when the convection becomes turbulent, even though the solution obtained here does not hold in the turbulent régime. This paradoxical result of the creation of a deep isothermal (adiabatic) layer by convection at a large imposed temperature difference is very important for the understanding of the convective processes in nature, where observations usually give a critical temperature gradient instead of a supercritical gradient.

It may be pointed out that even though the non-linear interactions between different modes of convection do not contribute to the total heat transport, they are very important for the modification of the mean temperature distribution, because these terms do not cancel except at the boundaries.

8. Pattern of isotherms

Since the temperature θ is a cosine series in x and therefore is symmetric with respect to $x = 0$, it is sufficient to consider only a half cell. We therefore

† The coefficients $\theta_{0,2n}$ in figure 3*c* give a very small reversed gradient near $z = \frac{1}{2}$ for $\lambda \geqslant 3\lambda_0$, which is numerically much less than the errors of the approximations and therefore should not be taken as a real feature.

restrict attention to the region $0 \leqslant \xi \leqslant \pi$ and $0 \leqslant \zeta \leqslant \pi$, where $\xi = k\pi x$ and $\zeta = \pi z$. Expressed in terms of $\Theta \equiv (T - T_0)/R$, we have

$$\Theta = \overline{\Theta} - \frac{4}{\pi\lambda} \sum_{\gamma} \theta_\gamma \cos l\xi \sin n\zeta,$$

where $\overline{\Theta}$ is the horizontal average of Θ and is given by equation (7.1). It can easily be shown that Θ is diagonally antisymmetric about the point $\xi = \frac{1}{2}\pi$, $\zeta = \frac{1}{2}\pi$.

In order to demonstrate the effects of the higher-order terms we take as our example the solution for $\lambda = 7\lambda_0$. For this λ we find that the values of the coefficients θ_{ln} for $\sigma = 10$ are

$$\begin{aligned}
\theta_{11} &= \ \ 12{\cdot}145, & \theta_{13} &= \ \ 4{\cdot}810, & \theta_{15} &= \ \ 0{\cdot}831, & \theta_{17} &= \ \ 0{\cdot}066; \\
\theta_{22} &= \ \ 2{\cdot}160, & \theta_{24} &= -0{\cdot}298, & \theta_{31} &= \ \ 2{\cdot}900, & \theta_{33} &= -0{\cdot}060; \\
\theta_{02} &= -20{\cdot}72, & \theta_{04} &= -4{\cdot}670, & \theta_{06} &= -0{\cdot}448, & \theta_{08} &= -0{\cdot}024.
\end{aligned}$$

The other coefficients are very small, and therefore will be neglected. The isotherms given by this solution are shown in figure 6*a*. The most prominent features are the concentration of large temperature gradients in the boundary regions where the ascending and descending currents are approaching the boundaries, whereas in the boundary regions where these currents are moving away as well as in the main bodies of these currents the temperature gradients are very small. Another feature of the temperature distribution is the mushroom-like spreading of the ascending and descending currents, which is a characteristic feature of convection due to isolated hot bubbles, but also appears in this solution. The curve in figure 6*b* represents the temperature distribution at the level $z = \frac{1}{2}$, as given by the solution. It illustrates more clearly the effect of the higher mode (3, 1). This distribution is surprisingly similar to that given by Silveston (1958) which is deduced from observations.

Because the ψ_{ln} of the higher modes are much smaller than the ψ_{11}, the distortion of the streamline field is not so pronounced as that of the temperature field.

9. Discussion

There is no doubt that the non-linear solution obtained in the present work converges more rapidly and is valid over a much larger range of the imposed temperature difference than the solutions obtained in previous studies. It has also revealed many interesting features of the convective motion, such as the concentration of the mean temperature gradient in the boundary layers and the creation of a deep mean isothermal layer in the main body of the fluid, and the mushroom-like spreading of the warm-ascending and cold-descending currents.

A number of questions may be raised concerning this solution, such as its uniqueness and its most likely modification in order to embrace the turbulent régime.

Since this solution is based on the assumption that convection starts at the critical Rayleigh number R_0 in the form of the fundamental mode and proceeds to create higher modes through the non-linear cascade effect and to reach the equilibrium steady state, the solution can be unique only under these stated

conditions, and only when this solution converges and is stable. The last qualification is necessary because if the solution represents an unstable state, then the motion must be replaced by another motion which is stable for the given value of λ. The solution which represents this new state of convection may be composed

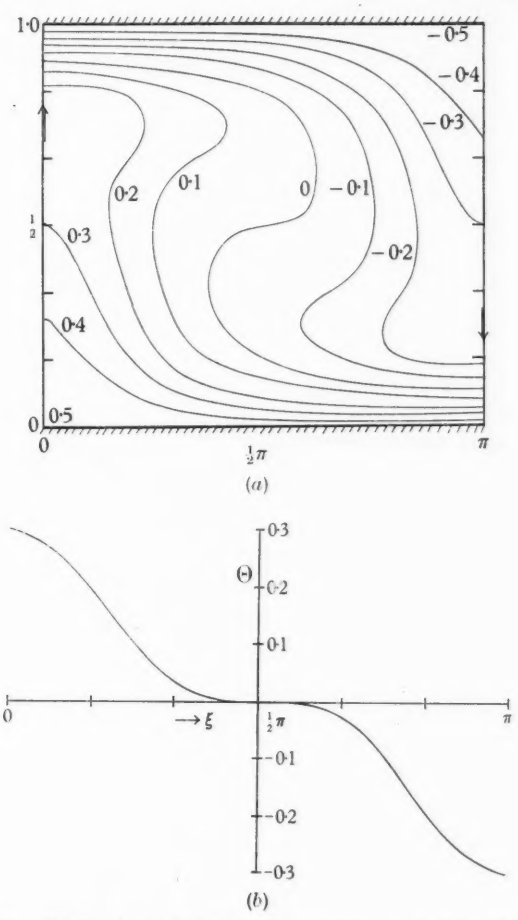

FIGURE 6. (*a*) The distribution of the total temperature as given by the non-linear solution for $\lambda = 7\lambda_0$ and $\sigma = 10$.

(*b*) The temperature distribution at the level $z = \frac{1}{2}$ as given by the solution.

of the same modes as given in figure 1, but with intensities different from that given by our present solution, or it could be composed of new components in addition to the modes in figure 1. In the former case the added parts of the various modes must appear in unsteady form, while in the latter case the new modes may either be steady or unsteady. In order to determine whether any new perturbation is needed, it seems necessary to examine the stability of the convective state represented by our non-linear solution.

Another point worth mentioning is that even though this solution is valid for a much larger range of temperature difference than the solutions obtained in the previous works, it also shows a tendency to divergence for values of λ greater than ten times the critical value. The reason for this divergence is apparently due to the fact that for large values of λ, the amplitudes of the higher modes ψ_{ln} increase as the factor $(\lambda_{ln}-\lambda_0)^{-1}$ and are no longer arranged according to their orders of appearances in the non-linear cascade effect depicted in figure 1. We note that for $\lambda > \lambda_{ln}$, we have

$$\frac{1}{\lambda_{ln}-\lambda_0} \simeq \frac{1}{\lambda-\lambda_0}\left\{1+\frac{\lambda-\lambda_{ln}}{\lambda-\lambda_0}\right\}.$$

Therefore for large λ the various modes behave somewhat like self-excited ones. It seems therefore that a different type of solution is needed for higher temperature differences, which may end up in the turbulent régime in which all modes are present.

A different solution of the non-linear equations which includes perturbations with horizontal scales longer as well as shorter than the fundamental mode can be obtained if the horizontal dimension L of the fluid is finite and is not an integral multiple of the horizontal scale a corresponding to the minimum critical Rayleigh number R_0. Then the motion must be delayed until λ reaches a value $\lambda_1(a_1)$ corresponding to the critical value for the horizontal scale a_1 such that $L = ma_1$, where m is an integer. We assume that λ_1 is the lowest λ which sustains convection which is compatible with the dimension L. Since a is the horizontal scale for which the critical λ_0 is an absolute minimum, there is another scale a_2 on the opposite side of a for which the critical value $\lambda_2(a_2)$ is equal to λ_1. Suppose $a_2 > a > a_1$ and $L = (m-1)\,a_2$. Then convection will start when λ reaches $\lambda_1 = \lambda_2$ and the initial motions must be represented by a fundamental mode consisting of two waves with horizontal wavelengths a_1 and a_2. In this case the non-linear interactions will produce new modes with both longer and shorter horizontal scales, and the spectrum will then be a complete spectrum. It seems that this consideration is important for the harmonic representation of the solution of the turbulent régime

REFERENCES

Globe, S. & Dropkin, D. 1959 Natural convection heat transfer in liquids confined by two horizontal plates and heated from below. *J. Heat Transfer*, **81**, 24–8.

Jakob, M. 1949 *Heat Transfer*, vol. 1. New York: John Wiley.

Kuo, H. L. & Platzman, G. W. 1960 A normal mode nonlinear solution of the Rayleigh convection problem—to be published in *Beit. Phys. frei Atmos.*

Malkus, W. V. R. & Veronis, G. 1958 Finite amplitude cellular convection. *J. Fluid Mech.* **4**, 225–60.

Nakagawa, Y. 1960 Heat transport by convection. *Phys. Fluids*, **3**, 82–6.

Pellew, Anne & Southwell, R. V. 1940 On maintained convective motion in a fluid heated from below. *Proc. Roy. Soc.* A, **176**, 312–43.

Rayleigh, Lord 1916 On convection currents in a horizontal layer of fluid when the higher temperature is on the under side. *Phil. Mag.* **32**, 529–46.

Silveston, P. L. 1958 Warmedurchgang in waagerechten Flussigkeitsschichten. *Forsch. Ing.* **24**, 29–32 and 59–69.

Appendix I

Table of the interacting pairs γ_1, γ_2 that contribute to the γ mode of B_γ and H_γ and their order of magnitude r

In this table, the two interacting pairs γ_1 and γ_2 are separated by a semicolon, the components l and n in each γ are separated by a comma, while the different interacting pairs are separated by a period.

γ	r	$\gamma_1; \gamma_2$				
02	2	1, 1; −1, 1.				
	4	1, −1; −1, 3.	−1, −1; 1, 3.			
	8	−2, −2; 2, 4.	2, −2; −2, 4.	−1, −3; 1, 5.	1, −3; −1, 5.	
04	4	1, 1; −1, 3.	−1, 1; 1, 3.			
	6	1, −1; −1, 5.	−1, −1; 1, 5.			
	8	2, 2; −2, 2.				
06	6	1, 3; −1, 3.	1, 1; −1, 5.	−1, 1; 1, 5.		
	8	−1, −1; 1, 7.	1, −1; −1, 7.	2, 2; −2, 4.	−2, 2; 2, 4.	
08	8	2, 4; −2, 4.	1, 1; −1, 7.	−1, 1; 1, 7.	1, 3; −1, 5.	−1, 3; 1, 5.
11	3	1, −1; 0, 2.				
	5	1, 3; 0, −2.				
	7	1, −3; 0, 4.	2, −2; −1, 3.	2, 4; −1, −3.		
	9	1, 5; 0, −4.	−2, 2; 3, −1.	−2, 4; 3, −3.	2, −4; −1, 5.	−2, −4; 3, 5.
13	3	1, 1; 0, 2.				
	5	1, −1; 0, 4.	−1, 1; 2, 2.	−1, −1; 2, 4.		
	7	1, 5; 0, −2.				
15	5	1, 1; 0, 4.	1, 3; 0, 2.	−1, 1; 2, 4.		
	7	1, −1; 0, 6.	−1, 3; 2, 2.	−1, −1, 2, 6.		
17	7	1, 1; 0, 6.	1, 3; 0, 4.	1, 5; 0, 2.	−1, 1; 2, 6.	−1, 3; 2, 4.
22	4	1, −1; 1, 3.				
	6	−1, 1; 3, 1.	2, 4; 0, −2.			
	8	−1, 3; 3, −1.	1, −3; 1, 5.	−1, −3; 3, 5.	2, −2; 0, 4.	
24	4	1, 1; 1, 3.				
	6	2, 2; 0, 2.	1, −1; 1, 5.	−1, 1; 3, 3.	−1, −1, 3, 5.	
	8	−1, 3; 3, 1.	2, 6; 0, −2.			
26	6	1, 1; 1, 5.	−1, 1; 3, 5.	2, 4; 0, 2.		
	8	1, −1; 1, 7.	−1, −1; 3, 7.	−1, 3; 3, 3.	2, 2; 0, 4.	
31	5	1, −1; 2, 2.				
	7	1, 3; 2, −2.	1, −3; 2, 4.	−1, −1; 4, 2.	3, −1; 0, 2.	3, 3; 0, −2.
33	5	1, −1; 2, 4.				
	7	−1, 1; 4, 2.	3, 1; 0, 2.	3, 5; 0, −2.		
35	5	1, 1; 2, 4.				
	7	1, 3; 2, 2.	3, 3; 0, 2.			
37	7	1, 1; 2, 6.	1, 3; 2, 4.	1, 5; 2, 2.	3, 5; 0, 2.	
42	6	1, 1; 3, 1.	1, −1; 3, 3.			
44	6	1, −1; 3, 5.				
46	6	1, 1; 3, 5.				

Appendix II

Expansions of the mean temperature spectral functions $\theta_{0,2n}$ and the advection spectral functions B_γ and H_γ

$$\theta_{02}/k = -\psi_{11}(\theta_{11}-\theta_{13})+\psi_{13}(\theta_{11}+\theta_{15})+\psi_{15}\theta_{13}+2\psi_{22}\theta_{24} + 2\psi_{26}\theta_{24}+2\psi_{24}(\theta_{22}+\theta_{26})-3\psi_{31}\theta_{31} + 3\psi_{33}(\theta_{31}+\theta_{35})+3\theta_{33}(\psi_{31}+\psi_{35})+\ldots. \tag{A.1}$$

$$2\theta_{04}/k = \psi_{11}(\theta_{15}-\theta_{13})+\theta_{11}(\psi_{15}-\psi_{13})-2\psi_{22}\theta_{22}+\psi_{13}\theta_{17} + \psi_{17}\theta_{13}+2(\psi_{22}\theta_{26}+\psi_{26}\theta_{22})-3\psi_{31}(\theta_{33}-\theta_{35}) - 3\theta_{31}(\psi_{33}-\psi_{35})+\ldots. \tag{A.2}$$

$$3\theta_{06}/k = -\psi_{13}\theta_{13}-\psi_{11}(\theta_{15}-\theta_{17})-\theta_{11}(\psi_{15}-\psi_{17})-3\psi_{33}\theta_{33} - 2(\psi_{22}\theta_{24}+\psi_{24}\theta_{22})-3(\psi_{31}\theta_{35}+\psi_{35}\theta_{31})+\ldots. \tag{A.3}$$

$$\left.\begin{aligned} H_{11}/2 &= \theta_{02}(\psi_{13}-\psi_{11})-2\theta_{04}(\psi_{13}-\psi_{15})-2\psi_{22}(\theta_{13}+\theta_{31}) \\ &\quad -2\theta_{22}(\psi_{13}+\psi_{31})+\psi_{24}(\theta_{13}+\theta_{35}-3\theta_{33}-3\theta_{15}) \\ &\quad +\theta_{24}(\psi_{13}+\psi_{35}-3\psi_{33}-3\psi_{15})+\ldots. \\ B_{11}/2 &= 2(\alpha_{13}^2-\alpha_{22}^2)\psi_{13}\psi_{22}+(\alpha_{24}^2-\alpha_{13}^2)\psi_{13}\psi_{24}+(\alpha_{35}^2-\alpha_{24}^2)\psi_{24}\psi_{35} \\ &\quad +2(\alpha_{22}^2-\alpha_{31}^2)\psi_{22}\psi_{31}+3\psi_{24}\{(\alpha_{24}^2-\alpha_{33}^2)\psi_{33}-(\alpha_{24}^2-\alpha_{15}^2)\psi_{15}\}+\ldots. \end{aligned}\right\} \tag{A.4}$$

$$\left.\begin{aligned} H_{13}/2 &= \psi_{11}(\theta_{02}-2\theta_{04}+2\theta_{22}-\theta_{24})+\theta_{11}(2\psi_{22}-\psi_{24})+\theta_{02}\psi_{15}+\ldots. \\ B_{13}/2 &= 2(\alpha_{22}^2-\alpha_{11}^2)\psi_{11}\psi_{22}-(\alpha_{24}^2-\alpha_{11}^2)\psi_{11}\psi_{24}+\ldots. \end{aligned}\right\} \tag{A.5}$$

$$\left.\begin{aligned} H_{22}/4 &= \theta_{02}\psi_{24}-2\theta_{04}\psi_{22}-\psi_{11}(\theta_{13}-\theta_{31})+\theta_{11}(\psi_{13}+\psi_{31}) \\ &\quad -\psi_{13}(2\theta_{31}+2\theta_{15}-\theta_{35})+\theta_{13}(2\psi_{31}-2\psi_{15}+\psi_{35})+\ldots. \\ B_{22}/4 &= (\alpha_{31}^2-\alpha_{11}^2)\psi_{11}\psi_{31}-(\alpha_{13}^2-\alpha_{11}^2)\psi_{11}\psi_{13}+2(\alpha_{15}^2-\alpha_{13}^2)\psi_{13}\psi_{15} \\ &\quad -(\alpha_{35}^2-\alpha_{13}^2)\psi_{13}\psi_{35}-2(\alpha_{13}^2-\alpha_{31}^2)\psi_{13}\psi_{31}+\ldots. \end{aligned}\right\} \tag{A.6}$$

$$\left.\begin{aligned} H_{31}/2 &= 3\theta_{02}(\psi_{33}-\psi_{31})-\psi_{11}(2\theta_{22}-\theta_{42})+\theta_{11}(2\psi_{22}+\psi_{42}) \\ &\quad +\psi_{13}(4\theta_{22}-5\theta_{24})-\theta_{13}(4\psi_{22}-5\psi_{24})+\ldots. \\ B_{31}/2 &= (\alpha_{42}^2-\alpha_{11}^2)\psi_{11}\psi_{42}-2(\alpha_{22}^2-\alpha_{11}^2)\psi_{11}\psi_{22}+4(\alpha_{22}^2-\alpha_{13}^2)\psi_{13}\psi_{22} \\ &\quad -5(\alpha_{24}^2-\alpha_{13}^2)\psi_{13}\psi_{24}+\ldots. \end{aligned}\right\} \tag{A.7}$$

Appendix III

Tables of the expansion coefficients

(*a*) Expansion coefficients of the odd functions

	q^2	q^4			q^6				
		σ^0	σ^{-1}	σ^{-2}	σ^0	σ^{-1}	σ^{-2}	σ^{-3}	σ^{-4}
$10^5\,\psi_{133}$	484	—	—	—	—	—	—	—	—
$10^5\,\psi_{135}$	726	−163	−266	−76	—	—	—	—	—
$10^5\,\psi_{137}$	908	−407	−666	−189	89	178	166	113	31
$10^3\,\theta_{133}$	618	—	—	—	—	—	—	—	—
$10^3\,\theta_{135}$	927	−208	−8	—	—	—	—	—	—
$10^3\,\theta_{137}$	1158	−519	−21	−1	113	23	14	4	2
$10^7\,\psi_{155}$	—	546	336	274	—	—	—	—	—
$10^7\,\psi_{157}$	—	1364	840	684	−260	−242	−161	−206	−88
$10^3\,\theta_{155}$	—	502	2	0	—	—	—	—	—
$10^3\,\theta_{157}$	—	1254	4	0	−239	−26	−4	−0·5	0
$10^9\,\psi_{177}$	—	—	—	—	715	517	500	349	257
$10^6\,\theta_{177}$	—	—	—	—	2479	40	111	120	0
$10^4\,\psi_{315}$	—	175	89	25	—	—	—	—	—
$10^4\,\psi_{317}$	—	439	221	63	−106	−61	−60	−40	−11
$10^3\,\theta_{315}$	—	250	19	7	—	—	—	—	—
$10^3\,\theta_{317}$	—	625	48	16	−96	9	−6	−9	−3
$10^6\,\psi_{335}$	—	−260	−118	−99	—	—	—	—	—
$10^6\,\psi_{337}$	—	−650	−296	−247	253	73	−146	−52	2
$10^4\,\theta_{335}$	—	−223	1	−1	—	—	—	—	—
$10^4\,\theta_{337}$	—	−558	2	−3	218	91	16	−7	0
$10^8\,\psi_{355}$	—	821	826	682	—	—	—	—	—
$10^8\,\psi_{357}$	—	2052	2065	1705	−735	−741	−410	−494	−208
$10^5\,\theta_{355}$	—	337	−3	0	—	—	—	—	—
$10^5\,\theta_{357}$	—	842	−7	1	−302	−41	−2	1	0
$10^9\,\psi_{377}$	—	—	—	—	250	229	187	134	110
$10^6\,\theta_{377}$	—	—	—	—	337	19	1	−0	0

(*b*) Expansion coefficients of the even functions

	q^2		q^3			
	σ^0	σ^{-1}	σ^0	σ^{-1}	σ^{-2}	σ^{-3}
$10^4\,\psi_{224}$	146	40	—	—	—	—
$10^4\,\psi_{226}$	292	80	−101	−91	−61	−17
$10^3\,\theta_{224}$	371	6	—	—	—	—
$10^3\,\theta_{226}$	742	13	−258	−36	−17	−3
$10^6\,\psi_{244}$	−254	−208	—	—	—	—
$10^6\,\psi_{246}$	−507	−415	192	134	151	63
$10^4\,\theta_{244}$	−581	−1	—	—	—	—
$10^4\,\theta_{246}$	−1162	−2	439	22	1	0
$10^8\,\psi_{226}$	—	—	−513	−430	−304	−249
$10^5\,\theta_{266}$	—	—	−524	−6	0	0
$10^6\,\psi_{426}$	—	—	380	732	384	80
$10^4\,\theta_{426}$	—	—	193	0·5	5	1
$10^8\,\psi_{446}$	—	—	476	270	277	231
$10^6\,\theta_{446}$	—	—	968	22	−3	2
$10^9\,\psi_{466}$	—	—	−192	−203	−206	−171
$10^6\,\theta_{466}$	—	—	−132	2	1	−0

(c) Coefficients for θ_{04} and θ_{06}

		q^3			q^4				
	q^2	σ^0	σ^{-1}	σ^{-2}	σ^0	σ^{-1}	σ^{-2}	σ^{-3}	σ^{-4}
$10^4\,\theta_{044}$	−2742	—	—	—	—	—	—	—	—
$10^4\,\theta_{046}$	−5483	911	74	12	—	—	—	—	—
$10^4\,\theta_{048}$	−8225	2734	233	37	−488	−134	−82	−31	−5
$10^5\,\theta_{066}$	—	−1524	−8	−3	—	—	—	—	—
$10^5\,\theta_{068}$	—	−4571	−23	−8	774	165	36	7	0
$10^5\,\theta_{088}$	—	—	—	—	−59	−2	−3	−3	0

REVIEWS

Turbulent Flows and Heat Transfer. (Volume v of **High Speed Aerodynamics and Jet Propulsion.**) Edited by C. C. Lin. Princeton University Press and Oxford University Press, 1959. 549 pp. £5. 5*s*.

I believe that, even in the present state of development, the results obtained from fundamental studies of turbulent flow can be useful in practical problems of fluid motion but I am unable to think of any book published in the last twenty years that provides evidence for this belief. The trouble is that most of the books belong to one of two distinct groups, the first describing experimental studies of highly specialized flows and relating them to mathematical theories based on insecure assumptions and the second providing design information for engineers. A typical book of the first group usually stops well short of being useful and, in spite of encouraging words on the jacket, makes little attempt to show how it could be useful. In a typical book of the second group, useful observational material is presented in the proper non-dimensional form and interpreted in terms of mixing-length theory, with a supplementary account of, say, the theory of diffusion by continuous movements which has no obvious relation to the rest of the book and confirms one's suspicion that the aim of the statistical theory of turbulence is full employment for mathematicians. To quote the preface to the volume under review: 'future developments in our knowledge should result in the merging of these two approaches into a comprehensive and unified treatment'. However the initiative lies with those engaged in fundamental studies and the cause of unity is not advanced by describing work interesting only to specialists. In this respect, this volume, or at least the part concerned with turbulent flow, is disappointing as one in my second group with a considerable amount of space allowed for description of basic theory.

The first section (by H. L. Dryden) is concerned with the phenomenon of transition from laminar to tubulent flow, for the most part in boundary layers, and it is a good account of present experimental knowledge related in a sensible way to the little theory that exists. Ample references are given as in all the sections and anyone needing information about the problem of transition should read this article. The next section on turbulent flow (by G. B. Schubauer and C. M. Tchen) must have been very difficult to write, and I am in complete sympathy with the authors in their desire to link theory and practice but I am most unhappy about the result of this mixture. The introductory chapter, discussing the general nature of turbulent flow, is good but the following chapters on equations of motion, compressible boundary-layers and wall-flow suffer from a lack of selection and organization of the theoretical background. Although the incompressible boundary-layer is used as the standard of comparison for compressible layers, the latter are described first and with inadequate forward reference. For example, two equations for the variation of skin friction with Reynolds number appear in chapter 3 as respective consequences of the Karman similarity hypothesis (12–17) and the Prandtl hypothesis for the

mixing-length (12–18) but, in chapter 4, they appear, more accurately, as a consequence of the 'law of the wall' and the 'law of the wake' (18–5) and as an explicit interpolation valid over moderate ranges of Reynolds number. Again, section 23 is a clear and accurate account of the effect of surface roughness, but the result that surface conditions can only cause a velocity shift is most relevant to the existence of the logarithmic velocity-distribution and should be mentioned when that is discussed. Some of the theory in this brief account is of very limited interest, e.g. the development of a modified form of the mixing-length theory from the Boltzmann equation; and the 'proof' that stagnation temperature and stream velocity are linearly related if the laminar Prandtl number is one (p. 91, § B.9) is just wrong. (The similarity of two equations is not established by similarity of their mean values.) Good selection of experimental material and very full references make this section useful but, on this evidence, meteorologists are far ahead of aerodynamicists in understanding wall flow.

The section on the statistical theory of turbulence (by C. C. Lin) has very little connexion with the rest of the book and it omits, or describes only very briefly those parts of the theory that are relevant to practical problems. The theory of isotropic turbulence is developed in some detail with brief reference to the Kolmogoroff theory of local similarity, and the various theories of the decay of isotropic turbulence are compared with experimental measurements. In the remaining 12 pages, we hear of the theory of diffusion by continuous movements, of temperature fluctuations in isotropic turbulence (with no mention of the more important topic of the spectrum in the range of local similarity), of turbulent motion in a compressible fluid and the production of sound, and of the effect of damping screens on homogeneous turbulence. Since this group of subjects includes nearly all those parts of the statistical theory that may be used with profit in the study of practical problems, some of the previous 45 pages should have been diverted to their use.

The other sections on flow problems, on convective heat transfer in liquids (by R. G. Deissler) and in gases (by E. R. van Driest) correlate experiment with theory in a way which should be useful to the experimentalist and which is not unduly disturbing to the theoretically minded. The remaining sections, on heat conduction, on boiling heat-transfer and on radiative transfer, are of less interest to hydrodynamicists.

Although the contributors to this volume were allowed less space, it is natural to compare it with a classic work in fluid dynamics, *Modern Development in Fluid Dynamics*, edited by Goldstein, and also the result of collaboration. Today, much of the value of this latter two-volume work lies in its comprehensive account of experiment and the simple theoretical interpretations. The greater part of *Turbulent Flows and Heat Transfer* shares these qualities. The exceptional unity and organization of the older work is missing but, if the reader wants practical information, he will find it here. For the basic theory of turbulent flow, he must wait or work it out from the literature.

A. A. Townsend

The Atmosphere and the Sea in Motion. Edited by B. Bolin. Oxford University Press, 1960. 105*s*.

This volume is a collection of articles prepared as a tribute to Carl-Gustaf Rossby, the Swedish–American meteorologist and oceanographer whose personality and scientific contributions have played a unique role in the spectacular growth of our knowledge of geophysical fluid systems during the past forty years. The collection was originally planned in honour of Rossby's sixtieth birthday, but following his death in Stockholm in August 1957, it was reorganized as a memorial volume.

The roster of distinguished contributors—a selection of Rossby's colleagues, collaborators, and students—is itself an impressive testimonial to the extraordinary role Rossby played in the development of many phases of modern geophysics. Virtually every aspect of physical meteorology, and much of physical oceanography, is represented. Articles in theoretical meteorology are interspersed with essays emphasizing synoptic or climatologic techniques of analysis. Discussions of laboratory experiments with rotating or stratified fluids are followed by articles on numerical methods in meteorological research and forecasting. Contributions also on geochemistry, cloud physics, atmospheric radiation, the mechanics of convection and many more fields are to be found in this scientific potpourri.

Unfortunately, the result is a collection of scientific papers lacking any semblance of organization or direction. Everyone with an interest in meteorology or oceanography can find something of interest in the Rossby memorial volume; few will find it a reference which they will frequently consult in their research.

This conclusion is not based solely on the wide variety of subjects discussed. The volume suffers also from the sheer number of contributions—thirty-nine in all—and the resulting raggedness of quality. Several of the articles are of trivial interest; others, by individuals well known for their research, are below the expected high standard of originality and competence. The number of significant articles is unfortunately low. One feels instinctively that many authors, finding themselves without a contribution of substantial importance, chose whatever topic was readily available in order to participate in the venture.

Nevertheless, it is difficult to blame either the individual contributors or the group of five meteorologists and oceanographers whose decision to solicit such a large number of contributions from such a heterogeneous group of scientists set the tenor of the volume. More than most leading scientists of our time, Rossby was a citizen of the world. His winning personality, flair for organization, and peripatetic restlessness—combined with his catholic interests and originality—led him to develop close associations with geophysicists throughout the world. Despite the fact that there were almost fifty contributors to the memorial volume, the five organizers (Bolin, Charney, Eliassen, Platzman and Stommel) find it necessary to apologize in their brief Preface for 'the number of colleagues or former students...we were forced to exclude in order to satisfy the rather stringent requirements of economy'.

This attitude is understandable. Yet the reviewer cannot help but regret the decisions which led to a volume of this nature. The array of talent available was formidable. A rigorously controlled number of major contributions, each devoted to a topic of substantial interest, might have proved a more enduring memorial to a great man.

The collection of articles in the volume is loosely grouped into six sections. The first is biographical in nature, and includes a major article by Rossby, translated from Swedish, which appeared in *Svensk Naturvetenskap* in 1956. The reviewer found this article to be one of the most interesting of the entire volume. Although it is written for the non-specialist, the paper illustrates the breadth of Rossby's interests and his comprehensive grasp of the atmosphere as a geophysical system. Those of us who knew Rossby only in his later years will also appreciate 'The young Carl-Gustaf Rossby', by Tor Bergeron.

The remaining sections are entitled: 'The Sea in Motion': 'Distribution of Matter in the Sea and Atmosphere'; 'The General Circulation of the Atmosphere'; 'Characteristic Features of Atmospheric Motion'; and 'Weather Forecasting'. It would be pointless to review individual contributions in detail. Articles of greatest interest will vary according to the background of the reader. The reviewer would like to call attention, however, to 'Ein numerisches Experiment mit dem primitiven Gleichung', by Von K. Hinkelman. This paper summarizes a substantial research effort, and holds considerable promise for the successful use of the primitive equations of motion in numerical research and forecasting.

GEORGE S. BENTON

INDEX

ASHKENAS, HARRY. *See* WEGENER

BENJAMIN, T. BROOKE. The development of three-dimensional disturbances in an unstable film of liquid flowing down an inclined plane, 401

BENNEY, D. J. A non-linear theory for oscillations in a parallel flow, 209

BLYTHE, P. A. Comparison of exact and approximate methods for analysing vibrational relaxation regions, 33

BREACH, D. R. Slow flow past ellipsoids of revolution, 306

BRETHERTON, F. P. The motion of long bubbles in tubes, 166

BROWN, D. R. A study of the behaviour of a thin sheet of moving liquid, 297

BRYSON, A. E. and GROSS, R. W. F. Diffraction of strong shocks by cones, cylinders, and spheres, 1

CABANNES, HENRI and STAEL, CLAUDE. Singularities of attached shock waves in steady axially symmetric flow, 289

CASE, K. M. Hydrodynamic stability and the inviscid limit, 420

CHESTER, W. The effect of a magnetic field on the flow of a conducting fluid past a body of revolution, 459

CHESTER, W. and MOORE, D. W. The effect of a magnetic field on the flow of a conducting fluid past a circular disk, 466

CORRSIN, S. *See* KENNEDY

COSART, W. P. *See* SCHWARZ

DAVEY, A. Boundary-layer flow at a saddle point of attachment, 593

DRAZIN, P. G. Discontinuous velocity profiles for the Orr–Sommerfeld equation, 571

DUNGEY, J. W. The action of Vlasov waves on the velocity distribution in a plasma, 473

ECKHAUS, WIKTOR. Theory of flame-front stability, 80

FRANCIS, J. R. D. A further note on the speed of floating bodies in a stream, 48

GLAUERT, M. B. A study of the magnetohydrodynamic boundary layer on a flat plate, 276

GOURDINE, MEREDITH C. Magnetohydrodynamic flow constructions with fundamental solutions, 439

GROSS, R. W. F. *See* BRYSON

HORLOCK, J. H. *See* MARSH

HOWARD, LOUIS N. Note on a paper of John W. Miles, 509

HUGHES, B. A. and STEWART, R. W. Interaction between gravity waves and a shear flow, 385

JOHANNSEN, N. H. Analysis of vibrational relaxation regions by means of the Rayleigh-line method, 25

KAHN, F. D. A dispersion relation for waves of finite amplitude in a two-stream plasma, 357

KANWAL, R. P. Slow steady rotation of axially symmetric bodies in a viscous fluid, 17

KENNEDY, D. A. and CORRSIN, S. Spectral flatness factor and 'intermittency' in turbulence and in non-linear noise, 366

KUO, H. L. Solution of the non-linear equations of cellular convection and heat transport, 611

LIEPMANN, HANS W. Gaskinetics and gasdynamics of orifice flow, 65

LIN, C. C. Some mathematical problems in the theory of the stability of parallel flows, 430

LONGUET-HIGGINS, M. S. and STEWART, R. W. The changes in amplitude of short gravity waves on steady non-uniform currents, 529

LUDFORD, G. S. S. The effect of a very strong magnetic cross-field on a steady motion through a slightly conducting fluid, 141

MARSH, H. and HORLOCK, J. H. Diabatic gas flows, 513

MICHAEL, D. H. Note on the stability of plane parallel flows, 525

MILES, JOHN W. On the stability of heterogeneous shear flows, 496

MOORE, D. W. *See* CHESTER

MORTON, B. R. On a momentum-mass flux diagram for turbulent jets, plumes and wakes, 101

NARASIMHA, RODDAM. Orifice flow at high Knudsen numbers, 371

PAIN, H. J. and SMY, P. R. Experiments on power generation from a moving plasma, 51

ROSHKO, ANATOL. Experiments on the flow past a circular cylinder at very high Reynolds number, 345

SATAPATHY, R. and SMITH, W. The motion of single immiscible drops through a liquid, 561

SCHWARZ, W. H. and COSART, W. P. The two-dimensional turbulent wall-jet, 481

SHINNAR, REUEL. On the behaviour of liquid dispersions in mixing vessels, 259

SMITH, W. *See* SATAPATHY

SMY, P. R. *See* PAIN

SPENCE, D. A. The theory of the jet-flap for unsteady motion, 237

STAEL, CLAUDE. *See* CABANNES

STEWART, R. W. *See* HUGHES

STEWART, R. W. *See* LONGUET-HIGGINS

STEWART, R. W. The wave drag of wind over water, 189

TAYLOR, G. I. Deposition of a viscous fluid on the wall of a tube, 161

TAYLOR, R. J. A new approach to the measurement of turbulent fluxes in the lower atmosphere, 449

TOWNSEND, A. A. A continuum theory of the isothermal flow of liquid helium II, 113

WARREN, F. W. G. A stationary-phase approximation to the ship-wave pattern, 584

WEGENER, PETER P. and ASHKENAS, HARRY. Wind tunnel measurements of sphere drag at supersonic speeds and low Reynolds numbers, 550

WERNER, J. E. Unsteady interaction of a shock wave with a cellular vortex field, 195

WU, T. YAO-TSU. Swimming of a waving plate, 321

YIH, CHIA-SHUN. Flow of a non-homogeneous fluid in a porous medium, 133

REVIEWS

Handbook of Supersonic Aerodynamics, 156

Hydromagnetic Channel Flows, 158

Non-Newtonian Fluids, 315

Heat Transfer, 317

Turbulence. An Introduction to Its Mechanism and Theory, 319

Similitude Physique: Examples d'Applications à la Mécanique des Fluides, 480

Turbulent Flows and Heat Transfer, 635

The Atmosphere and the Sea in Motion, 637

JOURNAL OF FLUID MECHANICS

Volume 10, Part 4 June 1961

CONTENTS

The two-dimensional turbulent wall-jet
by W. H. SCHWARZ and W. P. COSART *page* 481

On the stability of heterogeneous shear flows
by JOHN W. MILES 496

Note on a paper of John W. Miles
by LOUIS N. HOWARD 509

Diabatic gas flows
by H. MARSH and J. H. HORLOCK 513

Note on the stability of plane parallel flows
by D. H. MICHAEL 525

The changes in amplitude of short gravity waves on steady non-uniform currents
by M. S. LONGUET-HIGGINS and R. W. STEWART 529

Wind tunnel measurements of sphere drag at supersonic speeds and low Reynolds numbers
by PETER P. WEGENER and HARRY ASHKENAS 550

The motion of single immiscible drops through a liquid
by R. SATAPATHY and W. SMITH 561

Discontinuous velocity profiles for the Orr–Sommerfeld equation
by P. G. DRAZIN 571

A stationary phase approximation to the ship-wave pattern
by F. W. G. WARREN 584

Boundary-layer flow at a saddle point of attachment
by A. DAVEY 593

Solution of the non-linear equations of cellular convection and heat transport
by H. L. KUO 611

REVIEWS

Turbulent Flows and Heat Transfer 635

The Atmosphere and the Sea in Motion 637

INDEX TO VOLUME 10 639

Printed in Great Britain at the University Press, Cambridge
(Brooke Crutchley, University Printer)